UNIVERSIDADE FEDERAL DE MINAS GERAIS

Escola de Engenharia

Programa de Pós Graduação em Engenharia Metalúrgica, Materiais e Minas

Tese de Doutorado

# Estruturas tridimensionais (3D) porosas de derivados tiolados de quitosana produzidas por rota sustentável para potenciais aplicações ambientais e biológicas

Aluna: Fernanda Guerra Lima Medeiros Borsagli

Orientador: Prof. Dr. Herman Sander Mansur

Julho/2018

UNIVERSIDADE FEDERAL DE MINAS GERAIS

Escola de Engenharia

Programa de Pós Graduação em Engenharia Metalúrgica, Materiais e Minas

Fernanda Guerra Lima Medeiros Borsagli

# Estruturas tridimensionais (3D) porosas de derivados tiolados de quitosana produzidas por rota sustentável para potenciais aplicações ambientais e biológicas

Tese de doutorado apresentada ao Programa de Pós-Graduação em Engenharia Metalúrgica, Materiais e de Minas da Escola de Engenharia da Universidade Federal de Minas Gerais, como requisito parcial para obtenção do grau de Doutor em Engenharia Metalúrgica, Materiais e de Minas.

Área de Concentração: Ciência e Engenharia de Materiais

Orientador: Prof. Dr. Herman Sander Mansur

Universidade Federal de Minas Gerais

Programa de Pós Graduação em Engenharia Metalúrgica, Materiais e Minas

Belo Horizonte

2018

Borsagli, Fernanda Guerra Lima Medeiros.

B738e Estruturas tridimensionais (3D) porosas de derivados tiolados de quitosana produzidas por rota sustentável para potenciais aplicações ambientais e biomédicas [manuscrito] / Fernanda Guerra Lima Medeiros Borsagli. – 2018.

xx, 188 f., enc.: il.

Orientador: Herman Sander Mansur.

Tese (doutorado) - Universidade Federal de Minas Gerais, Escola de Engenharia.

Apêndice: f.144-145.

Inclui bibliografia.

1. Materiais - Teses. 2. Ciência dos materiais - Teses. 3. Engenharia de tecidos - Teses. 4. Quitosana - Teses. 5. Tiois - Teses. I. Mansur, Herman Sander, 1962-. II. Universidade Federal de Minas Gerais. Escola de Engenharia. III. Título.

CDU: 620(043)

***Dedico esse trabalho a todos aqueles que buscam conhecimento e amor, pois através dessa caminhada angariamos muito mais do que simples ciência, mas uma maneira de conviver e aprender uns com os outros.***

**Agradecimentos**

Primeiramente, gostaria de agradecer a Deus e ao Mestre Jesus por toda essa empreitada, pois se não fossem os mestres queridos jamais teria chegado até aqui.

Aos meus pais, Ubiratan e Sonia, por sempre me apoiarem e estarem ao meu lado em toda a empreitada da vida. Também por me auxiliarem a ser quem sou hoje.

Ao meu amado esposo, Alessandro, por estar ao meu lado em todos os momentos, pela paciência, compreensão, carinho e apoio e por acreditar em todo o meu potencial.

Ao meu orientador, Professor Dr. Herman Sander Mansur, por acreditar em meu potencial e em meu trabalho, por me apoiar nessa empreitada com ensinamentos e conhecimento, mesmo diante das diferenças de opiniões e pensamentos, mas que com certeza levarei para a vida toda.

A Professora Dra. Virginia Sampaio Teixeira Ciminelli a minha imensa gratidão pelos ensinamentos adquiridos, pela orientação durante a produção do segundo artigo, pela atenção e disponibilidade em me escutar e me ensinar a trilhar esse caminho, assim como por disponibilizar alguns dos equipamentos necessários às análises. Assim como, a Dra. Maria Sylvia Silva Dantas pelas análises de Raman necessárias ao projeto.

Ao coordenador do Programa de Pós Graduação em Engenharia Metalúrgica, Materiais e Minas, o Professor Ph.D Rodrigo Órefice, pela atenção, confiança em meu trabalho na entrega da representação discente do colegiado e por me ouvir em relação aos problemas enfrentados durante essa jornada.

Aos colegas da sala da pós, Aislan, Priscila, Dircilene, Daniela, Luana, Graziele Braga, Marys, Monique, entre outros que fizeram os momentos mais difíceis passarem rápido, com ombros amigos, muita alegria e muitas risadas.

Aos colegas do LASMAT, Aislan, Vítor, Nádia, Fábio, Anderson, Isadora, Alice e a Dra Alexandra Mansur pela ajuda e colaboração nessa empreitada. Assim como a Dra Sandhra Carvalho pelas análises biológicas necessários ao projeto, por me escutar e por ser uma pessoa tão maravilhosa quanto ela é.

Aos meus queridos amigos da Fundamigo, que sempre me fortaleceram e me ajudaram a construir minha nova jornada, dando-me força em todos os momentos e me auxiliando a lembrar que sempre tem alguém olhando e orando por nós.

À doutoranda do Departamento da Química, Poliane Chagas, e ao Professor Dr. Luiz Cláudio, pela disponibilidade de tempo e análises de RMN necessárias no material produzido nesse projeto. Também ao doutorando Dionei Haas e ao Professor Andrey P Lage da Escola de Medicina Veterinária pela disponibilidade de tempo e análises da atividade antibacteriana.

Aos funcionários do DEMET e do Programa de Pós Graduação em Engenharia Metalúrgica, Materiais e Minas, Cida, Nelson, Ilda, Isabel, Claúdia e Patrícia, em especial a grande Cida pela atenção, compreensão, ombros e abraços durante essa caminhada.

E, por último, mas não menos importante ou especial, à CAPES, CNPq, FAPEMIG, FINEP – CTINFRA pelo suporte financeiro, pelas instalações e equipamentos necessários a essa jornada, pois sem isso nada seria possível.

## Sumário

**Lista de Figuras**

**Lista de Tabelas**

**Lista de Equações**

**Lista de Siglas**

**As** Arsênio

**ATCC** *American Type Culture Collection*

**ATR** Reflectância Total Atenuada (*Total reflectance*)

**CCD** *Charge-coupled device*

**COOH** Grupo Carboxílico

**$COO^-$** Grupo Carboxilato

**Cd** Cádmio

**CGA** Glicosaminoglicano

**CHI** *Chitosan*

**CHICys** Quitosana funcionalizada com cisteína

**CHIMerc** Quitosana funcionalizada com ácido mercaptoundodecanóico

**$CH_3$** Metil

**$CH_4$** Metano

**$CO_2$** Gás Carbônico

**$C_0$** Concentração Inicial

**$C_e$** Concentração no equilíbrio

**CYS** Cisteína (*L-cysteine*)

**DD** *Degree of deacetylation*

**DF** Grau de Funcionalização (*Degree of functionalization*)

**DI** Água Deionizada

**DLS** Espalhamento dinâmico da luz

**DMEM** *Dulbecco's modified eagle medium*

**DTNB** 5,5-ditio-bis-[acido 2-nitrobenzoíco]

**ε** *Porosity* (Porosidade)

**ECM** *Extracellular matrix*

**EDC** *N*-(3-Dimetil aminopropil)-*N*-etilcarbodiimida

**EDTA** *Ethylenediaminetetraacetic acid*

**EDX** *Energy Dispersive Spectroscopy* - Espectroscopia por Dispersão de Energia

**FAO** *Food and Agriculture Organization of United Nations* – Organização de Alimento e Agricultura das Nações Unidas

**FBS** *Fetal bovine serum* (Soro fetal bovino)

**Fig** *Figure* (Figura)

**FTIR** *Infrared Spectroscopy Fourier Transform* - Espectroscopia no infravermelho com Transformada de Fourier

**GAG** *Glycosaminoglycan*

**GD** Grau de Desacetilação

**GF** *Gel-Fraction* (Degradação por solvatação)

**GI ou SD** Grau de Intumescimento (*Swelling Degree*)

**GLcN** 2 – amino – 2 – desoxi – *D* – glicopiranose

**GLcNAc** 2 – acetamido – 2 – desoxi – *D* – glicopiranose

**HCl** Ácido clorídrico

**HEK** *kidney cell line of human embryos* (Célula embrionária de rim)

**HEMA – chitosan – MWCNT** (*nanocomposite of multi-walled carbon nanotube (MWCNT) functionalized (f) with chitosan (CS) and poly-2- hydroxyethyl methacrylate* (pHEMA))

**$H_2O$** Água

**$^1$H NMR** *Proton nuclear magnetic resonance*

**IPT** Instituto de Pesquisa Tecnológica

**IR** *Infrared*

**KCl** Cloreto de Potássio

**kDa** Kilodalton

**MEC** Matriz extracelular

**MERC** Ácido mercaptoundodecanóico (*11-mercaptoundecanoic acid*)

**MEV** Microscopia Eletrônica de Varredura

**Micro-CT** Microtomografia Compuradorizada (*X-ray microcomputed tomography*)

**MM** Massa Molar

**MO** *Methyl Orange* (Laranja de metila)

**MTT** Ensaio colorimétrico com Brometo de 3-(4,5-Dimetiltiazol-2-yl)-2,5-difeniltetrazólio

**Mw** *Molecular weight* (Peso molecular)

**NIH** *National Institutes of Health*

**$NH_2$** Amina

**$NH_3^+$** Amina Protonada

**NHS** *N*-Hidroxisuccinimida

**OH** Hidroxila

**ONU** Organização das Nações Unidas

**PBS** *Phosphate Buffer Solution* – Solução Salina Tampão de Fosfato

**PHA** poli(hidroxialcanoatos)

**PHB** polihidroxibutirato

**PLA** Ácido Poliláctico

**PZ** Potencial Zeta

**ρ** *Density* (densidade)

**$q_e$** Capacidade de adsorção/complexação no equilíbrio

**$q_m$** Capacidade Máxima de Adsorção do Adsorvente (*Maximum uptake*)

**$q_t$** Capacidade de adsorção/complexação em um determinado tempo

**QS** *Quorum signals*

**QUI** Quitosana

**RMN ou NMR** Ressonância Magnética Nuclear (*Nuclear Magnetic Resonance*)

**RT** Temperatura ambiente (*Room temperature*)

**SAOS** *Human osteosarcoma cells* (Célula de osteosarcoma)

**SAP** *Polyelectrolyte-based hydrogel* (Polímeros superabsorventes)

**$S_a$** *Surface area (*Área superficial)

**SE** *Secondary electron*

**SEM** *Scanning Electron Microscope*

**-SH** Grupo Tiol

**Sulfo – NHS** *N*-Hidroxisulfosuccinimida

**SD** *Swelling degree*

**SDS** *Sodium Dodecyl Sulfate* - Dodecil Sulfato de Sódio

**S-S** *Dissulfide bond* (Ligação dissulfeto ou dissulfídica)

**3D** Estrutura tridimensional

**TGA** Ácido tioglicólico

**UFMG** Universidade Federal de Minas Gerais (*Federal University of Minas Gerais*)

**UNESCO** *United Nations Education, Scientific and Cultural Organization* – Organização das Nações Unidas para a Educação, Ciência e a Cultura

| | |
|---|---|
| **USA** | *United States of America* |
| **USP** | Universidade de São Paulo |
| **UV** | Ultravioleta |
| **UV vis** | Ultravioleta visível |
| **WA** | *Water adsorption* (Adsorção de água) |

**Resumo**

Um dos grandes desafios atuais da ciência e engenharia de materiais é o desenvolvimento de materiais sustentáveis, produzidos por rotas quimicamente amigáveis, que não impactem o meio ambiente proporcionando materiais com multifuncionalidade. Nesse sentido, a modificação da quitosana incorporando o grupo tiol é bastante promissora, pois essa modificação abre um leque de aplicações que vão desde engenharia de tecido até tratamento de água, pois esse grupamento possibilita uma melhor adesão celular, assim como uma seletividade e interação química ampliada com diversos materiais. Nesse enfoque, o presente trabalho buscou a produção de materiais tridimensionais por meio do processo *freeze-drying* (liofilização), funcionalizando a quitosana com diferentes precursores contendo o grupo tiol (-SH) (cisteína (CHICys) e ácido mercaptoundodecanóico (CHIMerc)) por uma rota química sustentável, para potenciais aplicações na regeneração tecidual e no tratamento de água. Para melhor compreensão dos mecanismos envolvidos na funcionalização, técnicas de caracterização como espectroscopia no infravermelho, espectroscopia Raman, ressonância magnética nuclear, intumescimento, degradação por solvatação (*Gel-fraction*, GF), ângulo de contato, microscopia eletrônica de varredura, microtomografia computadorizada, Arquimedes e definição do grau de funcionalização com o reagente *Ellman*, utilizando a espectroscopia no ultravioleta visível, foram utilizadas. Além disso, para avaliar a aplicação do material na regeneração de tecido, ensaios biológicos de citotoxicidade, como o ensaio colorimétrico de MTT e o LIVE/DEAD com as células de osteosarcoma (SAOS) e de rim embrionário (HEK) foram reproduzidos. Além de ensaios antibacterianos com a bactéria *Pseudomona aeroginosa* e ensaios de adsorção do pigmento laranja de metila, avaliando a cinética de adsorção, isotermas, influência do pH e dessorção para a potencial aplicação do material no tratamento de água com o patógeno e com corantes. Os resultados mostraram que os precursores apresentaram diferentes graus de funcionalização em razão das diferenças de cada um e do método utilizado (CHICys = 5 % e CHIMerc = 26 %). Além disso, a estrutura tridimensional das quitosanas modificadas apresentaram uma morfologia mais homogênea comparada com a da quitosana, diâmetros de poros ((223±72 µm), (225±95 µm) para a CHICys e CHIMerc, respectivamente), porosidade (> 80 %) e interconectividade (> 90 %) adequados para crescimento celular. Também a estabilidade química e a lipofilicidade do material foi diferente apresentando-se maior (CHIMerc, GF = 96±3 %) ou menor (CHICys, GF = 36±4 %) dependendo do precursor. Os resultados também indicaram que essa

estabilidade química está relacionada ao grau de funcionalização (CHICys = 409±27 µm.g$^{-1}$ e CHIMerc = 2218±100 µm.g$^{-1}$), já que o grupo tiol possibilita a formação de ligações cruzadas por meio de ligações dissulfetos, bem evidentes na amostra CHIMerc. Essa diferença na funcionalização, possibilitou a amostra CHIMerc a aplicação como adsorvente do pigmento laranja de metila, apresentando uma alta adsorção (400 – 450 mg.g$^{-1}$ em pH = 7,0±0,2), sendo o modelo de Freundlich o mais apropriado para explicar a adsorção, indicando uma afinidade química do *scaffold* pelo pigmento e com eluição do pigmento após 2 h de ultrassonicação ((82±1) %, (76±2) % e (37±2) % para o EDTA, KCl e $HNO_3$, respectivamente). A avaliação da adsorção do pigmento e de água em diferentes pH mostrou que o grupo tiol é influenciado pelo pH (sob condições básicas sofre oxidação e a adsorção sofre uma diminuição (18±1 %), comparada com condições ácidas (42±3 %) e neutras (91±2 %)). Essa amostra também apresentou atividade antibacteriana contra *Pseudomona aeroginosa*, uma bactéria bastante resistente e presente em efluentes e água residuais propiciando o uso desse *scaffold* como um adsorvente em água contaminadas com esse patógeno. E ambos os *scaffolds* não apresentaram citotoxicidade *in vitro* avaliada pelos ensaios de MTT e LIVE/DEAD nas células HEK e SAOS propiciando sua aplicação em regeneração tecidual em razão da morfologia, das propriedades físico-químicas e da não toxicidade no meio biológico.

**Palavras chaves:** Quitosanas Tiolizadas, Estrutura Tridimensional (3D), Tiol (SH), Engenharia de Tecido, Bioadsorção.

**Abstract**

One of the major challenges today in materials science and engineering is the development of sustainable materials produced by chemically friendly routes that do not impact the environment by providing multifunctional materials. In this sense, the modification of the chitosan incorporating the thiol group is very promising, since this modification opens a range of applications ranging from tissue engineering to water treatment, since this grouping allows a better cellular adhesion, as well as a selectivity and chemical interaction enlarged with several materials. In this approach, the present work sought the production of three-dimensional materials from a sustainable source through the freeze-drying process, using chitosan modified with different precursors containing the thiol group (SH) (cysteine (CHICys) and mercaptoundodecanoic acid (CHIMerc)) by a friendly chemical route for applications in tissue regeneration and water treatment. In order to understand the mechanisms involved in the functionalization, characterization techniques were used as infrared spectroscopy, Raman spectroscopy, visible ultraviolet spectroscopy, nuclear magnetic resonance, swelling degree, gel-fraction, surface contact, scanning electron microscopy, microtomography, Archimedes, biological cytotoxicity assays such as MTT and LIVE/DEAD with SAOS and HEK cells, and antibacterial activity against *Pseudomona aeroginosa*. In addition, the scaffolds were applied in the adsorption of the methyl orange, evaluating the kinetics of adsorption, isotherms and the influence of the pH in this adsorption. As the desorption of the pigment was carried out to evaluate the feasibility of reuse. The results showed that the different precursors led to different degrees of functionalization due to the differences in the chains and the method used (CHICys = 5 % and CHIMerc = 26 %). In addition, the three-dimensional structure of thiolated chitosans presented different morphology compared with chitosan, as the porous size ((223±72 μm), (225±95 μm) para a CHICys e CHIMerc, respectively), porosity (> 80 %) and interconnectivity (> 90 %) were suitable to cell growth. The chemical stability and lipophilicity of the material was also different (CHIMerc, GF = 96±3%) or lower (CHICys, GF = 36±4%) depending on the precursor. The results further indicated that the higher chemical stability was provided by the presence of the higher amount of thiol group (CHICys = 409±27 $\mu m.g^{-1}$ and CHIMerc = 2218±100 $\mu m.g^{-1}$, obtained with the *Ellman*'s reagent), which provides crosslinks formed by the disulfide bonds, most evident in the CHIMerc sample. This difference in the functionalization and the presence of the thiol group allowed the CHIMerc sample to be

applied as an adsorbent to the methyl orange, which presented a high adsorption (400 - 450 $mg.g^{-1}$ at pH = 7.0±0.2), and the Freundlich model was more suitable to explain the adsorption, which indicates a chemical affinity of the scaffold for the pigment. In addition, the adsorption of the pigment and water at different pH showed that the thiol group is influenced by pH (under basic conditions undergoing oxidation and the adsorption process suffer a decrease (18±1 %), compare with acid (42±3 %) and neutral (91±2 %) conditions). Moreover, the recovery of methyl orange after 2 h of ultrasonication was (82±1) %, (76±2) % and (37±2) % for the EDTA, KCl, and $HNO_3$, respectively indicated the feasibility of its reuse. In addition, this sample presented antibacterial activity against *Pseudomona aeroginosa*, a very resistant bacterium present in effluents and residual water, which allowed the use of this scaffold as an adsorbent wastewater with this patogen. As well as both scaffolds did not present *in vitro* cytotoxicity evaluated by the MTT and LIVE/DEAD assays with HEK and SAOS cells favoring its application in tissue regeneration due to the morphology, physicochemical properties and non-toxicity to the biological environment.

**Keywords:** Thiolated Chitosan, Three Dimensional Structure (3D), Thiol (SH), Tissue Engineering, Bioadsorption

**Organização da Tese**

A estrutura desta tese segue uma divisão por capítulos de 1 a 7, sendo que os capítulos 3 e 4 correspondem a um manuscrito publicado e submetido à publicação. O capítulo 1 apresenta a introdução ao tema e os objetivos dessa tese, sendo destacados a relevância do trabalho. O capítulo 2 relata uma breve revisão bibliográfica do assunto, abordando os tópicos principais expostos na literatura pertinentes a pesquisa trabalhada.

O capítulo 3 aborda o manuscrito publicado no periódico *International Journal of Biological Macromolecule* (Qualis A2) em março de 2018, onde é abordado a produção de estruturas tridimensionais pelo processo de liofilização (*freeze-drying*) a partir de quitosana modificada com diferentes precursores contendo o grupo tiol, compreendendo as diferenças de funcionalização em relação a morfologia e grau de funcionalização proporcionado pelos diferentes precursores para aplicação na regeneração tecidual de cartilagem.

O capítulo 4 é composto do manuscrito submetido à publicação em junho de 2018 para o periódico *Biochemical Engineering Journal* (Qualis A1). Nesse manuscrito é abordado a compreensão da funcionalização da quitosana para aplicação no tratamento de água com corantes (pigmentos) e sua atividade antibacteriana com a bactéria *Pseudomona aeroginosa*, compreendendo os diferentes mecanismos em cada aplicação e a influência do grupo tiol nessas aplicações.

O capítulo 5 aborda as considerações finais referentes ao trabalho de pesquisa aqui presente, entendendo a importância e a influência que o grupo tiol exerceu nas diferentes aplicações propostas nessa tese. Assim como as contribuições originais desse trabalho.

Por fim, os capítulos 6 e 7 abordam as contribuições para a literatura desse trabalho, assim como sugestões de trabalho futuro dessa pesquisa.

## Capítulo 1. Introdução

Um dos grandes desafios atuais da ciência e engenharia de materiais é o desenvolvimento de materiais sustentáveis, produzidos por rotas quimicamente amigáveis, que não impactem o meio ambiente produzindo materiais com multifuncionalidade. Logo, a proposta de funcionalização de polímeros provenientes de fontes naturais torna-se bastante promissora, pois esses polímeros possuem como vantagens serem biodegradáveis, provenientes de fontes renováveis, manufatura mais fácil e muitas vezes serem produzidos a partir de resíduos [1-3].

Nesse enfoque, a quitosana é um biopolímero bastante promissor, pois engloba propriedades, como biocompatibilidade, propriedades antibacterianas [4], apresenta propriedades únicas com funções fisiológicas altamente sofisticadas devido à sua atividade biológica versátil e biodegradabilidade em combinação com baixa toxicidade [5-7]. Além disso, apresenta em sua cadeia grupamentos químicos como as aminas e hidroxilas, que lhe proporcionam uma grande capacidade de captação de íons de metais pesados, de compostos organometálicos, assim como de óleos e derivados [8], e ainda permitem diversas modificações químicas na cadeia desse polímero viabilizando múltiplas aplicações como na indústria farmacêutica, cosmética, biomédica, biotecnológica, agrícola, indústrias de alimentação, bem como no tratamento de água, papel e têxteis [9-11]. Essas modificações químicas podem ser realizadas por meio de ligações cruzadas e conjugação oferecendo diversas alternativas, como inserção de grupos químicos funcionais e ativos, através de ligações covalentes com os grupamentos aminas ou hidroxilas tornando sua aplicação final mais viável [12-14].

A incorporação de grupos químicos específicos que proporcionem não somente uma alta capacidade de retenção de água, por meio da formação de redes tridimensionais, mas que possibilitem uma interação específica com determinados grupos químicos presentes tanto no meio celular, como no meio ambiental, em especial a água, apresenta-se como um desafio e uma oportunidade de aliar a ciência dos materiais a engenharia de sustentabilidade em aplicações ambientais e biológicas. Nesse sentido, as quitosanas modificadas com o grupo tiol (-SH) são cientificamente e industrialmente atraentes, pois a presença desse grupo

melhora a estabilidade química da quitosana, por meio da formação de ligações dissulfídicas (S-S), assim como possibilitam uma interação específica com diversos materiais e com o meio biológico [15]. Essa modificação é feita com base na imobilização do grupo tiol nos grupamentos aminas na cadeia da quitosana e vários compostos podem ser utilizados nessa incorporação do grupo tiol, como ácido tioglicólico [16], cisteína [15,16] e mercaptos [17,18].

De maneira geral, essas incorporações melhoraram a propriedade mucoadesiva e de reforço da quitosana, proporciona novas propriedades físico-químicas tais como a formação de organizações poliméricas, incluindo géis, vesículas poliméricas, filmes Langmuir-Blodgett, cristais líquidos, membranas e fibras, promovem atividade antibacteriana [18-22] e formação de matrizes tridimensionais mais homogêneas e estáveis quimicamente [17,23]. A incorporação desse grupo na cadeia da quitosana dá origem a algumas características sinérgicas interessantes para uso em engenharia de tecidos, bem como outras propriedades biomédicas potencialmente úteis, incluindo anticoagulante e atividades de colesterol [24,25]. Assim como potencial para aplicações ambientais, como tratamento de água, já que a incorporação do grupo tiol possibilita uma melhora na afinidade química com diversos íons como arsênio, cádmio e prata [26-28].

No entanto, embora existam vários estudos apontando o uso dessas quitosanas modificadas com o grupo tiol, existe um vasto campo a ser explorado com base na combinação de funcionalidades químicas com o esqueleto da quitosana produzindo uma nova classe de quitosanas tiolizadas, tais como quitosanas modificadas com cistéina e com grupos acilados contendo o grupo tiol, como os mercaptanos, para numerosas aplicações. Um material ideal combinará todas as características mencionadas da quitosana e do grupo tiol em um único projeto [18].

Considerando que a disponibilidade de água para o desenvolvimento econômico e conservação da vida é um tema de grande preocupação [29], cirurgiões ortopédicos e pesquisadores em todo o mundo enfrentam continuamente o desafio de regenerar os defeitos dos tecidos, pois o corpo humano tem uma capacidade restrita de auto-regenerar

adequadamente a maioria de seus principais tecidos [30] e antibióticos e bactérias resistentes são amplamente encontrados no ambiente como resultado do aumento do uso de medicamentos em aplicações médicas, veterinárias e agrícolas [31,32]. Encontrar um material que alie a possibilidade de aplicação no tratamento de água, regeneração tecidual e atividade antibacteriana é um grande desafio. Nesse contexto, essas quitosanas tiolizadas são interessantes, pois aliam a capacidade de mimetizar a matriz extracelular e possibilitar uma melhor adesão das células devido a presença do grupo tiol [33], promover atividade antibacteriana [18] e interação química com íons presentes em água [26-28]. Assim, há um vasto campo a ser explorado com base na combinação de funcionalidades químicas da quitosana com grupos tiol como *N*-cisteína-quitosana e *N*-acetil-quitosana para inúmeras aplicações e na literatura publicada não há relatos em relação a investigação de estruturas tridimensionais produzidas a partir de quitosanas tiolizadas para aplicações em reparo de tecidos moles e na adsorção de pigmentos.

Dessa forma, o propósito da presente tese foi desenvolver estruturas tridimensionais a partir de quitosana modificada com a incorporação de diferentes precursores contendo o grupo tiol em sua estrutura, a *L*-cistéina (CYS) e o ácido mercaptoundodecanóico (MERC), por meio de uma rota quimicamente sustentável, para potenciais aplicações na regeneração tecidual e no tratamento de água com corantes (pigmentos), além de promover a atividade antibacteriana. Compreendendo os mecanismos de funcionalização química, a engenharia química envolvida no processo e a interação química com os diferentes componentes trabalhados nessa pesquisa.

## 1.1. Objetivos

### 1.1.1 Objetivo Geral

O objetivo geral dessa tese foi produzir estruturas tridimensionais (3D) pelo processo de *freeze-drying*, a partir da quitosana modificada com diferentes precursores contendo o grupo tiol, a *L*-cisteína e o ácido mercaptoundodecanóico, por uma rota quimicamente sustentável, para aplicações na regeneração tecidual e na adsorção de corantes (pigmentos), além de promover a atividade antibacteriana.

### 1.1.2 Objetivos Específicos

Como objetivos específicos dessa tese encontram-se:

- Funcionalizar a quitosana com diferentes precursores contendo o grupo tiol por meio de uma rota quimicamente amigável, mantendo a mesma razão molar entre os precursores e avaliar as diferenças de funcionalidades em cada um;
- Promover a formação de estruturas tridimensionais através do processo de liofilização (*freeze-drying*) e estudar as diferenças proporcionadas na estrutura 3D com os diferentes precursores pelas técnicas de microscopia eletrônica de varredura (MEV), microtomografia computadorizada (micro-CT) e pelo Princípio de Arquimedes;
- Entender os mecanismos de funcionalização proporcionado pelo uso dos *zero-crosslinker* (*N*-(3-Dimetil aminopropil)-*N*-etilcarbodiimida (EDC) e *N*-Hidroxisulfosuccinimida (sulfo-NHS)) por meio de diferentes técnicas de caracterização, como espectroscopia no infravermelho (FTIR), espectroscopia Raman e Ressonância Magnética Nuclear (RMN) e espectroscopia no ultravioleta visível usando o reagente *Ellman*;
- Compreender a modificação nas propriedades da quitosana com a incorporação do grupo tiol e sua interação com os diferentes meios por meio do uso de técnicas como intumescimento, degradação por solvatação (*Gel-fraction*), espectroscopia Raman e ângulo de contato;
- Avaliar a citoxicidade *in vitro* das diferentes quitosanas tiolizadas para averiguar a possibilidade da sua aplicação em regeneração de tecido por meio de ensaios colorimétrico de redução do brometo de 3-(4,5-Dimetiltiazol-2-yl)-2,5-difeniltetrazólio (MTT) e LIVE/DEAD;
- Entender os mecanismos químicos envolvidos na adsorção do pigmento laranja de metila, assim como a interação do grupo tiol com o pigmento;
- Avaliar a cinética e a adsorção do pigmento laranja de metila por meio de isotermas de adsorção;
- Avaliar a influência do pH na adsorção do laranja de metila, assim como o comportamento da estrutura tridimensional em diferentes pH sem o corante, verificando as modificações no grupo tiol;

- Compreender a influência do grupo tiol na atividade antibacteriana contra a bactéria *Pseudomona aeroginosa*.

**Referências**

[1] De Paoli, M. A. Degradação e Estabilização de Polímeros. Cemkeys, 2008.

[2] Plank, J. Applications of biopolymers and other biotechnological products in building materials. Appl. Microbiol. Biot., 66 (2004) 1-9.

[3] Mohanty, S. P., Kougianos, E. Biosensors: a tutorial review. IEEE Potentials, 25 (2006) 35-40.

[4] Saraiva, S. M. et al. Synthesis and characterization of a photocrosslinkable chitosan–gelatin hydrogel aimed for tissue regeneration. RSC Adv., 5 (2015) 63478–63488.

[5] Costa, H. S. Caracterização e Avaliação do Comportamento Degradativo de Híbridos Porosos de Poli (Álcool Vinílico)/Vidro Bioativo. Tese (Doutorado em Engenharia Metalúrgica e de Minas) – Escola de Engenharia da Universidade Federal de Minas Gerais, UFMG, 2010.

[6] Costa Junior, E. S., et al. Preparation and Characterization of Chitosan/Poly(Vinyl Alcohol) Chemically Crosslinked Blends for Biomedical Applications, Carbohydr Polym, 76 (2009) 472-481.

[7] Costa Jr., E. S., Mansur, H. S. Preparação e caracterização de blendas de quitosana/poli(álcool vinílico) reticuladas quimicamente com glutaraldeído para aplicação em engenharia de tecido. Quim. Nova., 31 (2008) 1460-1466.

[8] Medeiros Borsagli, F. G. L., et al. O-carboxymethyl functionalization of chitosan: Complexation and adsorption of Cd (II) and Cr (VI) as heavy metal pollutant ions, React Func Polym, 97 (2015) 37-47.

[9] Muzzarelli, et al. Spray-drying of solutions containing chitosan together with polyuronans and characterisation of the microspheres. Carbohyd. Polym. 57 (2004) 73-82.

[10] Muzzarelli, et al. Current views on fungal chitin/chitosan, human chitinases, food preservation, glucans, pectins and inulin: A tribute to Henri Braconnot, precursor of the carbohydrate polymers science, on the chitin bicentennial. Carbohyd. Polym., 87 (2012) 995-1012.

[11] Muzzarelli, R. A. A. Chitosan composites with inorganics, morphogenetic proteins and stem cells, for bone regeneration. Carbohyd. Polym., 83 (2011) 1433-1445.

[12] Gonçalves, A. A., et al. Diferentes estratégias para reticulação de quitosana. Quím. Nov 34 (2011) 1215-1223.

[13] Mansur, H. S., et al. Functionalized-chitosan/quantum dots nano-hybrids for nanomedicine applications: towards biolabeling and biosorbing phosphate metabolites. J. Mater. Chem. B., 1 (2013) 1696-1711.

[14] Ramanery, F. P., et al. Green and Facile Synthesis of Water-Soluble ZnS Quantum Dots Nanohybrids using Chitosan Derivative Ligands. J. Nanopart. Res., 16 (2014) 2504-2519.

[15] Liu, D., et al. Potential advantages of a novel chitosan-N-acetylcysteine surface modified nanostructured lipid carrier on the performance of ophthalmic delivery of curcumin, Sci Rep, 28796 (2015) 1-14.

[16] Sarti, F., Bernkop-Schnürch, A. Chitosan and thiolated chitosan. In R. Jayakumar, M. Prabaharan, & R. A. A. Muzzarelli (Eds.), Advances in polymer science. chitosan for biomaterials I (243) (pp. 93–110). Berlin, Heidelberg: Springer Berlin Heidelberg.

[17] Medeiros Borsagli, F. G. L.; Carvalho, I. C.; Mansur, H. S. Amino acid-grafted and N-acylated chitosan thiomers: Construction of 3D bio-scaffolds for potential cartilage repair applications. Inter J Biol Macromol, 114 (2018) 270-282.

[18] Croce, M., et al. Synthesis and screening of N-acyl thiolated chitosans for antibacterial applications. Carbohydr Polym, 151 (2016) 1184-1192.

[19] Inta, O., Yoksan, R., Limtrakul, J. Hydrophobically modified chitosan: abio-based material for antimicrobial active film. Mater Sci Eng. C, 42 (2014) 569–577.

[20] Vallapa, N., et al. Enhancing antibacterial activity of chitosan surface by heterogeneous quaternization. Carbohydr Polym, 83 (2011) 868–875.

[21] Sarti, F., Bernkop-Schnürch, A. (2011). Chitosan and thiolated chitosan. In R. Jayakumar, M. Prabaharan, & R. A. A. Muzzarelli (Eds.), Advances in polymer science. chitosan for biomaterials I (243) (pp. 93–110). Berlin, Heidelberg: Springer Berlin Heidelberg.

[22] Dragostina, O. M., et al. New antimicrobial chitosan derivatives for wound dressing applications. Carbohydr Polym, 141 (2016) 28-40.

[23] Bae, I.-H., et al. Evaluation of a Thiolated Chitosan Scaffold for Local Delivery of BMP-2 for Osteogenic Differentiation and Ectopic Bone Formation. BioMed Res Int, 2013 (2013) 1-11.

[24] Schmitz, T., Grabovac, V., Palmberger, T. F., Hoffer, M. H., Bernkop-Schnurch, A., Synthesis and characterization of a chitosan-N-acetyl cysteine conjugate, Inter J Pharm, 347 (2008) 79-85.

[25] Casettari, L., Biomedical applications of amino acid-modified chitosans: A review. Biomaterials, 33 (2012) 7565-7583.

[26] Teixeira, M. C., et al. Raman spectroscopy and DFT calculations of As(III) complexation with a cysteine-rich biomaterial. J. Colloid Interface Sci 315 (2007) 128-134.

[27] Yong, S. K., et al. Synthesis and Characterization of Thiolated Chitosan Beads for Removal of Cu (II) and Cd (II) from Wastewater. Water Air Soil Pollut, 224 (2013) 1720-1735.

[28] Guimarães, A. M. F., Ciminelli, V., Vasconcelos, W., Smectite organofunctionalized with thiol groups for adsorption of heavy metal ions. Appl. Clay Sci., 42 (2009) 410-414.

[29] Ali, I., Gupta, K., Advances in water treatment by adsorption, Taylor & Francis, New York, 2007.

[30] Chen, F-M., Liu, X.., Advancing biomaterials of human origin for tissue engineering, Prog Polym Sci, 53 (2016) 86–168.

[31] Halling-Sorensen, B., et al. Occurrence, fate and effects of pharmaceutical substances in the environment – a review. Chemosphere, 36 (1998) 357-393.

[32] Subbaiah, M. V., Kim, D-S., Adsorption of methyl orange from aqueous solution by aminated pumpkin seed powder: kinetics, isotherms, and thermodynamic studies, Ecotoxicol. Environ. Saf. 128 (2016) 109-117.

[33] Diekjürgen, D., Grainger, D. W., Polysaccharide matrices used in 3D in vitro cell culture systems, Biomaterials,141 (2017) 96-115.

# Capítulo 2. Revisão Bibliográfica

## 2.1 A química verde e aspectos de sustentabilidade

As tecnologias de Química Verde e Engenharia são "ferramentas" que fornecem soluções inovadoras para hoje e amanhã em muitas áreas de produtos e pesquisa de processo e aplicação [1]. Os esforços em Química Verde e Engenharia precisam estar focados nas principais questões para a sustentabilidade, as quais incluem vários fatores como alterações climáticas, produção sustentável de energia, esgotamento de recursos não renováveis, a dissipação de materiais tóxicos e perigosos no meio ambiente, assim como tratamentos de resíduos sólidos e líquidos, entre eles a água [2,3].

Anasta & Warner (1998) [4] definem a química verde como a utilização de um conjunto de princípios que reduz ou elimina o uso ou a geração de substâncias perigosas no projeto, fabricação e aplicação de produtos químicos. Uma das distintas características desse conceito é a ação para fazer um produto químico ou processo inerentemente menos perigoso [4]. Já a sustentabilidade foi definida pela Comissão Mundial sobre Meio Ambiente e Desenvolvimento da Organização das Nações Unidas (ONU) (1987) como uma iniciativa em atender às necessidades da geração atual, sem comprometer a capacidade das gerações futuras de atender suas necessidades [5].

Dessa forma, aliar processos que sejam menos perigosos ao ser vivo e ao meio ambiente e promover a produção de materiais que atendam as necessidades das gerações atuais e futuras, sem um grande impacto no meio ambiente, torna-se um desafio cada vez maior para a ciência dos materiais, já que com o passar dos anos o homem tem comprometido não só seu desenvolvimento presente, mas principalmente das gerações futuras que encontram um ambiente pouco promissor para as práticas sociais e de trabalho, com diminuição e impactos constantes nos recursos naturais, como a água, assim como um acúmulo cada vez maior de resíduos no ambiente [1,6].

Nesse enfoque, os produtos químicos devem ser em sua grande maioria biodegradáveis para que não persistam no meio ambiente. Substâncias químicas e processos devem ser capazes de minimizar os riscos potenciais de produtos químicos como derramamentos, explosões e incêndios [1,4]. O uso de derivados desnecessários devem ser evitados para reduzir o desperdício químico que pode ser gerado. Assim como a preferência pelo uso de matérias primas provenientes de fontes renováveis no lugar de materiais provenientes de fontes não renováveis [1,4].

Logo, o objetivo do projeto deve ser a durabilidade direcionada ao produto e não a imortalidade. Atender às necessidades e minimizar o excesso deve ser considerado como uma prioridade no design e produtos multicomponentes devem ser projetados para minimizar os impactos causados durante o processamento [7]. A integração e a interconectividade com os fluxos disponíveis de energia e material devem ser projetados de forma a diminuirem os impactos causados no meio ambiente. Assim como a escolha de rotas químicas mais sustentáveis com uso racionado de materiais que impactem o meio ambiente devem ser escolhidas [7].

Nesse sentido, uso de materiais como os biopolímeros é cientificamente e industrialmente atraente, pois estão disponíveis em grandes quantidades, apresentam grande potencial para uso em razão do seu baixo custo, representando recursos praticamente inexplorados, amplamente disponíveis e ambientalmente amigáveis, já que muitos são de origem natural e biodegradável [8-11].

## 2.2 Biopolímeros

Os biopolímeros, também conhecidos como bioplásticos, começaram a ter seu uso industrial há muitos anos atrás, no entanto sua participação ainda é mínima no mercado internacional, mesmo apresentando vantagens de aplicações [12]. No Brasil, o seu desenvolvimento se iniciou na década de 90 com a cana de açúcar, por meio de uma parceria do Instituto de Pesquisa Tecnológica (IPT), da Copersucar e da Universidade de São Paulo (USP). Esses

estudos se iniciaram com os polímeros da família dos poli(hidroxialcanoatos) (PHA), os quais são produzidos por bactérias em biorreatores a partir de açúcares [13].

Esses biopolímeros são classificados estruturalmente como polissacarídeos, poliésteres ou poliamidas. A sua manufatura é possível por meio de uma fonte de carbono renovável, geralmente carboidratos derivados de plantios comerciais de larga escala ou de óleos vegetais, ou provenientes das paredes celulares de fungos ou casca de crustáceos [14]. Essas fontes renováveis possuem um ciclo de vida mais curto comparado com as fontes fósseis, como o petróleo que leva milhares de anos para se formar, levando ao crescente interesse no uso dos biopolímeros, em razão de alguns fatores ambientais e sócio econômicos, pois reduzem os grandes impactos ambientais causados pelos processos de extração e refino utilizados para produção dos polímeros provenientes do petróleo [15].

Uma vantagem do uso desses materiais é que grande parte deles apresentam uma degradação mais sustentável, pois são biodegradáveis [16]. Os principais polímeros biodegradáveis de base biológica incluem polihidroxialcanoatos, polihidroxibutirato (PHB) e copolímeros afins, como o ácido poliláctico (PLA), a celulose regenerada e polímeros à base de amido. O consumo desses materiais tem crescido cada vez mais, principalmente na América do Norte (2º maior produtor) e na Europa Ocidental (1º maior produtor), sendo os mais consumidos o ácido poliláctico (PLA) e o amido, com 41 % e 38 % de consumo, respectivamente [17].

Polímeros de origem natural e biodegradáveis de grande interesse atual estão presentes na classe dos polissacarídeos. Os polissacarídeos são os carboidratos mais abundantes presentes na natureza desempenhando diversas funções, entre elas fornecimento de energia, pois liberam grandes quantidades de calorias [18].

### 2.2.1 Polissacarídeos

Os polissacarídeos são polímeros naturais e biodegradáveis com cadeias de dez a milhares de monossacarídeos unidos por ligações glicosídicas (Figura 2.1). Apresentam grupamentos químicos que lhes possibilitam diversas modificações químicas. Assim como apresentam

biocompatibilidade e a possibilidade de interação com diversos meios, como o biológico e a água [19-22].

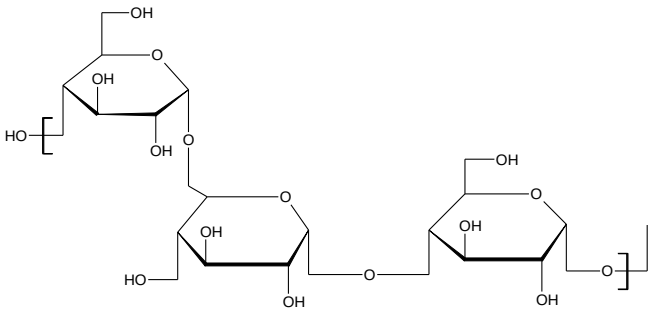


Figura 2. 1. Estrutura de um polissacarídeo com as ligações glicosídicas
Fonte: Adaptado de Kaplan (1998) [23]

Os benefícios de utilizar esses polissacarídeos em diversas aplicações são enormes, pois são polímeros ambientalmente amigáveis, provenientes de fontes renováveis, apresentam biodegradabilidade, propriedades reológicas interessantes, podem apresentar interações intermoleculares de maneiras diferenciadas, a depender da classe, implicando nas mais diversas aplicações em ciências dos materiais, são biocompatíveis, além de comporem a composição alimentar essencial da maioria dos seres vivos [18,23-25].

O primeiro polissacarídeo foi descoberto em fungos comestíveis durante estudo relativo ao seu valor nutricional em 1811, posteriormente denominado quitina. A presença de grupos funcionais como hidroxilas, aminas, acetamida, carboxílicos e sulfatos proporcionam a esse grupo características interessantes como biocompatibilidade, atoxicidade, hidrofilicidade e multifuncionalidade [21]. Esses polissacarídeos podem ser classificados quanto à função como estruturais (celulose e quitina) ou de reserva (amido). Os estruturais são compostos de polímeros lineares, arranjados na forma de fibras constituindo paredes de plantas, animais, insetos e vegetais. Já os de reserva são cadeias mais complexas que ao serem degradadas fornecem energia [26].

Um dos polissacarídeos mais abundantes no Planeta é a celulose. Ela compõe a estrutura de plantas, alguns animais marinhos, algas e líquens. Estima-se que sua produção no mundo seja

superior a $10^{12}$ toneladas sendo considerada uma fonte quase inesgotável de matéria prima no ecossistema [27]. A celulose é composta de uma unidade elementar denominada anidro – *D* – glicose, sendo que os monômeros da glicose são esterificados por ligações do tipo ß - (1,4) – glicosídicas permitindo a celulose um arranjo linear devido à configuração do carbono anomérico (Figura 2.2). Esse arranjo linear resulta numa distribuição uniforme das hidroxilas na cadeia levando a constituições de fortes interações de hidrogênio, proporcionando um arranjo cristalino na celulose o que a torna um polímero com certa rigidez e hidrofilicidade [28,29].

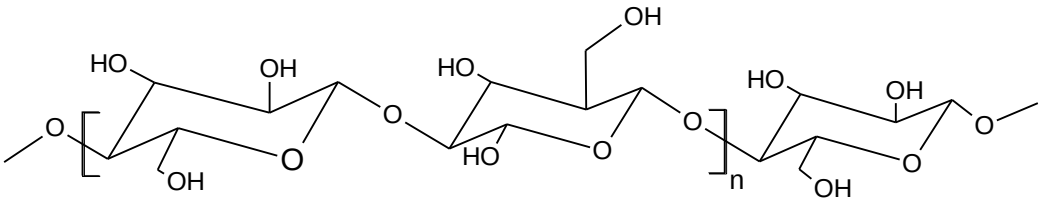


Figura 2. 2. Estrutura da celulose
Fonte: Adaptado de Taipina (2012) [29]

A celulose vem sendo estudada há mais de 70 anos e mesmo nos dias de hoje a sua aplicabilidade e modificação tem ampla divulgação no meio científico. Vários estudos como o de Innerlohinger, et al. (2006) [30] e Wang, et al. (2013) [31], envolvendo a produção de aerogéis mostraram resultados interessantes em relação a porosidade e outras propriedades. Além de trabalhos como produção de nanocristais de celulose [32,33], ou a produção de celulose através dos mais diferentes tipos de fungos para diferentes aplicações [34], produção de nanofibras, aplicações de celuloses e modificações de celuloses em tratamento de água e adsorção [35-37].

No entanto, outros polissacarídeos são estudados além da celulose, como o amido ou a quitina [37-39]. Assim como modificações desses mesmos polissacarídeos, como a carboximetilcelulose [19,40], a quitosana [41,42], a carboximetilquitosana [42], a trimetilquitosana [43], entre outros. No caso do amido, a sua vantagem é que ele faz parte da principal reserva alimentar de plantas, sendo comercialmente derivado de grãos e tubérculos. Ele é composto de uma mistura de dois polissacárideos (glucanos), a amilose (menor

composição) e a amilopectina (maior composição). Muitas das propriedades químicas e físicas do amido dependem da sua natureza granular [39].

Além do amido, nos últimos anos um grande número de polissacarídeos vem sendo estudado. As xiloglucanas, encontradas na parede celular de plantas que possuem um esqueleto celulósico (1→4) – ß – *D* - glicopirano agregado a resíduos α – *D* - xilopiranose no carbono 6, ligadas por meio de ligações de hidrogênio às fibras de celulose na parede celular, é outro representante desse grupo. Esse polissacarídeo é de extrema importância para o não rompimento das células durante a pressão osmótica [44], sendo muito utilizada como aditivo na indústria de papel celulósico, pois a sua inserção nas fibras de celulose durante a produção de papel torna a superfície mais fina proporcionando maior resistência ao papel [45].

Outro polissacarídeo presente em grande abundância é a quitina, considerado o segundo mais abundante desse grupo por alguns autores na literatura. A quitina compõe a estrutura de exoesqueletos de crustáceos, fungos e paredes celulares [46]. Além disso, por meio da desproteinização, desmineralização, descoloração e desacetilação alcalina de estruturas contendo quitina é possível obter a quitosana (Figura 2.3), um biopolímero biodegradável de grande interesse atual [47].

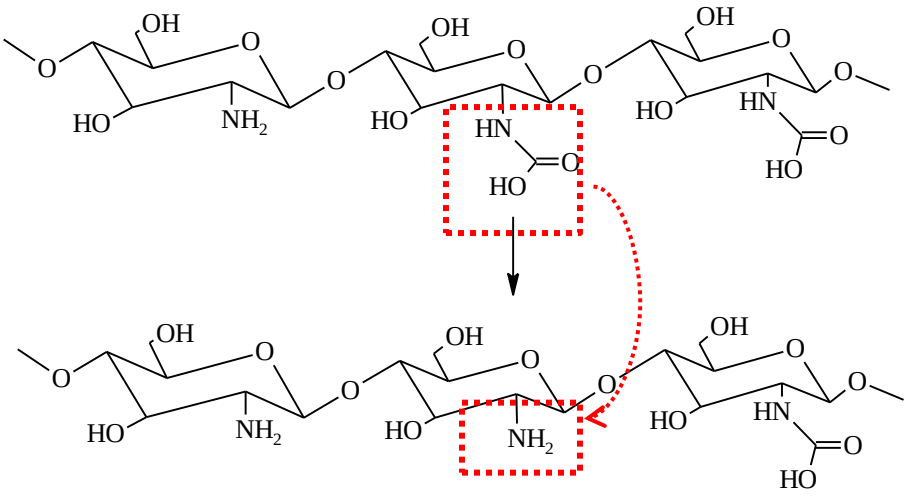


Figura 2. 3. Representação esquemática da desacetilação da quitina para obtenção da quitosana, destacando os grupamentos aminas livres

Fonte: Adaptado de Pires (2010) [48]

### 3.2.1.1 Quitosana e Quitosana tiolizada

A quitosana é obtida pela *N*-desacetilação da quitina sendo considerada um copolímero composto por unidades estruturais de 2 – amino – 2 – desoxi – *D* – glicopiranose (*GlcN*) e 2 – acetamido – 2 – desoxi – *D* – glicopiranose (*GlcNAc*) unidos por ligações glicosídicas do tipo β (1→4), mas com a unidade glicosamina (*GlcN*) sempre em maior proporção (Figura 2.4) [49].

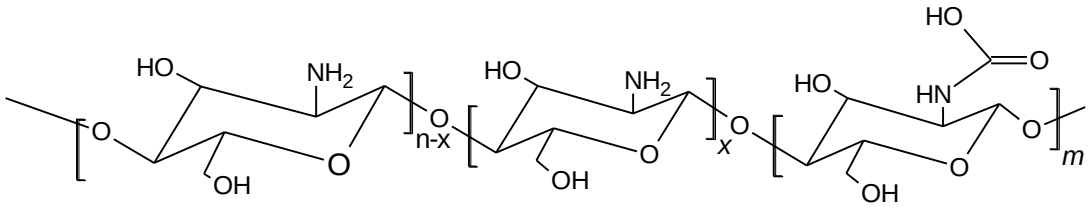


Figura 2. 4. Estrutura química da quitosana
Fonte: Adaptado de Gonçalves, et al. (2011)

A escolha da fonte da quitina e o seu processo de isolamento afetam a qualidade e as propriedades físico-químicas da quitosana significativamente [50]. A maior parte da quitosana disponível comercialmente é produzida a partir da desacetilação da quitina retirada de cascas de camarão em condições alcalinas, a altas temperaturas e por longos períodos de tempo [51]. No entanto, o fornecimento das matérias-primas é variável lote a lote, sazonal, sendo o processo laborioso e dispendioso [52].

A formação da quitosana é determinada pelo grau de desacetilação (GD), que está associada à porcentagem de grupamentos aminos livres, permitindo a distinção entre a quitina e a quitosana [53,54]. Quando o GD alcança valores maiores que 50 %, a quitina se torna solúvel em meio aquoso ácido sendo então denominada de quitosana [53]. O processo de desacetilação alcalina de ligações *N* - acetil presentes na quitina, resultando na formação de *D* - glucosamina, que contém um grupo amina livre, proporciona à quitosana um relativo caráter hidrofílico [48].

O GD da quitosana pode ser determinado por diversas técnicas como análise elementar, titulação potenciométrica [55], espectroscopia no ultravioleta visível (UV vis) [56], espectroscopia no infravermelho (FTIR) [57] e pela ressonância magnética nuclear [42]. A escolha da técnica depende do processo de purificação, da solubilidade da amostra e da disponibilidade de equipamento.

Nahalka, et al. (1998) [57] relata que o GD da quitosana está relacionado à quantidade de grupos amidos acetilados, podendo dessa forma ser utilizada a espectroscopia no infravermelho para detecção do seu valor. Nesse caso, usa-se a razão das absorbâncias (A) definindo o *baseline* e realizando os cálculos conforme colocado na Equação (2.1).

$$A_{1320}/A_{1420} = 0{,}3822 + 0{,}03133(100 - GD) \qquad (2.1)$$

Onde:

$A_{1320}$ é a absorbância (relacionada a altura) centrada próximo a banda 1320 $cm^{-1}$ é a banda da amida III.

$A_{1420}$ é a absorbância (relacionada a altura) centrada próximo a banda 1420 $cm^{-1}$ referente a banda da deformação anti-assimétrica do grupo $CH_3$.

O grau de desacetilação e a massa molar da quitosana influenciam na maioria de suas propriedades, tais como solubilidade em água, comportamento mecânico, transparência óptica, biodegradabilidade, estabilidade química, entre outras [41-43]. A espectroscopia no infravermelho é muito valiosa na caracterização química da quitosana e seus derivados, pois além de ser possível a obtenção do GD ela analisa as emissões de energia devido à ação de um campo eletromagnético, ocorrendo assim transferência de energia entre o campo e a molécula sendo possível determinar as ligações químicas presentes na cadeia [58]. A Tabela 2.1 mostra as bandas relativas aos grupos químicos associados à estrutura química da quitosana e a Figura 2.5 mostra um espectro da quitosana.

Tabela 2. 1. Números de onda e grupos químicos característicos da quitosana [42,43,54,57].

| **Bandas ($cm^{-1}$)** | **Grupo Químico** | **Bandas ($cm^{-1}$)** | **Grupo Químico** |
|---|---|---|---|
| 3570 – 3200<br>3450 | ν OH | 1340 – 1250<br>1380 | δ C-N (Amida III) |
| 2955 – 2845<br>2922 | ν CH (assimétrico) | 1321 | ν CN (Amida III) |
| 2878 | ν CH (simétrico) | 1260 | ν CN (Amida II) |
| 1550 – 1500<br>1590 - 1500 | ν $NH_3^+$ (simétrico)<br>$NH_2$ e Amida II | 1150 e 896 | ν C-O-C |
| 1640 – 1600<br>1650 | ν $NH_3^+$ (anti-simétrico)<br>-C=O (Amida I) | 1090 – 1075<br>1060 – 1020 | ν -C-O (C3-OH álcool secundário)<br>ν -C-O (C6-OH álcool primário) |
| 1640 – 1690 | ν C=N (fraco) (Base de Schiff) | 1300 – 1000<br>1070 | ν C-O (cíclico) |
| 1570-1515<br>1560 | δ N-H (II) | 1030 | ν C-O (cíclico) |
| 1465<br>1420 | δ OH deformação antisimétrica $CH_3$ | 897 | ν C-O |

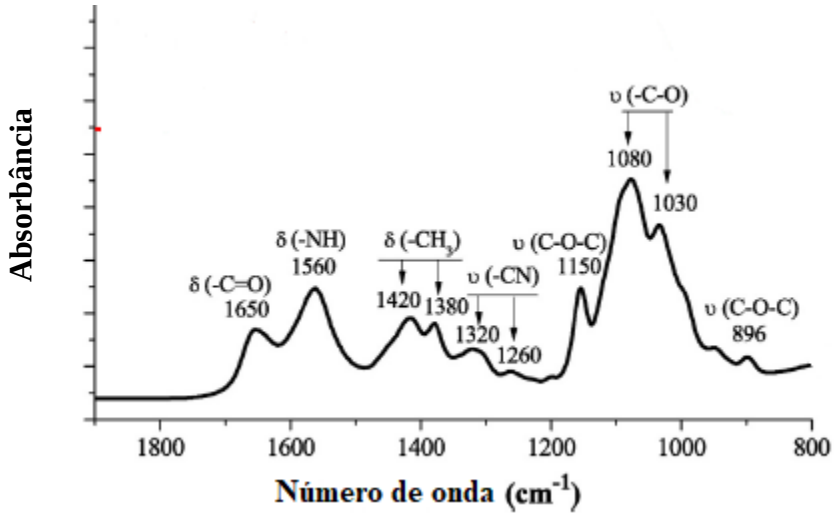


Figura 2. 5. Espectro no infravermelho da quitosana na faixa de 800 a 1800 $cm^{-1}$
Fonte: Adaptado de Medeiros Borsagli, et al. (2015) [42]

Outra ferramenta que pode ser aliada ao FTIR é a espectroscopia Raman. O efeito Raman consiste do espalhamento inelástico de luz. Um fóton incidente perde ou ganha energia no processo de espalhamento com o material, tendo o fóton espalhado energia inferior ou superior à energia do fóton incidente. As diferenças de energia entre a luz incidente e a espalhada estão relacionadas às diversas propriedades vibracionais de cada material [59].

Uma das características mais importantes dessa técnica é a identificação de grupos químicos característicos nas quais muitas moléculas estão envolvidas, além da obtenção de uma ampla faixa de número de onda ($cm^{-1}$), o que muitas vezes é inviável por espectroscopia no infravermelho [59]. Além disso, a espectroscopia no Raman permite a observação de bandas, como por exemplo o grupo tiol (-SH) e ligações dissulfídicas (S-S), que são pouco ou nada perceptíveis pela espectroscopia no infravermelho [20].

Várias outras técnicas como MEV, micro-CT, espalhamento dinâmico da luz (DLS) [60], entre outras, são utilizadas para caracterizar a quitosana, seja ela obtida comercialmente ou produzida em laboratório a partir da quitina extraída, em geral de crustáceos. Além dessas técnicas, o potencial zeta (PZ) é uma técnica bastante interessante, pois permite determinar a solubilidade e mecanismos iônicos envolvidos na cadeia da quitosana em diferentes pH, já

que é possível estimar a carga de superfícies, sendo possível predizer sobre a estabilidade da suspensão [61] (Figura 2.6).

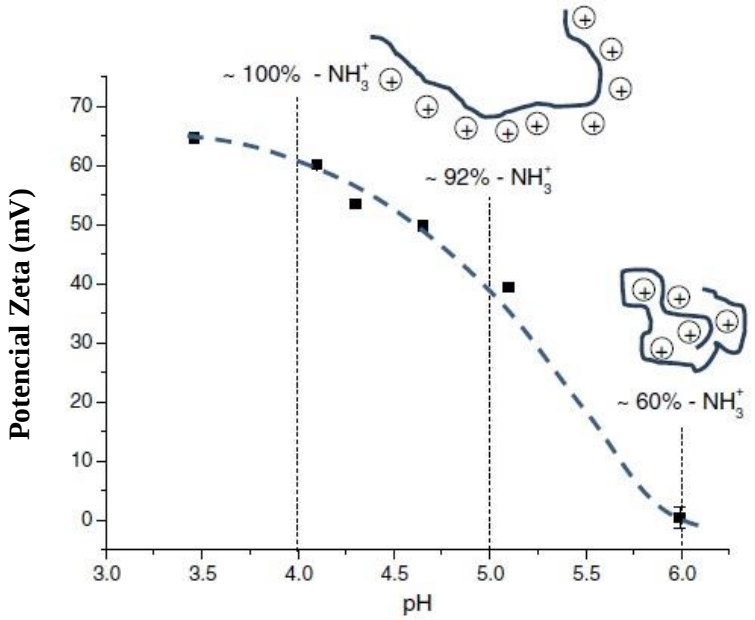


Figura 2. 6. Potencial zeta da quitosana em diferentes pH mostrando a extensão da protonação das aminas

Fonte: Ramanery, et al. (2013) [41].

O valor do pKa, associado a dissociação da quitosana em água, é o fator determinante em relação ao mecanismo de captação iônica. Sorlier, et al. (2001) [62] revelou que o valor do pKa está diretamente ligado ao GD da quitosana, sendo que para a completa dissociação iônica o seu valor deve estar entre 6,3 e 7,2. O valor do *Ka* pode ser determinado pela Equação (2.2). Esse valor de pKa é dependente do pH da solução, em meios neutros (pH ≈ 7,0) cerca de 50 % dos grupamentos aminas encontram-se desprotonados (-$NH_2$) [63].

$$Ka = \{[QUI - NH_2][H_3O^+]/[QUI - NH_3^+]\} \quad (2.2)$$

Alguns autores na literatura [41,42] propuseram por meio da espectroscopia no ultravioleta visível, potencial zeta e espectroscopia no infravermelho os mecanismos químicos envolvido no processo de solubilização em água da quitosana definidas nas Equações (2.3) e (2.4) descritas a seguir.

$$QUI - NH_2 + H^+(aq) \rightarrow QUI - NH_3^+ \quad (2.3)$$

$$QUI - NH_3^+ + OH^-(aq) \rightarrow QUI - NH_2 + H_2O \quad (2.4)$$

Segundo esses autores [41,42], o intervalo de solubilidade da quitosana e derivados pode ser explicado com base no equilíbrio global de cargas negativas e positivas na cadeia polimérica. Sob condições ácidas (pH < pKa ≈ 6,5), o grupamento da amina na quitosana é protonado em graus diferentes (Equação 2.3). Esses grupos aminas protonados ($NH_3^+$) repelem-se uns aos outros, favorecendo a interação da quitosana com a água, superando o modelo associativo de ligações de hidrogênio e interações hidrofóbicas entre as correntes. Em meios moderadamente ácidos a neutros, o número de espécies -$NH_3^+$ diminui resultando em uma atração da cadeia acabando por diminuir a solubilidade da quitosana em água (Equação 2.4).

Em razão das diversas características presentes na quitosana, suas aplicações são as mais diversas. As suas propriedades únicas a tornam uma classe de materiais bastante interessante [67,65]. Devido ao caráter hidrofílico proporcionado pela presença dos grupos aminas e hidroxilas livres, a quitosana apresenta uma grande capacidade de adsorção, assim como uma boa compatibilidade com o meio fisiológico [42,54].

Contudo, devido a sua limitação em relação à atuação em pH maiores que 6,5, muitas modificações são propostas para melhorar sua aplicabilidade [64-66]. Portanto, a modificação química da quitosana fornece um meio poderoso para promover novas atividades biológicas e propriedades específicas. A versatilidade da funcionalização da quitosana é essencialmente devida à presença de grupos amino primários na macromolécula. Esses grupos são reativos e fornecem um mecanismo para a fixação de grupos laterais usando uma variedade de condições de reações [66].

Além disso, pela seleção adequada da natureza do grupo lateral a ser anexado às cadeias poliméricas, as propriedades físico-químicas e biológicas podem ser ajustadas para fornecer funcionalidades específicas [67-69]. Com base nesta abordagem, uma gama de grupos (por exemplo, carboxilatos, acilas, alquilas, tióis, amino quaternários, etc.) foram inseridos em

quitosana fornecendo características adicionais, tais como melhor solubilidade em água, características aniônicas ou catiônicas, atividades antibacterianas, comportamento anfifílico e outras características [43,68,69].

Uma estratégia inovadora para a modificação da quitosana está associada à introdução de unidades de aminoácidos (isto é, unidades monoméricas de proteínas) com características ácidas, básicas ou hidrofóbicas, na estrutura da cadeia polimérica. Essa estratégia tem sido usada para modificar e melhorar as propriedades físico-químicas da quitosana, como solubilidade e mucoaderência, e dá origem a algumas características sinérgicas interessantes para uso em engenharia de tecidos, bem como outras propriedades biomédicas potencialmente úteis, incluindo anticoagulante, antibacteriana, atividades de colesterol [70,71]. As reações de conjugação de aminoácidos com quitosana foram conduzidas principalmente nos grupos amino livres da cadeia, em geral formando ligações amida covalentes com uso de agentes de reticulação como os *zero crosslinkers* EDC e sulfo-NHS [71] os quais apenas ativam o processo sem incorporarem a cadeia (Figura 2.7).

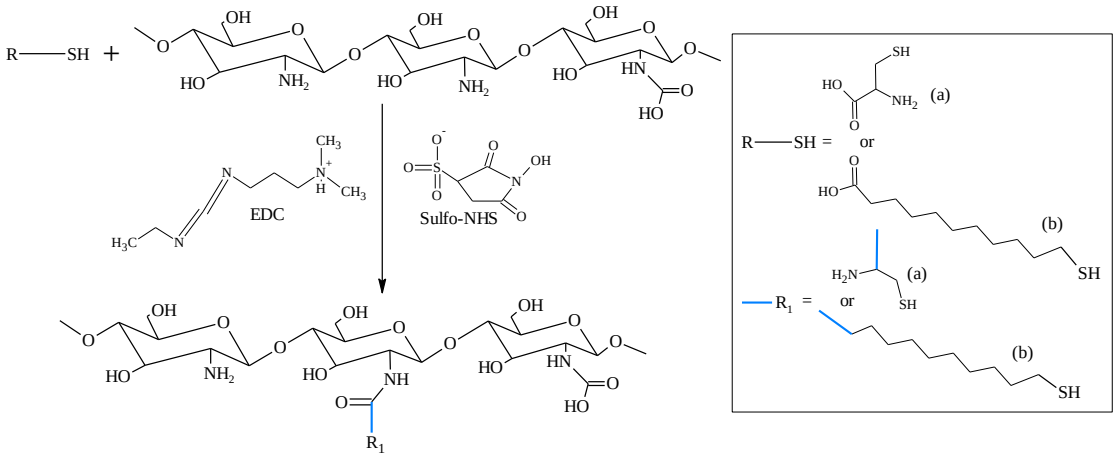


Figura 2. 7. Representação esquemática da modificação da quitosana com incorporação de cadeias contendo o tiol com o uso dos *zero crosslinkers*.
Fonte: Medeiros Borsagli, et al. (2018) [20]

Um fenômeno interessante resultante da funcionalização da quitosana com aminoácidos é a introdução de grupos carboxílicos e grupos amino adicionais, que, em combinação, aumentam a solubilidade em água da quitosana em valores de pH neutros e alcalinos. Esta

característica é altamente desejável considerando a limitada solubilidade da quitosana, o que pode comprometer sua aplicação em várias áreas biomédicas [71].

Nesse enfoque, a incorporação de cadeias que apresentem o grupo tiol é bastante promissora, pois esse grupo possibilita uma melhor adesão das células [71], a possibilidade de atividade antibacteriana [72] e formação de matrizes tridimensionais, hidrogéis [73]. Os tiomeros (ou polímeros tiolizados) são produzidos pela imobilização de cadeias contendo o grupo tiol (-SH) no esqueleto do polímero, o que resulta numa melhora significativa na mucoadesão [74]. A quitosana tiolizada tem características predominantes, como a estabilidade química melhorada com base nas ligações covalentes formadoras de dissulfeto, e a interação seletiva com várias substâncias [67,75]. Além disso, a quitosana tiolizada tem um alto nível de propriedades coesivas, mucoadesivas, inibidoras da enzima e que melhoram a permeação [75]. Assim, há um vasto campo a ser explorado com base na combinação de funcionalidades químicas com o esqueleto da quitosana produzindo uma nova classe de quitosanas tiolizadas como *N*-acetilcisteína-quitosana e *N*-acetil-quitosana para inúmeras aplicações [75].

A imobilização de grupos tiol para formar derivados de quitosana (isto é, quitosana tiolizadas) pode promover e melhorar numerosas propriedades biológicas e bioquímicas devido à formação de ligações dissulfidicas com subdomínios ricos em cisteína comumente encontradas em sistemas biológicos (por exemplo, células e tecidos) [75-78]. Curiosamente, embora haja um interesse crescente nos últimos anos no desenvolvimento de polímeros tiolizados e derivados de quitosana para diversas aplicações, como transportadores de liberação de fármacos, transfecção de nucleotídeos para terapia gênica, atividades mucoadesivas e antibacterianas, adsorção e tratamento de água, não havia na literatura publicada nenhum relato em relação a investigação de estruturas tridimensionais produzidas a partir de quitosanas tiolizadas para aplicações em reparo de tecidos moles e na adsorção de pigmentos.

Além disso, o efeito das quitosanas tiolizadas em microrganismos, incluindo atividade antibacteriana, apresenta um grande *gap* [72,79-82], pois os autores relacionam o efeito antibacteriano com a lipofilicidade da quitosana modificada, adquirida com a incorporação

de substituintes mercapto, os quais apresentam o grupo tiol, no entanto, esta hipótese não foi confirmada pelos resultados experimentais [72]. Assim como, relatam o aumento da atividade antimicrobiana para cadeias alquílicas mais longas [79], enquanto outros afirmaram a tendência oposta [80].

De fato, existe um vasto campo a ser explorado com base na combinação de funcionalidades químicas com o esqueleto da quitosana produzindo uma nova classe de polímeros de quitosana tiolizadas tais como quitosanas modificadas com aminoácido (cistéina) e com grupos mercaptos (ácido mercaptoundodecanóico) para numerosas aplicações. Um material ideal combinará todas as características mencionadas da quitosana e dos tiomeros em um único projeto, para abordar os diferentes aspectos de um processo dinâmico de adsorção, reparo tecidual e atividade antibacteriana.

### 3.3 Engenharia de Tecido e a regeneração de tecido

A expectativa de vida aumentou muito ao longo dos anos o que levou ao ser humano apresentar uma estrutura física mais sobrecarregada. Embora muitos dos fatores responsáveis pelo envelhecimento não serem completamente compreendidos, as consequências são muito claras. Articulações passam a apresentar sérios problemas como artroses, ou os ossos se tornam frágeis e quebram. A capacidade da visão e da audição são perdidas ou diminuem. O sistema circulatório mostra sinais de aterosclerose e o coração perde o controle do seu ritmo de batimento vital ou suas válvulas se tornam danificadas [83]. E diversos outros processos tornam-se cada vez mais presentes. Como consequência dessas causas, naturais ou não, de deterioração do corpo humano, é que entre dois e três milhões de dispositivos artificiais e próteses são implantadas em indivíduos nos Estados Unidos a cada ano [83].

Órgãos de saúde nos Estados Unidos colocam que os gastos com saúde estão acima de 2,5 trilhão de dólares somente nesse país [84]. Danos e doenças relacionadas ao sistema esquelético representam uma parcela significante desse custo. Nesse sentido, a engenharia de tecidos tem evoluído como um campo excitante e multidisciplinar de pesquisa com o objetivo de recriar e restaurar tecidos doentes ou danificados [85]. E, a indústria de biomateriais

seguiu esse mesmo caminho crescendo muito nas últimas décadas, sendo esperada uma taxa de crescimento anual de 15 % para os próximos anos [86,87].

Alguns tecidos não são capazes de recuperar grandes lesões teciduais, ainda que sejam capazes de se regenerar. Além disso, a capacidade de regeneração de tecidos é substancialmente reduzida com o envelhecimento [85]. A reconstrução cirúrgica, ainda que seja uma solução muito utilizada, é incapaz de reparar plenamente tecidos e órgãos perdidos, muitas vezes devido à indisponibilidade de doadores [86]. Biomateriais inteligentes são biodegradáveis e participam ativamente do processo de regeneração de tecidos danificados, estimulando respostas celulares específicas em nível molecular [67,86]. Para atender a esses requisitos, modelos de matrizes tridimensionais podem ser projetados em nível macro, micro e nanoestruturais [86]. Esses materiais podem ser combinados e ajustados às condições *in vivo* de infinitas formas, modificando suas propriedades tridimensionais e sua composição para criar matrizes porosas degradáveis para o reparo do tecido em questão [86] (Figura 2.8).

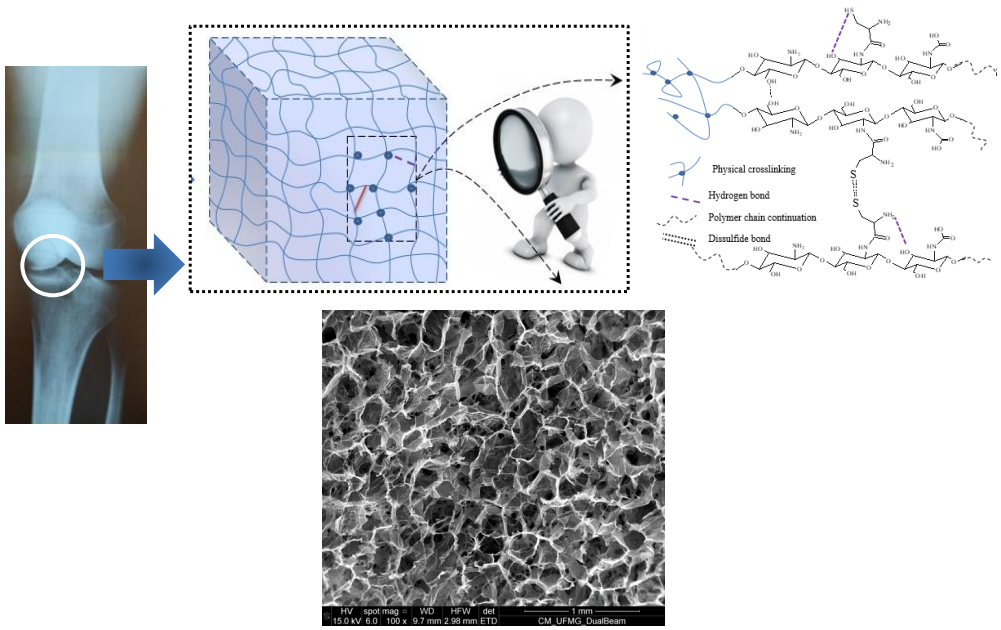


Figura 2. 8. Ilustração da estrutura porosa de biomateriais para aplicação em cartilagem óssea.

Fonte: Medeiros Borsagli, et al. (2018) [20]

Além disso, a adesão celular nos biomateriais é um pré-requisito crucial para a reparação e regeneração tecidual, e neste caso a morfologia e estrutura da superfície dos biomateriais são consideradas características chaves que afetam a capacidade das células de aderirem. Assim, é muito importante entender a morfologia da estrutura, em particular a porosidade, porque esse parâmetro afeta fortemente o desempenho mecânico e biológico das estruturas desenvolvidas [20,67,88]. Foi demonstrado pela literatura que o tamanho ideal de poro para a atividade de células de osteoblastos em estruturas de engenharia de tecidos, por exemplo, ainda é controverso, pois houve relatos conflitantes [89,90]. Akay et al. (2011) [89] mostrou que os osteoblastos preenchiam poros menores (40 µm) quando eles foram cultivados em estruturas com diferentes tamanhos de poros, mas maiores tamanhos de poros (100 µm) facilitaram a migração celular. No entanto, os diferentes tamanhos de poros não tiveram nenhum efeito sobre a extensão da mineralização ou profundidade de penetração celular [89]. Outros autores mostraram que tamanho de poros entre 50 a 200 µm era capaz de promover a diferenciação celular e infiltração de por exemplo de fibroblastos dérmicos [91], ou ainda que tamanhos de poros maiores de aproximadamente 160 a 270 µm eram importantes para facilitar a angiogênese em toda a estrutura, assim como a vascularização das estruturas requer poros maiores que 300 µm [89,92].

Dentro dessa perspectiva, cirurgiões ortopédicos e pesquisadores em todo o mundo enfrentam continuamente o desafio de regenerar os defeitos da cartilagem articular. O corpo humano tem uma capacidade restrita de auto-regenerar adequadamente a maioria de seus principais tecidos se a integridade original do tecido tiver sido seriamente prejudicada por causa de distúrbios médicos envolvendo uma carga cada vez maior de trauma, anormalidades congênitas e doenças degenerativas [93]. Embora o campo da engenharia de tecidos tenha progredido desde o artigo publicado na revista Science em 1993 por Langer e Vacanti (1993) [94], que listou as principais estratégias para o desenvolvimento de biomateriais, incluindo matrizes de construção para células a serem semeadas, ainda não é possível imitar inteiramente as propriedades físico-químicas, bioquímicas e biológicas da cartilagem articular usando tecnologia disponível e estratégias de desenvolvimento [95]. Portanto, o desenvolvimento de biomateriais miméticos com propriedades específicas relevantes para a cartilagem articular está associada a produção de materiais inteligentes, funcionais e

inovadores para potencial aplicação clínica [20]. Essencialmente, a cartilagem articular é um tecido conjuntivo composto por uma matriz extracelular (MEC) contendo colágeno, glicosaminoglicano (CGA) e água.

Devido à sua complexidade, a engenharia de um substituto de tecido requer uma combinação de vários campos de pesquisa com uma abordagem multidisciplinar, como a ciência dos materiais, química de materiais, bioquímica, biologia molecular e engenharia biomédica [96-101]. Dessa forma, a seleção de biomateriais é crucial para o sucesso do candidato a potenciais aplicações de reparo de tecidos e outros processos regenerativos, uma vez que uma grande variedade de materiais naturais e sintéticos com propriedades biológicas e físico-químicas distintas foi desenvolvida nos últimos anos [102].

### 3.4 Processos de Adsorção

A água é um dos mais importantes elementos naturais compondo de maneira essencial a vida animal e vegetal, assim como possuí um papel fundamental na manutenção das propriedades do funcionamento equilibrado do ecossistema. No entanto, ainda há algumas partes do mundo onde não se encontra água limpa disponível e, embora se saiba do seu desempenho e importância na manutenção da vida, ela vem se deteriorando de forma exponencial devido à contaminação proporcionada pelas ações antrópicas [6,103]. Essa contaminação, recentemente tem trazido à tona uma preocupação cada vez mais crescente na sociedade em razão da possibilidade de esgotamento de tal recurso, pois além de mudanças climáticas mais intensas e constantes ocorrendo, o crescente desmatamento e despejo de resíduos de todos os tipos na água pelas indústrias e agricultura tem proporcionado uma redução no nível de água potável do Planeta [42,104].

Várias técnicas são utilizadas para a remoção de materiais nos meios aquosos, o que as diferencia são as aplicações, custos, seletividade e manutenção [105]. Atualmente, vários processos têm sido desenvolvidos com o intuito de melhorar o processo de remoção de materiais e proporcionar melhor seletividade na remoção. No entanto, alguns desses métodos podem ser ineficazes para a remoção de vestígios de grandes volumes de águas residuais e

apresentam deficiências, como altos custos de manutenção, geração de lama tóxica e procedimentos complicados envolvidos no tratamento [106-108]. Por esse motivo, é necessário um processo seletivo de tratamento para a captura/imobilização de materiais específicos, além da reutilização de resíduos.

Nesse sentido, um processo bastante usado é a adsorção. Esse processo tem como vantagem sobre as demais técnicas o fato de utilizar equipamentos comercialmente acessíveis, ter baixa geração de resíduos, ser possível a recuperação dos materiais, além da possibilidade de reutilização do adsorvente e, dependendo do material adsorvente que é utilizado no processo, pode-se tornar um método de custo competitivo para o tratamento de efluentes industrialmente [104,109].

A adsorção é um processo de separação no qual certos componentes de uma fase são transferidos para a superfície de um sólido adsorvente [110]. O material aderido denomina-se adsorvato e a superfície sólida onde ele é aderido é o adsorvente [111]. Há sistemas onde o processo de adsorção é acompanhado da absorção, ocorrendo a penetração de fluido na fase sólida, sendo mais apropriado o uso do termo sorção, que abrange os dois processos [112]. A adsorção ocorre principalmente nas paredes dos poros ou em sítios específicos dentro da partícula podendo envolver processos físicos e/ou químicos [113].

Essa adsorção é uma operação de transferência de massa, na qual se estuda a habilidade de certos sólidos em concentrar na sua superfície determinadas substâncias existentes em fluidos líquidos ou gasosos, possibilitando a separação dos componentes desses fluidos. Uma vez que os componentes adsorvidos, concentram-se sobre a superfície externa, quanto maior for esta superfície externa por unidade de massa sólida, tanto mais favorável será a adsorção [113]. Por isso, geralmente os adsorventes são sólidos com porosidade. O adsorvente consegue reter de maneira seletiva uma ou mais das espécies contidas inicialmente no fluido, e essa seletividade irá depender da natureza da superfície do adsorvente e do poder de interação com as moléculas adsorvidas [114]. O processo de adsorção pode ocorrer nas interfaces líquido-gás, líquido-líquido, sólido-gás e sólido-líquido. O contato entre as fases ocorre devido às interações entre elas.

A adsorção está baseada em três mecanismos distintos, o mecanismo estérico, os mecanismos de equilíbrio e os mecanismos cinéticos. No caso do mecanismo estérico, os poros do material adsorvente possuem dimensões características, as quais permitem que determinadas moléculas possam entrar, excluindo as demais. Já os mecanismos de equilíbrio, os diferentes sólidos possuem habilidades para acomodar diferentes espécies de adsorvatos, que são adsorvidos, preferencialmente, a outros compostos. E, por último, o mecanismo cinético está baseado nas diferentes difusividades das diversas espécies nos poros adsorventes [115].

A natureza das forças envolvidas no processo de adsorção a classificam quanto a sua intensidade em dois tipos, adsorção física e adsorção química. Na primeira, conhecida como fisissorção, a ligação do adsorvato à superfície do adsorvente envolve uma interação relativamente fraca que pode ser atribuída às forças de Van der Walls, que são similares às forças de coesão molecular. Já na segunda, conhecida como quimissorção, ocorre a troca ou partilha de elétrons entre as moléculas do adsorvato e a superfície do adsorvente, resultando em uma reação química. Isso resulta essencialmente numa nova ligação química e, portanto, bem mais forte que no caso da fisissorção [113,115]. Embora os conceitos de quimissorção e fisissorção sejam distintos, os dois mecanismos de adsorção não são completamente independentes. No entanto, a distinção quanto à espécie ser física ou quimicamente adsorvida não é muito clara [116], pois, muitas vezes, ambos os processos podem ser descritos em termos dos princípios da adsorção física. De uma maneira geral, as diferenças entre adsorção física e adsorção química podem ser sumarizadas como no caso da primeira, ela é inespecífica, já a adsorção química é altamente específica e nem todas as superfícies sólidas possuem sítios ativos capazes de adsorver quimicamente o adsorvato [116].

A adsorção é resultado de uma combinação entre os tipos de forças envolvidas na adsorção física e química. Nesse sentido, vários fatores influenciam o processo de adsorção como a área superficial, as propriedades do adsorvente e do adsorvato, a temperatura do sistema, natureza do solvente e o pH do meio. Logo, depende da natureza do adsorvente, do adsorvato e das condições operacionais. Algumas características do adsorvente como área superficial, tamanho do poro, densidade, grupos funcionais presentes na superfície e hidrofobicidade do material, também influem nesse processo. Por outro lado, a natureza do adsorvato depende

da polaridade, do tamanho da molécula, da solubilidade e da acidez ou basicidade. As condições operacionais incluem, principalmente, temperatura, pH e natureza do solvente [118].

Dentre os mais diversos processos de adsorção, a biossorção tem sido vista como uma solução verde em aplicações ambientais, como o tratamento de efluentes. Nesse sentido, muitas pesquisas têm focado em adsorventes biológicos ou biocompatíveis, pois apresentam grande capacidade de adsorção e estão disponíveis em abundância [119]. Na remoção de íons metálicos, por exemplo, o uso desses biossorventes para remoção não é baseada num único mecanismo, mas vários que de forma quantitativa e qualitativa são diferentes a depender do biossorvente utilizado e do metal [120].

Para melhor compreensão dos processos de adsorção, as análises e os projetos dos processos de adsorção requerem o conhecimento dos dados de equilíbrio. Esses dados permitem a compreensão dos processos físico-químicos e, assim, pode ser avaliada a aplicabilidade do processo de adsorção como uma operação unitária [117]. A quantidade da substância adsorvida por massa de adsorvente ($q_e$) (Equação 2.5) em função da concentração de adsorvato ($C_e$) em solução é a maneira de se expressar essa adsorção [121,122]. Além disso, curvas da concentração do soluto em função da fase fluida, à temperatura constante, podem ser traçadas e definir esse equilíbrio, essas curvas são denominadas isotermas de adsorção. Essas curvas mostram a relação de equilíbrio entre a concentração na fase fluida e a concentração nas partículas adsorventes em uma determinada temperatura. Portanto, diversos modelos de equilíbrio, especialmente os multicomponentes, têm sido desenvolvidos levando em conta a sua simplicidade e aplicabilidade [104,109].

$$q_e = \{(C_0 - C_e)x\ (V/m)\} \qquad (2.5)$$

Onde $C_0$ é a concentração inicial total ($mg.L^{-1}$),$C_e$ é a concentração total no equilíbrio ($mg.L^{-1}$), $V$ é o volume de solução usado, $m$ é massa de adsorvente utilizada e $q_e$ ($mg.g^{-1}$) é a capacidade de adsorção no equilíbrio expressa em relação à concentração total do adsorvato [104].

### 3.4.2 Isotermas de Adsorção

A adsorção é geralmente descrita por isotermas que demostram a quantidade de soluto que pode ser adsorvida pelo adsorvente a uma dada temperatura e tempo. A isoterma de adsorção examina a interação entre o adsorvato e o adsorvente e como a adsorção varia com a concentração do adsorvato em um dado valor de pH e de temperatura [123]. As isotermas são usadas para representar os resultados da adsorção, elas relacionam as quantidades adsorvidas por unidade de massa do adsorvente a uma temperatura constante. Sendo assim, uma isoterma de adsorção representa a relação de equilíbrio entre a quantidade de material adsorvido e a concentração (líquidos) na fase fluida a temperatura constante [123]. Estes valores são determinados experimentalmente, mas também existem modelos de prevê-los, tanto para adsorção de um único material, como para a adsorção de mais materiais [123].

Esses modelos são expressos por equações matemáticas que relacionam a concentração do adsorvato na interface à concentração do adsorvente no equilíbrio na fase líquida. Dessa forma obtém-se uma interpretação molecular do processo e, com os parâmetros obtidos compara-se o comportamento de adsorção [124]. Experimentalmente, a curva obtida determina o grau de adsorção através de uma massa conhecida de material sólido em uma solução de concentração conhecida numa dada temperatura. Quando não mais é percebida mudança significativa dessa relação estabelecida, a condição de equilíbrio é então atingida [124].

Dentre os modelos que mais se aplicam para a interface sólido-líquido, é possível citar as de Langmuir e Freundlich. O modelo de Langmuir assume que a superfície do adsorvente possuí idêntica energia e que cada molécula adsorvida encontra-se em um único site. Dessa forma, é possível prever a formação de uma monocamada do adsorvato na superfície do adsorvente [104]. Esse modelo é preferencialmente usado em estudos de adsorção em solução, onde $q_e$ e $C_e$ são a quantidade adsorvida e a concentração em solução, respectivamente, ambos em equilíbrio, $K_L$ é a constante de Langmuir e $q_m$ é a capacidade máxima de adsorção da monocamada formada no adsorvente (Tabela 2.2). No entanto, esse modelo é limitado, pois coloca que a adsorção é reversível e limitada em apenas uma camada, a superfície interna do

sólido é homogênea, as moléculas adsorvidas não interagem entre si, não existe adsorção competitiva, cada molécula é adsorvida em apenas um único sítio de adsorção e os sítios são energeticamente equivalentes. Já o modelo de Freundlich preenche a limitação da equação de Langmuir por assumir que a adsorção em um ponto da superfície do sólido adsorvente não influencia na adsorção do sítio vizinho e que cada sítio pode reter mais de uma molécula do adsorvato. Trata-se de uma equação empírica, sendo uma das isotermas mais amplamente utilizadas para a descrição de multi sitíos de adsorção, pois considera a existência de uma estrutura em multicamadas e não prevê a saturação da superfície durante a adsorção (Tabela 2.2). Trata-se de um modelo matemático introduzido como uma correlação empírica de dados experimentais. Nessa isoterma, $K_F$ e n são constantes da isoterma de Freundlich indicando a capacidade de adsorção e intensidade de adsorção, respectivamente [104]. A Tabela 2.2 mostra as principais equações relacionadas aos modelos matemáticos propostos para a adsorção.

Tabela 2. 2. Relação matemática das principais isotermas [125].

| Isoterma | Equação | Observações |
|---|---|---|
| **Freundlich** | $q_e = K_F C_e^{1/n}$ | $K_F$ e n são parâmetros empíricos, sendo que n é usualmente < 1 |
| **Langmuir** | $q_e = (K_L C_e q_m)/(1 + K_L C_e)$ | $q_{e,\,max}$ é o máximo de adsorção e |
| **BET** | $q_e = q_{e,max}\ k_b C_{eq} / (C_s - C_{eq})[1 + (k_b - 1)\left(\frac{C_{eq}}{C_s}\right)]$ | $q_{e,\,max}$ é o máximo de adsorção e $k_b$ é uma constante, $C_s$ é a concentração total no sítio saturado. Modelo válido para multicamadas numa superfície homogênea[#] |
| **Redlich-Peterson** | $q_e = kRC_{eq} / (1 + a_R C b R_{eq})$ | $k_R$ e $a_R$ são constantes, sendo o valor de $b_R$ entre 0 e 1 |
| **Temkin** | $q_e = (RT / b_T)\ ln(a_T C_{eq})$ | $R$ é a cosntante universal dos gases, $T$ é a temperatura absoluta e $a_T$ e $b_T$ são constantes |
| **Dubinin – Radushkevich** | $q_e = q_D exp^{(-BDx^2)}$ | $x = RTln\ (P/P_0)$, $q_D$ é a máxima capacidade de Dubbinin-Radushkevich para uma camada, x é o potencial de Polyani, $P$ é a pressão das espécies adsorvidas e $P_0$ é a pressão de vapor |
| **Toth** | $q_e = q_{e,max} a_t C_{eq} / (1 + (a_t C_{eq})tT)/tT$ | $a_t$ é a constante do inverso do potencial de adsorção e o expoente $tT$ caracteriza a heterogeneidade do processo de adsorção, sendo seu valor menor que 1. |
| **Langmuir – Freundlich** | $q_e = \frac{q_{mas\,1}}{b_s C_{eq\,1}} / b_s(1 + \frac{(a_s C_{eq})1}{b_s})$ | $a_s$ e $b_s$ são parâmetros da isoterma |

Alguns tipos de isotermas de adsorção comumente encontrados são apresentados na Figura 2.9. Essas isotermas podem assumir diferentes formas a depender do tipo de adsorção, das forças predominantes, das características físico-químicas do adsorvato e das propriedades do sistema. Quando a isoterma é linear, passando pela origem, a quantidade adsorvida é

proporcional à concentração do fluido. Já aquelas que apresentam a concavidade para baixo são ditas favoráveis, apresentando capacidade de remoção relativamente alta, mesmo em condições de baixa concentração de adsorvato na solução. Nesse caso, há uma diminuição da disponibilidade dos sítios de adsorção quando a concentração da solução aumenta. No entanto, quando o conteúdo adsorvido é independente da concentração do adsorvato, diz-se que a isoterma é irreversível. Já uma isoterma com a concavidade para cima é denominada desfavorável porque a quantidade adsorvida é relativamente baixa [110].

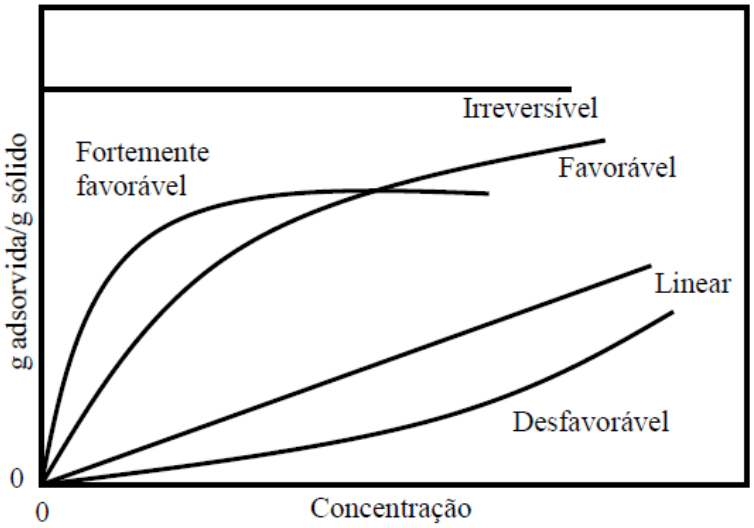


Figura 2. 9. Representação esquemática dos diferentes tipos de isoterma.
Fonte: Adaptado de Macbe, et al. (1993) [110].

### 3.4.1 Cinética de Adsorção

A cinética de adsorção é governada pelas reações de sorção e transferência de massa, as quais governam a transferência dos materiais da solução para os sítios presentes na superfície do adsorvente [123]. Essa cinética de adsorção deve ser investigada, pois os adsorventes utilizados, em sua maioria, são porosos, e a velocidade global de adsorção é limitada pela capacidade das moléculas do adsorvato se difundirem para o interior da partícula. A velocidade da adsorção pode ser afetada pela temperatura, pH, concentração inicial, agitação, tamanho das partículas, distribuição dos poros e tipo de solução [123]. No caso da quitosana

os mecanismos são dependentes da forma física da quitosana, sendo intrínseco a estrutura da mesma em relação à desacetilação, cristalinidade e massa molecular, além da natureza dos materiais e as condições de temperatura e pH [123].

Em geral os modelos de pseudo primeira ordem, pseudo segunda ordem e de difusão intra-partículas são os mais utilizados para descrever a cinética de adsorção do adsorvato pelo adsorvente [104,125,126]. A Equação (2.6) da taxa de Lagergreen foi uma das primeiras equações utilizadas para descrever o processo de adsorção de fases líquida e sólidas num sistema, baseando-se na capacidade do sólido. Ela está relacionada com os modelos de pseudo primeira ordem [126].

$$\ln(q_e - q_t) = \ln(q_e) - K_1 t \qquad (2.6)$$

Onde $q_e$ é a quantidade do íon complexado por unidade de massa do complexante, a capacidade de complexação no equilíbrio ($mg.g^{-1}$) e $q_t$ é a quantidade de íon complexado por unidade de massa do complexante em qualquer determinado tempo ($t$). $K_1$ é a constante de velocidade da pseudo primeira ordem. O $K_1$ tem seus valores calculados a partir da linearização do $\ln(q_e - q_t)$ versus $t$ na concentração estabelecidas nas análises realizadas [126].

Segundo Gerente, et al. (2007) [125] esse modelo apresenta como desvantagem o fato de que o valor de $q_e$ é dependente de dados experimentais. Além disso, a curva dos pontos é linear apenas nos primeiros 30 minutos, depois de passado esse tempo não há correlação entre os dados experimentais e teóricos. Esse modelo é largamente usado no processo de quelação da quitosana pelos íons metálicos. Para alguns casos o valor $k_1$ cabe adequadamente pelos valores determinados experimentalmente [125,126], contudo em outros casos o modelo de pseudo segunda ordem torna-se mais adequado. A Equação (2.7) mostra a taxa de adsorção segundo o modelo de pseudo segunda ordem [126].

$$t/q_t = 1/((K_2 . q_e^2)) + (1/q_e).t \qquad (2.7)$$

Onde $K_2$ é a constante de velocidade de complexação da pseudo segunda ordem (g.mg$^{-1}$. min$^{-1}$). Os valores de $K_2 . q\,{}_e^{\,2}$ foram calculados a partir da linearização do $t/qt$ versus $t$ na concentração estabelecida [125,126].

No entanto, o modelo de pseudo segunda ordem é apenas adequada para descrever os dados medidos perto do equilíbrio. Esse modelo assume que o passo determinante da velocidade pode ser uma reação química na superfície [127,128]. O modelo de difusão intra partícula (modelo de Weber & Morris [123]) controlado leva em consideração uma resistência do filme em relação à transferência de massa (Equação 2.8). Assim como leva em consideração que o formato das partículas seja esférico. Sendo um modelo muito pouco utilizado no processo de quelação pela quitosana e derivados, além de apresentar o inconveniente de não prever a adsorção em relação aos primeiros minutos, pois o modelo é baseado numa relação de tempo levada a 1/2 [123].

$$q(t) = K_{IP}\, t^{0.5} + C \qquad (2.\ 8)$$

Onde, $K_{IP}$ é a constante de difusão e $C$ é o efeito da camada limite, dando uma ideia da espessura da camada [126].

### 3.4.3 Corantes e a adsorção

A presença de corantes em efluentes industriais é uma causa significativa de poluição devido à sua natureza recalcitrante, dando cor indesejável à água e reduzindo a penetração da luz solar, além do fato de que seus produtos de degradação podem ser tóxicos ou mesmo mutagênicos e carcinogênicos [129]. Aproximadamente 10.000 diferentes tipos de pigmentos e mais de 700.000 toneladas por ano são produzidos mundialmente anualmente, sendo 10 a 15 % perdidos no efluente durante o processo de tingimento [19,109,130].

Esses corantes são um grupo relativamente grande de produtos químicos orgânicos geralmente classificados com base em sua estrutura molecular, que são amplamente utilizados em muitas indústrias, como têxtil, impressão em papel, plástico, cosméticos,

borracha, curtume e tintas. Normalmente, os corantes são difíceis de degradar devido às suas complexas estruturas aromáticas. Eles podem causar várias doenças em humanos e animais, como alergia, irritação, dermatite e até câncer [132-134]. Para remoção desses materiais, métodos como floculação, oxidação e eletrólise são comuns. No entanto, esses métodos possuem alto custo e habilidade na operação [104]. Nesse sentido, a adsorção é o processo mais comumente usado, em razão da sua eficácia e simplicidade para a remoção de corantes não degradáveis, mesmo em baixas concentrações de água potável ou de efluentes industriais [135,136].

Convencionalmente, o carvão ativado tem sido utilizado para a adsorção de corantes em vários tipos de efluentes, mas sua aplicação é muitas vezes limitada devido ao seu alto custo e natureza recalcitrante. Portanto, nos últimos anos, o interesse em buscar novos substitutos eficazes baseados em polímeros naturais e derivados como amido, celulose, quitosana e lignina aumentou significativamente considerando o conceito de materiais econômicos e ecologicamente corretos [134,136]. Nesse sentido, entre diversas alternativas, os adsorventes à base de polímeros têm sido utilizados para descontaminação de água e tratamento de efluentes, pois apresentam redes hidrofílicas com grupos funcionais para o desenvolvimento de interações químicas com íons metálicos e compostos orgânicos [137]. Para este fim, hidrogéis poliméricos altamente absorventes (ou polímero superabsorvente, SAP) têm sido amplamente utilizados em uma variedade de aplicações, tais como produtos farmacêuticos na distribuição de medicamentos, nutrição, agricultura e como bio-adsorventes para tratamento e remediação de água [19,138-141].

Nesse enfoque, o uso da quitosana tiolizada é vantajoso, pois apresenta em sua estrutura além dos grupos químicos presentes na quitosana, o acréscimo do grupo tiol. Esse grupo já tem suas propriedades conhecidas no estudo de adsorção de metais pesados e arsênio [142,143]. Esses estudos apontam que o grupo tiol apresenta-se como uma base de Lewis, o que lhe torna um metal macio com comportamento básico, em razão da presença de grupos de elétrons disponíveis em sua estrutura, o que lhe possibilita ligações fortes com vários íons, como cádmio, arsênio e prata [142,145]. Entretanto, não há relatos na literatura do uso dessas quitosanas na adsorção de corantes em água, em especial o pigmento laranja de metila.

O laranja de metila é um pigmento que contém orto-substituintes e a presença do grupo para-dimetilamino ativando o grupo azo. Em meios ácidos, esse corante protona e o dimetilamino forma um íon amônio (Figura 3.9 2), ou o grupo azo forma uma azônio (Figura 2.9). Estudos com dimetilaminoazobenzeno sugerem que o íon azônio pode ser a espécie predominante em pH menores. Já em meios maiores do que seu pka (pka = 3,49) [109], ele passa de carga neutra a negativa [109,146].

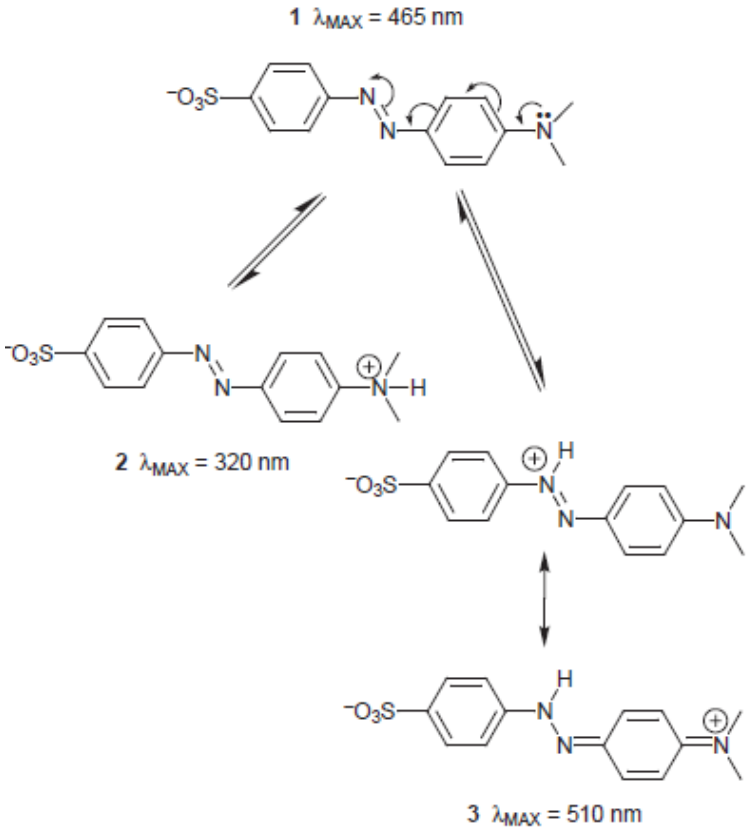


Figura 2. 10. Representação esquemática das cargas do laranja de metila em meios ácidos
Fonte: Oakes et al. (1998) [146].

### 3.5 Atividade antibacteriana da quitosana

Atualmente, o efluente hospitalar tem se tornado uma grande preocupação, pois muitos antibióticos e bactérias resistentes são descartados em grandes quantidades no meio ambiente em decorrência do aumento e do uso frequente e indiscriminado de antibióticos nos processos

médico, veterinário e agrícola, e como a água do rio é o principal receptor desse poluente essa contaminação pode contribuir para a resistência de muitos agentes [147,148].

Esses efluentes hospitalares são responsáveis por liberar muitas substâncias nos meios aquosos, como antibióticos, farmacêuticos, metais pesados, drogas, desinfetantes, que não são metabolizados pelos pacientes. Esta situação provoca um ambiente que fornece um meio seletivo para bactérias causando um aumento da resistência bacteriana [149]. Estudos mostram que os efluentes hospitalares apresentam maior resistência bacteriana do que os efluentes de outras fontes e a concentração de antibacterianos na água que recebe o esgoto hospitalar também é maior, criando um ambiente com forte seletividade [150]. Além disso, as condições precárias de tratamento de efluentes hospitalares podem causar uma rota de disseminação de bactérias multirresistentes [149-151].

*Pseudomonas aeruginosa* (*P. aeruginosa*) é um patógeno altamente resistente e oportunista. Devido à barreira de permeabilidade na membrana externa, é naturalmente resistente a muitos antibióticos [152]. Infecções causadas por *P. aeruginosa* estão aumentando tanto em hospitais como na comunidade em geral e tem sido relatada como uma das principais causas de patógenos nosocomiais, particularmente entre pacientes imunocomprometidos [153]

Concomitantemente, o uso extensivo de agentes antibacterianos e as estratégias evolutivas de resistência das bactérias a esses agentes resultaram no surgimento de bactérias resistentes a drogas. A eficácia de muitos antibióticos no tratamento de infecções tornou-se bastante limitada devido ao desenvolvimento de resistência e a ameaça de organismos resistentes aos antibacterianos [153-155].

Além da característica intrínseca de apresentar baixos níveis de sensibilidade a agentes antibacterianos, vários mecanismos de resistência foram identificados em *P. Aeruginosa*, como hiperexpressão de bombas de efluxo, produção de β-lactamases, perda ou expressão reduzida de proteínas de membrana externas [156]. Por essas razões, infecções causadas por cepas de *P. aeruginosa* multirresistentes representam um desafio substancial para o tratamento antibacteriano, trazendo para o cenário atual a identificação dessas bactérias

multirresistentes no efluente hospitalar e avaliando sua contribuição para a disseminação da resistência em amostras de águas superficiais [157].

Biopolímeros naturais são cientificamente e industrialmente atraentes por causa de sua capacidade de atividade antibacteriana [153]. Nesse sentido, a quitosana é um dos biopolímeros mais atraentes com atividade antibacteriana estudada [157]. As propriedades antibacterianas da quitosana continuam atraindo crescente interesse de pesquisa, principalmente no que diz respeito ao seu alto potencial de aplicação na tecnologia em saúde [158]. Contudo, todas as pesquisas relacionadas a atividade antibacteriana da quitosana e derivados estão relacionadas a aplicação como biomaterial associando essa atividade antibacteriana na melhora, por exemplo de cicatrização de feridas por queimadura [153-158]. Praticamente, não há nenhum relato associando essa atividade antibacteriana ao tratamento de água, onde essas bactérias estão bastante presentes, em especial a *Pseudomona aeroginosa*.

A atividade antibacteriana da quitosana varia de acordo com suas propriedades físicas (grau de desacetilação, massa molecular), solvente, espécie de microrganismo e fonte. A atividade antibacteriana da quitosana é relatada como dependente dos métodos envolvidos na preparação de diferentes GD e massa molar de quitosana (quanto maior a massa da quitosana menor sua atividade antibacteriana) [159-163]. Portanto, há ainda muitos estudos sobre a atividade antibacteriana da quitosana, pois seu mecanismo ainda é intensamente debatido. Nesse sentido, algumas hipóteses são publicadas como quelação de íons metálicos essenciais, penetração celular em razão da baixa massa molar seguida por inibição da síntese de proteínas através de ligação a ácidos nucléicos e, mais amplamente aceito, a destruição de estruturas da parede celular bacteriana [164-167].

Nesse enfoque, as quitosanas tiolizadas foram recentemente utilizadas como portadores de drogas para aumentar a interação com resíduos de cisteína na mucosa, aumentando assim os tempos de retenção *in situ*. Além disso, estudos anteriores revelaram um forte efeito do ácido quitosano-tioglicólico (TGA) em diferentes microorganismos, incluindo *Streptococcus sobrinus* (bactérias gram-positivas), *Neisseria subflava* (bactérias gram-negativas) e *Candida*

*albicans* (fungos) [168-170]. Curiosamente, as bactérias gram-positivas, que são geralmente menos sensíveis à baixa massa molar da quitosana e seus derivados, foram atacadas de forma seletiva e eficiente pelos tíomeros com TGA, ou com substituintes mercapto, identificando esse composto como um agente antibacteriano promissor e versátil [72]. No entanto, embora haja diversos estudos da atividade antibacteriana da quitosana e quitosana tiolizada, esses estudos apresentam um grande *gap*, pois apresentam resultados contraditórios e não explicativos em relação ao mecanismo da atividade antibacteriana, o que viabiliza a necessidade de mais estudos. Além do fato de que nenhum dos estudos abordando o uso das quitosanas tiolizadas como promissores antibacterianos tenha abordado o grupo tiol como um dos agentes dessa atividade.

**Referências**

[1] Gonzalés, M. N. G. Development and life cycle assessment of polymeric materials from renewable sources. Thesis (PhD. Thesis in Materials Engineering), Politecnico di Milano, Department of Chemistry, Materials and Chemical Engineering, 2014.

[2] Anastas, P. T, Lankey, R. L. Sustainability through green chemistry and engineering. ACS Syrup Series, 823 (2002) 1-11.

[3] Marteel-Parrish, A. E, Abraham, M. A. Green Chemistry and Engineering: A Pathway to Sustainability. Chapter 2. Principles of green chemistry and green engineering. John Wiley & Sons, Inc, 2014.

[4] Anastas, P. T., Warner, J. C. Green Chemistry: Theory and Practice. Oxford University Press, New York. (1998).

[5] ONU, Organização das Nações Unidas Our Common Future, Report. Organização das Nações Unidas. United Nations (1987) 167.

[6] UNESCO. Scientific and Cultural Organization, Report. UNESCO (United Nations Educational) (2015) 267.

[7] Anastas, P. T., Zimmerman, J. B. Design through the twelve principles of green engineering. Environ Sci Technol 37 (2003) 94A-101A.

[8] Brooks, C. S. Metal Recovery from Industrial Wastes. Chelsea, Michigan: Lewis Publishers, 1991.

[9] Erosa, M. S. D., et al. Cadmium sorption on chitosan sorbents: kinetic and equilibrium studies. Hydrometallurgy, 61 (2001) 157-167.

[10] Spinellli, V. A., Laranjeira, M. C. M., Fávere, V. T. Preparation and characterization of quaternary chitosan salt: adsorption equilibrium of chromium(VI) ion. React. Funct. Polym., 61 (2004) 347-352.

[11] Vendrusco, G. S., Mentz, L. A. Study of use citations agreement and importance of medicinal used species and families to the community of Ponta Grossa neighborhood. Acta Botanica Brasilica, 20 (2006) 367-382.

[12] Korner, C., et al. Carbon Flux and Growth in Mature Deciduous Forest Trees Exposed to Elevated $CO_2$. Science, 309 (2005) 1360-1362.

[13] Chandra, R., Rustgi, R. Biopolymers, Biodegradable polymer or bioplastic. Prog. Polym. Sci., 23 (1998) 1273.

[14] Plank, J. Applications of biopolymers and other biotechnological products in building materials. Appl. Microbiol. Biot., 66 (2004) 1-9.

[15] Mohanty, A. K., et al. Natural Fibers, Biopolymers, and Biocomposites: An Introduction. Boca Raton: Taylor & Francis, 2005.

[16] De Paoli, M. A. Degradação e Estabilização de Polímeros. Cemkeys, 2008.

[17] Handbook Chemical Economics. Biodegradable polymers, (2015). Disponível em: https://www.ihs.com/products/biodegradable-polymers-chemical-economics-andbook.html.

[18] Slavin, J., Carlson, J. Carbohydrates. Adv. Nutr. Inter. Rev. J., 5 (2014) 760-761.

[19] Capanema, N.S.V., et al. Eco-friendly and Biocompatible Crosslinked Carboxymethylcellulose Hydrogels as adsorbents for the Removal Organic Dye Pollutants for Environmental Applications, Environ Technol, 38 (2017) 1-42.

[20] Medeiros Borsagli, F. G. L.; Carvalho, I. C.; Mansur, H. S. Amino acid-grafted and N-acylated chitosan thiomers: Construction of 3D bio-scaffolds for potential cartilage repair applications. Inter J Biol Macromol, 114 (2018) 270-282.

[21] Habibi, Y., Lucia, L. A. Polysaccharide building blocks: A sustainable approach to the development of Renewable Biomaterials. New Jersey: Wiley, John & Wiley Sons, 2012.

[22] Heinze, T. Advances in polymer Science: Polysaccharides I Struture, Characterization and Use. Heidelberg: Springer Verlag, 2005.

[23] Kaplan, D. L. Bipolymers from Renewable Resources. New York: Springers, 1998.

[24] Aplin, J. D., Hall, L. D. Nitroxide spin-labels as molecular probes of the microviscosity of aqueous solurions of carbohydrates: alginate, other polysaccharides, and sucrose. Carbohyd. Polym., 59 (1977) c20-c24.

[25] Shah, A. A., et al. Biological degradation of plastics: A Comprehensive review. Biotechnol., 26 (2008) 246-265.

[26] Witt, M. A. Obtenção e caracterização de filmes finos de multicamadas de polieletrólitos naturais depositados por layer-by-layer. Tese (Doutorado em Química), Departamento de Química da Universidade Federal de Santa Catarina, UFSC, Florianopólis, 2012.

[27] French, A., et al. Kirk-Orthmer Encyclopedia of chemical Technology. New York: John Wiley & Sons, 2004.

[28] Solomons, W. G., Fryhle, C. B. Química Orgânica. Rio de Janeiro: LTC, 2006.

[29] Taipina, M. O. Nanocristais de cellulose: Obtenção, caracterização e modificação de superfície. Dissertação (Mestrado em Química), Departamento de Química da Universidade Estadual de Campinas, UNICAMP, Campinas, 2012.

[30] Innerlohinger, J., Weber, H. K., Kraft, G. Aerocellulose: Aerogels and Aerogel like Materials made from Cellulose. Macromol. Symp., 2044 (2006) 126-135.

[31] Wang, et al. Fluorescent cellulose aerogels containing covalently immobilized (ZnS)x(CuInS2)12x/ZnS (core/shell) quantum dots. Cellulose, 20 (2013) 3007-3024.

[32] He, X., et al. Adsorption and Desorption of Methylene Blue on Porous Carbon Monoliths and Nanocrystalline Cellulose. Appl Mater Interf., 5 (2013) 8796-8804.

[33] Jiang, F., Hsieh, Y-L. Chemically and mechanically isolated nanocellulose and their self-assembled structures. Carbohyd. Polym., 35 (2013) 32-40.

[34] Zhang, Y., et al. Cellulose Nanofibrils: From Strong Materials to Bioactive Surfaces. J. Renew. Mater. (JRM)., 1 (2013) 195-211.

[35] Wan, C., et al. Ultralight and hydrophobic nanofibrillated cellulose aerogels from coconut shell with ultrastrong adsorption properties. J APPL POLYM SCI., 42037 (2015) 1-7.

[36] Cervin, N. T., et al. Lightweight and Strong Cellulose Materials Made from Aqueous Foams Stabilized by Nanofibrillated Cellulose. Biomacromolecules, 14 (2012) 503-514.

[37] Hubbe, M. New Horizons for Use of Cellulose-Based Materials to Adsorb Pollutants from Aqueous Solutions. Review. Lignocellulose, 2 (2013) 386-411.

[38] Rudnik, E. Compostable polymer materials. Oxford: Elsevier, 2008.

[39] Whistler, R. L., Daniel, J. R. Starch. Kirk-Othmer Encyclopedia of Chemical Technology/ University Purdue. United Kingdom: John Wiley & Sons, 2000.

[40] Capanema, N. S. V., et al. Bioengineered carboxymethyl cellulose-doxorubicin prodrug hydrogels for topical chemotherapy of melanoma skin cancer. Carbohydr. Polym., 195 (2018) 401-412.

[41] Ramanery, F. P., Mansur, A. A. P., Mansur, H. S. One-step colloidal synthesis of biocompatible water-soluble ZnS quantum dot/chitosan nanoconjugates. Nano. Res. Lett., 8 (2013) 512.

[42] Medeiros Borsagli, F. G., et al. O-carboxymethyl functionalization of chitosan: Complexation and adsorption of Cd (II) and Cr (VI) as heavy metal pollutant ions, React Func Polym, 97 (2015) 37-47.

[43] Santos, J. C., et al. Functionalized chitosan derivatives as nonviral vectors: physicochemical properties of acylated *N*,*N*,*N*-trimethyl chitosan/oligonucleotide nanopolyplexes, Soft Matter, 41 (2015) 8113-8125.

[44] Heinze, T. Advances in polymer Science: Polysaccharides I Struture, Characterization and Use. Heidelberg: Springer Verlag, 2005.

[45] Stiernersted, J., et al. Friction between cellulose surfaces and effect of xyloglucan adsorption. Biomacromolecules, 7 (2006) 2147-2153.

[46] Vendruscolo, G. S., Mentz, L. A. Study of use citations agreement and importance of medicinal used species and families to the community of Ponta Grossa neighborhood. Acta Botan. Bras., 20 (2006) 367-382.

[47] Dutta, P. K., Dutta, J., Tripathi, V. S. Chitin and chitosan: chemistry, properties and applications. J. Sci. Ind. Res. India., 63 (2004) 20-31.

[48] Pires, G. Biomateriais derivados de quitosana e hidroxiapatita com potencial para preenchimento ósseo. Tese (Doutorado em Química) – Departamento de Química da Universidade Estadual de Campinas, UNICAMP, Campinas, 2010.

[49] Gonçalves, A. A., et al. Diferentes estratégias para reticulação de quitosana. Quím. Nov 34 (2011) 1215-1223.

[50] Pochanavanich, P., Suntornsuk, W. Fungal chitosan production and its characterization. Lett. Appl. Microbol., 35 (2002) 17-21.

[51] Kannan, M., et al. Production and Characterization of Mushroom Chitosan under Solid-State Fermentation Conditions. Adv. Biol. Res., 4 (2010) 10-13.

[52] Crestini, C., Kovac, B., Giovannozzi-Sermanni, G. Production and isolation of chitosan by submerged and solid-state fermentation from Lentinus edodes. Biotechnol. Bioeng., 50 (1996) 207-210.

[53] Costa Junior, E. S., et al. Preparation and Characterization of Chitosan/Poly(Vinyl Alcohol) Chemically Crosslinked Blends for Biomedical Applications, Carbohydr Polym, 76 (2009) 472-481.

[54] Costa Jr., E. S., Mansur, H. S. Preparação e caracterização de blendas de quitosana/poli(álcool vinílico) reticuladas quimicamente com glutaraldeído para aplicação em engenharia de tecido. Quim. Nova., 31 (2008) 1460-1466.

[55] Tan, S.C., et al. The degree of deacetylation of chitosan: advocating the first derivative UV-spectrophotometry method of determination. Talanta, 45 (1998) 713-719.

[56] Wu, T., Zivanovic, S. Determination of the degree of acetylation (DA) of chitin and chitosan by an improved first derivative UV method. Carbohyd. Polym., 73 (2008) 248-253.

[57] Nahalka, et al. Elicitation of plumbagin by chitin and its release into the medium in Drosophyllum lusitanicum. Link suspension cultures. Biotechnol. Lett., 20 (1998) 841–845.

[58] Evans Jr., C. A., Brundle, C. R., Wilson, S. Encyclopedia of materials caracterization. New York: Butterworth-Heinemann, 1992.

[59] Silva, G. C. Mecanismo de acumulação de ferro e arsênio em biomassa vegetal fibrosa. Dissertação (Mestrado em Engenharia Metalúrgica, Materiais e Minas) – Escola de Engenharia da Universidade Federal de Minas Gerais, UFMG, Belo Horizonte, 2008.

[60] Dumont, V. C., et al. Glycol/Chitosan nanohydroxyapatite biocomposites for potential bone tissue engineering and regenerative medicine, Inter J Biol Macromol Part B, 93 (2016) 1465-1478.

[61] Heurtault, B., et al. Physico-chemical stability of colloidal lipids particles. Biomaterials, 74 (2003) 4283-4300.

[62] Solier, P., et al. Relation between the Degree of Acetylation and the Electrostatic Properties of Chitin and Chitosan. Biomacromolecules, 2 (2002) 765-772.

[63] Guibal, E. Interactions of metal ions with chitosan-based sorbents: a review. Sep. Purif. Technol., 38 (2004) 43-74. [63] Muzzarelli, et al. Current views on fungal chitin/chitosan,

human chitinases, food preservation, glucans, pectins and inulin: A tribute to Henri Braconnot, precursor of the carbohydrate polymers science, on the chitin bicentennial. Carbohyd. Polym., 87 (2012) 995-1012.

[64] Muzzarelli, et al. Spray-drying of solutions containing chitosan together with polyuronans and characterisation of the microspheres. Carbohyd. Polym. 57 (2004) 73-82.

[65] Muzzarelli, R. A. A. Chitosan composites with inorganics, morphogenetic proteins and stem cells, for bone regeneration. Carbohyd. Polym., 83 (2011) 1433-1445.

[66] Liu, D., et al. Potential advantages of a novel chitosan-N-acetylcysteine surface modified nanostructured lipid carrier on the performance of ophthalmic delivery of curcumin, Sci Rep, 28796 (2015) 1-14.

[67] Carvalho, I. C., Mansur, H. S., Engineering 3D scaffolds of photocrosslinked chitosan-gelatin hydrogel hybrids for cronic wound dressings and regeneration, Mater Sci Eng C, 78 (2017) 690-705.

[68] Mansur, H. S., et al. Bioconjugation of quantum-dots with chitosan and *N*,*N*,*N*-trimethyl chitosan. Carbohydr. Polym., 90 (2012) 189-196.

[69] Schmitz, T., et al. Synthesis and characterization of a chitosan-N-acetyl cysteine conjugate, Inter J Pharm, 347 (2008) 79-85.

[70] Casettari, L., Biomedical applications of amino acid-modified chitosans: A review. Biomaterials, 33 (2012) 7565-7583.

[71] Diekjürgen, D., Grainger, D. W., Polysaccharide matrices used in 3D in vitro cell culture systems, Biomaterials,141 (2017) 96-115.

[72] Croce, M., et al. Synthesis and screening of N-acyl thiolated chitosans for antibacterial applications. Carbohydr. Polym., 151 (2016) 1184-1192.

[73] Bae, I.-H., et al. Evaluation of a Thiolated Chitosan Scaffold for Local Delivery of BMP-2 for Osteogenic Differentiation and Ectopic Bone Formation. BioMed Res Int, 2013 (2013) 1-11.

[74] Talaei, F., et al. Thiolated chitosan nanoparticles as a delivery system for antisense therapy, Inter J Nanomedicine, 6 (2011) 1963–1975.

[75] Bernkop-Schnurch, A., Guggi, D., Pinter, Y., Thiolated chitosans: development and in vitro evaluation of a mucoadhesive, permeation enhancing oral drug delivery system, J Control Release, 94 (2004) 177– 186.

[76] Bernkop-Schnurch, A., Thiomers: A new generation of mucoadhesive polymers, Adv Drug Deliv Rev, 57 (2005) 1569– 1582.

[77] Dheer, D., et al. Polysaccharides based nanomaterials for targeted anti-cancer drug delivery, J Drug Target, 25 (2017) 1-16.

[78] Shah, K. U., et al. Thiomers and their potential applications in drug delivery, Expert Opin Drug Deliv, 14 (2017) 601-610.

[79] Inta, O., Yoksan, R., Limtrakul, J. Hydrophobically modified chitosan: abio-based material for antimicrobial active film. Mater Sci Eng. C, 42 (2014) 569–577.

[80] Vallapa, N., et al. Enhancing antibacterial activity of chitosan surface by heterogeneous quaternization. Carbohydr Polym, 83 (2011) 868–875.

[81] Sarti, F., Bernkop-Schnürch, A. (2011). Chitosan and thiolated chitosan. In R. Jayakumar, M. Prabaharan, & R. A. A. Muzzarelli (Eds.), Advances in polymer science. chitosan for biomaterials I (243) (pp. 93–110). Berlin, Heidelberg: Springer Berlin Heidelberg.

[82] Dragostina, O. M., et al. New antimicrobial chitosan derivatives for wound dressing applications. Carbohydr Polym, 141 (2016) 28-40.

[83] Costa, H. S. Síntese, Caracterização e Avaliação do Comportamento Degradativo de Híbridos Porosos de Poli (Álcool Vinílico)/Vidro Bioativo. Tese (Doutorado em Engenharia Metalúrgica e de Minas) – Escola de Engenharia da Universidade Federal de Minas Gerais, UFMG, Belo Horizonte, 2010.

[84] HCUP - Healthcare Cost & Utilization Project, Agency for Healthcare Research and Quality, 2007. MERRILL, Chaya; ELIXHAUSER, Anne. Hospital Stays Involving Musculoskeletal Procedures, 1997–2005. Disponível em http://www.hcup-us.ahrq.gov/reports/statbriefs/sb34.pdf.

[85] Saraiva, S. M. et al. Synthesis and characterization of a photocrosslinkable chitosan–gelatin hydrogel aimed for tissue regeneration. RSC Adv., 5 (2015) 63478–63488.

[86] Holzapfel, B. M., et al. How smart do biomaterials need to be? A translational science and clinical point of view. Adv. Drug Deliv. Rev., 65 (2013) 581–603.

[87] Groeber, F., et al. Skin tissue engineering - In vivo and in vitro applications. Adv. Drug Deliv. Rev., 63 (2011) 352–366.

[88] Mansur, H. S.,et al. 3D-macroporous hybrid scaffolds for tissue engineering: network design and mathematical modeling of degradation kinetics. Mater. Sci. Eng. *C*, 32 (2012) 404-415.

[89] Akay, G., Birch, M. A, Bokhari, M. A. Microcellular polyHIPE polymer supports osteoblast growth and bone formation in vitro. Biomaterials, 25 (2011) 3991-4000.

[90] Mandal, B., Kundu, S. Cell proliferation and migration in silk fibroin 3D scaffolds. Biomaterials, 30 (2009) 2956-2695.

[91] Lien, S. M., Ko, L. Y., Hunag, T. J. Effect of pore size on ECM secretion and cell growth in gelatin scaffold for articular cartilage tissue engineering. Acta Biomateralia, 5 (2009) 670-679.

[92] Murphy, C. M., O'Brien, F. J. Understanding the effect of mean pore size on cell activity in collagen-glycosaminoglycan scaffolds. Cell Adh. Migr, 4 (2010) 377-381.

[93] Chen, F-M., Liu, X.., Advancing biomaterials of human origin for tissue engineering, Prog Polym Sci, 53 (2016) 86–168.

[94] Langer, R., Vacanti, J. P., Tissue Engineering, Science, New Series, 260 (1993) 920-926.

[95] Griffith, L. G., Naughton, G., Tissue Engineering-Current Challenges and Expanding Opportunities. Science, 295 (2002) 1009-1014.

[96] Vial, X., Andreopoulos, F. M., Novel biomaterials for cartilage tissue engineering, Curr Rheumatol Rev, 500 (2009) 51-57.

[97] Shoichet, M. S., Polymer scaffolds for biomaterials applications, Macromol, 43 (2010) 581-591.

[98] Campos, D. F. D., Supporting Biomaterials for Articular Cartilage Repair, Cartilage, 3 (2012) 205–221.

[99] Alves da Silva, M. L., et al. Chondrogenic differentiation of human bone marrow mesenchymal stem cells in chitosan-based scaffolds using a flow-perfusion bioreactor, J Tissue Eng Regen Med, 5 (2011) 722-732.

[100] Abarrategi, A., et al. Chitosan scaffolds for osteochondral tissue regeneration. J Biomed Mater Res A, 95 (2010) 1132-1141.

[101] Chevrier, A., et al. Temporal and spatial modulation of chondrogenic foci in subchondral microdrill holes by chitosan-glycerol phosphate/blood implants, Osteoarthr Cartil, 19 (2011) 136-144.

[102] Suh, J-K. F., Mathew, H. W. T., Application of chitosan-based polysaccharide biomaterials in cartilage tissue engineering: a review, Biomaterials, 21 (2000) 2589-2598.

[103] Ali, I., Gupta, K., Advances in water treatment by adsorption, Taylor & Francis, New York, 2007.

[104] Laus, R., Fávere, V. T., Competitive adsorption of Cu (II) and Cd (II) ions by chitosan crosslinked with epichlorohydrin-triphosphate, Biosour. Technol. 102 (2011) 8769-8776.

[105] Bandeira, L. F. M. Remoção de metal pesado de efluentes aquosos através da combinação dos processos de osmose inversa e adsorção. Dissertação (Mestrado em Engenharia Química) – Escola de Engenharia da Universidade federal do Rio de Janeiro, Rio de Janeiro, 2007.

[106] Bhatnagar, A., Sillanpää, M., Witek-Krowiak, A. Agricultural waste peels as versatile biomass for water purification — a review. Chem. Eng. J. 270 (2015) 244–271.

[107] Monier, M., Adsorption of $Hg^{2+}$, $Cu^{2+}$ and $Zn^{2+}$ ions from aqueous solution using formaldehyde cross-linked modified chitosan-thioglyceraldehyde Schiff's base, Int. J. Biol. Macromol. 50 (2012) 773-781.

[108] Gautam, R. K., et al. Biomass-derived biosorbents for metal ions sequestration: Adsorbent modification and activation methods and adsorbent regeneration. J. Environ. Chem. Eng. 2 (2014) 239–259.

[109] Subbaiah, M. V., Kim, D-S. Adsorption of methyl orange from aqueous solution by aminated pumpkin seed powder: kinetics, isotherms, and thermodynamic studies, Ecotoxicol. Environ. Saf. 128 (2016) 109-117.

[110] Mccabe, W. L., Smith, J. C., Harriott, P. Unit Operations of Chemical Engineering. 5$^{th}$ ed. 1993.

[111] Ali, I., Asim, M., Khan, T.A. Low Cost Adsorbents for the Removal of Organic Pollutants from Wastewater. Department of Chemistry, New Delhi, India, p. 170-183, 2012.

[112] Rouquerol, F., Rouquerol, J., Sing, K. Adsorption by powders & porous solids: principles, Methodology and application. Academic Press. 1999.

[113] Ruthven, D. M. Principles of Adsorption and Adsorption Processes. 1st ed. New York: Wiley-Interscience. 1984.

[114] Souza, R. S. Avaliação da Lama Vermelha na Remoção de Derivados de Petróleo – Benzeno, Tolueno, Xileno (BTX). Tese (Doutorado em Engenharia Química), Faculdade de Engenharia Química da Faculdade Estadual de Campinas, UNICAMP, Campinas, 2013.

[115] Do, D. D. Adsorption analysis: equilibria and Kinetics. London: Imperial College Press, 1998.

[116] Adamson, A. W., Gast, A. P. Physical Chemistry of Surfaces. New York: Wiley, 1997.

[117] Kumar, K.V., Ramamurthi, V., Sivanesan, S. Modeling the mechanism involved during the sorption of methylene blue onto fly ash. J. Coll. Inter. Sci., 284 (2005) 14–21.

[118] Cooney, D. O. Adsorption Design for Wastewater Treatment. Florida: CRC Press, 1999.

[119] Lordeiro, P., Cordero, B., Barriada, J. L. Biosorption of Cadmium by Biomass of Brown Marine Macroalgae. Biosour. Technol., 96 (2006) 1796-1803.

[120] Summer, M. E. Handbook of Soil Science, manuals. Washington, D. C., USA: Library of Congress, section B, 1999.

[121] Oscik, J., Cooper, I. L. Adsorption. John Wiley & Sons, 1982.

[122] Letterman, R. D. Water quality and treatment: a handbook of community water supplies. 5th ed. New York: McGraw-Hill: American Water Works Association, 1999.

[123] Benavente, M. Adsorption of metallic ions onto chitosan: equilibrium and kinetic studies. Tese (Doutorado em Engeharia Química) – Departamento em Engenharia Química do Royal Institute of Technology), KTH, 2008.

[124] Richardson, J. F., Harker, J. H. Particle Technology and Separation Processes. Coulson and Richardson's Chemical Engineering. Butterworth-Heinemann: Woburn, 2002.

[125] Gerente, C., et al. Aplication of Chitosan for the remove of metals from wastewater by adsorption - Mecanism and Models Review. Crit. Rev. Env. Sci. Tec., 37 (2007) 41-127.

[126] Simonin, J-P. On the comparison of pseudo-first and pseudo-second order rate laws in the modeling of adsorption kinetics, Chem. Eng. J. 300 (2016) 254-263.

[127] Plazinski, W., Rudzinski, W., Plazinska, A. Theoretical models of sorption kinetics including a surface reaction mechanism: A review. Adv. Colloid Interface Sci., 152 (2009) 2-13.

[128] Zhao, F., et al. Adsorption of Cd(II) and Pb(II) by a novel EGTA-modified chitosan material: Kinetics and isotherms. J. Colloid. Interface. Sci., 409 (2013) 174-182.

[129] Halling-Sorensen, B., et al. Occurrence, fate and effects of pharmaceutical substances in the environment – a review. Chemosphere, 36 (1998) 357-393.

[130] Li, X., et al. Preparation and characterization of new foam adsorbents of poly(vinyl alcohol)/chitosan composites and their removal for dye and heavy metal from aqueous solution, Chem. Eng. J. 183 (2012) 88-97.

[131] Emmanuel, E., et al. Ecotoxicological risk assessment of hospital wastewater: a proposed framework for raw effluents discharging into urban sewer network. J Hazard Mater, A117 (2005) 1-11.

[132] Peng, N., et al. Superabsorbent cellulose–clay nanocomposite hydrogels for highly efficient removal of dye in water. ACS Sustainable Chem. Eng. 4 (2016) 7217−7224.

[133] Zhang, G., Yi, L., Deng, H., Sun, P. Dyes adsorption using a synthetic carboxymethyl cellulose-acrylic acid adsorbent. J. Environ. Sci. 26 (2014) 1203–1211.

[134] Lin, Q., et al. Adsorption properties of crosslinking carboxymethyl cellulose grafting dimethyldiallylammonium chloride for cationic and anionic dyes. Carbohydr. Polym. 151 (2016) 283–294.

[135] Mahfoudhi, N., Boufi, S. Nanocellulose as a novel nanostructured adsorbent for environmental remediation: a review. Cellulose 24 (2017) 1171–1197.

[136] Rangabhashiyam, S., Anu, N., Selvaraju, N. Sequestration of dye from textile industry wastewater using agricultural waste products as adsorbents. J. Environ. Chem. Eng., 1 (2013) 629–641.

[137] Tran, T.H., et al. Removal of metal ions from aqueous solutions using carboxymethyl cellulose/sodium styrene sulfonate gels prepared by radiation grafting. Carbohydr. Polym. 157 (2017) 335–343.

[138] Demitri, C., et al. Novel superabsorbent cellulose-based hydrogels crosslinked with citric acid. J. Appl. Polym. Sci. 110 (2008) 2453–2460.

[139] Esposito, F., et al. Water sorption in cellulose-based hydrogels. J. Appl. Polym. Sci. 60 (1996) 2403–2407.

[140] Passauer, L., Liebner, F., Fischer, K. Synthesis and properties of novel hydrogels from cross-linked starch phosphates. Macromol. Symp., 244 (2006) 180–193.

[141] Raju, K.M., et al. Synthesis of superabsorbent copolymers as water manageable materials. Polym. Int., 52 (2003) 768–772.

[142] Teixeira, M. C., et al. Raman spectroscopy and DFT calculations of As(III) complexation with a cysteine-rich biomaterial. J. Colloid Interface Sci 315 (2007) 128-134.

[143] Yong, S. K., et al. Synthesis and Characterization of Thiolated Chitosan Beads for Removal of Cu (II) and Cd (II) from Wastewater. Water Air Soil Pollut, 224 (2013) 1720-1735.

[145] Guimarães, A. M. F., Ciminelli, V., Vasconcelos, W., Smectite organofunctionalized with thiol groups for adsorption of heavy metal ions. Appl. Clay Sci., 42 (2009) 410-414.

[146] Oakes, J., Graton, P. Kinetic investigations of the oxidation of Methyl Orange and substituted arylazonaphthol dyes by peracids in aqueous solution. J. Chem. Soc. Perkin Trans. 2 (1998) 2563-2568.

[147] Halling-Sorensen, B., et al. Occurrence, fate and effects of pharmaceutical substances in the environment – a review. Chemosphere, 36 (1998) 357-393.

[148] Goni-Urriza, M., et al. Impact of an urban effluent on antibiotic resistance of riverine Enterobacteriaceae and Aeromonas spp. Appl. Environ. Microbiol., 66 (2000) 125-132.

[149] Emmanuel E, et al. Ecotoxicological risk assessment of hospital wastewater: a proposed framework for raw effluents discharging into urban sewer network. J. Hazard. Mater., A117 (2005) 1-11.

[150] Linton, K. B, et al. Antibiotic resistance and R factors in coliform bacilli isolated from hospital and domestic sewage. J. Med. Microbiol., 7 (1974) 91-103.

[151] Baquero F. From pieces to patterns: evolutionary engineering in bacteril pathogens. Nature Rev. Microbiol., 2 (2004) 510-518.

[152] Lee, Y. C, et al. Molecular characterization of Pseudomonas aeruginosa isolates resistant to all antimicrobial agents, but susceptible to colistin, in Daegu. Korea. J Microbiol, 45 (2007) 358-363.

[153] Tin, S., et al. Activity of Chitosans in combination with antibiotics in *Pseudomonas Aeruginosa.* Inter. J. Biol. Sci., 5 (2009) 153-160.

[154] Falagas, M. E., et al. Outcome of infections due to pandrug-resistant (PDR) Gram-negative bacteria. BMC Infect. Dis, 5 (2005) 24-30.

[155] Bosso, J. A. The antimicrobial armamentarium: evaluating current and future treatment options. Pharmacotherapy, 25 (2005) 55S–62S.

[156] Li, X. Z., Barre, N., Poole, K. Influence of the MexA-MexB-oprM multidrug efflux system on expression of the MexC-MexD-oprJ and MexE-MexF-oprN multidrug efflux systems in *Pseudomonas aeruginosa*. J. Antimicrobial Chemother., 46 (2000) 885-893.

[157] Anitha, A., et al. Chitin and chitosan in selected biomedical applications. Prog. Polym. Sci., 39 (2014) 1644–1667.;

[158] Jayakumar, R., et al. Biomaterials based on chitin and chitosan in wound dressing applications. Biotechnol. Adv., 29 (2014) 322–337.

[159] Qin C. Q, et al. Water-solubility of chitosan and its antimicrobial activity. Carbohydr. Polym., 63 (2006) 367-374.

[160] Chen, Y. M, et al. Antibacterial activity of chitosan- based matrixes on oral pathogens. J. Environ Sci Health A Tox Hazard Subst Environ Eng., 37 (2002) 1379-1390.

[161] No, H. K, et al. Antibacterial activity of chitosans and chitosan oligomers with different molecular weights. Inter. J. Food Microbiol., 74 (2002) 65-72.

[162] Liu, H., et al. Effect of ultrasonic treatment on the biochemphysical properties of chitosan. Carbohydr. Polym., 64 (2006) 553-559.

[163] Rhoades, J., Roller, S. Antimicrobial Actions of Degraded and Native Chitosan against Spoilage Organisms in Laboratory Media and Foods. Appl. Environ. Microbiol., 66 (2000) 80-86.

[164] Pittler, M. H., et al. Randomised, double – blind trial of chitosan for body weight reduction. Eur J Clin Nutr., 53 (1999) 379-381.

[165] Liu, X. F., et al. Antibacterial effects of chitosan and its water-soluble derivatives on E. coli, plasmids DNA, and mRNA. J. Appl. Polym. Sci., 103 (2011) 3521–3528.

[166] Liu, H., et al. Chitosan kills bacteria through cell membrane damage. Inter. J. Food Microbiol., 95 (2004) 147–155.

[167] Raafat, D., et al. Insights into the mode of action of chitosan as an antibacterial compound. Appl. Environ. Microbiol., 74 (2008) 3764–3773.

[168] Kumar, R., Sinha, V. R. Thiomer: a potential carrier for therapeuticdelivery. Reac. Func. Polym., 73 (2013) 1156–1166.

[169] Sarti, F., Bernkop-Schnürch, A. Chitosan and thiolated chitosan. In R. Jayakumar, M. Prabaharan, & R. A. A. Muzzarelli (Eds.), Advances in polymer science. chitosan for biomaterials I (243) (pp. 93–110). Berlin, Heidelberg: Springer Berlin Heidelberg.

[170] Geisberger, G., et al. Chitosan-thioglycolic acid as a versatile antimicrobial agent. Biomacromolecules, 14 (2013) 1010–1017.

# Capítulo 3. Amino Acid-grafted and *N*-acylated Chitosan Thiomers: Construction of 3D Bio-Scaffolds for Potential Cartilage Repair Applications

# Amino Acid-grafted and *N*-acylated Chitosan Thiomers: Construction of 3D Bio-Scaffolds for Potential Cartilage Repair Applications

Fernanda G. L. Medeiros Borsagli[1a], Isadora C. Carvalho[1b], Herman S. Mansur[1*]

[1]Center of Nanoscience, Nanotechnology and Innovation - CeNano2I, Department of Metallurgical and Materials Engineering, Federal University of Minas Gerais/UFMG, Brazil.

amedeirosfernanda80@gmail.com; bisadora.cota@gmail.com; *hmansur@demet.ufmg.br

**Abstract**

In this work novel three-dimensional (3D) scaffolds were developed with chitosan thiomer derivatives for potential soft tissue repair applications. Amino acid-grafted chitosan (cysteine, CHICys) and *N*-acylated chitosan (11-mercaptoundecanoic acid, CHIMerc) derivatives were synthesized by covalent coupling reaction and hydrogel scaffolds were produced by freeze-drying process. They were comprehensively characterized by swelling and degradation behaviors, NMR, FTIR and Raman spectroscopy, SEM and X-ray microcomputed tomography. The results demonstrated the synthesis of chitosan thiomers with distinct degree of thiol substitution (CHICys = 5 % and CHIMerc = 26 %), producing highly porous scaffolds (porosity > 80 %) with hierarchical interconnected 3D pore structures. Additionally, their physicochemical properties and architectural features were significantly tuned by the thiol-modifier, evidenced by the swelling degrees ranging from approximately 2300 % (CHICys) to 1800 % (CHIMerc) and chemical stability against degradation. Moreover, they exhibited cytocompatibility based on *in vitro* bioassays, which hold promise as suitable platform in soft tissue engineering applications.

**Keywords: Chitosan; Thiolated chitosan; Thiomers; 3D Scaffold; Cytocompatibility; Soft tissue biomaterial.**

---

[*] **Corresponding author: Prof. H Mansur.** Department of Metallurgical and Materials Engineering, Federal University of Minas Gerais, Av. Antônio Carlos, 6627– Escola de Engenharia, Bloco 2 – Sala 2233, 31.270-901, Belo Horizonte/MG, Brazil, Phone/FAX: +55 31 34091843; email: hmansur@demet.ufmg.br

# Graphical Abstract

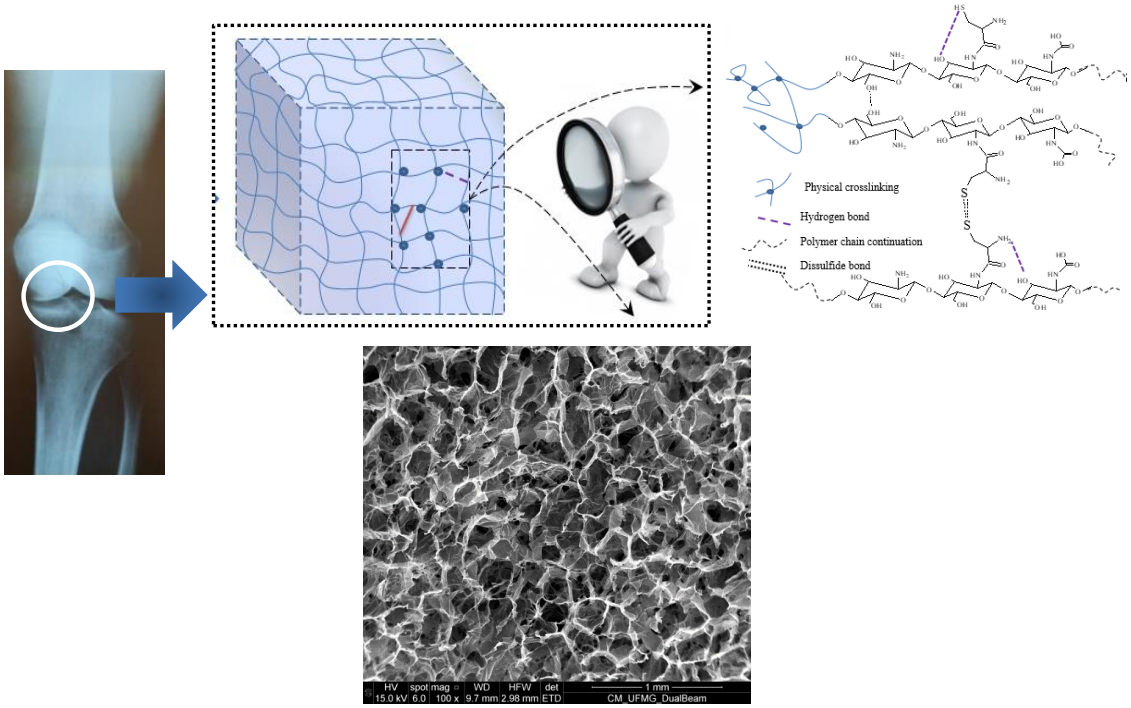


**3D Scaffolds of chitosan thiomers for potential soft tissue engineering applications.**

## 3.1 Introduction

Orthopedic surgeons and researchers worldwide are continuously faced with the challenge of regenerating articular cartilage defects. The human body has a restricted ability to properly auto-regenerate most of its major tissues if the original tissue integrity has been seriously injured because of medical disorders involving an ever-increasing burden of trauma, congenital abnormalities and degenerative diseases [1]. Although the field of tissue engineering has progressed since the landmark article published in *Science* in 1993 by Langer and Vacanti (1993) [2], which listed key strategies for the development of biological substitutes, including building matrices for cells to be seeded on, it is not yet possible to entirely mimic the physicochemical, biochemical and biological properties of articular cartilage using available technology and development strategies [3]. Therefore, the development of mimetic biomaterials with specific properties relevant to articular cartilage native tissue will support the promotion of improved, functional, and novel engineered smart materials for potential clinical application. Essentially, articular cartilage is a connective tissue composed of an extracellular matrix (ECM) containing collagen, glycosaminoglycan (GAG), and water. Due to its complexity, engineering an articular cartilage substitute requires a combination of several fields of research with a multidisciplinary approach such as materials science, materials chemistry, biochemistry, molecular biology, and biomedical engineering [4-9]. Therefore, the biomaterial selection is crucial to the success of the candidate for potential cartilage repair applications, as a large variety of natural and synthetic materials with distinct biological and physicochemical properties have been developed in recent years. Ideally, the biomaterial scaffold should closely mimic the environment occurring in the original articular cartilage tissue structure [10].

To this end, hydrogel scaffolds made from natural and synthetic polymers have become increasingly important within the field of soft tissue repair and restoration, where natural polymers possess more favorable biocompatibility and relative abundance. Among several alternatives of natural polymers, polysaccharides (*e.g.*, chitosan, hyaluronic acid, starch) have attracted the special attention of researchers for producing three-dimensional (3D) scaffolds suitable as extracellular matrix mimics for cell culture in tissue repair applications [11].

Chitosan, which is a partially de-acetylated derivative of chitin, usually extracted from exoskeletons of crustaceans, is an interesting alternative to polysaccharides for producing scaffolds. Chitosan is a linear polysaccharide consisting of $\beta$-(1-4) linked D-glucosamine residues with randomly located *N*-acetyl-glucosamine groups, where its applications depend mostly on the degree of acetylation. In addition, chitosan presents some characteristics similar to several GAGs and hyaluronic acid, which are commonly found in articular cartilage [10]. The *N*-acetylglucosamine moiety in chitosan is a structural feature present in GAGs, which suggests that the analogous structure may also present similar bioactivity. Moreover, one of the most promising features found in chitosan is related to the exceptional ability to be processed into porous structures to be applied in tissue regeneration. Porous chitosan structures can be shaped by distinct methods such as freezing and lyophilizing slightly acid solutions of chitosan in appropriate molds [10,12].

Despite the numerous advantages of chitosan (*e.g.*, abundant natural polysaccharide, biodegradable and non-toxic), it is soluble only under an acidic aqueous medium, which can restrict some of its potential applications in the biomedical field at a physiological pH and with mildly alkaline environmental conditions. Therefore, chemical derivatization of chitosan provides a powerful means to promote new biological activities and specific properties. The versatility of chitosan functionalization is essentially due to the presence of primary amino groups in the macromolecule (*i.e.*, degree of deacetylation). These groups are reactive and provide a mechanism for side group attachment using a variety of mild reaction conditions. Moreover, by the proper selection of the nature of the side group to be attached to the polymer chains, the physicochemical and biological properties can be tuned to provide specific functionalities. Based on this approach, a myriad of groups (*e.g.*, carboxylates, acyls, alkyls, thiols, quaternized amino, *etc.*) have been inserted into chitosan providing additional characteristics such as improved water solubility, anionic or cationic features, antifouling and antimicrobial activities, amphiphilic behavior and other characteristics [12-14].

Some studies have developed *N*-alkyl derivatives of chitosan exhibiting reasonable water solubility, swelling behavior, and micellar aggregation in solution for applications as drug carriers, nucleic acid transfection in gene therapy and blood compatibility [13,15]. The *N*-

acylation of chitosan with fatty acids with different alkyl chain lengths and degree of substitution can add adjustable hydrophobic interactions for use as hydrogel matrices in tissue engineering [15,16].

Another innovative strategy for the derivatization of chitosan is associated with the introduction of amino acid moieties (*i.e.,* monomeric units of proteins) with acidic, basic or hydrophobic characteristics, to the backbone of the polymer chain. This strategy has been used to modify and improve the physicochemical properties of chitosan such as solubility and mucoadhesiveness and gives rise to some interesting synergistic features for using in tissue engineering, as well as other potentially useful biomedical properties, including anticoagulant, antimicrobial, and anti-cholesterol activities as well as the increasing interest in the field of tissue engineering [17,18]. The conjugation reactions of amino acids with chitosan have been conducted principally on the free amino groups of chitosan, usually by direct coupling forming covalent amide bonds [18]. An interesting phenomenon resulting from the functionalization of chitosan with amino acids is the introduction of carboxylic groups and additional amino groups, which in combination, increase the water-solubility of chitosan at neutral and up to alkaline pH values. This characteristic is highly desirable considering the limited solubility of chitosan (*i.e.,* pH > 6.0), which can compromise its application in several biomedical areas [18].

Thiomers (or thiolated polymers) are produced by the immobilization of thiol-bearing ligands onto the polymer backbone, which results in a significant improvement in mucoadhesion. Thiolated chitosan has a high level of cohesive-, mucoadhesive-, enzyme inhibitory-, and permeation-enhancing properties. Thus, there is a vast field to be exploited based on the combination of chemical functionalities with the chitosan polysaccharide backbone producing a new class of thiolated chitosan polymers such as *N*-acetyl cysteine-chitosan and *N*-acetyl-chitosan for numerous biomedical applications [19]. The immobilization of thiol groups to form chitosan derivatives (*i.e.,* thiolated chitosan) can promote and enhance numerous biological and biochemical properties due to the formation of disulfide bonds with cysteine-rich subdomains of glycoproteins commonly encountered in biological systems (*e.g.,* cells and tissues) [20-23]. Interestingly, although there is an increasing interest in recent

years in the development of thiolated polymers and chitosan derivatives for biomedical applications such as drug delivery carriers, nucleotide transfection for gene therapy, mucoadhesive and antimicrobial activities, no report was found in the published literature investigating the production of 3D porous scaffold hydrogels made of cysteine-chitosan and *N*-acetyl-chitosan for potential applications in soft tissue repair [20,21,23].

Thus, in this study novel multifunctional thiolated polysaccharides were designed and produced based on the chemical functionalization of chitosan backbone with cysteine amino acid and *N*-acyl-thiol moiety for producing 3D scaffolds aiming at potential soft tissue engineering applications. The highly porous 3D scaffold hydrogels with complex interconnected and hierarchical architecture demonstrated physicochemical properties and *in vitro* biocompatibility suitable to be prospectively applied as biomaterial support for cartilage repair in soft tissue engineering.

## 3.2 Materials and Methods

### 3.2.1 Materials

All the reagents and precursors, sodium hydroxide (Sigma, USA, ≥ 99 %, NaOH), hydrochloric acid (Sigma-Aldrich, USA, 36.5 – 38.0 %, HCl), 11-Mercaptoundecanoic acid (Sigma-Aldrich, USA, ≥ 95 %, MM = 218.36 g.mol$^{-1}$, $HSCH_2(CH_2)_8CH_2COOH$), ethanol (Synth, Brazil, 99.8 %, $CH_3CH_2OH$), 2-Propanol (Sigma-Aldrich, USA, anhydrous 99.5 %, $(CH_3)_2CHOH$), Acetic acid (Synth, Brazil, 99.8 %, MM = 60.05 g.mol$^{-1}$, $CH_3CO_2H$), L-cysteine (Aldrich, USA, $HSCH_2CH(NH_2)CO_2H$, MM = 121.16 g.mol$^{-1}$), *Ellman's* reagent (Sigma-Aldrich, USA, DTNB, 5,5′-Dithiobis(2-nitrobenzoic acid), MM = 396.35 g.mol$^{-1}$, [-$SC_6H_3(NO_2)CO_2H]_2$), EDC (Sigma-Aldrich, USA, $C_8H_{17}N_3{\cdot}HCl$ *N*-(3-Dimethylaminopropyl)-*N*′-ethylcarbodiimide hydrochloride, MM = 191.7 g.mol$^{-1}$), Sulfo-NHS (*N*-hydroxysulfosuccinimide sodium salt, Aldrich, USA, ≥ 98 %, $C_4H_4NNaO_6S$, MM = 217.13 g.mol$^{-1}$), sodium phosphate dibasic (Sigma-Aldrich, USA, ≥ 99.0 %, MM = 141.96 g.mol$^{-1}$, $Na_2HPO_4$), potassium phosphate monobasic (Sigma-Aldrich, USA, ≥ 99.0 %, MM = 136.09 g.mol$^{-1}$, $KH_2PO_4$), potassium chloride (Sigma-Aldrich, USA, ≥ 99.0 %, MM = 74.55 g.mol$^{-1}$, KCl), sodium chloride (Sigma-Aldrich, USA, ≥ 99.0 %, MM = 58.44 g.mol$^{-1}$, NaCl) were used as-received. High-molecular-mass chitosan powder (CHI, molar mass, MM

= 310,000 to >375,000 g.mol$^{-1}$, deacetylation degree (DD) ≥ 75.0 %, and viscosity 800-2000 cPoise, at 1 % in 1 % acetic acid, Aldrich, USA) was used for polymer modification. Deionized water (DI-water) (Millipore Simplicity™) with a resistivity of 18 MΩ·cm was used to prepare all solutions. All preparations and syntheses were performed at room temperature (RT, 25 ± 2) ˚C unless otherwise specified.

### 3.2.2 Synthesis of thiolated chitosan derivatives - Thiomers

#### 3.2.2.1 Amino acid functionalization of chitosan with cysteine (CHICys)

The synthesis of chitosan (CHI) with cysteine (CYS) was performed according to the molar ratio of reagents 1:2:2 (CHI:EDC:CYS) adapted from the process reported in the literature [17]. Briefly, 0.5 g of chitosan powder was dissolved in 30 mL of 2 % (v/v) acetic acid aqueous solution overnight for complete solubilization. The pH was adjusted to 4.5±0.5 (NaOH, 1.0 mol·L$^{-1}$). In the sequence, 0.7 g of cysteine powder was dissolved in 20 mL of phosphate-buffered saline (PBS) solution, 1.2 g of EDC and 0.32 g of sulfo-NHS were added and maintained under moderate stirring for 1 h at room temperature (referred to as CYS/EDC/NHS solution). Then, the CYS/EDC/NHS solution was added to the chitosan/acetic acid solution (*i.e.*, total volume = 57 mL, molar ratio of 1:2:2/CHI:EDC:CYS) and the pH was adjusted to 5.0±0.5 (NaOH, 1.0 mol·L$^{-1}$). The coupling reaction *via* the formation of amides was performed at room temperature under moderate stirring for 5 h in the darkness. Next, the mixture was dialyzed in the darkness against distilled water using a membrane (12–14 kDa, Sigma, USA) for 7 days at RT to remove unreacted species and water-soluble contaminants for further preparing the hydrogels.

#### 3.2.2.2 *N*-Acylation of chitosan with 11-mercaptoundecanoic acid (CHIMerc)

Although not previously reported in the literature, the *N*-acylation of chitosan with 11-mercaptoundecanoic acid (MERC), a similar procedure using the modification of chitosan with cysteine was adapted for the synthesis of chitosan functionalized with the hydrophobic acyl chain using MERC. Thus, based on the molar ratio of reagents 1:2:2 (CHI:EDC:MERC), 0.5 g of chitosan powder was dissolved in 30 mL of 2 % (v/v) aqueous acetic acid solution overnight for complete solubilization, and the pH was adjusted to 4.5±0.5 (NaOH, 1.0 mol·L$^{-1}$). In the sequence, 1.36 g of MERC was dissolved in 60 mL of PBS buffer

solution/isopropanol (30/30) (v/v). Next, 1.2 g of EDC and 0.32 g of sulfo-NHS were added to the solution and maintained under moderate stirring for 1 h at room temperature (referred to as MERC/EDC/NHS solution). The MERC/EDC/NHS solution was added to chitosan/acetic acid solution (*i.e.*, total volume = 91 mL, molar ratio of 1:2:2/CHI:EDC:MERC), and the pH was adjusted to 5.0±0.5 (NaOH, 1.0 $mol \cdot L^{-1}$). The acylation reaction was performed at room temperature under moderate stirring for 5 h in the darkness. In the sequence, the mixture was dialyzed in the darkness against distilled water using a membrane (12–14 kDa, Sigma, USA) for 7 days at RT to remove unreacted species and water-soluble contaminants for further preparing the hydrogels.

### 3.2.3 Preparation of 3D porous scaffolds of chitosan thiomers

To obtain polymer matrices with porous three-dimensional structures, samples of the previously prepared solutions (CHICys and CHIMerc) were poured into plastic tubes (1.5 mL in *Eppendorfs*) and frozen at -4±2 ˚C for 72 h and freeze-dried (ModulyoD, Thermo Electron Corporation, Wathan, Massachusetts, USA) at -50 ˚C and 400±100 µbar until the samples reached a constant mass (approximately 72 h). The freeze-drying process was the same, and the parameters (temperature, pressure, time) were maintained unchanged for all the samples produced. The thiolated-chitosan scaffolds were produced with a foam-like aspect and stored at 4±2 ˚C until further use.

### 3.2.4 Characterization of chitosan thiomers and 3D porous scaffolds

#### 3.2.4.1 Determination of thiol functionalization of chitosan by *Ellman's* reagent protocol

The determination of the total of the thiol groups in the CHICys chain was performed using the *Ellman's* reagent protocol as reported previously in the literature [24]. Briefly, 5 mg of CHICys polymer was dissolved in 2 mL of deionized water. Next, the test solution was prepared by mixing 100 µL of the CHICys solution with 900 µL of 0.5 M phosphate buffer (PBS, pH 8.0) and 1 mL of *Ellman's* reagent (DTNB, 3 mg in 10 mL of 0.5 M PBS, pH 8.0). After incubation for 2 h at room temperature with light protection, the polymer/PBS/DTNB solution was centrifuged at 4000 rpm for 10 min. The absorbance of the supernatant was measured at a wavelength of $\lambda$ = 450 nm with a Lambda EZ-2100 spectrophotometer (Perkin

Elmer, USA) using a quartz cell with an optical path length of 10 mm. The amount of thiol groups was calculated from a calibration curve of cysteine in a concentration range of 1600 – 20 µM prepared exactly like the samples (Fig. S1.a). Analogously, a similar procedure was performed to determine the total number of thiol groups in the CHIMerc samples, but with the minor alteration of dissolving the chitosan thiomers in ethanol instead of in DI water because of the relative hydrophobicity (*i.e.*, 5 mg of CHIMerc polymer was dissolved in 2 mL of ethanol). Thus, the total amount of thiol functionalization was calculated using the calibration curve of 11-mercaptoundecanoic acid in a concentration range of 2400 – 90 µM and made in the exactly same way as the samples (Fig. S1b). All experiments were conducted in triplicate (n = 3) unless specifically noted. Statistical analysis of the results was performed using the mean and standard deviation, where necessary.

The degree of functionalization (DF) of chitosan with CYS and MERC was estimated based on the total number of available reaction sites in the chitosan chains before the functionalization reactions and on the results obtained by the *Ellman's* method (µmol.g$^{-1}$) (Equation 3.1):

$$DF\ \% \ = \ [(N_{Ellman} \times 161)\ /(W_{CHI} \times DD)]\ x\ 100 \qquad (3.\ 1)$$

where $N_{Ellman}$ is the number of thiol groups obtained by the *Ellman's* method (mol); $W_{CHI}$ is the mass of chitosan used in the synthesis (g); 161 is the average molar mass of 2-amino-2-desoxi-D-glucose units of chitosan (g.mol$^{-1}$); *DD* is the degree of deacetylation of chitosan (DD = 0.85, obtained by NMR in our previous study) [25].

### 3.2 Spectroscopic characterization of chitosan thiomers and 3D porous scaffolds

Fourier transform infrared (FTIR) spectra were obtained using an attenuated total reflectance method for all samples (ATR, ZnSe crystal prism, 4000 – 650 cm$^{-1}$ using 32 scans and a 4 cm$^{-1}$ resolution - Nicolet 6700, Thermo-Fischer). All of the experiments were conducted in triplicate (n = 3) unless specifically noted.

Raman spectroscopy was performed with a LabRam-HR 800 (Horiba/Jobin Yvon) equipped with an Olympus BX-41 microscope provided with lenses of 10×, 50× and 100× and an additional macro lens of 40 mm for all samples. A 632.8 nm excitation from a helium-neon laser was focused on a spot of 1-2 $\mu m^2$ in the samples. The back-scattered light collected was dispersed by a monochromator and detected by the $LN_2$ (liquid nitrogen)-cooled CCD (charge-coupled device) system. The spectra ranged from 200 $cm^{-1}$ to 3300 $cm^{-1}$ with a step size of 1.1 $cm^{-1}$. Depending on the background fluorescence, the acquisition time was set from approximately 60 s to 300 s, with a minimum ten replicates to increase the signal-to-noise ratio.

$^1$H-NMR (proton nuclear magnetic resonance) spectra of CHI, CHICys and CHIMerc samples were recorded at 50 ˚C in $D_2O$/DCl using a Bruker-400 MHz Varian spectrometer (90° pulse and 16 scans).

### 3.2.4.3 Characterization of swelling degree and gel-fraction behavior of thiolated-chitosan 3D porous scaffolds

The swelling degree (SD) of all samples was evaluated in deionized water (pH = 5.5±0.5) as described in the literature [12, 26]. Briefly, the samples were weighed before ($W_i$, "dry state") and after immersion in DI water ($W_s$, "swollen state") for the specific time period. After the immersion, any excess of solution was gently removed from the sample surface with a cellulose filter paper and then weighed. In the sequence, the sample was dried at 40±2 ˚C in an oven for 24 h (*i.e.,* faster drying process compared to room temperature, until mass stabilization) and the final weight was recorded. This process was repeated for different time intervals 1, 2, 3, 4 and 24 h to assess the swelling degree until reaching the equilibrium for the chitosan-based hydrogels, which was evaluated using Equation 3.2:

$$SD\ (\%) = [(W_s - W_i)/W_i]\ x\ 100 \qquad (3.\ 2)$$

where $W_s$ is the weight of the swollen polymer, and $W_i$ is the initial weight of the polymer.

The chemical stability *in vitro* in aqueous solution (referred to as the gel fraction, GF) of thiolated chitosan samples was assessed by measuring the GF, according to Equation 3.3 [27].

$$GF\ (\%) = \left\{1 - \left[\left(W_i - W_f\right)/W_i\right]\right\} x\ 100 \qquad (3.\ 3)$$

where $W_i$ is the initial mass of the polymer, and $W_f$ is the mass of the dried polymer after the swelling procedure.

These experiments were performed with 21 samples for each system (n = 21, 7 samples of 3 different synthesis of each polymer, CHI, CHICys, CHIMerc). The results were averaged and statistical analysis was performed using ANOVA (one way included Tukey's test, $p < 0.05$, software Origin v.8.1, OriginLab Corporation, USA).

**3.2.4.5 Morphological analysis of thiolated-chitosan 3D porous scaffolds**

The morphologies of the freeze-dried CHICys and CHIMerc scaffolds were evaluated using a scanning electron microscope (SEM, FEI-FEG-FIB-QUANTA 3D) coupled with energy dispersion X-ray spectroscopy (EDX, EDAX Bruker, 0.8 nm). Before examination, the samples were coated with a thin carbon film *via* sputtering using a low deposition rate, cooling the substrate, and ensuring the maximum distance between the target and the sample to avoid sample damage; the film formed was 30 nm. Images of secondary electrons (SEs) were obtained using an accelerating voltage of 15 kV for all samples on two different planes (transversal and superficial). SEM images were collected and the pore size was estimated based on at least 50 random measurements using the open source image processing program (ImageJ v.1.50+, National Institutes of Health, NIH). The results were averaged, and statistical analysis was performed using ANOVA (one way included Tukey's test, $p < 0.05$, software Origin v.8.1, OriginLab Corporation, USA).

The three-dimensional structures of the scaffolds were investigated using 3D microtomography (SkyScan 1174, Bruker micro-CT) at a resolution of 12.18 μm, at 40 kV voltage, 100 μA current, 0.7° rotation step, and no filter. Images were reconstructed using

NRecon Reconstruction software (v.1.6.1.18, Bruker micro-CT). CTAn software (v.1.15.4.0, Bruker micro-CT) was used to analyze the micro-CT datasets in 2D and 3D for morphometry and densitometry, and CTVol software (v. 2.3.1.0, Bruker micro-CT) was used for 3D visualization of the scaffolds.

Additionally, the mass of the dry, wet and submerged scaffolds was measured using the accessory SMK-301/400 (Shimadzu) coupled to a balance (±0,0001 g) and the densities ($\rho_a$, Equation 3.4) were calculated according to the equipment manual. The porosities (ε) were calculated according to the *Archimedes's* Method [28] (Equation 3.5). The surface areas ($S_a$) were estimated by a method used to determine the surface area of powder materials (Equation 3.6) [29].

$$\rho_a = (W_{(d)}/(W_{(d)} + W_{(l)}))\, x\, \rho_{(l)} \quad (3.4)$$

$$\varepsilon\,(\%) = [(W_{(w)} - W_{(d)})/(W_{(w)} - W_{(l)})]\, x\, 100 \quad (3.5)$$

$$S_a = 3/(\rho_a.(d_m/2)) \quad (3.6)$$

Where $W_{(d)}$ is the mass of sample dry (g), $W_{(w)}$ is the mass of sample in water or alcohol (g), $W_{(l)}$ is the mass of the sample submerged, $\rho_{(l)}$ is the density of water or alcohol at the temperature of experimental analysis (19 ˚C; 0.9984 and 0.79 g.cm$^{-3}$ to water and alcohol, respectively), $S_a$ is the surface area (m$^2$·g$^{-1}$), $\rho_a$ is the bulk density, and $d_m$ is the average diameter (*m*) obtained by micro-CT or by SEM analysis.

**Surface Contact Angle (SCA)**

The effect of thiolation of chitosan with CYS and MERC moieties on the hydrophilic/hydrophobic behavior was evaluated *via* contact angle measurements. The tests were performed by pouring DI water droplets using a microsyringe (50 μL) onto CHI, CHICys and CHIMerc films and capturing the images for contact angle calculations (Lumix FZ-47 digital camera, Panasonic, Tokyo, Japan and open source image processing program, ImageJ Fijji, NIH).

### 3.2.5 Biological assays of thiolated-chitosan 3D porous scaffolds

**Cell viability assay by MTT (3-(4,5-dimethylthiazol-2yl) 2,5-diphenyl tetrazolium bromide):** Human osteosarcoma cells (SAOS) and the kidney cell line of human embryos (HEK 293 T) were kindly provided by Prof. A. Goes of the Department of Immunology and Biochemistry, UFMG. The cells were cultured in Dulbecco's modified eagle medium (DMEM) with 10 % fetal bovine serum (FBS), penicillin G sodium (10 units·mL$^{-1}$), streptomycin sulfate (10 mg·mL$^{-1}$), and 25 µg·mL$^{-1}$ amphotericin-b (all from Gibco BRL, NY, USA) in a humidified atmosphere of 5 % $CO_2$ at 37 ˚C. The cells were used for the experiments at passage twelve. All of the biological tests were conducted according to ISO standards (ISO 10993-5:2009/(R)2014 (Biological evaluation of medical devices: Tests for *in vitro* cytotoxicity)). SAOS and HEK 293 T cells were plated ($3 \times 10^4$ cells) on each sample material. The plates were subjected to UV radiation for 60 min in a sterile flow and washed quickly in ice-cold PBS. The samples were sterilized by UV radiation for 60 min in a sterile flow. Controls were created using cells and the DMEM medium (10 %); Triton x-100 (1 %; Sigma-Aldrich, St. Louis, MO, USA) was used as a positive control, and chips of sterile polypropylene (1 mg·mL$^{-1}$; Eppendorf, Hamburg, Germany) were used as a negative control. After 24 h, all media were aspirated and replaced with 210 µL of culture medium with serum. MTT (170 µL, 5 mg·mL$^{-1}$; Sigma-Aldrich, St. Louis, MO, USA) was added to each well and incubated for 4 h followed by incubation 16 h with SDS/4 % HCl. Subsequently, 100 µL was removed from each well and transferred to a 96-well plane, and the absorbance was quantified using a Varioskan Reader (Thermo Scientific) with a 595-nm filter. The values obtained were expressed as the percentage of viable cells according to Equation 3.7.

$$Cell\ viability\ (\%) = \frac{Absorbance\ \text{of}\ samples\ and\ SAOS\ cells \times 100}{Absorbance\ (control)} \qquad (3.\ 7)$$

All of the experiments were performed in triplicate (n = 3). The results were averaged, and statistical analysis was performed using ANOVA (one way included Tukey's test, $p < 0.05$, software Origin v.8.1, OriginLab Corporation, USA).

**Cell viability assay by LIVE/DEAD®:** SAOS and HEK 293 T cells on passage 13 and 8, respectively, were synchronized in a serum-free medium for 24 h. After this period, cells

were trypsinized and seeded ($3 \times 10^5$ cells/well) on hydrogel foams (1 mg hydrogel and 200 µL medium, w/v) and placed in a 96-well plate. The reference controls were cells cultured in the DMEM medium with 10 % FBS. After 24 h, all of the media were aspirated, and the cells were washed two times with 10 mL of phosphate buffered saline (PBS, Gibco BRL, NY, USA). Cells were treated with the LIVE/DEAD® Viability/Cytotoxicity kit (Life Technologies of Brazil Ltd., São Paulo, Brazil) for 30 min, according to the manufacturer's specifications. Images of fluorescent emissions were separately acquired, calcein at 530±12 nm, and EthD-1 (ethidium homodimer-1) at 645±20 nm, with an inverted optical microscope (Leica DMIL LED, Germany).

## 3.3 Results and Discussion

### 3.3.1 Characterization of chitosan thiomers and 3D porous scaffolds

#### 3.3.1.1 Characterization of degree of substitution *via* Ellman's reagent method

The primary amino group at the 2-position of the glucosamine subunits of chitosan is the main target for the immobilization of thiol groups. The sulfhydryl-bearing reagents can be attached to this primary amino group *via* the formation of covalent amide bonds, using the carboxylic acid groups of the CYS and MERC molecules reacting with the primary amino group of chitosan mediated by a water soluble carbodiimide as schematically depicted in Figure 3.1A.

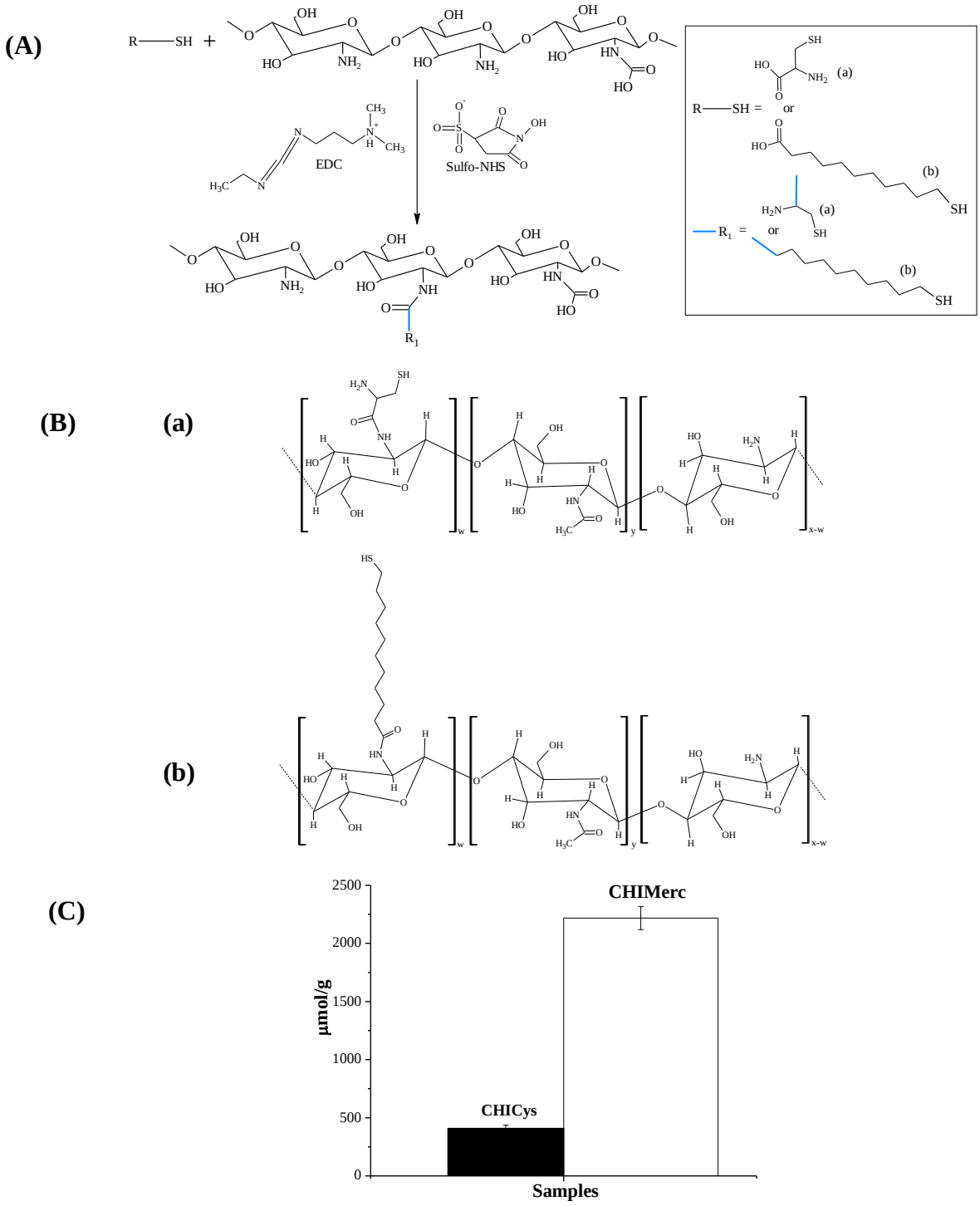


Figure 3. 1. (A) Schematic representation of chemical functionalization of chitosan with thiol precursors (a) CYS and (b) MERC. (B) Chitosan thiomers produced (a) CHICys and (b) CHIMerc (x = 0.85, y = 0.15, and w = 0.85 x DF; DF is 0.05 and 0.26 for CYS and MERC, respectively). (C) Histogram of thiol content inserted in chitosan chain estimated by Ellman´s reagent (µmol.g$^{-1}$).

The number of thiol groups on the chitosan-based thiomers was determined *via Ellman's* reagent [20]. Figure 3.1B shows the chemical structure of the chitosan thiomers of CHICys (a) and CHIMerc (b), respectively. Figure 3.1C presents the results of the concentration of thiol groups of CHICys (409±27) $\mu mol \cdot g^{-1}$ and CHIMerc (2218±100) $\mu mol \cdot g^{-1}$ obtained by *Ellman´s* method. The degree of substitution of thiol groups in this study was relatively higher than others found in the literature [20,24,30,31], although the *N*-acylation of chitosan using 11-mercaptoundecanoic acid has not been reported before. This more effective thiolation process can be assigned to distinct optimized experimental conditions such as the buffer solution and solvent (*i.e.*, PBS in water), the use of sulfo-NHS combined with EDC as a zero-length coupling agent (stabilization of intermediates formed), temperature, pH, concentration of reagents, time of reaction, degree of deacetylation and molar mass of chitosan and others. In addition, a much higher concentration (over 400 %) of thiol groups was verified in the CHIMerc compared to CHICys, which was suggested to be mostly caused by the orientation of the reacting molecule MERC as an amphiphilic molecule (*i.e.*, "polar carboxylic head" and "hydrophobic thiol-acyl tail") favoring the formation of amide bonds with amino groups of chitosan. However, as cysteine is a polarizable amino acid, it can be repelled by electrostatic forces with charged groups of chitosan (amino) leading to a reduction of the degree of substitution [32,33].

Nonetheless, the high concentration of thiol groups found in this study (degree of substitution of 5±1 % and 26±2 %, CHICys and CHIMerc, respectively) possesses advantages for improving the properties of pristine chitosan in potential biomedical applications such as water solubility, cytocompatibility and mucoadhesion [24,31].

### 3.3.1.2 Spectroscopic characterization of chitosan thiomers

Chitosan is a copolymer composed of *N*-acetyl-D-glucosamine and D-glucosamine repeating units with several chemical groups, which can be extensively characterized by FTIR spectroscopy. As a general analysis of the FTIR spectra (Figure 3.2A), the typical chitosan bands can be identified in all samples: The amide I bands at ~1655 $cm^{-1}$; the amide II band at 1560 $cm^{-1}$; the amide III band at 1315–1320 $cm^{-1}$; the broad OH and NH stretching bands at 3450 $cm^{-1}$; C-H stretching bands between 2800–2900 $cm^{-1}$; the $–CH_2$ bending at 1420 $cm^{-}$

[1]; the bands assigned to C-O stretching at 1030 $cm^{-1}$ and 1075 $cm^{-1}$; and the band at 897 $cm^{-1}$, related to C-O-C glycosidic linkage [12,13].

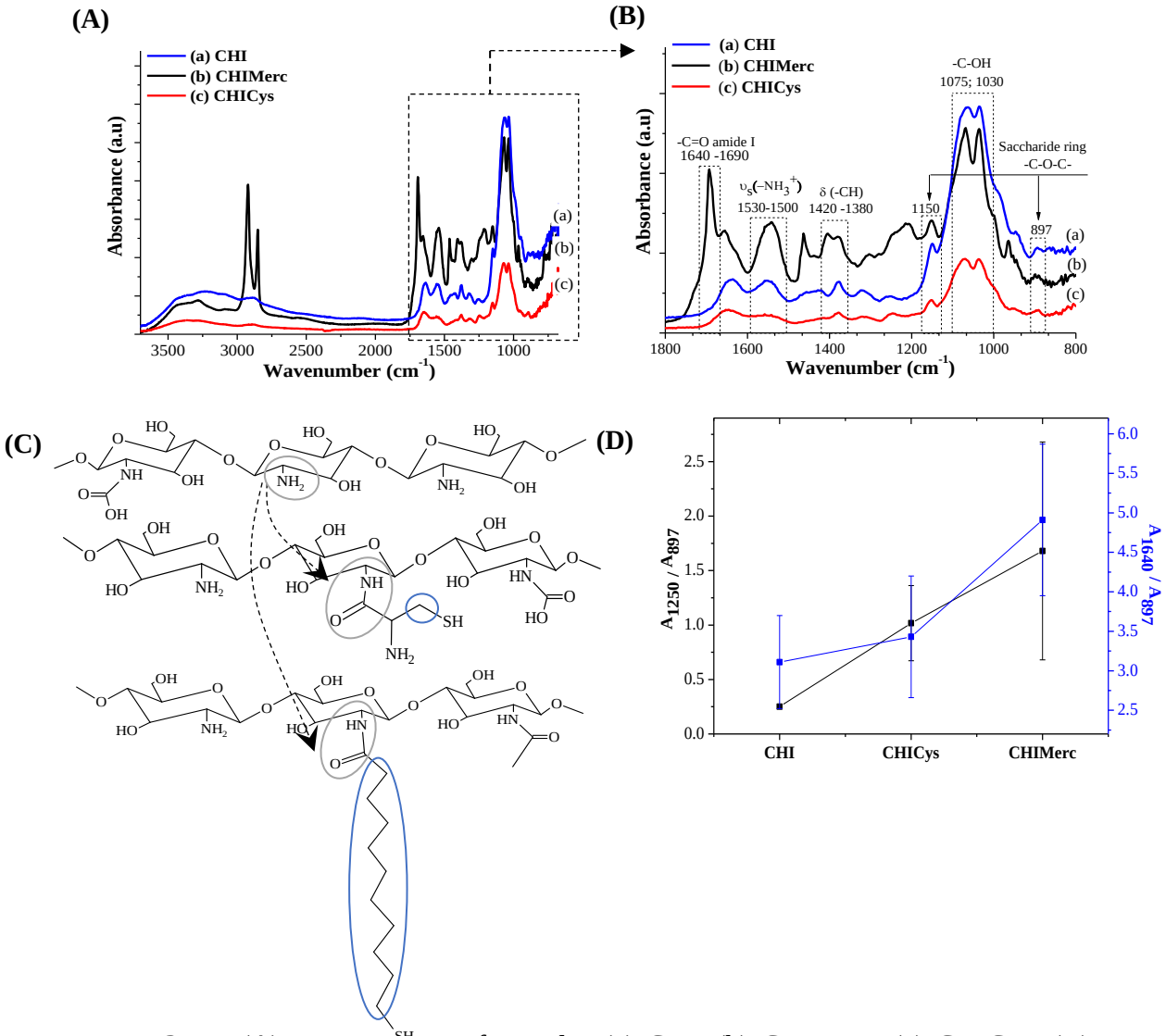


Figure 3. 2. (A) FTIR spectra of samples (a) CHI, (b) CHIMerc, (c) CHICys; (B) FTIR spectra with changes of bands of amine and amide groups (a) CHI, (b) CHIMerc, (c) CHICys; (C) Chemical representation highlighting the changes in the chitosan chains with the thiol functionalization (a) CHI, (b) CHIMerc, (c) CHICys; (D) The relationship between bands at 1640/897 $cm^{-1}$ and 1250/897 $cm^{-1}$ for each sample.

The differences observed by comparing the IR spectra can be associated with the functionalization by the thiol precursors (*i.e.*, CYS and MERC) with the primary amine in chitosan glucosamine units (Figure 3.2B In CHIMerc (b), and CHICys (c) spectra, the C-N

(1250 - 1320 $cm^{-1}$) and NH (~1550 $cm^{-1}$) bands shifted towards lower frequencies, which can be attributed to the addition of a heavier group after the amide bond formation [13,16]. In addition, the formation of amide groups also increases the amide I band due to the augmentation of C=O stretching vibrations. Moreover, for both functionalization moieties, *i.e.*, CYS and MERC, there is an insertion of $CH_2$ groups in the chitosan polymer structure, especially for CHIMerc, which possess an alkyl chain with 10 carbons. Therefore, the thiolation of chitosan in this study was qualitatively confirmed by the increase in bands related to $CH_2$ vibrations at approximately 2900 $cm^{-1}$ and 1420 $cm^{-1}$. Moreover, the FTIR spectra indicated the presence of weak signals of sulfur-based groups at approximately 770 – 730 $cm^{-1}$ (-S-C) and 2560 – 2500 $cm^{-1}$ (-SH) in thiol-containing chitosan samples (CHICys and CHIMerc).

Considering the glycoside linkage band (897 $cm^{-1}$) of chitosan as the reference, which is not expected to be significantly affected by the chemical reaction at the primary amino group [12], and comparing the relative changes in amide III band (C-N bond) associated with the amide bond formation, it was possible to estimate the extension of the functionalization process. Changes in amide I region (~1640 $cm^{-1}$) can also be used to estimate the degree of functionalization. Compared with the CHI spectrum (Figure 3.2B (a)), the changes in CHIMerc spectrum (Figure 3.2B (b)) are more remarkable than those in the CHICys spectrum (Figure 3.2B (c)), attributed to the length of the alkyl chain and the higher degree of functionalization, as verified by *Ellman´s* reagent in the previous section. The chemical representations of the changes in chitosan chains with the thiol functionalization, according to the FTIR analysis, are shown in Figure 4.2C. The ratio between reference (897 $cm^{-1}$) and amide (1640 $cm^{-1}$ and 1250 $cm^{-1}$) bands (related to both areas and intensities of these selected bands) are shown in Figure 4.2 D [30,34-36].

As thiol bands are weakly detectable in FTIR, Raman spectroscopy was used as a complementary technique for further characterization of the chitosan thiomers. The results are shown in the Raman spectra in Figure 3.3A highlighting the bands related to sulfur groups of thiol chitosan samples (CHICys and CHIMerc) at 2800 – 2700 $cm^{-1}$ (-S-$CH_2$-$CH_2$), 610 $cm^{-1}$, 530 $cm^{-1}$ (S-S), 770 – 730 $cm^{-1}$ (-S-C), and 2560 – 2500 $cm^{-1}$ (-SH) [37,38]. However,

the major band related to thiol groups (-SH) at 2560 – 2500 $cm^{-1}$ appeared only in the CHIMerc (Figure 3.3B), most likely due to the much higher degree of substitution compared to CHICys evaluated by *Ellman´s* method in the previous section [37,38]. Moreover, the bands associated with stretching and bending vibrations of the $CH_2$ species at 2800-3000 and 1400 – 1200 $cm^{-1}$ were stronger in the CHIMerc sample than in the CHICys and CHI samples, which were assigned to the contributions of *N*-acylation of the chitosan polymer with the MERC alkyl chain (*i.e.*, inserting 10 $CH_2$ groups) [37,38]. Minor signals were detected at 530 $cm^{-1}$ in the CHICys and the CHIMerc samples, which indicated the formation of disulfide bonds (S-S) by adjacent thiol groups [37,38].

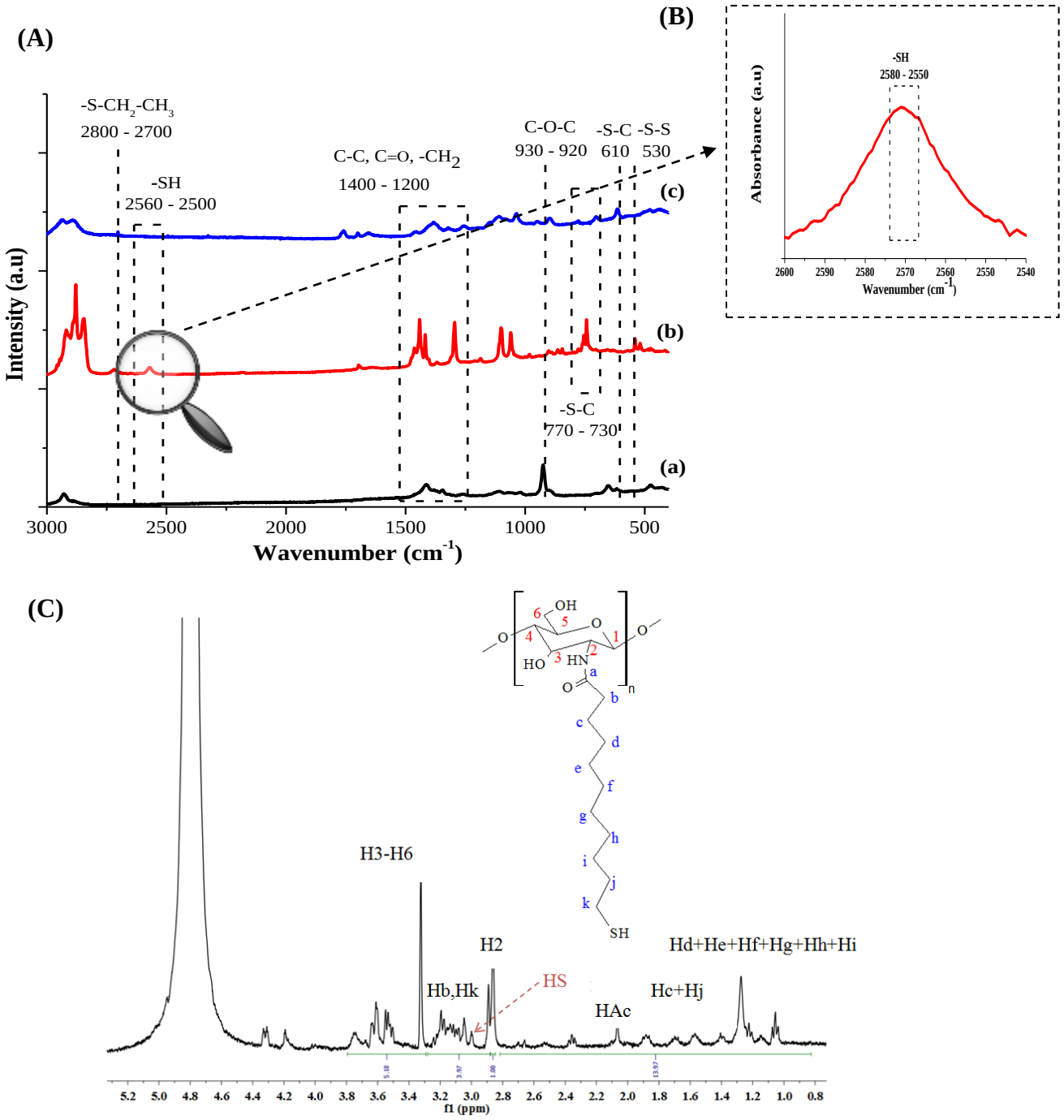


Figure 3. 3. (A) Raman spectra of samples (a) CHI; (b) CHIMerc and (c) CHICys; (B) Raman spectra of all thiol chitosan samples highlighted the thiol group and (C) $^{1}$H-NMR spectrum of CHIMerc.

Nuclear magnetic resonance spectroscopy (NMR) has been widely used as a characterization tool for evaluating polysaccharides such as chitosan and its functionalized derivatives. Thus,

in this study, $^{1}$H-NMR spectroscopy was used as a supporting technique for further investigating the functionalization of the chitosan backbone by thiol modifiers (*i.e.*, cysteine and MERC). Principally, both samples (CHICys, Fig. S2 and CHIMerc, Figure 3.3C) showed the peak at approximately 2.0 ppm indicating the three *N*-acetyl protons of the *N*-acetyl glucosamine residue ($NHCOCH_3$) due to the incomplete deacetylation of chitosan. In addition, the saccharide ring protons of chitosan usually resonating at approximately 3.4 – 5.0 ppm were detected [13,24,25,36,39]. Regarding the functionalization of chitosan, the protons in thiol groups can easily be replaced by D in $D_2O$ used for NMR sample preparation, making it undetectable in the NMR spectrum. Nonetheless, the signal at δ 2.7 - 2.9 ppm is commonly assigned to methylene protons adjacent to thiol groups ($-S-CH_2$), which can be perceived as evidence for the existence of thiol groups immobilized on chitosan backbones [24,36,39,40]. Moreover, the $^{1}$H-NMR spectrum of CHIMerc indicated the incorporation of aliphatic chain residues due to the appearance of signals corresponding to acyl chain protons at 3.1 - 3.3 ppm, 1.9 - 1.4 ppm and 1.3 - 1.0 ppm (greater δ related to α $-CH_2-$ and β $-CH_2-$ and smaller δ for $-(CH_2)_{d-i}-$) as indicated in Figure 3.3C [13]. These results confirmed that CYS and MERC were successfully grafted onto the chitosan backbone forming thiomer-functionalized structures.

### 3.3.1.3 Swelling and degradation properties of thiolated-chitosan scaffolds

The results of swelling degree of chitosan and chitosan-thiolated scaffolds are presented in Figure 3.4A. A significant decrease of the swelling degree (SD) at equilibrium of chitosan from 2600 % to 2280 % and 1810 % for the thiomers, CHICys and CHIMerc, respectively, was observed after 24 h of immersion in deionized water (pH = 5.5±0.5, at room temperature, 26±2 ˚C). Although several methods are reported in the literature for evaluating the swelling degree of hydrogels, most of them present well-correlated results with no relevant difference for the overall tendency analyzed. These results are consistent with the FTIR findings and the degree of functionalization discussed in the previous sections, where the thiolation of chitosan occurred *via* the formation of amide bonds (*i.e.*, replacing $-NH_2$ groups by -SH groups), which led to a less chemically hydrophilic (or more hydrophobic) polymer matrix for water swelling. In addition, the introduction of thiol groups to the chitosan backbone favored further crosslinking of the polymer network by the formation of disulfide bonds

between adjacent groups *(i.e.*, -SH/-SH) [17, 24, 30]. Therefore, this effect contributed to the reduction of the swelling capacity of the chitosan-thiolated scaffolds produced. To this end, the reduction of swelling degree was more prominent in CHIMerc scaffolds due to the grafting of the hydrophobic acyl chain with terminal sulfhydryl group to the chitosan backbone, associated with a higher degree of functionalization compared to CHICys.

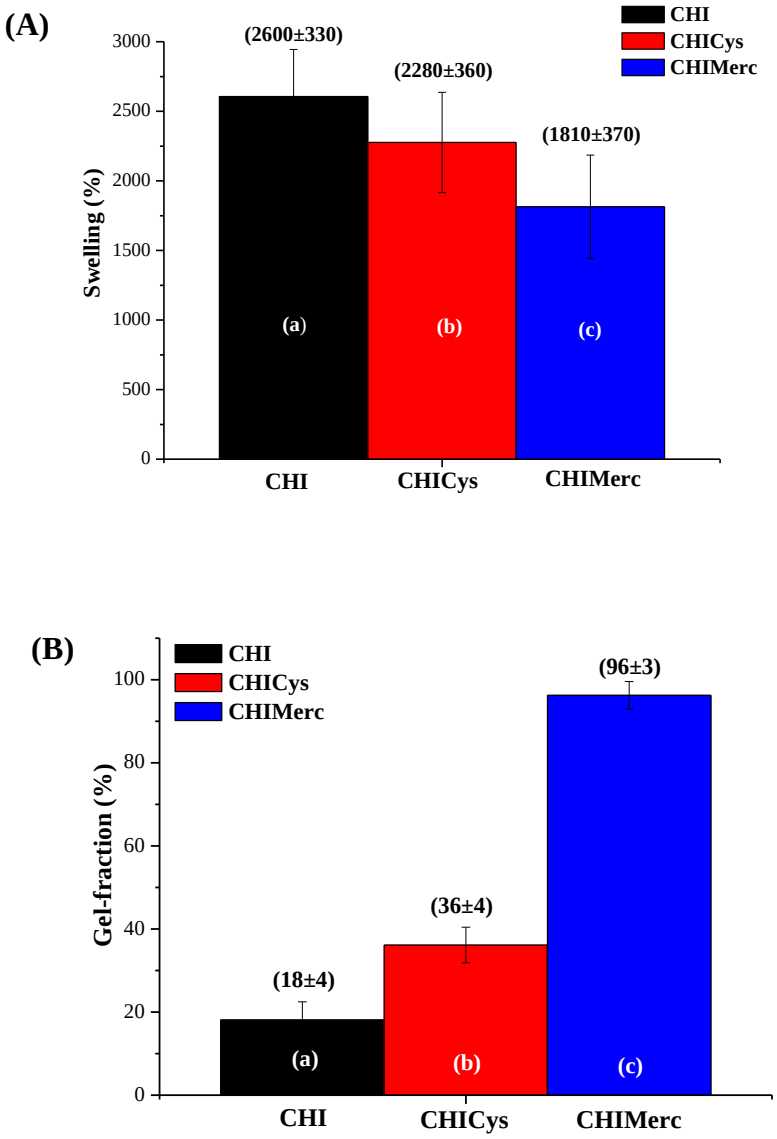


Figure 3. 4. (A) Swelling degree in deionized water (pH = 5.5±0.5) for all samples at 24 hours (n = 21) and (B) Gel fraction in deionized water (pH = 5.5±0.5) at 24 hours for all samples (n = 21).

Analogously, the *in vitro* chemical stability of these scaffolds was assessed by a gravimetric method after 24 h of immersion in deionized water (pH = 5.5±0.5), at room temperature (26±2 ˚C), which was applied to estimate the gel fraction (or degradation by solvation), and the results are presented in Figure 3.4B. As expected, the opposite trend for the GF compared to the swelling degree was verified. The swelling degree was decreased by grafting thiol moieties to the chitosan backbone. The results of GF indicated a higher chemical stability of the scaffolds produced with chitosan derivatives, *i.e.*, GF = 100 % and 36 % for CHIMerc and CHICys, respectively, and 18 % for chitosan. These results endorsed the previous findings, demonstrating the more hydrophobic behavior of thiolated chitosan derivatives due to the substitution of primary amino groups by thiol groups in the polymer chain and the incorporation of the acyl groups by coupling with MERC. Similar trends were reported in the literature for thiolated chitosan derivatives [17,36,41].

Thus, the results of swelling degree and gel fraction measurements demonstrated that these thiomer-based scaffolds made of chitosan derivatives showed physicochemical properties suitable for biomedical applications in soft tissue engineering where hydrophilic networks are highly needed associated with chemical stability in aqueous media. Moreover, the grafting of thiol groups onto the chitosan backbone tuned these properties, which may promote chemical interactions with more hydrophobic molecules (peptides, antibodies, proteins, enzymes, drugs, *etc*.) present in the biological microenvironment (*e.g.*, cells and tissues) [42-45].

#### 3.3.1.4 Morphological analysis by SEM, micro-CT and Archimedes' Method

The presence of thiol groups is a very interesting characteristic because the thiol groups can give the system bio-adhesive characteristics, permeation enhancement and anti-protease properties, and these characteristics are important because they influence the capacity of cells to adhere and proliferate [42]. In addition, if the tissue engineering applications are envisioned, cell adhesion to biomaterials is a crucial prerequisite for tissue repair and regeneration, and in this case, the morphology and structure of the surface of biomaterials are considered key features affecting the capacity of cells to adhere and proliferate [12,46]. Therefore, it is very important to understand the morphology of the scaffold, in particular

porosity, because this parameter strongly affects the mechanical and biological performance of the developed structures [12,46]. Among many alternatives, appropriate techniques for this purpose must be selected, because each technique has limitations, and a combination of different techniques is often required to achieve an in-depth study of the morphological properties of the scaffold. Then, for that proposal, scanning electron microscopy (SEM) analysis associated with micro-computed tomography (micro-CT) as nondestructive techniques can provide a comprehensive set of data and fulfill this role. In addition, the surface areas of the scaffolds were estimated based on the results obtained by the *Archimedes'* Method.

SEM is considered a traditional technique to characterize the material surface. This technique presents excellent resolution at the sub-micrometer range and is available in research centers and universities worldwide. However, the micro-CT, which was used initially to characterize the 3D trabecular microarchitecture of bone, has been exploited for several research studies for the morphological porous biomaterial characterization, and this technique enables a full assessment of porous structures, both in terms of pore size and interconnected porosity for the development of scaffold-based tissue engineering applications [12]. In that sense, the SEM analysis was performed, and all samples have presented highly tridimensional porous structure at the micrometer range (Figure 3.5). However, although all scaffolds presented sponge-like structures with pore size typically ranging from 100 and 350 µm, they clearly showed distinct morphological aspects. Chitosan scaffolds presented relatively larger average pore size of 389±188 µm than CHICys and CHIMerc thiomer derivatives of 223±72 and 225±95 µm, respectively. Moreover, CHICys scaffolds (Figure 3.5B) presented a more uniform pore size distribution than the CHIMerc sample despite similar average pore size values (Figure 3.5C), assigned to the possible interactions of the hydrophobic acyl chain of MERC with the water solvent during the freeze-drying process. Nonetheless, as far as biomedical application is concerned, these features of highly porous structures are very important to facilitate the diffusion of nutrients, biomolecules and cell metabolic by-products. In addition, pore sizes ranging from 100 to 350 µm are ideal for cell proliferation and the formation of new tissue [12,47-52].

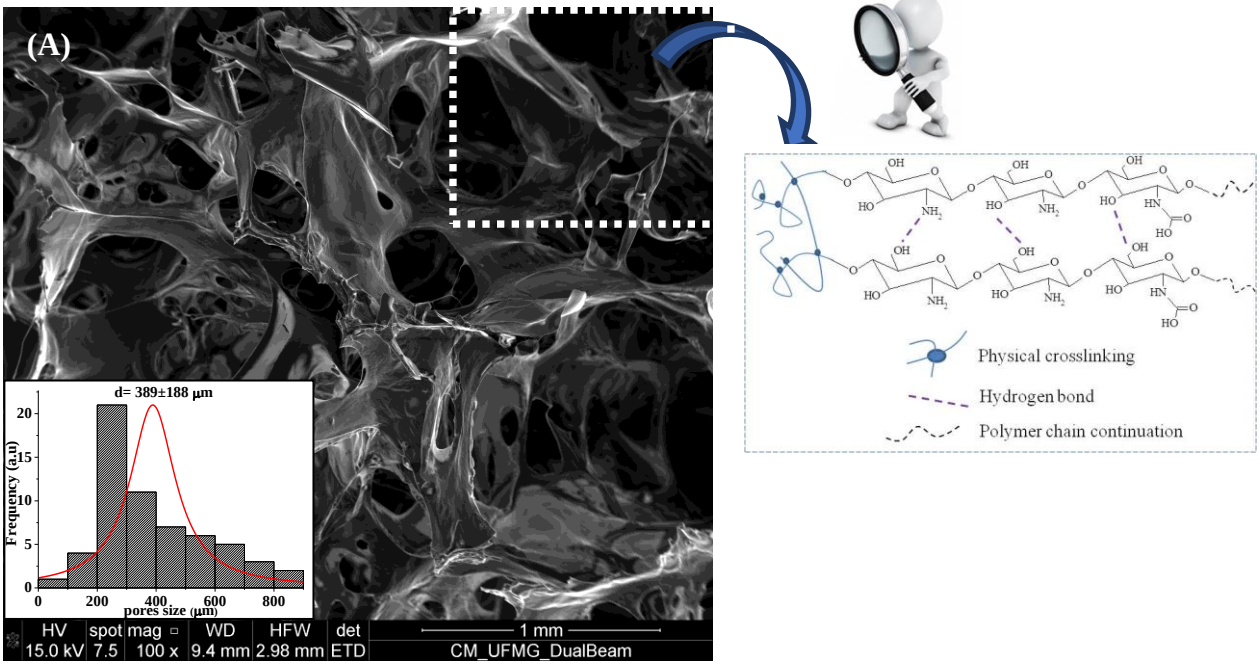
(A)
d= 389±188 µm
Frequency (a.u)
pores size (µm)
HV spot mag WD HFW det
15.0 kV 7.5 100 x 9.4 mm 2.98 mm ETD
1 mm
CM_UFMG_DualBeam
Physical crosslinking
Hydrogen bond
Polymer chain continuation

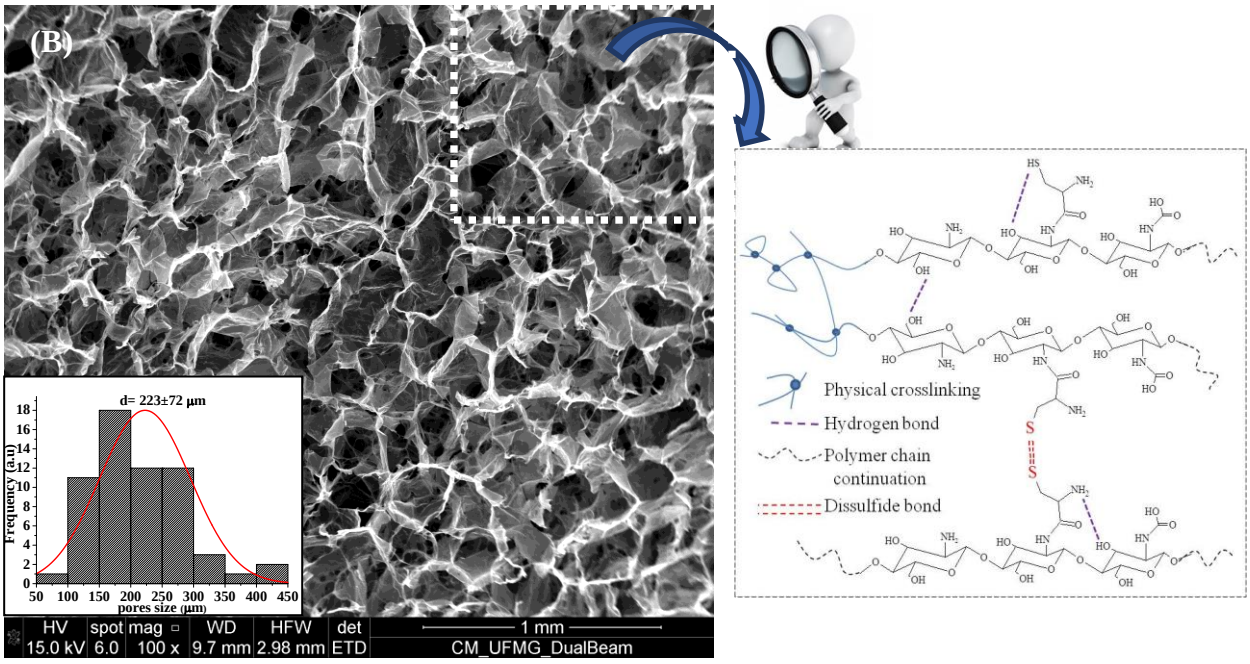
(B)
d= 223±72 µm
Frequency (a.u)
pores size (µm)
HV spot mag WD HFW det
15.0 kV 6.0 100 x 9.7 mm 2.98 mm ETD
1 mm
CM_UFMG_DualBeam
Physical crosslinking
Hydrogen bond
Polymer chain continuation
Dissulfide bond

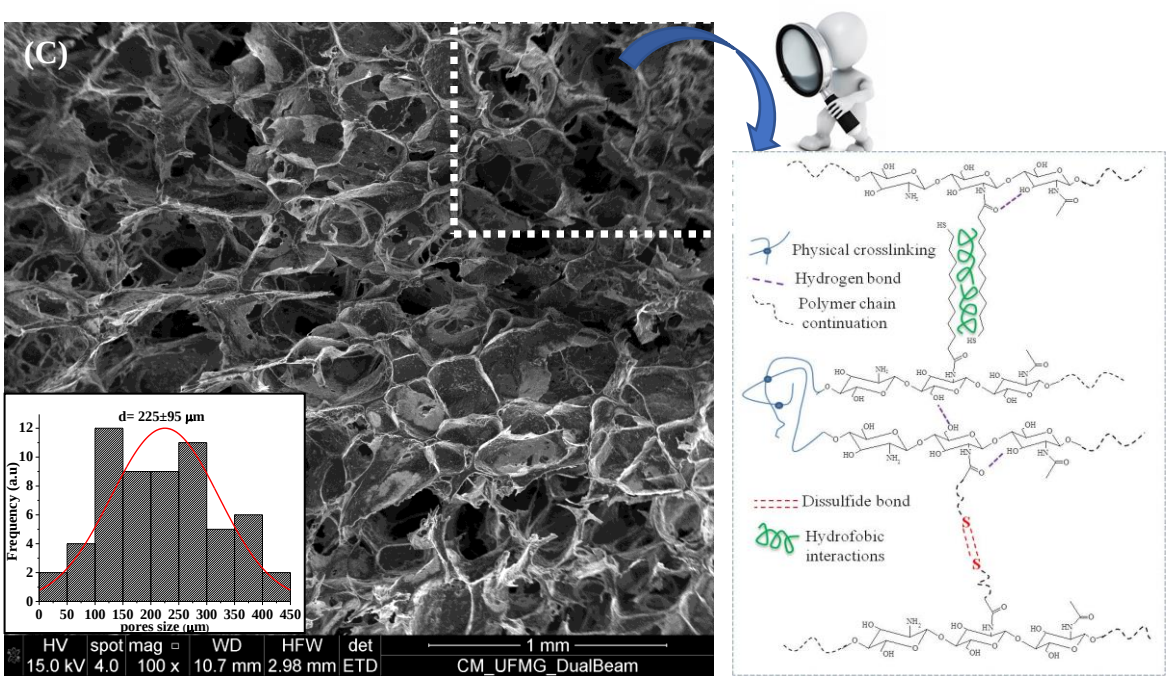


Figure 3. 5. SEM images with 100 x at left and distribution of porous size obtained manually with 30 measures and Chemical/Physical crosslinking between the chains at right of (A) CHI, (B) CHICys and (C) CHIMerc.

The X-ray microtomography analysis (micro-CT) showed that the average porosity was higher than 80 % in all samples, and the average pore size was 204±6 and 214±3 µm for CHICys and CHIMerc, similar to the values estimated by SEM. The interconnectivity of CHICys and CHIMerc was > 90 % (Table 3.1), which is suitable for better cell proliferation aiming at potential biomedical applications in tissue repair [49,52,53] as it allows the flow transport of nutrients and metabolic waste and cell functions pertinent to the new tissue formation and tissue ingrowth.

Table 3. 1. Morphological aspects obtained by micro-CT analysis for 3D porous scaffolds of thiolated-chitosan derivatives.

| **Morphological Aspects** | **CHICys** | **CHIMerc** |
|---|---|---|
| Average pore size (µm) | (204±6) | (214±3) |
| Porosity (%) | (86±4) | (82±3) |
| S/V ($\mu m^{-1}$) | (0.026±0.003) | (0.085±0.001) |
| Interconnectivity (%) | > 90 | > 90 |

The *Archimedes'* method was also used to assess the surface area and the porosity of the scaffolds [54,55]. The results indicated that all chitosan-based thiomer scaffolds presented porosity higher than 90 % (like the micro-CT method) but CHIMerc showed the largest surface area and lowest density (Table S1). These results were interpreted as the contribution of the hydrophobic chain inserted in the 3D scaffold of CHIMerc, which caused repulsion to water molecules during the synthesis of the 3D porous structure. In addition to the pores with size ranging from 100 - 350 µm, this has led also to the formation of ultra-small pores in the scaffolds causing a much higher surface area and lower density, which was detected at the higher magnification of the SEM analysis (Fig. S3). Therefore, the contact angles of these systems were evaluated using water droplets spread onto polymer films as a qualitative method for assessing the relative variation of hydrophobic/hydrophilic behavior of the chitosan and thiolated chitosan samples. The results of the contact angle (Figure 3.6) were 60±1° for chitosan and 64±1° and 84±2° for CHICys and CHIMerc, respectively. The thiolation of chitosan has significantly increased the average value of the contact angle of almost 40 % for CHIMerc, which demonstrated the hydrophobic interactions of the acyl groups inserted into the polymer backbone. To this end, such a large specific surface area, high porosity and tunable hydrophilic/hydrophobic characteristics may promote cell adhesion and proliferation regarding to the potential biomedical applications of these systems [41,51,56].

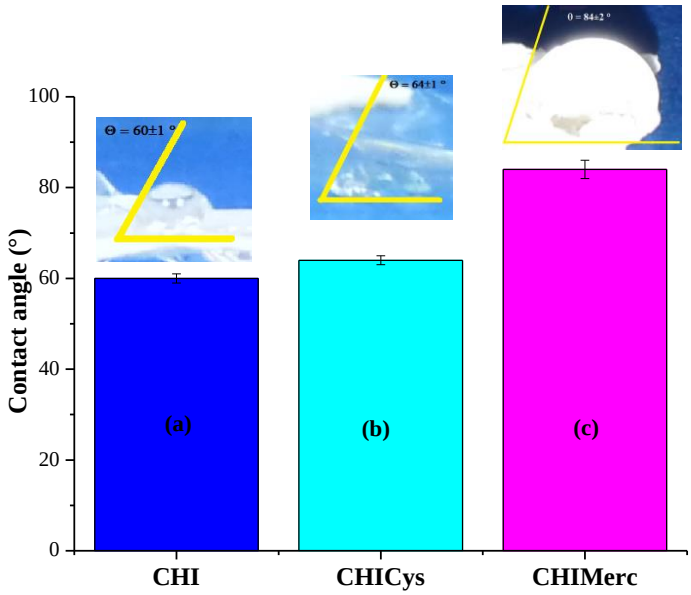


Figure 3. 6. Contact angle measurements of (a) CHI (b) CHICys and (c) CHIMerc films.

### 3.3.1.5 Biological characterization of thiolated-chitosan 3D porous scaffolds

#### 3.3.1.5.1 Cell viability assay by MTT

The cytocompatibility of the 3D hydrogel scaffolds was characterized through MTT *in vitro* assays to further validate the potential of these hydrogels to be applied in the biomedical field for cartilage repair [12,26]. HEK 293 T and SAOS were used as models, since they share similarities with cells that are involved in the production of ECM components essential for the repair of soft and hard tissues [4-9]. Therefore, in this study, the toxicity of the CHI, CHICys and CHIMerc biopolymeric scaffolds was preliminary evaluated based on analysis of the cell viability using the direct contact method of the MTT assay. This test was specifically used to evaluate mitochondrial function and cell viability and is widely accepted to access the cytotoxicity of novel biomaterials according to the international standard (ISO 10993-5:2009/(R)2014, Biological evaluation of medical devices: Tests for *in vitro* cytotoxicity). Figure 3.7A shows the results towards HEK 293 T where no cytotoxic effects were observed for all systems, as there were cell viability responses of over 90 %, like the reference control condition (100 %, within statistical variation). Despite differences in the morphological and architectural features of CHI, CHICys and CHIMerc scaffolds and their physicochemical properties characterized in the previous sections, they demonstrated equivalent cytocompatibility to HEK 293 T cells, which was attributed to the high

biocompatibility of the chitosan biopolymer favoring cell metabolic mitochondrial activity. For the confluence of these cells (Figure 3.7B), no significant difference was observed for the polymeric samples compared with the control group with nearly 100 % surface coverage after 24 h of incubation in the direct contact method. Analogously, equivalent results were observed for SAOS cells where no cytotoxicity was verified towards all scaffolds tested (Fig. S4).

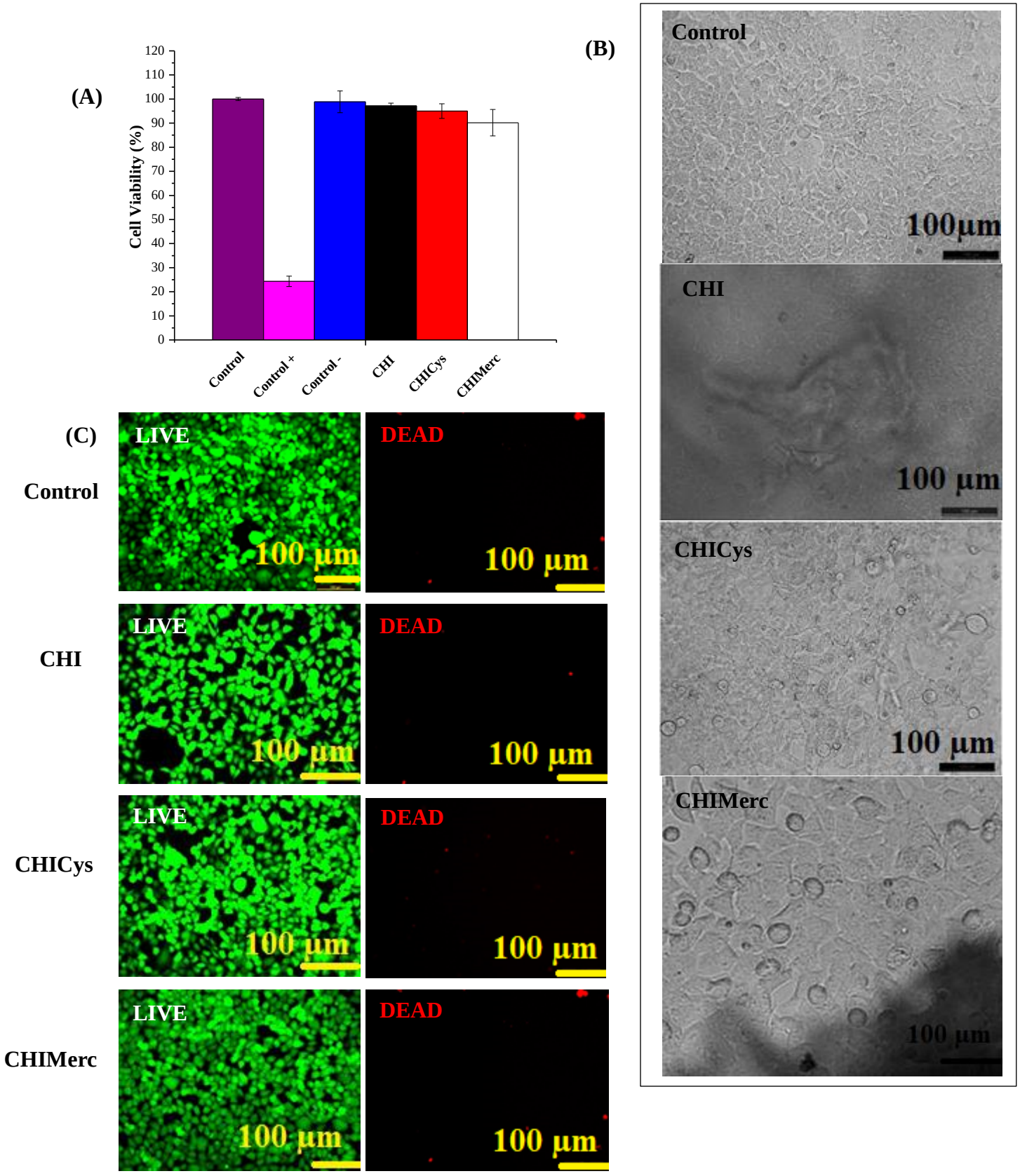


Figure 3. 7. (A) Histogram of cell viability of embryonic cell lines (HEK 293 T) towards all samples; (B) Optical images of HEK 293 T responses after 24h using MTT assay and (C)

The LIVE/DEAD® test with HEK 293 T cells after 24 h incubation. Live cells (green) and Dead cells (red) in control of with 200 x.

#### 3.3.1.5.2 *LIVE/DEAD® assay*

Essentially, the LIVE/DEAD® viability/cytotoxicity assay provides a two-color fluorescence cell viability test, based on the simultaneous determination of live (stained in green, $\lambda_{ex}$ 495 nm, $\lambda_{em}$ 515 nm) and dead cells (stained in red, $\lambda_{ex}$ 495 nm, $\lambda_{em}$ 635 nm) with two probes, Calcein AM (acetoxymethyl ester of calcein) and EthD-1 (ethidium homodimer), that measure known parameters of cell viability, the intracellular esterase activity and plasma membrane integrity [57,58]. Therefore, the LIVE/DEAD® cytotoxicity assay was performed to confirm the results of the MTT tests using the kidney cell line of a human embryo (HEK 293 T) with chitosan and thiolated derivatives (CHICys and CHIMerc). Figure 3.7C shows that the cells tested with the samples CHI, CHICys and CHIMerc had a fluorescence pattern similar to the control group, *i.e.*, high green fluorescence (viable cells) and little or no red fluorescence (dead cells). Thus, as expected, the LIVE/DEAD test validated the previous results shown in the cell viability assays by MTT. In that sense, it may be suggested that the CHICys and CHIMerc scaffolds have shown promising potential to find applications as biomaterials for tissue engineering.

## 3.5 Conclusions

In this study, we focused on the synthesis and comprehensive characterization of new 3D hydrogel scaffolds based on thiol-functionalized high molecular mass chitosan. The hydrogels were produced by the freeze-drying method for obtaining porous scaffolds. The FTIR, Raman and NMR spectroscopy results evidenced the mechanisms involved in the conjugation process *via* the formation of amide bonds between carboxyl groups from thiol precursors (*i.e.*, cysteine and MERC) with amino groups of the chitosan backbone. Moreover, the results demonstrated that the chitosan and chitosan-thiolated hydrogels were produced with different degree of functionalization and swelling degree depending on the thiol-modifier precursors used in the synthesis. Analogously, degradation behavior was reduced by increasing the hydrophobicity of the thiol precursor and the crosslinking of the network by the formation of disulfide bonds. SEM analysis associated with micro-CT X-ray imaging

of the hydrogel scaffolds presented highly porous and interconnected 3D structures, with distinct morphological features such as porosity, surface area and density significantly affected by the thiol moieties inserted in the chitosan polymeric network. These three-dimensional hydrogel scaffolds were cytocompatible, based on the *in vitro* MTT assay with over 90 % of the cell viability responses of HEK 293 T and SAOS cells and LIVE/DEAD cell viability results. Therefore, novel biocompatible chitosan-derived thiomer scaffolds were designed and produced with properties that are modified by the selection of sulfhydryl precursors, with the ability to absorb large amounts of water while maintaining their architectural features and three-dimensional stability. The scaffolds are promising for potential use in cartilage tissue repair applications.

**Acknowledgments**

The authors acknowledge the financial support from the following Brazilian research agencies: CNPq (140810/2015-3; PQ1B–306306/2014-0; UNIVERSAL-457537/2014-0; PIBIC-2016/2017), CAPES (PROEX-2010-2017; PNPD; PROINFRA2010-2014), FAPEMIG (PPM-00760-16), and FINEP (CTINFRA-PROINFRA 2008/2010/2011). The authors express their gratitude to the staff at the Microscopy Center at UFMG for SEM analysis. Finally, the authors thank the staff at the Center of Nanoscience, Nanotechnology and Innovation-CeNano$^2$I/CEMUCASI/UFMG for the spectroscopy analyses.

**Author Contributions**

The manuscript was written through equally contributions from all authors. All authors have read and given approval to the final version of the manuscript.

**Conflicts of Interest**

The authors declare that they have no competing interests.

**References**

[1] Chen, F-M., Liu, X.., Advancing biomaterials of human origin for tissue engineering, Prog Polym Sci, 53 (2016) 86–168.

[2] Langer, R., Vacanti, J. P., Tissue Engineering, Science, New Series, 260 (1993) 920-926.

[3] Griffith, L. G., Naughton, G., Tissue Engineering-Current Challenges and Expanding Opportunities. Science, 295 (2002) 1009-1014.

[4] Vial, X., Andreopoulos, F. M., Novel biomaterials for cartilage tissue engineering, Curr Rheumatol Rev, 500 (2009) 51-57.

[5] Shoichet, M. S., Polymer scaffolds for biomaterials applications, Macromol, 43 (2010) 581-591.

[6] Campos, D. F. D., Supporting Biomaterials for Articular Cartilage Repair, Cartilage, 3 (2012) 205–221.

[7] Alves da Silva, M. L., Martins, A., Costa-Pinto, A. R, Correio, V. M, Sol, P., Bhattacharya, M., Faria, S., Reis, R. L., Neves, N. M., Chondrogenic differentiation of human bone marrow mesenchymal stem cells in chitosan-based scaffolds using a flow-perfusion bioreactor, J Tissue Eng Regen Med, 5 (2011) 722-732.

[8] Abarrategi, A., Lopiz-Morales, Y., Ramos, V., Civantos, A., Lopez-Duran, L., Marco, F., López-Lacomba, J. L., Chitosan scaffolds for osteochondral tissue regeneration. J Biomed Mater Res A, 95 (2010) 1132-1141.

[9] Chevrier, A., Hoemann, C. D, Sun J., & Buschmann, M. D., Temporal and spatial modulation of chondrogenic foci in subchondral microdrill holes by chitosan-glycerol phosphate/blood implants, Osteoarthr Cartil, 19 (2011) 136-144.

[10] Suh, J-K. F., Mathew, H. W. T., Application of chitosan-based polysaccharide biomaterials in cartilage tissue engineering: a review, Biomaterials, 21 (2000) 2589-2598.

[11] Diekjürgen, D., Grainger, D. W., Polysaccharide matrices used in 3D in vitro cell culture systems, Biomaterials,141 (2017) 96-115.

[12] Carvalho, I. C., Mansur, H. S., Engineering 3D scaffolds of photocrosslinked chitosan-gelatin hydrogel hybrids for cronic wound dressings and regeneration, Mater Sci Eng C, 78 (2017) 690-705.

[13] Santos, J. C., Moreno, P. M. D., Mansur, A. A. P., Leiro, V., Mansur, H. S., Pêgo, A. P., Functionalized chitosan derivatives as nonviral vectors: physicochemical properties of acylated *N*,*N*,*N*-trimethyl chitosan/oligonucleotide nanopolyplexes, Soft Matter, 41 (2015) 8113-8125.

[14] Mansur, H. S., Mansur, A. A. P., Curti, E., Almeida, M. V., Bioconjugation of quantum-dots with chitosan and *N*,*N*,*N*-trimethyl chitosan. Carbohydr Polym, 90 (2012) 189-196.

[15] Lee, K. Y., Ha, W. S., Park, W. H., Blood compatibility and biodegradability of partially N-acylated chitosan derivatives, Biomaterials, 16 (1995) 1211-1216.

[16] Le Tien, C., Lacroix, M., Ispas-Szabo, P., Mateescu, M. A., N-acylated chitosan: hydrophobic matrices for controlled drug release, J Control Release, 93 (2003) 1-13.

[17] Schmitz, T., Grabovac, V., Palmberger, T. F., Hoffer, M. H., Bernkop-Schnurch, A., Synthesis and characterization of a chitosan-N-acetyl cysteine conjugate, Inter J Pharm, 347 (2008) 79-85.

[18] Casettari, L., Biomedical applications of amino acid-modified chitosans: A review. Biomaterials, 33 (2012) 7565-7583.

[19] Talaei, F., Azizi, E., Dinarvand, R., Atyabi, F., Thiolated chitosan nanoparticles as a delivery system for antisense therapy, Inter J Nanomedicine, 6 (2011) 1963–1975.

[20] Bernkop-Schnurch, A., Guggi, D., Pinter, Y., Thiolated chitosans: development and in vitro evaluation of a mucoadhesive, permeation enhancing oral drug delivery system, J Control Release, 94 (2004) 177– 186.

[21] Bernkop-Schnurch, A., Thiomers: A new generation of mucoadhesive polymers, Adv Drug Deliv Rev, 57 (2005) 1569– 1582.

[22] Dheer, D., Arora, D., Jaglan, S., Rawal, R. K., Shankar, R., Polysaccharides based nanomaterials for targeted anti-cancer drug delivery, J Drug Target, 25 (2017) 1-16.

[23] Shah, K. U., Shah, U. S., Dilawar, N., Khan, G. M., Gibaud, S., Thiomers and their potential applications in drug delivery, Expert Opin Drug Deliv, 14 (2017) 601-610.

[24] Liu, D., Li, J., Pan, H., He, F., Liu, Z., Wu, Q., Bai, C., Yu, S., Yang, X., Potential advantages of a novel chitosan-N-acetylcysteine surface modified nanostructured lipid carrier on the performance of ophthalmic delivery of curcumin. Sci Rep *6*, 28796 (2016)1-14.

[25] Medeiros Borsagli, F. G., Mansur, A. A. P., Chagas, P., Oliveira, L. C., Mansur, H. S., O-carboxymethyl functionalization of chitosan: Complexation and adsorption of Cd (II) and Cr (VI) as heavy metal pollutant ions, React Func Polym, 97 (2015) 37-47.

[26] Costa Junior, E. S., Mansur, A. A. P., Stancioli, E. F., Vasconcelos, W. L., Mansur, H. S., Preparation and Characterization of Chitosan/Poly(Vinyl Alcohol) Chemically Crosslinked Blends for Biomedical Applications, Carbohydr Polym, 76 (2009) 472-481.

[27] Mozalewska, W., Czechowska-Biskupa, R., Olejnika, A. K., Wacha, R. A., Ulańskia, P., Rosiak, J. M., Chitosan-containing hydrogel wound dressings prepared by radiation technique, Radiat Phys Chem, 134 (2017) 1-7.

[28] Ho, S. T., Hutmacher, D. W., A comparison of micro CT with other techniques used in the characterization of scaffolds, Biomaterials, 27 (2006) 1362-1376.

[29] Lowell, S., Shields, J. E., Thomas, M. A., Thommes, M., Characterization of Porous Solids and Powders: Surface Area, Pore Size and density. Springer, New York, 2004.

[30] Teng, D.-Y., Wu, Z.-M., Zhang, X.-G., Wang, Y.-X., Zheng, C., Wang, Z., Li, C.-X., Synthesis and characterization of in situ cross-linked hydrogel based on self-assembly of thiol-modified chitosan with PEG diacrylate using Michael type adition, Polymer, 51 (2010) 639-646.

[31] Kafedjiiski, K., Krauland, K. H., Hoffer, M. H., Bernkop-Schnurch, A., Synthesis and in vitro evaluation of a novel thiolated chitosan, Biomaterial, 26 (2005) 819-826

[32] Tawill, N., Hatef, A., Sacher, E., Maisonneuve, M., Gervais, T., Mandeville, R., & Meunier, M., Surface Plasmon Resonance Determination of the Binding Mechanisms of L-Cysteine and Mercaptoundecanoic Acid on Gold, J Phys Chem, 117 (2013) 6712−6718.

[33] Cavalleri, O., Oliveri, L., Dacca, A., Parodi, R., Rolandi, R., XPS Measurements on L-Cysteine and 1-Octadecanethiol Self-Assembled Films: A Comparative Study, Appl. Surf. Sci., 175 (2001) 357−362.

[34] Yang, R., Su, Y., Aubrecht, K. B., Wang, X., Ma, H., Grubbs, R. B., Hsiao, B. S., Chu, B., Thiol-functionalized chitin nanofibers for As (III) adsorption, Polymer, 60 (2015) 9-17.

[35] Robbinson, A. S., King, J., Disulphide-bonded intermediate on the folding and assembly pathway of a non-disulphide bonded protein. Nat Struct Mol, 4 (1997) 450-455.

[36] Rajawat, G. S., Shinde, U. A., Nair, H. A., Chitosan-N-acetyl cysteine microspheres for ocular delivery of acyclovir: Synthesis and in vitro/in vivo evaluation. J Drug Deliv Sci Technol, 35 (2016) 333-342.

[37] Edsall, J. T., Otvos, J. W., Rich, A., Raman Spectra of Amino Acids and Related Compounds. VII. Glycylglycine, Cysteine, Cystine and Other Amino Acids. J Am Chem Soc, 72 (1950) 474-477.

[38] Pawlukojc, L., Leciejewicz, J., Ramirez-Cuesta, A. J., Nowicka-Scheibe, J., l-Cysteine: Neutron spectroscopy, Raman, IR and ab initio study, Spectrochim Acta Mol Biomol Spectrosc, 61 (2005) 2474–2481.

[39] Liu, X, Yu, B., Huang, Q., Liu, R., Feng, Q., Cai, Q., Mi, S., In vitro BMP-2 peptide release from thiolated chitosan based hydrogel. Inter J Biol Macromol, 93 (2016) 314-321.

[40] Li, J., Liu, D., Tan, Z., Zhao, Z., Yang, X., Pan, W., A comparative study on the efficiency of chitosan-N-acetylcysteine, chitosan oligosaccharides or carboxymethyl chitosan surface modified nanostructured lipid carrier for ophthalmic delivery of curcumin, Carbohydr Polym, 146 (2016) 435-444.

[41] Santos, J. C., Mansur, A. A., Mansur, H. S., One-Step Biofunctionalization of Quantum Dots with Chitosan and N-palmitoyl Chitosan for Potential Biomedical Applications, Molecules, 18 (2013) 6550-6572.

[42] Bernkop-Schnurch, A., Krauland, A. H., Leitner, V. M., Palmberger, T., Thiomers: potential excipients for non-invasive peptide delivery systems, Eur J Pharm Biopharm, 58 (2004) 253-263.

[43] Nobs, L., Buchegger, F., Gurny, R., Alle'mann, E., Current Methods for Attaching Targeting Ligands to Liposomes and Nanoparticles, J Pharm Sci, 93 (2004) 1980-1992.

[44] Domínguez-Delgado, C. L., Rodríguez-Cruz, I. M., Fuentes-Prado, E., Escobar-Chávez, J. J., Vidal-Romero, G., García-Gonzáles, L., Fuente-Lee R. I., Drug Carrier Systems Using Chitosan for Non Parenteral Routes. In S. J. Thatha Gowder (Ed), Pharmacology and Toxicological and Pharmaceutics Science, (pp. 273-325). Intech, 2014.

[45] Werle, M., Bernkop-Schnurch, A., Thiolated chitosans: useful excipients for oral drug delivery, J Pharm Pharmacol, 60 (2008) 273-281.

[46] Bertoldi, S., Farè, S., Tanzi, M. C., Assessment of scaffold porosity: the new route of micro-CT. J Appl Biomater Biomech, 9 (2011) 165-175.

[47] Bae, I.-H., Jeong, B.-C., Kook, M.-S., Kim, S.-H., Koh, J.-T., Evaluation of a Thiolated Chitosan Scaffold for Local Delivery of BMP-2 for Osteogenic Differentiation and Ectopic Bone Formation. BioMed Res Int, 2013 (2013) 1-11.

[48] Mansur, H. S., Costa, H. S., Mansur, A. A., Pereira, M., 3D-macroporous hybrid scaffolds for tissue engineering: network design and mathematical modeling of degradation kinetics, Mater Sci Eng C, 32 (2012) 404-415.

[49] Mandal, B., Kundu, S., Cell proliferation and migration in silk fibroin 3D scaffolds, Biomaterials, 30 (2009) 2956-2695.

[50] Kim, H., Kim, U., Vunjak-Novakovic, G., Min, B., Kaplan, D., Influence of macroporous protein scaffolds on bone tissue engineering from bone marrow stem cells, Biomaterials, 26 (2005) 4442-4452.

[51] Akay, G., Birch, M. A., Bokhari, M. A., Microcellular polyHIPE polymer supports osteoblast growth and bone formation in vitro, Biomaterials, 25 (2004) 3991-4000.

[52] Murphy, C. M., O'Brien, F. J., Understanding the effect of mean pore size on cell activity in collagen-glycosaminoglycan scaffolds, Cell Adh Migr, 4 (2010) 377-381.

[53] Lien, S. M., Ko, L. Y., Hunag, T. J., Effect of pore size on ECM secretion and cell growth in gelatin scaffold for articular cartilage tissue engineering, Acta Biomate*r,* 5 (2009) 670-679.

[54] Allen, T., Particle size measurement, Chapman & Hall, Londres, 1990.

[55] Svarovski, L., Solid-gas separation, Elsevier Scientific P. Co., New York, 1981.

[56] Yasuda, T., Okuno, T., Contact angle of water on polymer surfaces. Langmuir, 10 (1994) 2435–2439.

[57] Moreira, C. D. F., Carvalho, S. M., Mansur, H. S., Pereira, M. M., Thermogelling chitosan-colagen-bioactive glass nanoparticle hybrids as potential injectable system for tissue engineering, Mater Sci Eng C, 58 (2016) 1207-1216.

[58] Dumont, V. C., Mansur, H. S., Mansur, A. A. P., Carvalho, S. M., Capanema, N. S. V., Barrioni, B. R., Glycol/Chitosan nanohydroxyapatite biocomposites for potential bone tissue engineering and regenerative medicine, Inter J Biol Macromol Part B, 93 (2016) 1465-1478.

**Supplementary Materials**

**Table S1.** Morphological parameters obtained for 3D porous scaffolds of chitosan and thiomer derivatives: Bulk density ($\rho_a$), porosity ($\varepsilon$) and surface area ($S_a$).

| **3D Porous Scaffolds samples** | $\boldsymbol{\rho_a}$ $(\boldsymbol{g.cm^{-3}})$ | $\boldsymbol{\varepsilon}$ **(%)** | $\boldsymbol{S_a}$ $(\boldsymbol{m^2.g^{-1}})$ | |
|---|---|---|---|---|
| | | | **SEM analysis** | **Micro-CT analysis** |
| CHI | (0.112±0.014) | (89±3) | (139±17) | NA* |
| CHICys | (0.066±0.008) | (95±2) | (466±61) | (426±55) |
| CHIMerc | (0.035±0.003) | (96±2) | (804±89) | (765±64) |

*NA = Not applied due to limitation of the method.

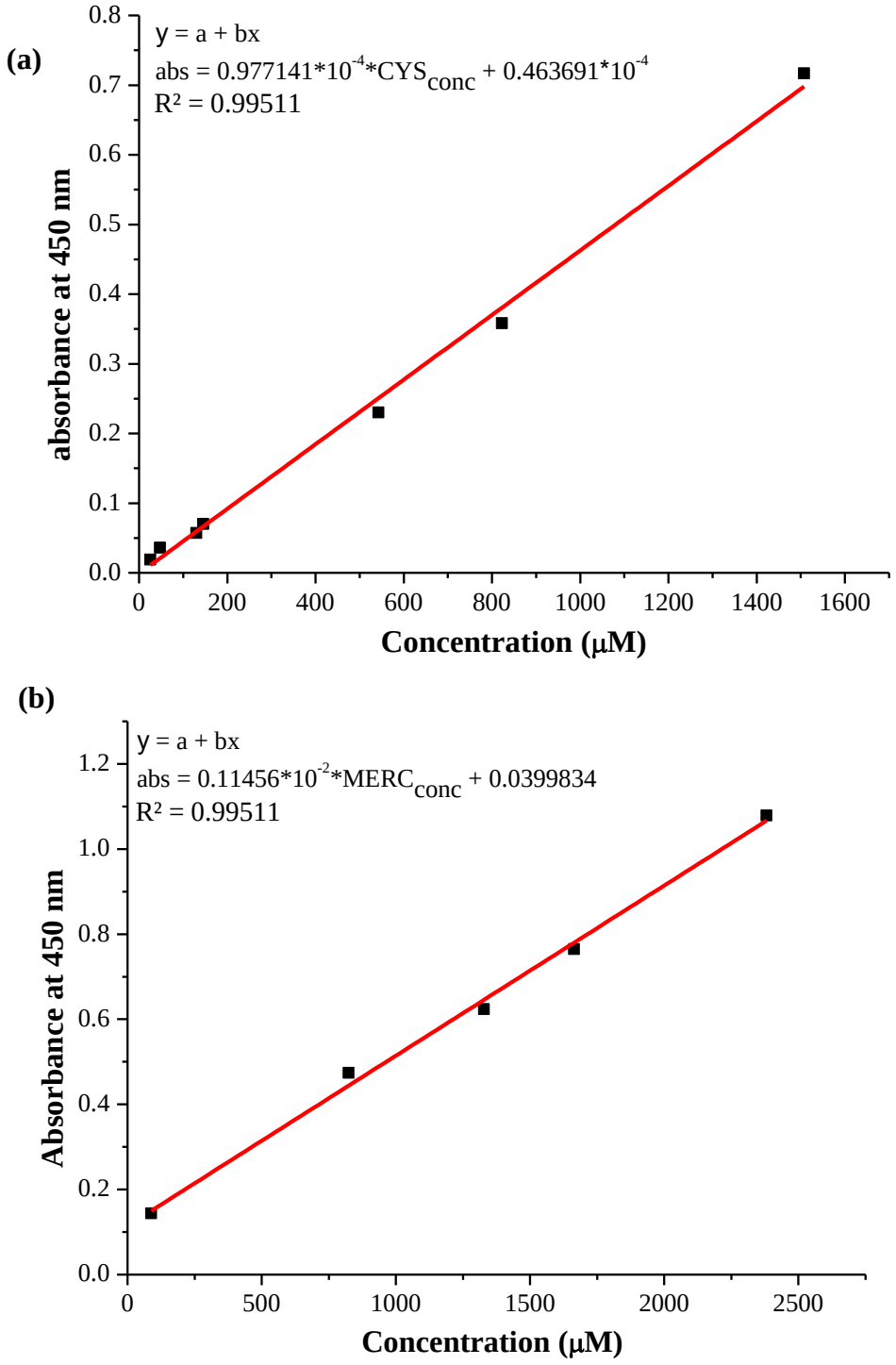


Figure S1. Calibration curves of (a) Cysteine (CYS) and (b) 11-mercaptoundecanoic acid (MERC)

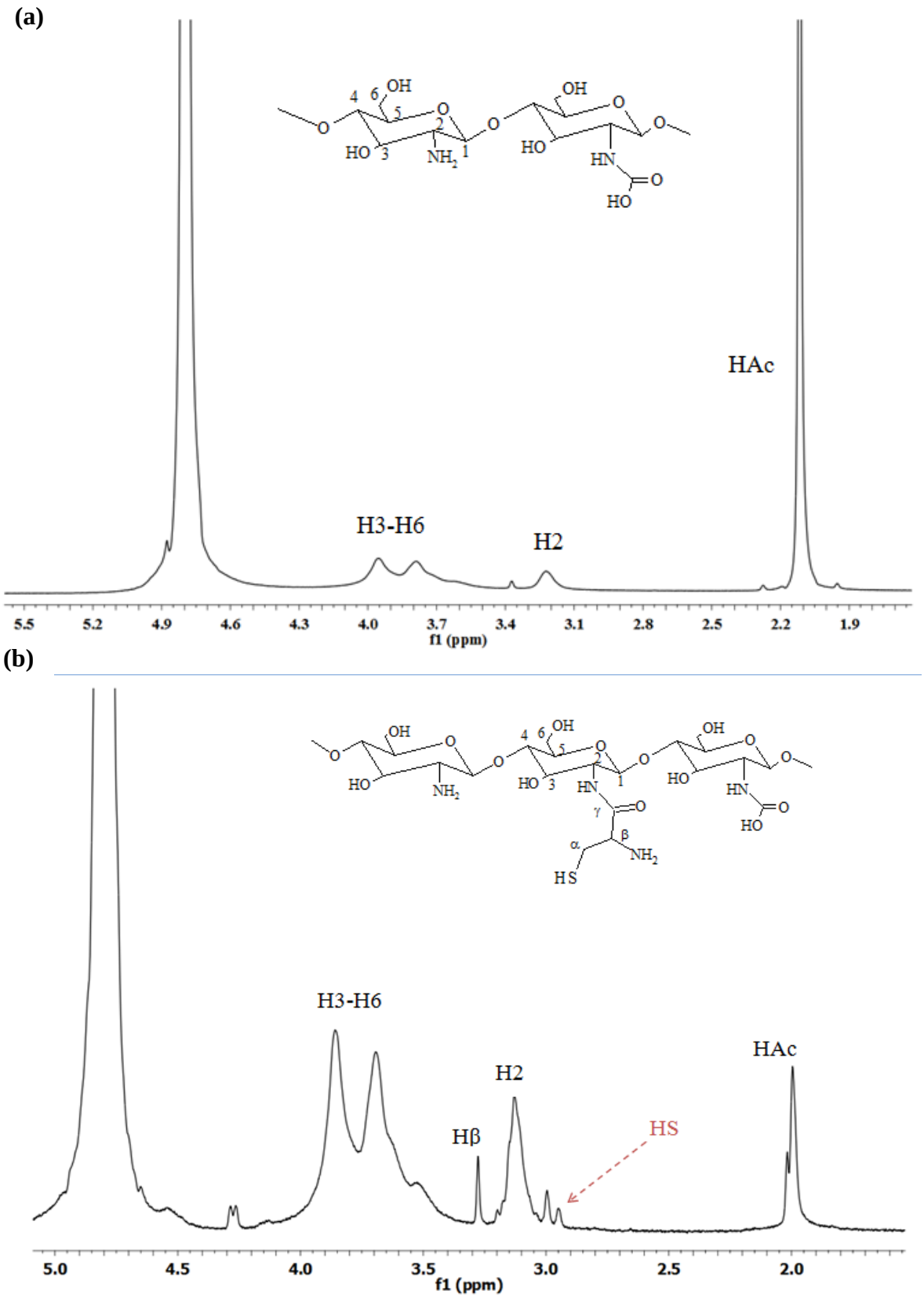


Figure S2. $H^1$ NMR spectra of (a) CHI and (b) CHICys

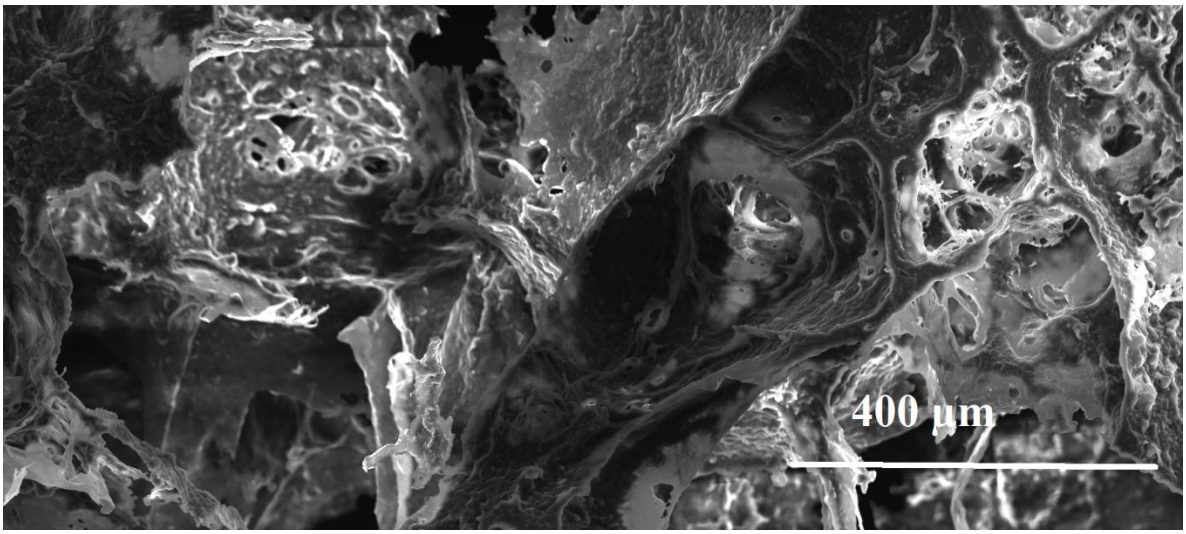


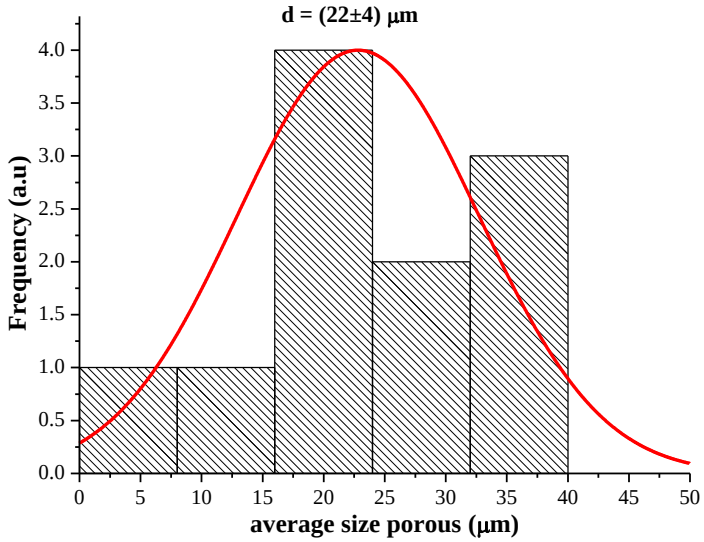


Figure S3. (a) SEM images with 350 x of CHIMerc showed the sub-micrometer pores and (b) Population distribution of distribution of pores size obtained manually with 50 measures

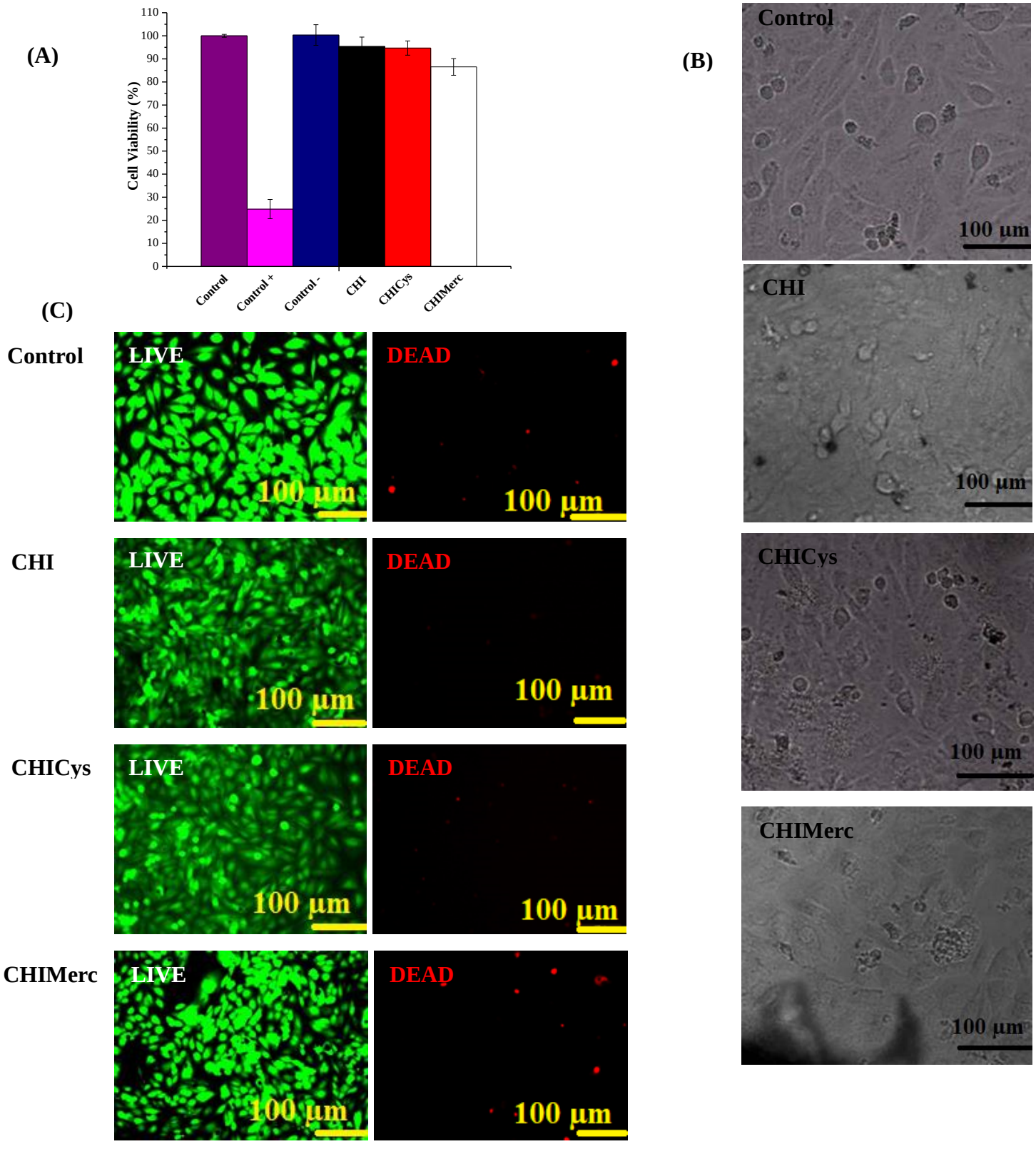


Figure S4. (A) Histogram of cell viability of embryonic cell lines (SAOS) towards all samples (B) Optical images of SAOS responses after 24h using MTT assay and (C) The

LIVE/DEAD® test with SAOS cells after 24 h of contact with extracts. Live cells (green) and Dead cells (red) in control of with 200 x.

# Capítulo 4. Bi-Functional Eco-friendly 3D Scaffolds based on *N*-acyl Thiolated Chitosan for Potential Adsorption of Dye Pollutants and Antibacterial Applications

# Bi-Functional Eco-friendly 3D Scaffolds based on *N*-acyl Thiolated Chitosan for Potential Adsorption of Dye Pollutants and Antibacterial Applications

Fernanda G. L. Medeiros Borsagli[1], Virginia S. T. Ciminelli[2], Dionei J. Haas[3], Andrey P. Lage[3], Herman S. Mansur[1*]

*[1]Center of Nanoscience, Nanotechnology, and Innovation - CeNano[2]I, Department of Metallurgical and Materials Engineering, Federal University of Minas Gerais/UFMG, Belo Horizonte, Brazil.*
*[2]National Institutes of Science and Technology: INCT-Acqua, Department of Metallurgical and Materials Engineering, Federal University of Minas Gerais, Brazil.*
*[3]Department of Preventive Veterinary Medicine, Veterinary School, Federal University of Minas Gerais, Brazil.*
Corresponding author: *hmansur@demet.ufmg.br

## Abstract

Unfortunately, the presence of organic dyes in industrial effluents has been continuously polluting waters leading to the formation of toxic sludge and/or carcinogenic compounds. To worsen this scenario, the proliferation of multidrug-resistant microorganisms in waters caused by anthropogenic activities and natural disasters has become major global concern because of serious health and environmental harms. Herein we designed and developed novel three-dimensional (3D) porous scaffolds made of *N*-acyl thiolated chitosan using 11-mercaptoundecanoic acid. These hydrogels exhibited 3D hierarchical pore structure (porosity > 82%) and high surface area (~ 804 $m^2.g^{-1}$), which demonstrated high adsorption capacity for methyl orange anionic dye pollutant (~ 450 $mg.g^{-1}$) in water. The adsorption data were well-fitted to a pseudo-second-order kinetics and Freundlich's isotherm. Moreover, the thiolated-chitosan proved antibacterial activity against *Pseudomonas aeruginosa* regularly found in hospital discharges. Thus, for the first time, bi-functional thiolated-chitosan 3D-scaffolds were produced combining *green* biosorbent behavior for organic dyes and antimicrobial activity against pathogenic bacteria, which offer innovative strategy for the treatment of multi-polluted and contaminated water bodies.

**Keywords: Biosorbent; Adsorption of Dyes; Antibacterial Hydrogel; Wastewater Treatment; Thiolated-chitosan; Porous Scaffolds.**

***Corresponding author**: Universidade Federal de Minas Gerais, Av. Antônio Carlos, 6627 – Escola de Engenharia, Bloco 2 – Sala 2233, 31.270-901, Belo Horizonte/MG, Brazil; Tel: +55-31-34091843; Fax: +55-31-34091843; E-mail: hmansur@demet.ufmg.br (H. Mansur).

## Graphical abstract

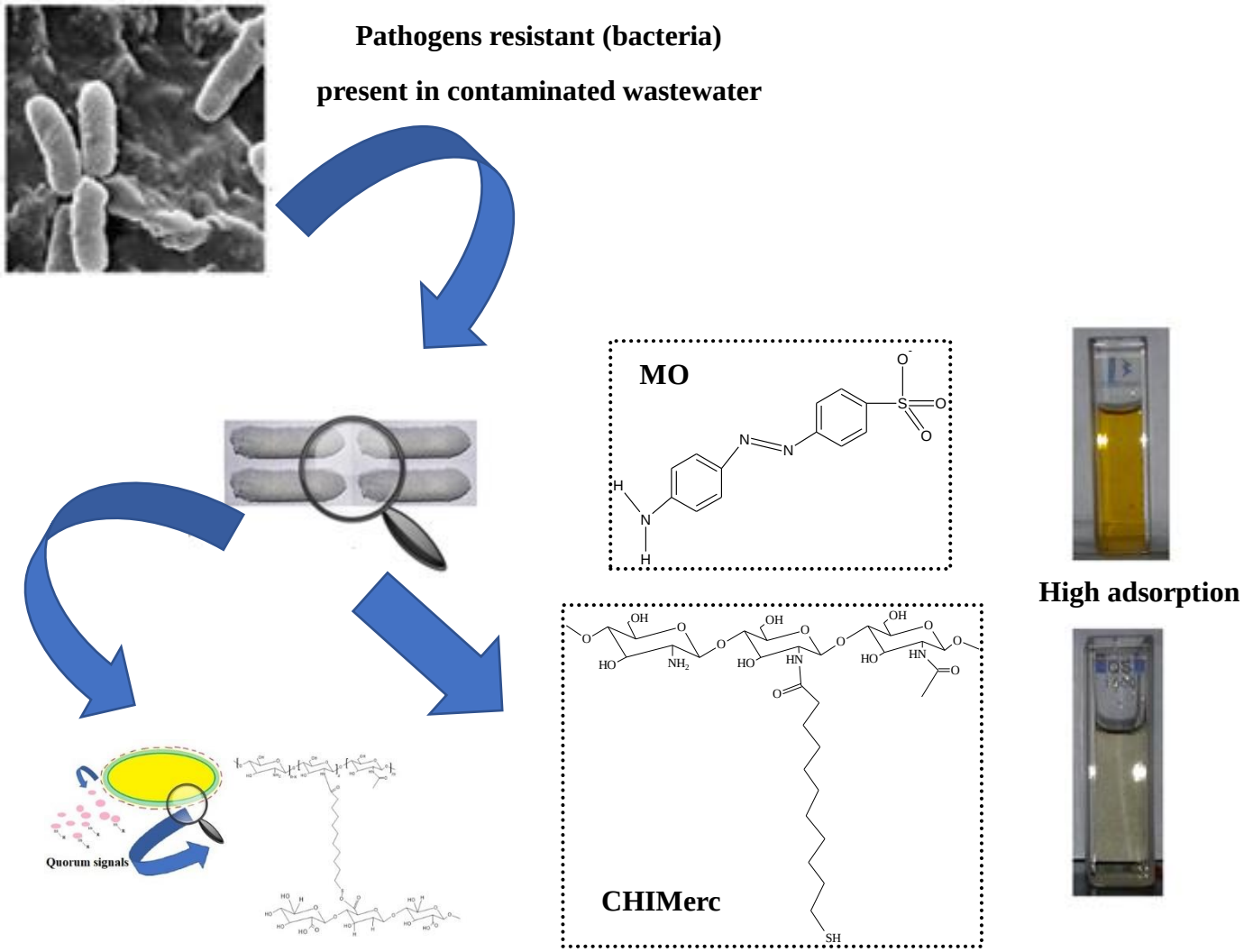


**Green Chemistry meets Environmental Science and Technology: Novel 3D Porous Scaffolds based on Chitosan Thiomers as Biosorbents with Antibacterial Activity for Wastewater Treatment**

## 4.1 Introduction

Water availability for economic development and conservation of life is a theme of great concern given the increasing occurrence of extreme events related to climate changes combined with the deterioration of water quality due to anthropogenic contamination [1]. Among these pollutants, dyes, phenolics, pharmaceutics, and pesticides have recently become of great concern because of their extreme toxicity and persistence in the environment. Although chemical and biological treatments are available for the removal of organic compounds, the by-products of their degradation can also be harmful and non-degradable [2-4]. Industrial effluents and hospital wastewater are some sources of water pollution. Industrial effluents runoffs may comprise colored substances that are released from textile, paint, paper, varnishes, ink, plastics, pulp, cosmetics, tannery and plastic [5,6]. The presence of dyes in industrial effluents are a significant cause of pollution due to their recalcitrance nature, giving undesirable color to the water and reducing sunlight penetration, associated with the fact that their degradation products may be toxic or even mutagenic and carcinogenic [5]. Approximately 10,000 different types of pigments and over 700,000 tons are produced worldwide annually, being 10 to 15 % lost in the effluent during the dyeing process [4,6,7]. To aggravate this scenario, many types of drugs, including antibiotics usually from inappropriate discard of medical, veterinary, and agricultural applications, heavy metals, and disinfectants are found in wastewater, thus contributing for increasing bacterial resistance [5,6,8,9]. Studies have shown that hospital effluents, in special, contain levels of bacteria with antibiotic resistance higher than effluent derived from other sources [8-10].

Effluents are usually treated by chemical precipitation, membrane separation, evaporation, electrolysis, among other processes. However, some of these methods may be ineffective for the removal of trace amounts from large volumes of wastewater and present shortcomings, such as high maintenance costs, generation of toxic sludge and complicated procedure involved in the treatment [11-14]. For this reason, selective wastewater treatment processes for the capture/immobilization of specific dyes, in addition to the reuse of waste is highly needed. In addition to the adopted adsorbents (*e.g.*, activated carbon) investigations on selective biosorbents based on natural polymers and derivatives have significantly increased under the concept of economic and environmentally friendly materials [15]. The natural

polymers such as starch, cellulose, chitosan, and lignin are scientifically and industrially attractive because they present hydrophilic networks with functional groups for developing chemical interactions with metallic ions and organic compounds [16, 17]. Moreover, the presence of pH-sensitive functional groups in the polymer backbone offers an attractive possibility for developing novel soft materials forming polyelectrolyte hydrogel platforms. These hydrogel networks can swell in aqueous medium instead of dissolving in it and therefore, are capable of retaining extremely large amounts of water relative to their own mass (referred to as superabsorbent polymer-based *hydrogel, SAP)*. The formation of hydrogen bonding between water molecules and functional groups of the polymer network leads to water absorption from 10-100 times its weight and this allows a variety of innovative environmental and biological applications [4,17].

Despite the several advantages of chitosan such as abundant natural polysaccharide, non-toxic and biodegradable, it is only soluble under acidic aqueous solution, which can limit some of its potential applications in the environmental and biomedical fields. Thus, the chemical derivatization of chitosan provides powerful means to promote new features and specific properties by the functionalization process based on the presence of primary amino groups in the macromolecule [18-25]. To this end, the chemical conjugation process of chitosan with thiol-bearing ligands produces thiomers with improved water solubility associated with a high level of cohesive-, mucoadhesive-, enzyme inhibitory-, and permeation-enhancing properties. Moreover, the effect of chitosan thiomers on microorganisms, including antibacterial activity has been recently reported [18-25].

Chitosan and derivatives have been widely investigated as sorbent for water treatment mostly in the removal of heavy metals and dyes [16, 24-27]. However, interestingly, no study was found in the consulted literature reporting the research of chitosan thiomer hydrogels for organic dye adsorption combined with antimicrobial features. Hence, there is a vast field to be exploited based on the combination of chemical functionalities with the chitosan polysaccharide backbone producing a new class of thiolated-chitosan polymers for numerous applications. An ideal material will combine all the mentioned features of chitosan and its thiomers into one single design, to address simultaneously the distinct aspects of a dynamic

adsorption process and antibacterial activity. Hence, such modifications should preserve the fundamental skeleton of the chitosan and improve selectivity according to the character of the introduced moieties. In that sense, further investigations of the effects of thiolated chitosan on the adsorption of toxic dyes and antibacterial activity pose highly attractive challenges to the research community and environmental professionals.

Thus, to the best of our knowledge, the present work reports for the first time a facile green synthesis of 3D porous scaffold bio-adsorbents combined with antibacterial activity based on thiolated chitosan produced using 11-mercaptoundecanoic acid. It was comprehensively evaluated the influence of grafting thiol groups to chitosan on the adsorption of model hazardous organic dye, including the kinetics and mechanisms involved, as well as the antibacterial activity against the resistant pathogen (*Pseudomonas aeruginosa*). It is foreseen the prospective use of these bi-functional 3D porous scaffolds as ecologically sustainable dye adsorbents combined with the antibacterial behavior for wastewater treatment with severe organic dye pollution and pathogen contamination.

## 4.2 Experimental section

### 4.2.1 Materials

All the reagents and precursors were used as received. These included sodium hydroxide (Sigma, USA, ≥ 99 %, NaOH), hydrochloric acid (Sigma-Aldrich, USA, 36.5–38.0 %, HCl), 11-mercaptoundecanoic acid (Sigma-Aldrich, USA, ≥ 95 %, MM = 218.36 g.mol$^{-1}$, $HSCH_2(CH_2)_8CH_2COOH$), 2-propanol (Sigma-Aldrich, USA, anhydrous 99.5 %, $(CH_3)_2CHOH$), acetic acid (Synth, Brazil, 99.8 %, MM = 60.05 g.mol$^{-1}$, $CH_3CO_2H$), *Ellman's* reagent (Sigma-Aldrich, USA, DTNB, 5,5′-dithiobis(2-nitrobenzoic acid), MM = 396.35 g.mol$^{-1}$, $[-SC_6H_3(NO_2)CO_2H]_2$), *N*-(3-dimethylaminopropyl)-*N*′-ethylcarbodiimide hydrochloride - EDC (Sigma-Aldrich, USA, $C_8H_{17}N_3{\cdot}HCl$, MM = 191.7 g.mol$^{-1}$), N-hydroxysulfosuccinimide sodium salt - sulfo-NHS ( Aldrich, USA, ≥ 98 %, $C_4H_4NNaO_6S$, MM = 217.13 g.mol$^{-1}$), sodium phosphate dibasic (Sigma-Aldrich, USA, ≥ 99.0 %, MM = 141.96 g.mol$^{-1}$, $Na_2HPO_4$), potassium phosphate monobasic (Sigma-Aldrich, USA, ≥ 99.0 %, MM = 136.09 g.mol$^{-1}$, $KH_2PO_4$), potassium chloride (Sigma-Aldrich, USA, ≥ 99.0 %, MM = 74.55 g.mol$^{-1}$, KCl), sodium chloride (Sigma-Aldrich, USA, ≥ 99.0 %, MM = 58.44

g.mol$^{-1}$, NaCl), ethylenediaminetetraacetic acid (EDTA, Synth, Brazil, $(HO_2CCH_2)_2NCH_2CH_2N(CH_2CO_2H)_2$, > 99.99 %, MM = 292.24 g.mol$^{-1}$), nitric acid ($HNO_3$, Sigma-Aldrich, USA, ≥ 90 %, MM = 63.01 g.mol$^{-1}$), methylene blue (MB, Synth, Brazil, $C_{16}H_{18}N_3SCl{\cdot}3H_2O$) and methyl orange (MO, Synth, Brazil, $C_{14}H_{14}N_3NaO_3S$). High-molecular-mass chitosan powder (CHI, molar mass, MM = 310,000 to > 375,000 g.mol$^{-1}$, deacetylation degree (DD) ≥ 75.0 %, and viscosity 800-2000 cP, at 1 % in 1 % acetic acid, Aldrich, USA) was used for polymer modification. Deionized water (DI-water) (Millipore Simplicity™) with a resistivity of 18 MΩ·cm was used to prepare all solutions. All preparations and syntheses were performed at room temperature (RT, 25±2 ˚C) unless otherwise specified.

### 4.2.2 N-Acylation of chitosan with 11-mercaptoundecanoic acid (CHIMerc)

The synthesis of chitosan with 11-mercaptoundecanoic acid (MERC) was performed according to the molar ratio of reagents 1:2:2 (CHI:EDC:MERC) as described at our previous work [25,26] which was slightly modified due to presence of the hydrophobic acyl chain (MERC). Briefly, 0.5 g of chitosan powder was dissolved in 30 mL of 2 % (v/v) acetic acid aqueous solution overnight for complete solubilization and the pH was adjusted to 4.5±0.5 (NaOH, 1.0 mol.L$^{-1}$). In the sequence, 1.36 g of MERC was dissolved in 60 mL of phosphate-buffered saline (PBS) solution/2-propanol (30/30) (v/v). Then, 1.2 g of *N*-(3-dimethylaminopropyl)-*N′*-ethylcarbodiimide hydrochloride (EDC) and 0.32 g of N-hydroxysulfosuccinimide sodium salt (sulfo-NHS) were added and maintained under moderate stirring for 1 h at room temperature (referred to as MERC/EDC/NHS solution). Then, the MERC/EDC/NHS solution was added to chitosan/acetic acid solution and the pH was adjusted to 5.0±0.5 (NaOH, 1.0 mol.L$^{-1}$) (*i.e.*, total volume = 91 mL, molar ratio of 1:2:2/CHI:EDC:MERC). This is required in order to increase number of de-protonated amino groups ($R\text{-}NH_3^+ \rightarrow R\text{-}NH_2$) to conjugate with carboxylic group from MERC [18,25]. The coupling reaction *via* the formation of amides was performed at room temperature (RT) under moderate stirring for 5 h in the darkness. Next, the mixture was dialyzed in the darkness against distilled water using a membrane (12–14 kDa, Sigma, USA) for 7 days at RT to remove unreacted species and water-soluble contaminants for further preparing the hydrogels. To obtain polymer matrices with porous three-dimensional structures, samples of

the previously prepared solutions (CHIMerc) were poured into plastic tubes (1.5 mL in *Eppendorfs*), frozen at -4±2 ˚C for 72 h and freeze-dried (ModulyoD, Thermo Electron Corporation, Waltham, Massachusetts, USA) at -50 ˚C and 400±100 µbar until the samples reached a constant mass (approximately 72 h). The freeze-drying process was the same and the parameters (temperature, pressure, time) were maintained unchanged for all the samples produced. The thiolated-chitosan scaffolds were produced with a soft foam-like aspect and stored at 4±2 ˚C until further use.

### 4.2.3 Thiolated chitosan characterization

#### 4.2.3.1 Determination of thiol group content grafted to chitosan

In our previous work [25], the determination of the total amount of thiol groups in the CHIMerc chain was performed using the *Ellman's* reagent protocol as reported previously in the literature [18]. This method was used because a solution of this compound produces a measurable yellow-colored product when it reacts with sulfhydryl, so this reagent (DTNB, 5,5′-dithiobis(2-nitrobenzoic acid)) is very useful as a sulfhydryl assay reagent because of its specificity for -SH groups at neutral pH, 11-mercaptoundecanoic acid at concentration range of 2400 – 90 µM was used because sulfhydryl groups may be estimated in a sample by comparison to a standard curve composed of known concentrations of a sulfhydryl-containing compound [19]. All experiments were performed in triplicate (n = 3), unless specifically noted. Moreover, the degree of functionalization (DF) of chitosan with MERC was estimated based on the total amount of available reaction sites in chitosan chains before the functionalization reactions and the results obtained by the *Ellman's* method as described in our recent work [25] with *DD (*degree of deacetylation of chitosan (*DD* = 0.85)) estimated by NMR according to our previous study [27].

#### 4.2.3.2 Statistical analysis

The results of all experiments were averaged and statistical analysis was performed using ANOVA (one way included Tukey's test, $p < 0.05$, software Origin v.8.1, OriginLab Corporation, USA) unless specifically noted.

#### 4.2.3.3 Characterization of thiomer samples

Raman spectroscopy was performed with a LabRam-HR 800 (Horiba/Jobin Yvon) equipped with an Olympus BX-41 microscope provided with lenses of 10×, 50× and 100× and an additional macro lens of 40 mm for all samples. A 632.8 nm excitation from a helium-neon laser was focused on a spot of 1-2 $\mu m^2$ in the samples. The back-scattered light collected was dispersed by a monochromator and detected by the $LN_2$ (liquid nitrogen)-cooled CCD (charge-coupled device) system. The spectra ranged from 200 $cm^{-1}$ to 3300 $cm^{-1}$ with a step size of 1.1 $cm^{-1}$. Depending on the background fluorescence, the acquisition time was set from approximately 60 s to 300 s, with a minimum of ten replicates to increase the signal-to-noise ratio. This analysis was performed on samples produced and after immersed in aqueous solutions with pH 3.0, 7.0, 9.0 and dried at room temperature.

To determine the swelling behavior of 3D scaffolds, the water adsorption (WA) was evaluated in aqueous solution at pH 3.0, 7.0 and 9.0 (adjusted with HCl or NaOH, 0.5 % aqueous solution), as described in the literature [4,25]. This process was performed for 24 hours and the Equation 4.1 was used to assess the water adsorption until reaching the equilibrium for the chitosan-based hydrogels [25]. These experiments were performed with 9 samples for each system (n = 9, 3 samples of 3 different syntheses of the 3D scaffolds).

$$WA\ (\%) = [(M_s - M_i)/M_i]\ x\ 100 \qquad (4.\ 1)$$

Where $M_s$ is the weight of the swollen polymer, and $M_i$ is the initial weight of the polymer.

The morphologies of the freeze-dried CHICys and CHIMerc scaffolds were evaluated using a scanning electron microscope (SEM, FEI-FEG-FIB-QUANTA 3D) coupled with energy dispersion X-ray spectroscopy (EDX, EDAX Bruker, 0.8 nm). Before the examination, the samples were coated with a thin carbon film *via* sputtering using a low deposition rate, cooling the substrate, and ensuring the maximum distance between the target and the sample to avoid sample damage; the film formed was 30 nm. Images of secondary electrons (SE) were obtained using an accelerating voltage of 15 kV for all samples. Moreover, the three-dimensional structures of the scaffolds were investigated using 3D microtomography

(SkyScan 1174, Bruker micro-CT) at a resolution of 12.18 μm, at 40 kV voltage, 100 μA current, 0.7° rotation step, and no filter. Images were reconstructed using NRecon Reconstruction software (v.1.6.1.18, Bruker micro-CT). CTAn software (v.1.15.4.0, Bruker micro-CT) was used to analyze the micro-CT datasets in 2D and 3D for morphometry and densitometry. Additionally, the mass of the dry, wet and submerged scaffolds was measured using the accessory SMK-301/400 (Shimadzu) coupled to a balance (± 0.0001 g) and the densities $\rho_a$, were calculated according to the literature [25]. The porosities (ε) were calculated according to the *Archimedes's* Method [25,28]. The surface areas ($S_a$) were estimated by a method used to determine the surface area of powder materials [25,29].

### 4.2.4 Antibacterial activity of 3D scaffolds

The samples were sterilized and pressed as disc format similar to the antibiotic disc, then it was sterilized again using UV radiation at 10 cm of distance (4.78 $mW.cm^{-2}$, 6 W, at λ = 254 nm, Boitton Instruments). It was prepared 18 discs of each sample with average mass presented in Table S.1. Then, the Gram-negative human bacterial pathogens (*Pseudomonas aeruginosa*, *P. aeruginosa*, ATCC 27853) obtained from the American Type Culture Collection (ATCC) was tested. The inoculums of the test organism were incubated at 37 °C in Muller–Hinton medium until reaching the logarithmic phase. The optical density of bacterial suspensions was measured at λ = 620 nm using a microplate reader (Spectra II Microplate Reader, Tecan) at absorbance mode. All of the materials were sterilized in the autoclave at 120 °C under 1 $kgf.cm^{-2}$ for 15 min.

### 4.2.5 Adsorption and desorption of organic dye pollutants

The adsorption of organic dye pollutants was made using methyl orange (MO) as a model of hazardous dyes in water, respectively. MO solutions were prepared from a stock solution of 100 $mg.L^{-1}$ in deionized water. The MO solutions were prepared with 3 concentrations (20 $mg.L^{-1}$, 50 $mg.L^{-1}$, and 100 $mg.L^{-1}$). Adsorption experiments were conducted by adding approximately 18 mg of the scaffolds (on a dry mass basis) into 5 mL of each MO solution. The experiments were performed at constant pH = (7.0±0.5) and temperature of (26±2) ºC in a dark chamber. All experiments were averaged, and statistical analysis was used. The removal efficiency (% removal by sorption) under the selected experimental conditions and

adsorption capacity ($mg.g^{-1}$) were determined according to the literature [27]. The correlation of the absorbance with the dye concentration was performed at the characteristic maximum absorption wavelength of MO (*i.e.*, $\lambda$ = 465 nm) by the standard working curve (Fig. S.1) using UV–vis spectroscopy (Lambda EZ-210, Perkin Elmer) in all experiments. Appropriate dilution was performed to ensure that the concentration of the solution was within the range of the standard working curve.

Adsorption kinetics experiments were performed to determine the time for equilibrium for the dye adsorption (at 20 $mg.L^{-1}$, final pH equal 7.0±0.5 and temperature of 26±2 °C). The fitting of the pseudo-first-order and pseudo-second-order models [4,30] to the experimental data at increasing time intervals up to 1440 min (*i.e.,* 24 h) was also investigated.

The Langmuir and Freundlich equations [13] were tested to determine the best model to describe the results, in a concentration range of 0-100 $mg.L^{-1}$, mass of adsorbent of 13 mg, final pH of 6.5±0.5 and temperature of (26±2) °C. The effect of the pH from 3.0±0.5 to 9.0±0.5 (adjusted with NaOH or HCl 1.0 $mol.L^{-1}$) on the adsorption of MO solutions (20 $mg.L^{-1}$) was also investigated. Before and after scaffold immersion and with increasing time intervals, aliquots of the MO solutions were collected and analyzed to determine the dye concentration. The CHIMerc sorbent, before and after 24 hours contact with MO was dried at room temperature and analyzed by Raman spectroscopy, according to the procedure described in section 4.2.3.3.

As a preliminary assessment of the potential recovery of MO, desorption experiments were performed. After adsorption of MO (at 100 $mg.L^{-1}$ after 24 h), saturated dye-loaded sorbents were immersed in aqueous KCl solution (3 $mol.L^{-1}$, ionic strength = 1.5), $HNO_3$ solution (pH = 4.0±0.5), NaOH solution (pH = 10.0±0.5), and EDTA (1 M, pH = 4.5±0.5) to evaluate desorption due to the ion exchange, pH variation and extraction by a complexant, respectively. After 2 h of ultrasonication, the final MO concentrations in solution were analyzed and compared to the amount of dye previously adsorbed.

## 4.3 Results and Discussion

### 4.3.1 Characterization of 3D scaffolds

#### 4.3.1.1 Analysis of synthesis and determination of total thiol group

The concentration of thiol groups on CHIMerc was (2218±100) µmol.g$^{-1}$ [24]. It can be observed that the degree of substitution of thiol groups was higher (300 to 700 % for CHIMerc) compared with other studies [18,19,26,31]). The *N*-acylation of chitosan using 11-mercaptoundecanoic was only previously reported in our recent work [24]. This effectiveness of the thiolation process can be assigned to optimized experimental conditions, such as the use of sulfo-NHS combined with EDC as a zero-length coupling agent (stabilization of intermediates formed), the buffer solution and solvent (*i.e.*, PBS solution), temperature, pH, concentration of reagents, kinetics of reaction, degree of deacetylation, molecular weight (Mw), DD of chitosan and others. The high concentration (over 400 %) of thiol groups at CHIMerc was suggested to be mostly caused by the orientation of the reacting molecule MERC as an amphiphilic molecule (*i.e.*, "polar carboxylic head" and "hydrophobic thiol-acyl tail") favoring the formation of amide bonds with the amino groups of chitosan [32]. Moreover, the high concentration of thiol groups found in CHIMerc (degree of substitution of 26±2 %) possesses advantages for improving the properties of pristine chitosan in many potential applications [18,31].

#### 4.3.1.2 Analysis of Raman spectra and Swelling as a function of pH (Mechanism)

Raman spectroscopy was used for the characterization of the chitosan thiomers, as thiol bands are weakly detectable in FTIR. The typical chitosan bands (Figure 4.1A) can be identified in the 3D scaffolds: the amide I bands at ~1696 cm$^{-1}$; the amide III band at 1297 cm$^{-1}$; the –$CH_2$ bending at ~1410 cm$^{-1}$; the bands assigned to C-O stretching at 890 cm$^{-1}$ and 920 cm$^{-1}$; C-H stretching bands between 2800 – 2900 cm$^{-1}$. In addition, the 3D scaffolds presented the bands related to sulfur groups at 610 cm$^{-1}$ (-S-C-), 540 cm$^{-1}$ (S-S) and 2560 – 2500 cm$^{-1}$ (-SH) [33, 34]. Moreover, the bands associated with stretching and bending vibrations of the C-H and $CH_2$ species at 2800 - 3000 and 1492 cm$^{-1}$, respectively, were stronger in the CHIMerc sample than in the CHI sample, which were assigned to the contributions of *N*-acylation of the chitosan polymer with the MERC alkyl chain (*i.e.*, inserting 10 $CH_2$ groups) [33]. Minor signals were detected at 540 cm$^{-1}$ in the CHIMerc sample, which indicated the formation of

disulfide bonds (S-S) by adjacent thiol groups [34]. The band located at 760 $cm^{-1}$, which may be attributed to the deformation $\rho(CH_2)$ in phase [34], only appeared at CHIMerc. Some other less intense bands (not highlighted) at CHIMerc were observed at 1037 and 1100 $cm^{-1}$ are assigned to the *cis* and *trans* (C–C) stretching, respectively, while the band at 1064 is characteristic of a random (C–C) skeletal conformation [33].

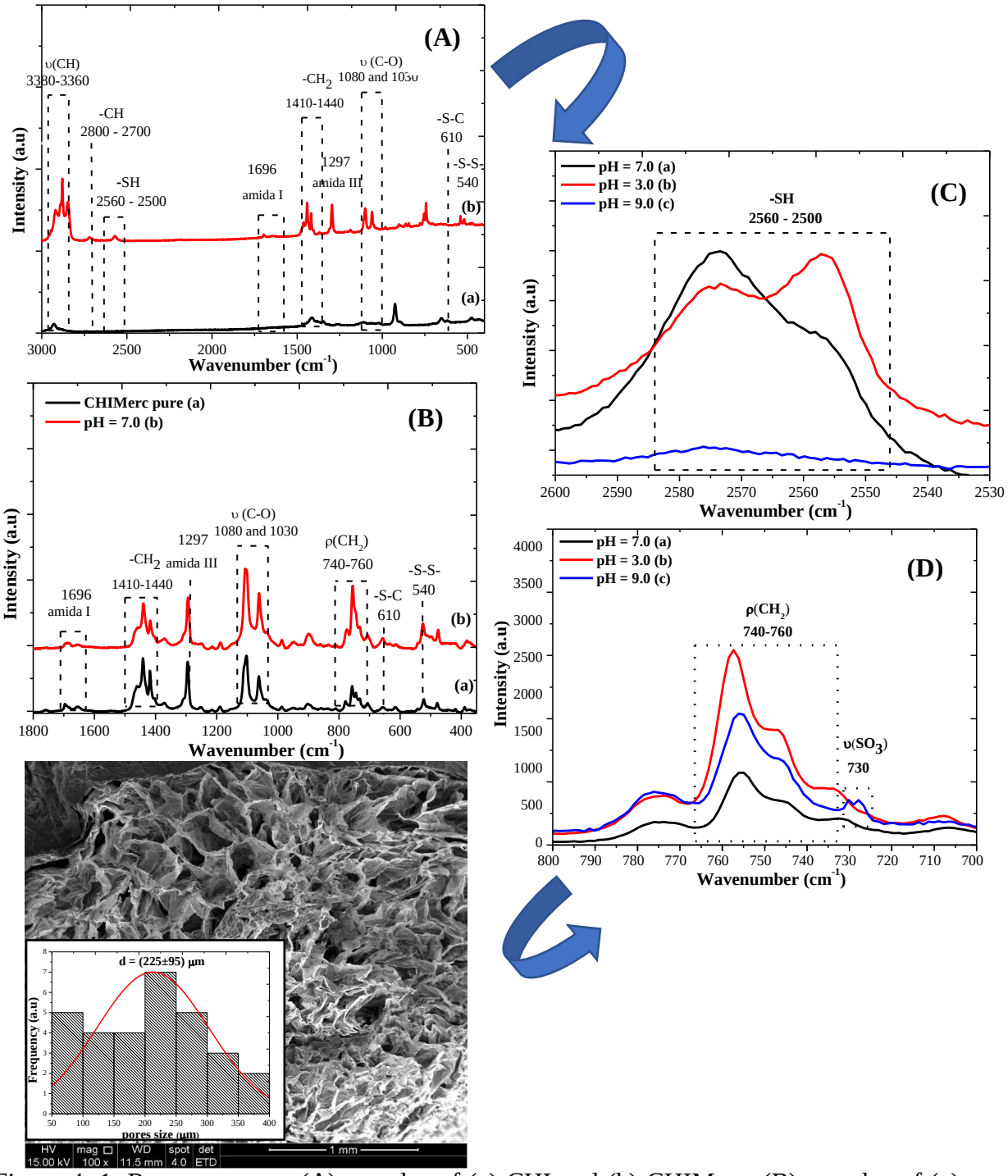


Figure 4. 1. Raman spectra: (A) samples of (a) CHI and (b) CHIMerc; (B) samples of (a) CHIMerc pure, (b) CHIMerc at pH=7.0±0.5; (C) detail of the 2550-2560 $cm^{-1}$ band (-SH) at (a) pH=7.0±0.5, (b) pH=3.0±0.5, (c) pH=9.0±0.5; (D) detail of the 730 $cm^{-1}$ band ($-SO_3$) at (a) pH=7.0±0.5, (b) pH=3.0±0.5, (c) pH=9.0±0.5; (E) Typical SEM image of 3D thiomer scaffold.

Raman spectroscopy helped to determine the mechanism of 3D scaffolds (CHIMerc) at different pH. Figure 4.1B shows the similarity between the spectra obtained under neutral conditions and that of pure CHIMerc. Under basic conditions the thiol band suffers a great decrease (Figure 4.1C), which can be attributed to the oxidation of SH groups at this pH. The vibration of $SO_3$ [35,36] by the additional weak mode appears at 730 $cm^{-1}$ (Figure 4.1D). In addition, the band at 956 $cm^{-1}$ is shifted towards lower frequencies at pH (9.0±0.5) compared with pH (7.0±0.5) and (3.0±0.5), which can be also attributed to the appearance of $SO_3$ [36,37].

Similar to Raman, the water adsorption was used to determine the mechanism of 3D scaffolds at different pH values. The results showed a significant difference in the swelling of CHIMerc between pH (3.0±0.5) and (9.0±0.5). The water adsorption (WA) was higher at acid (916±71 %) than at basic conditions (511±18 %). The largest water adsorption (1765±144 %) was observed under neutral conditions (pH=7.0±0.5).

Under acidic conditions (pH<pKa≈6.5 of chitosan [27]), the amine groups of chitosan are predominantly protonated to various degrees (Equation 4.2), which improve the water adsorption at this medium. Under basic conditions, the amino group is deprotonated (Equation 4.3). In addition, the thiol group is present in aqueous solution as dissolved neutral ($H_2S$) species or dissolved anions (*eg.* $HS^-$, $HSO_3^-$, $S_2O_3^-$) depending on the pH [38]. This group presents a great affinity by oxygen and can oxidize to form disulfide cross-linked hydrogel or -$SO_3$, spontaneously; the reaction is slow by exposure to air [31,39]. The basic conditions accelerated this oxidation process, thus decreasing the water adsorption at this medium (Equation 4.3). At neutral conditions all amine groups are deprotonated ($NH_3^+ \rightarrow NH_2$, no residual charges), the polymer chain increases the formation of dative bonds of groups (electron donor, :$NH_2$ or :SH), and the reaction of thiol oxidation is very slow, which improved the water adsorption (Equation 4.4).

$$CHI\,{}^{:NH_2}_{SH} + \; H^+(aq) \rightarrow CHI\,{}^{NH_3^+}_{SH} \qquad (4.2)$$

$$CHI_{SH}^{NH_3^+} + OH^-(aq) \rightarrow CHI_{SO_3}^{:NH_2} \quad (4.3)$$

$$CHI\ {}_{:SH}^{:NH_2} + H_2O_{(aq)} \rightarrow [CHI\ {}_{SH}^{NH_2}/H_2O] \quad (4.4)$$

#### 4.3.1.3 Morphological analysis of 3D scaffolds

SEM images of samples CHIMerc showed a highly porous structure for the thiomer scaffolds (Figure 4.1E) with average pore diameter of (225±95) µm. These CHIMerc scaffolds present a three dimensional interconnected hierarchical pore structure, which will contribute for the formation of surface sites for the adsorption process of organic dyes in water. These interconnected pores are very important to facilitate the diffusion of the adsorbate [6,39]. In addition, as reported in our previous study [25], micro-CT analysis indicated porous structures with a reasonably monodisperse distribution in the 3D volume. The CHIMerc showed an average pore size of (214±3) µm and porosity of (82±3) %. These results supported the SEM analysis, indicating that the combination of morphological features would favor the permeability and flux of adsorbate, improving the adsorption of azo dyes by the scaffolds. The surface area in the 3D scaffolds was determined by *Archimedes'* method. This method indicated that CHIMerc has the largest surface area (804±89 $m^2 \cdot g^{-1}$), because the presence of sub-micrometer pores [25]. The high porosity of the scaffolds and their high surface area likely provided a very large surface-to-volume ratio, thus offering abundant active sites for the adsorption of azo dyes [40].

### 4.3.2 Analysis of the Antibacterial activity of 3D scaffolds

The chitosan antibacterial activity depends on their physical properties (DD, Mw), type of solvent, microorganism species and biopolymer source [19,20,41]. According to the literature [19], the results also depend on the tested chitosan and on the method to measure the antibacterial activity. In this study, the antibacterial activity of 3D scaffolds was evaluated using agar-well diffusion method. The results are shown at Figure 4.2A. The absence of antibacterial activity of CHI is ascribed to the high molar mass of the sample used in the present investigation.

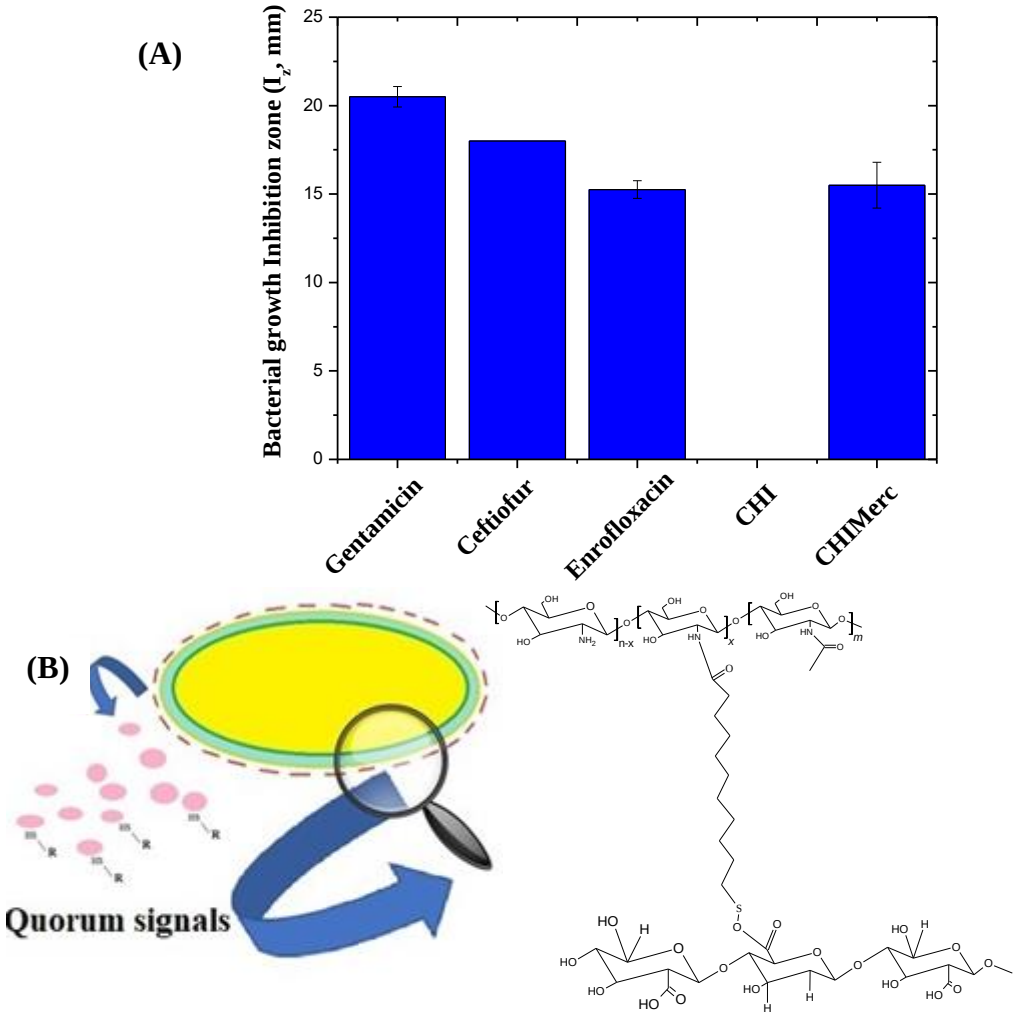


Figure 4. 2. (A) Sensitivity of bacterial activity against 3D scaffolds and (B) Illustration of some mechanisms proposed to explain CHIMerc antibacterial activity against *P. aeruginosa*.

Conversely, Figure 4.2A demonstrates the antibacterial activity of the synthesized CHIMerc against the *P. aeruginosa*. These bacteria are highly drug-resistant and opportunistic pathogen present at hospital effluents. Due to the permeability barrier in the outer membrane, it is naturally resistant to many antibiotics [20]. To explain the CHIMerc antibacterial result against *P. aeruginosa* some hypotheses are not discharged: the highest DF (26±2) %, the long alkyl-chain, which improves the hydrophobic interactions between the alkyl chain and the bacterial wall proteins [20], the interaction between the thiol group and the alginate

biofilm ((1–4)-linked β-D-mannuronate) formed at bacterial culture causing lyase of this biofilm [42], and the interaction with *quorum signals* (QS) (which is a mechanism by each bacteria communicate with each other [41]) prevented the increase of bacterial proliferation (Figure 4.2B).

Previous work [20] suggested the length of the thiol-alkyl chains of the chitosan substituents can enhance the antibacterial activity of the pristine compound through hydrophobic interactions between the alkyl chain and the bacterial wall proteins. Nevertheless, other authors reported the detrimental effect on antibacterial activity by the reaction of the thiol-moiety with cysteine, because this group can serve as nutrients for the bacteria [19,22].

### 4.3.3 Analysis of dye adsorption process

#### 4.3.3.1 Adsorption analysis of methyl orange (MO)

The adsorption pattern depicted by the scaffolds, CHIMerc, are shown in Figure 4.3. The CHIMerc scaffolds showed increasing MO uptake with time up to approximately 240 min, remaining constant at longer times. The decolorization of the MO solutions, changing from a darker orange to light orange (Figure 4.3C), was qualitatively observed after the contact with CHIMerc.

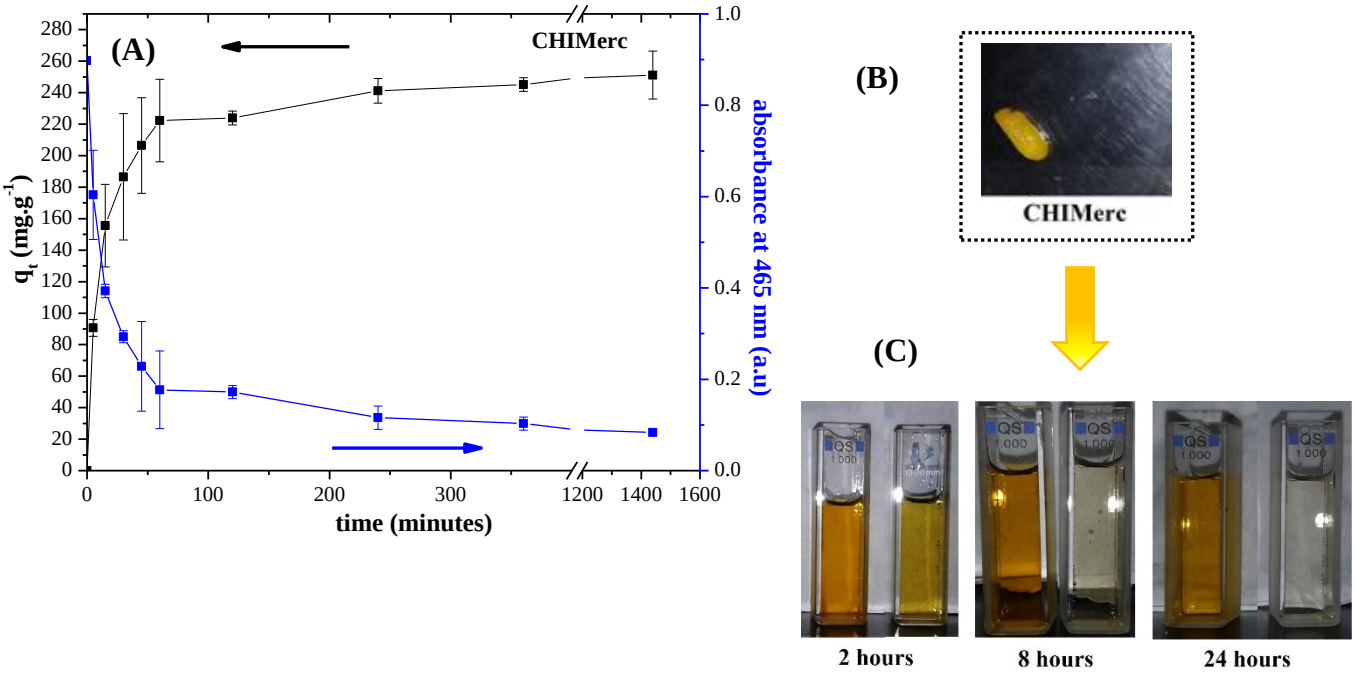


Figure 4. 3. (A) Methyl orange (MO) adsorption and absorbance profile as a function of time for CHIMerc, (B) CHIMerc after 8 hours in contact with MO solution (C) Initial solution of MO and after 2, 8 and 24 hours in contact with CHIMerc. Experimental conditions: MO initial concentration 20 mg.L$^{-1}$; initial pH (7.0±0.5); final pH (6.7±0.5); temperature of 26±2 °C.

The MO dye concentration was quantified by the Beer-Lambert correlation with absorbance analyzed by UV–vis spectroscopy at its characteristic maximum absorption wavelength (i.e., $\lambda = 465$ nm) (Fig S.2). The decrease of absorbance at 465 nm with the increase of time (Figure 4.3) depicts MO adsorption by the scaffold. The MO removal (S) after 2 hours contact time was calculated to be (88±1) % for CHIMerc. Under these conditions, the adsorption capacity (not $q_{max}$) of CHIMerc for MO was (251±15) mg.g$^{-1}$, which compares very positively with the literature (Table 4.1). The relative high adsorption of MO dye was related to the high concentration of thiol groups in the CHIMerc ((2218±100) µmol.g$^{-1}$), resulting in the formation of a MO-thiolate complex on the scaffold surfaces.

Table 4. 1. Comparison of MO uptake with data from the literature

| Reference | Adsorbent | $q_{max}$ ($mg.g^{-1}$) | pH |
|---|---|---|---|
| [6] | Aminated pumkin seed powder Zr (IV)-immobilized crosslinked | 126.1 | 3 |
| [43] | Chitosan/bentonite composite | 76.9 | 7 |
| [44] | HEMA-chitosan-MWCNT nanocomposite | 198 | 7 |
| [45] | Chitosan spheres | 5.8 | 7 |
| [46] | Chitosan biomass | 29 | 3 |
| [47] | Chitosan/alumina composite | 32.999 | 7 |
| This study | CHIMerc | 400 – 450 | 7 |

MO (Methyl orange)
HEMA – chitosan – MWCNT (nanocomposite of multi-walled carbon nanotube (MWCNT) functionalized (f) with chitosan (CS) and poly-2- hydroxyethyl methacrylate (pHEMA))
Zr (IV)-immobilized crosslinked (nanocomposite of chitosan with Zr (IV)

### 4.3.3.2 Kinetics of MO adsorption

The adsorption kinetics of the dye was calculated by monitoring the absorbance of the MO solution after the contact with CHIMerc sample. Figure 4.4 clearly shows that the adsorption process increased rapidly in the initial stages and then slowed down. According to the literature, the adsorption processes are generally described by the following kinetic equations, namely, the pseudo-first-order and pseudo-second-order rate laws [6,13]. The pseudo-second-order model fitted better the adsorption data as indicated by the fitting curves (Figure 4.4) to the experimental data, the higher correlation coefficient ($R^2$) (Table S.2). This conclusion was further confirmed by the Chi-square ($\chi^2$) test [4] as shown in the supplementary material. The pseudo-second-order rate constant calculated from Figure 4 was ($15x10^{-3}$) $g.mg^{-1}.min^{-1}$. The theoretical value of $q_e$ (251 $mg.g^{-1}$) also agrees very well with the experimental data.

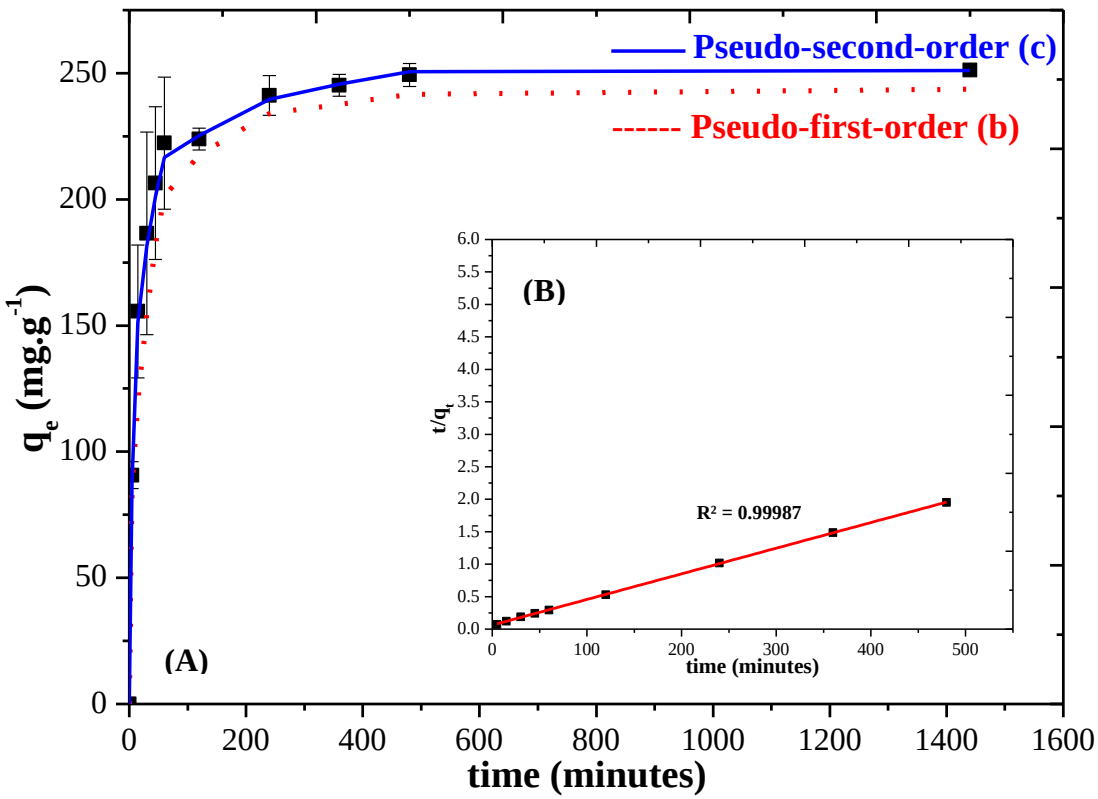


Figure 4. 4. Kinetic models applied to the experimental data (squares) of methyl orange (MO) adsorption on CHIMerc (a) pseudo-second-order (continuous line) and (b) pseudo-first-order (dash line); the inset shows the linearized form of pseudo-second-order model. Experimental conditions: MO initial concentration 20 mg.L$^{-1}$; initial pH of (7.0±0.5); final pH of (6.7±0.5); temperature of 26±2 °C.

#### 4.3.3.3 Adsorption Isotherms

The amount of solute adsorbed per unit mass of the adsorbent in equilibrium with the concentration of an adsorbate in bulk solution at a given temperature may be expressed by an adsorption isotherm. The two most common equations for describing solid-liquid sorption systems are the Langmuir and Freundlich (two-parameter isotherms) [6]. The fitted isotherms and the constants $K_L$, $K_F$, $R_L$, and $q_m$ are presented in Figure 4.5A and Table 4.2, respectively.

Table 4. 2. Parameters of Langmuir's and Freundlich's Equations

| **Langmuir** | | | | | **Freundlich** | | | |
|---|---|---|---|---|---|---|---|---|
| **$q_m$ ($mg.g^{-1}$)** | **$K_L$ ($L.mg^{-1}$)** | **$R_L$** | **$R^2$** | **D (%)** | **$K_F$ ($mg.g^{-1}$)** | **n** | **$R^2$** | **D (%)** |
| 588.24 | 0.85 | 0.062 | 0.92952 | 21 | 4.21 | 2.40 | 0.98974 | 12 |

$q_m$ (maximum uptake obtained by the Langmuir equation);
$K_L$ (Langmuir constant);
$R_L$ (dimensionless separation factor);
$K_F$ (constant relating the adsorption capacity);
n (empirical parameter related to the deviation of linearity);
D (average absolute percentage deviation).

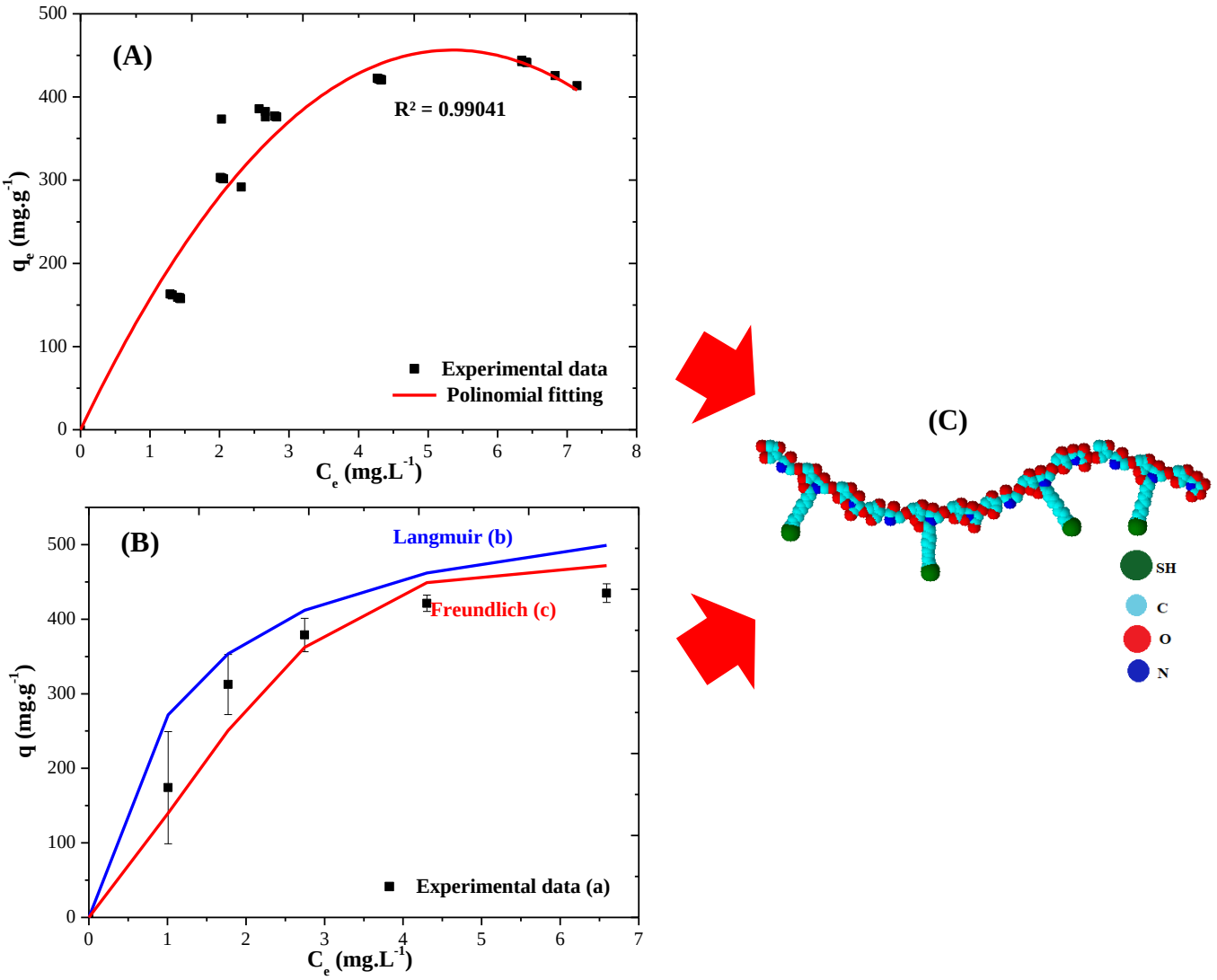


Figure 4. 5. Fitting of models to MO-CHIMerc experimental data (A) second-order degree polynomial, (B) Langmuir (b, blue square) and Freundlich (c, red circle) adsorption isotherms (C) 3D structure of CHIMerc showing the thiol group at chitosan chain (SH green). Experimental conditions: MO initial concentration 20 $mg.L^{-1}$; initial pH (7.0±0.5); final pH (6.7±0.5); temperature of 26±2 °C.

The best fitting was achieved with the Freundlich equation, as shown by $R^2$ and the average absolute percentage deviation (% D) [13] (Table 4.2). Figure 4.5 suggests that at lower concentrations the Langmuir equation fitted better than Freundlich, whereas at high concentrations the Freundlich equation prevails. This observation can be ascribed to the fact that at lower concentrations and surface coverage, adsorption may take place with no

interaction between the adsorbate molecules. As the surface coverage increases, the interaction between the adsorbate molecules will influence the adsorption process. This behavior may be also explained in terms of a non-uniform distribution of adsorption energy, which is consistent with the Freundlich model and MO adsorption on CHIMerc illustrated in Figure 4.5C. The adsorption involves the affinity of thiol groups, crafted on the chitosan chain, by the oxygen in the MO pigment. A favorable adsorption tends to have a value of n (Freundlich's constant) between 1 and 10 [48]. It is also noticeable the development of a plateau corresponding to a maximum adsorption capacity in range of 400 – 450 $mg.g^{-1}$, which is relatively high if compared to the other studies reported in the literature (Table 4.1) in similar systems. There are some investigations on the application of thiolated chitosan for the removal of metals. To the best of the authors' knowledge, the adsorption of dyes by thiolated chitosan porous scaffolds was not previously reported.

#### 4.3.3.4 Analysis of MO desorption

To offer the possibility of recovering the dyes extracted from the liquid phase and the adsorbent, it is desirable to regenerate the adsorbent material. For this experiment, four systems (EDTA, KCl, $HNO_3$, and NaOH) were chosen. The recovery of MO after just 2 h of ultrasonication was (82±1) %, (76±2) % and (37±2) % for the EDTA, KCl, and $HNO_3$, respectively (Figure 4.6). These results indicated the potential use of these new 3D scaffolds as biocompatible and eco-friendly bio-sorbents for MO dye removal and recovery in environmental applications.

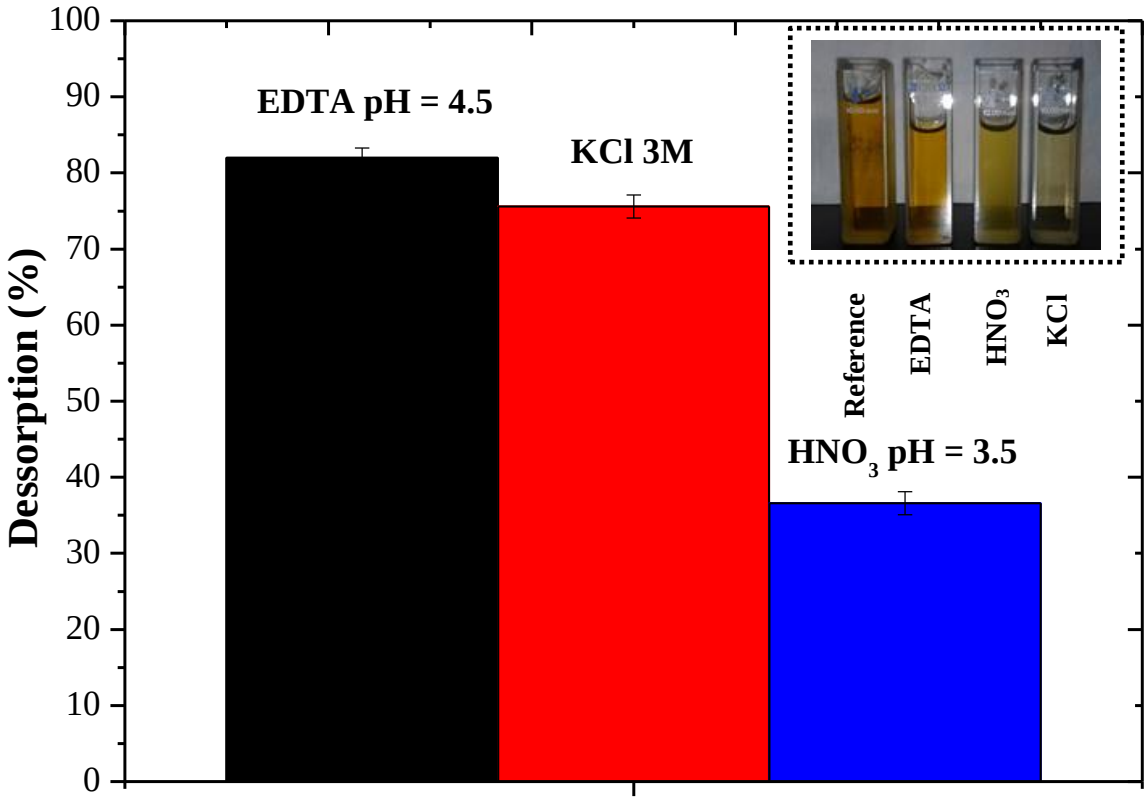


Figure 4. 6. Desorption of methyl orange from CHIMerc by different media, after 2 hours, T= (26±2) °C; the inset shows the solution with 20 mg.$L^{-1}$ MO and after desorption by EDTA, KCl and $HNO_3$.

#### 4.3.3.5 Mechanism of MO adsorption on thiolated chitosan

The pH of the solution will affect both the charges of the ionized dye molecules and the thiol group, thus the adsorption process. The previous section discussed the experiments carried out under neutral conditions (pH=7.0±0.5), the best one according to water adsorption and Raman spectroscopy. The effect of acid and alkaline conditions on MO adsorption was also studied and is shown in Figure 4.7.

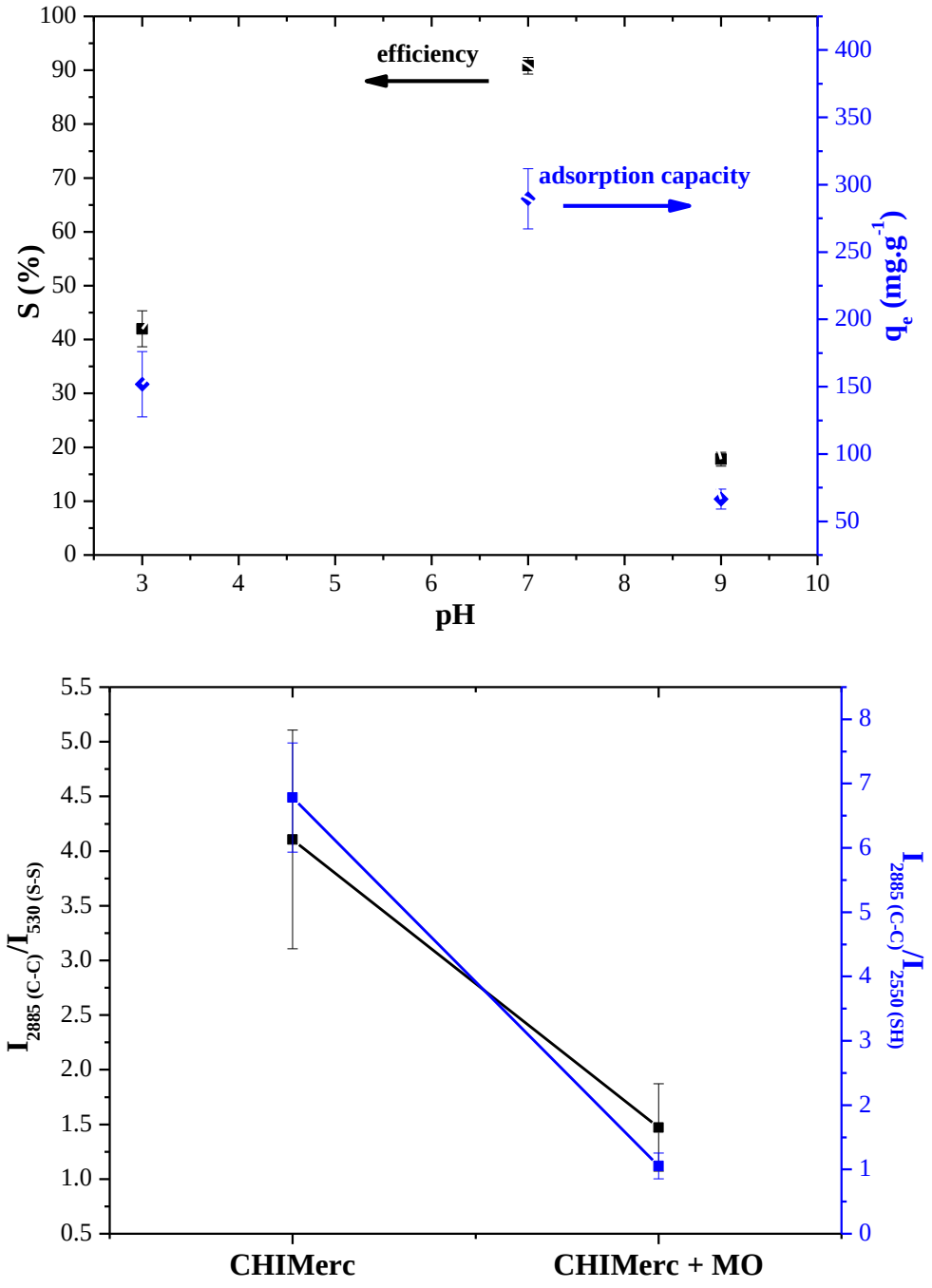


Figure 4. 7. (A) Uptake of methyl orange (MO) by CHIMerc at different pH. Experimental conditions: MO initial concentration 20 mg.L$^{-1}$; temperature of 26±2 °C (B) The relationship between band intensities at 2885 and 2550 cm$^{-1}$ and between bands at 2885 and 530 cm$^{-1}$.

Under acid conditions (MO pKa = 3.49), MO protonates: the dimethylamino group to form an ammonium ion ($R\text{-}NH_3^+$) or the azo group to form an azonium ion ($R{=}NH_2^+$). As pH increases, the MO charge changes from positive to neutral and finally to negative charge [49]. The study of the effect of pH was developed at pH (9.0±0.2), (7.0±0.2) and (3.0±0.2). During all of the adsorption experiments, pH variation was less than 0.2 units, thus indicating no net release of $H^+$ or $OH^-$ groups.

The obtained results showed the highest MO uptake at neutral conditions, thus indicating that the charge of dye does not influence directly dye adsorption on CHIMerc. Adsorption is rather dominated by the great affinity of MO by the thiol groups (Figure 4.8). At neutral conditions (Figure 4.8A), the polymer chain increases the formation of dative bonds (electron donor, : $NH_2$ or :SH), and the kinetic of thiol oxidation is very slow, as demonstrated in previous section by Raman spectroscopy. Under acid conditions (Figure 4.8B), the amine groups of CHIMerc are predominantly protonated ($\text{-}NH_3^+$) and so the MO groups, which may hinder MO adsorption, despite the great affinity of adsorbent by the dye (Figure 4.6B). Under basic conditions the oxidation process of a thiol group takes place, as demonstrated by the Raman spectroscopy (section 4.3.1.2), which contributes to decrease MO adsorption.

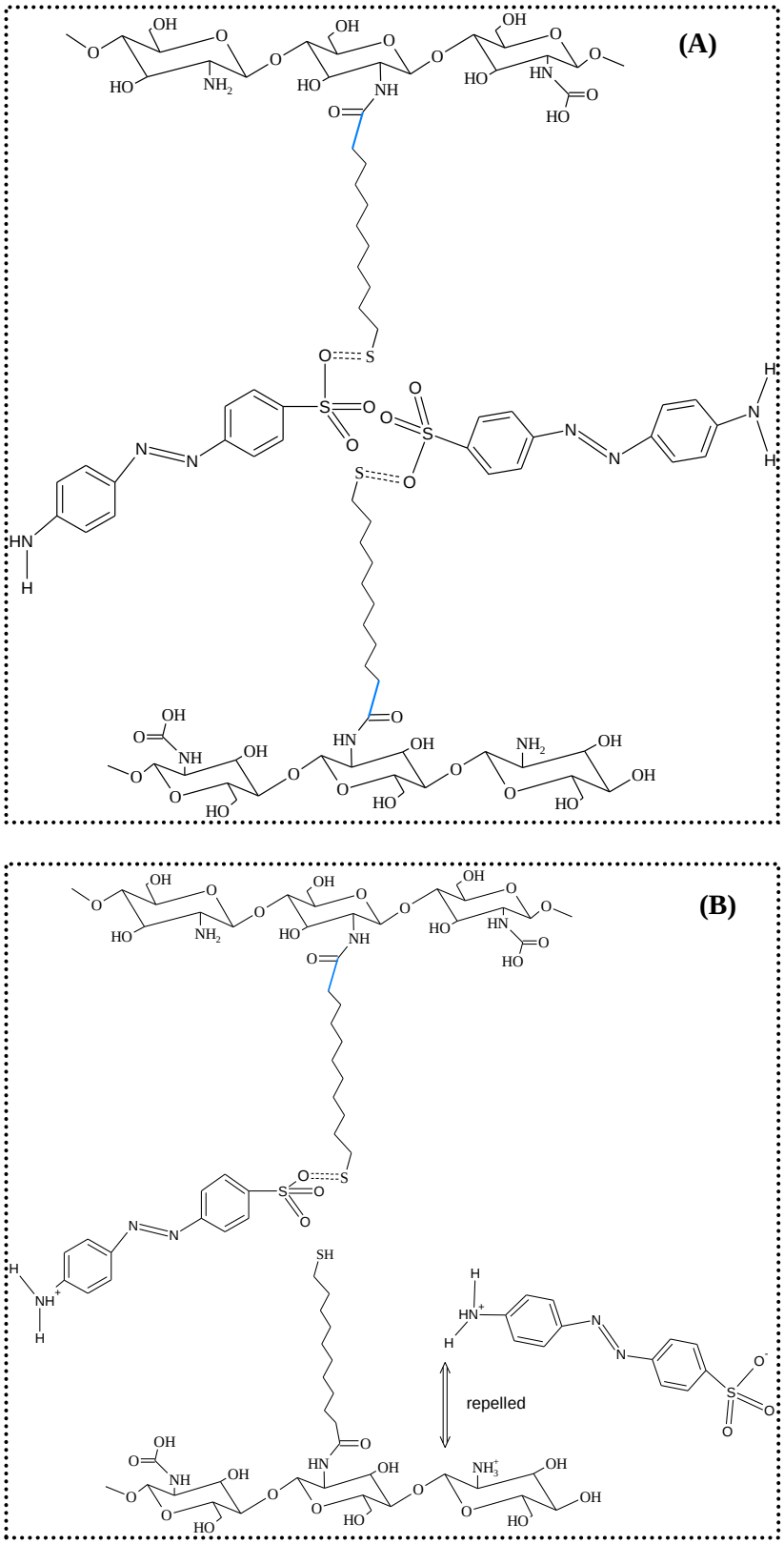


Figure 4. 8. Mechanism of MO adsorption by CHIMerc at (A) neutral and (B) acid conditions.

Raman spectroscopy was used to investigate role of thiol groups on MO adsorption. The spectra (Fig. S.3) showed the interaction between MO and the thiol at CHIMerc by the decrease of bands at 610 $cm^{-1}$ (-C-S), 540 $cm^{-1}$ (S-S) and 2560 – 2500 $cm^{-1}$ (-SH). Moreover, the ratio of the reference band intensity at 2885 $cm^{-1}$, which was not significantly affected by the chemical reaction with MO, and the intensities of the 540 $cm^{-1}$ (S-S) and 2560 – 2500 $cm^{-1}$ (-SH) bands were used to confirm the adsorption mechanism (Figure 4.8). The decrease of this ratio, observed in Figure 4.7B, indicates the interaction of sulfur-containing groups with MO during adsorption. Based on the results, it is possible to conclude that only a special type of S–S bonds is involved in MO adsorption. In fact, the atoms involved in the disulfide bonds (C–C–S–S–C–C) of adsorbent structure may assume different spatial orientations, causing three different conformations for the chemical bonds: *trans–gauche–trans*, *gauche–gauche–trans*, and *gauche–gauche–gauche* [34]. For the *trans-gauche–trans* and *gauche–gauche–trans* conformations, the expected wavenumbers for the S–S stretching vibration is 540 and 525 $cm^{-1}$, respectively, while for the *gauche–gauche–gauche* it is 510 $cm^{-1}$ [34]. The results indicated that the *trans-gauche–trans* disulfide bridges prevail in the CHIMerc and were preferably consumed during MO adsorption. Moreover, the sharp band at 2550 $cm^{-1}$ ($\nu$(S–H) vibrational mode) shown in the CHIMerc spectrum disappears after reaction with MO, which confirms that the higher concentration of thiol group (2218±100) µmol.$g^{-1}$ resulted in the formation of a MO-thiolated chitosan complex on the scaffold surface.

### 4.4 Conclusions

The application of 3D scaffolds with antibacterial activity, was evaluated for wastewater treatment. These thiolated chitosan derivatives showed a significant high thiolation degree (up to 700 % compare to other studies). The antibacterial activity was demonstrated against *P. aeruginosa*, a bacterium highly drug-resistant and an opportunistic pathogen. This feature was related to the presence of sulfhydryl groups, the high DF (26±2) %, the long alkyl-chain, with probable thiol interaction with the alginate biofilm, and the interaction with *quorum signals* (QS). The maximum adsorption capacity, in a range of 400 – 450 mg.$g^{-1}$, is higher than similar studies with other chitosan derivatives. The removal of dyes by thiolated chitosans were not previously reported, to the best of the authors' knowledge. Raman spectroscopy showed that the sulfhydryl groups at the 3D scaffolds are the active groups

involved in MO biosorption. The adsorption data were well-fitted to a pseudo-second-order kinetics and Freundlich's isotherm. Finally, the scaffolds showed MO dye recovery over 80 %. The 3D scaffolds are envisioned as promising bio-sorbents for potential wastewater treatment.

**Acknowledgments**

The authors acknowledge the financial support from the following Brazilian research agencies: CNPq (140810/2015-3; PQ1B–306306/2014-0; UNIVERSAL-457537/2014-0; PIBIC-2014/2015), CAPES (PROEX-433/2010; PNPD; PROINFRA2010-2014), FAPEMIG (PPM-00760-16; BCN-TEC 30030/12), and FINEP (CTINFRA-PROINFRA 2008/2010/2011), and they express their gratitude to the Center for Microscopy of the Federal University of Minas Gerais (UFMG) for the SEM/EDX analysis, the staff at the Center of Nanoscience, Nanotechnology and Innovation-CeNano$^2$I/CEMUCASI/UFMG for the spectroscopy analyses and to Dr. Maria Silva (INCT-Acqua) for the Raman spectroscopy analysis.

**Author Contributions**

The manuscript was written through the contributions of all authors. All authors have given their approval to the final version of the manuscript.

**Conflicts of Interest**

The authors declare that they have no competing interests.

**References**

[1] Ali, I., Gupta, K., Advances in water treatment by adsorption, Taylor & Francis, New York, 2007.

[2] Aksu, Z. Application of biosorption for the removal of organic pollutants: a review, Process. Biochem. 40 (2005) 997-1026.

[3] Peng, N., Hu4, D., Zeng, J., Li, Y., Liang, L.; Chang, C., Superabsorbent cellulose-clay nanocomposite hydrogels for highly efficient removal of dye in water, Acs Sustainable Chem. Eng. 4 (2016) 7217-7224.

[4] Capanema, N.S.V., Mansur, A.A.P., Mansur, H.S., Jesus, A.C., Carvalho, S.M., Chagas, P., Oliveira, L.C., Eco-friendly and Biocompatible Crosslinked Carboxymethylcellulose Hydrogels as adsorbents for the Removal Organic Dye Pollutants for Environmental Applications, Environ Technol, 38 (2017) 1-42.

[5] Halling-Sorensen, B., Nielsen, S.N., Lanzky, P.F, Ingerslev, F., Lützheft H.C.H, Jorgensen, S.E. Occurrence, fate and effects of pharmaceutical substances in the environment – a review. Chemosphere, 36 (1998) 357-393.

[6] Subbaiah, M. V., Kim, D-S., Adsorption of methyl orange from aqueous solution by aminated pumpkin seed powder: kinetics, isotherms, and thermodynamic studies, Ecotoxicol. Environ. Saf. 128 (2016) 109-117.

[7] Li, X., Li, Y., Zhang, S., Ye, Z., Preparation and characterization of new foam adsorbents of poly(vinyl alcohol)/chitosan composites and their removal for dye and heavy metal from aqueous solution, Chem. Eng. J. 183 (2012) 88-97.

[8] Emmanuel, E., Perrodin, Y., Keck, G., Blanchard, J.M., Vermande, P. Ecotoxicological risk assessment of hospital wastewater: a proposed framework for raw effluents discharging into urban sewer network. J Hazard Mater, A117 (2005) 1-11.

[9] Linton, K.B., Richmond, M.H., Bevan, R., Gillespie, W.A. Antibiotic resistance and R factors in coliform bacilli isolated from hospital and domestic sewage. J Med Microbiol, 7 (1974) 91-103.

[10] Baquero, F. From pieces to patterns: evolutionary engineering in bacterial pathogens. Nat Rev Microbiol, 2 (2004) 510-518.

[11] Bhatnagar, A., Sillanpää, M., Witek-Krowiak, A. Agricultural waste peels as versatile biomass for water purification — a review. Chem. Eng. J. 270 (2015) 244–271.

[12] Erosa, M.S.D., Medina T.I.S., Mendoza, R.N., Rodriguez, M.A., Guibal, E., Cadmiun sorption on chitosan sorbents: kinetics and equilibrium studies, Hydrometallurgy 61 (2001) 157-167.

[13] Laus, R., Fávere, V.T., Competitive adsorption of Cu (II) and Cd (II) ions by chitosan crosslinked with epichlorohydrin-triphosphate, Biosour. Technol. 102 (2011) 8769-8776.

[14] Monier, M., Adsorption of $Hg^{2+}$, $Cu^{2+}$ and $Zn^{2+}$ ions from aqueous solution using formaldehyde cross-linked modified chitosan-thioglyceraldehyde Schiff's base, Int. J. Biol. Macromol. 50 (2012) 773-781.

[15] Gautam, R. K., Mudhoo, A., Lofrano, G., Chattopadhyaya, M. C. Biomass-derived biosorbents for metal ions sequestration: Adsorbent modification and activation methods and adsorbent regeneration. J. Environ. Chem. Eng. 2 (2014) 239–259.

[16] Sanmugam, A., Vikraman, D., Park, H.J., Kim, H.-S. One-Pot Facile Methodology to Synthesize Chitosan-ZnO-Graphene Oxide Hybrid Composites for Better Dye Adsorption and Antibacterial Activity. Nanomaterials 7 (2017) 363.

[17] Raju, K.M., Raju, M.P., Mohan, Y.M., Synthesis of superabsorbent copolymers as water manageable materials. Polym. Int. 110 (2008) 2453-2460.

[18] Liu, D., Li, J., Pan, H., He, F., Liu, Z., Wu, Q., Bai, C., Yu, S. Yang, X., Potential advantages of a novel chitosan-N-acetylcysteine surface modified nanostructured lipid carrier on the performance of ophthalmic delivery of curcumin, Sci Rep, 28796 (2015) 1-14.

[19] Croce, M., Conti, S., Maake, C., Patzke, G.R. Synthesis and screening of N-acyl thiolated chitosans for antibacterial applications. Carbohydr Polym, 151 (2016) 1184-1192.

[20] Inta, O., Yoksan, R., Limtrakul, J. Hydrophobically modified chitosan: A bio-based material for antimicrobial active film. Mater Sci Eng. C, 42 (2014) 569–577.

[21] Vallapa, N., Wiarachai, O., Thongchul, N., Pan, J., Tangpasuthadol, V., Kiatkamjornwong, S. Enhancing antibacterial activity of chitosan surface by heterogeneous quaternization. Carbohydr Polym, 83 (2011) 868–875.

[22] Sarti, F., Bernkop-Schnürch, A. (2011). Chitosan and thiolated chitosan. In R. Jayakumar, M. Prabaharan, & R. A. A. Muzzarelli (Eds.), Advances in polymer science. chitosan for biomaterials I (243) (pp. 93–110). Berlin, Heidelberg: Springer Berlin Heidelberg.

[23] Dragostina, O. M., Samal, S. K., Dash, M., Lupascu, F., Pânzariu, A., Tuchilus, C., Ghetu, N., Danciu, M., Dubruel, P., Pieptu, D., Vasile, C., Tatia, R., Profire, L. New antimicrobial chitosan derivatives for wound dressing applications. Carbohydr Polym, 141 (2016) 28-40.

[24] Yong, S. K., Bolan, N., Lombi, E., Skinner, W. Synthesis and Characterization of Thiolated Chitosan Beads for Removal of Cu (II) and Cd (II) from Wastewater. Water Air Soil Pollut, 224 (2013) 1720-1735.

[25] Medeiros Borsagli, F. G. L.; Carvalho, I. C.; Mansur, H. S. Amino acid-grafted and N-acylated chitosan thiomers: Construction of 3D bio-scaffolds for potential cartilage repair applications. Inter J Biol Macromol, 114 (2018) 270-282.

[26] Schmitz, T., Grabovac, V., Palmberger, T.F., Hoffer, M.H., Bernkop-Schnurch, A., Synthesis and characterization of a chitosan-N-acetyl cysteine conjugate, Inter. J. Pharm. 347 (2008) 79-85.

[27] Medeiros Borsagli, F.G.L., Mansur, A.A.P., Chagas, P., Oliveira, L.C.A., Mansur, H.S., O-carboxymethyl functionalization of chitosan: Complexation and adsorption of Cd (II) and Cr (VI) as heavy metal pollutants ions, React. Funct. Polym. 97 (2015) 37-47.

[28] Ho, S. T., Hutmacher, D. W. (2006). A comparison of micro CT with other techniques used in the characterization of scaffolds. Biomaterials, 27, 1362-1376.

[29] Lowell, S., Shields, J. E., Thomas, M. A., Thommes, M., Characterization of Porous Solids and Powders: Surface Area, Pore Size and density. Springer, New York, 2004.

[30] Simonin, J-P., On the comparison of pseudo-first and pseudo-second order rate laws in the modeling of adsorption kinetics, Chem. Eng. J. 300 (2016) 254-263.

[31] Teng, D-Y., Wu, Z-M., Zhang, X-G., Wang, Y-X., Zheng, C., Wang, Z., Li, C-X., Synthesis and characterization of in situ cross-linked hydrogel based on self-assembly of thiol-modified chitosan with PEG diacrylate using Michael type addition. Polymer 31 (2010) 639-646.

[32] Tawill, N., Hatef, A., Sacher, E., Maisonneuve, M., Gervais, T., Mandeville, R., & Meunier, M. (2013). Surface Plasmon Resonance Determination of the Binding Mechanisms of L-Cysteine and Mercaptoundecanoic Acid on Gold. J Phys Chem Lett, 117, 6712−6718.

[33] Moller, K., Kobler, J., Bein, T. Colloidal suspensions of mercapto-functionalized nanosized mesoporous silica. J Matter Chem 17 (2007) 624-631.

[34] Teixeira, M. C., Ciminelli, V. S. T., Dantas, M. S. S., Diniz, S. F., Duarte, H. A. Raman spectroscopy and DFT calculations of As(III) complexation with a cysteine-rich biomaterial. J. Colloid Interface Sci 315 (2007) 128-134.

[35] Gillespie, R. J., Robinson, E. A. The Raman spectra of liquid sulfur trioxide and solutions of sulfur trioxide in inert solvents. Can J Chem 39 (1961) 2189-2200.

[36] Bondy, A. L., Craig, R. L., Zhang, Z., Gold, A., Surratt, J. D., Ault, A. P. Isoprene-Derived Organosulfates: Vibrational Mode Analysis by Raman Spectroscopy, Acidity-

Dependent Spectral Modes, and Observation in Individual Atmospheric Particles. J Phys Chem A 122 (2018) 303-315.

[37] Wan, Y., Wang, X., Hu, W., Chou, I-M., Wang, X., Chen, Y., Xu, Z. In situ optical and Raman spectroscopic observations of the effects of pressure and fluid composition on liquid–liquid phase separation in aqueous cadmium sulfate solutions (_400 _C, 50 MPa) with geological and geochemical

Implications. Geochim. Cosmochim. Acta 211 (2017) 133-152.

[38] Marcus, P. Surface science approach of corrosion phenomena. Electrochim. Acta 43 (1998) 109-118.

[39] Yang, R., Su, Y., Aubrecht, K.B., Wang, X., Ma, H., Grubbs, R.B., Hsiao, B.S., Chu, B., Thiol-functionalized chitin nanofibers for As (III) adsorption. Polymer 60 (2015) 9-17.

[40] He, X., Male, K. B., Nesterenko, P. N., Brabazon, D., Paull, B., Luong, J. H. T. Adsorption and Desorption of Methylene Blue on Porous Carbon Monolits and Nanocrystalline Cellulose, ACS Appl. Mater. Interface 5 (2013) 8796-8804.

[41] Liu, X. F., Song, L., Li, L., Li, S., De Yao, K. Antibacterial effects of chitosan and its water-soluble derivatives on E. coli, plasmids DNA, and mRNA. J Appl Polym Sci, 103 (2007) 3521–3528.

[42] Hurley, M.N., Càmara, M., Smith, A.R. Novel approaches to the treatment of Pseudomonas aeruginosa infections in cystic fibrosis. Eur Respir J., 40 (2012) 1014-1023.

[43] Zhang, L., Hu, P., Wang, J., Liu, Q., Huang, R. Adsorption of methyl orange (MO) by Zr (IV)-immobilized cross-linked chitosan/bentonite composite. Inter J Biol Macromol, 81 (2015) 818-827.

[44] Mahmoodian, H., Moradi, O., Shariatzadeha, B., Salehf, T. A., Tyagi, I., Maity, A., Asif, M., Gupta, V. K. Enhanced removal of methyl orange from aqueous solutions by poly HEMA–chitosan-MWCNT nano-composite. J Mol Liq, 2012 (2015) 189-198.

[45] Morais, W. A., Almeida, A. L. P., Pereira, M. R., Fonseca, J. L. C. Equilibrium and kinetics analysis of methyl orange sorption on chitosan spheres. Carbohydr Res, 343 (2008) 2489-2493.

[46] Allouche, F-N., Yassaa, N., Lounici, H. Sorption of Methyl Orange from Aqueous Solution on Chitosan Biomass. Proced Earth Plan Sci, 15 (2015) 596-601.

[47] Zhang, J., Zhou, Q., Ou, L. Kinetic, Isotherm, and Thermodynamic Studies of the Adsorption of
Methyl Orange from Aqueous Solution by Chitosan/Alumina Composite. J Chem Eng Data, 57 (2012) 412-419.

[48] Delle-Site, A. Factors affecting sorption of organic compounds in natural sorbent/water systems and sorption coefficients for selected pollutants. A review. J Phys Chem Ref Data, 30 (2001) 187-439.

[49] Oakes, J., Graton, P. Kinetic investigations of the oxidation of Methyl Orange and substituted arylazonaphthol dyes by peracids in aqueous solution. J. Chem. Soc. Perkin Trans. 2 (1998) 2563-2568.

**Supplementary Materials**

**Kinetics model – Equations**

pseudo-first-order

$$\ln(q_e - q_t) = \ln(q_e) - K_1 t \quad (1)$$

pseudo-second-order

$$t/q_t = 1/((K_2 . q_e^2)) + (1/q_e).t \quad (2)$$

Where, $q_e$ is the amount of dye adsorption per unit of mass of the adsorbent (adsorption capacity at equilibrium, mg.g$^{-1}$); $q_t$ is the amount of dye adsorption per unit of mass of the adsorbent at any given time ($t$); $K_1$ is the pseudo-first-order rate constant and it is calculated from the linearization of $\ln(q_e - q_t)$ vs. $t$ at the concentration established at 24 hours; $K_2$ is the pseudo-second-order rate constant (g.mg$^{-1}$·min$^{-1}$) [8].

The Chi square ($\chi^2$) test [4], a non-parametric test that can be used to determine the best fitted model [4], was used to confirm the results and confirmed that the pseudo-first-order was not properly fitted for CHIMerc ($R^2 = 0.8531$, $\chi^2 = 0.4050 << \chi_c^2 = 38.6314$ with significance level of 0.05; degree of freedom=9).

**Isotherms**

Equation 3 is preferentially used in studies on adsorption in solution, where $C_e$ are the adsorbate concentration in solution at equilibrium, $K_L$ is the Langmuir constant and $q_m$ is the maximum adsorption capacity of the monolayer formed on the adsorbent [8].

$$q_e = (K_L C_e q_m)/(1 + K_L C_e) \quad (3)$$

The Langmuir constant ($K_L$) is used to calculate $R_L$, a dimensionless separation factor given by Equation 4 [8].

$$R_L = 1/(1 + K_L C_0) \quad (4)$$

The $R_L$ values indicate whether the adsorption is unfavorable ($R_L$ > 1), linear ($R_L$ = 1), favorable (0 < $R_L$ < 1), or irreversible ($R_L$ = 0) [8].

The Freundlich isotherm is an empirical equation and is one of the most widely used isotherms for the description of multi-site adsorption. Mathematically, it is expressed by Equation 5 [8], where $K_F$ (mg.L$^{-1}$) is a constant relating the adsorption capacity and $1/n$ is an empirical parameter relating the adsorption intensity.

$$q_e = K_F C_e^{1/n} \quad (5)$$

**Linear form of isotherms**

The linear form of the Langmuir isotherm, represented by Equation 6, is employed to determine the $q_m$ and $K_L$ values from the angular and linear coefficients obtained by plotting $C_e/q_e$ as a function of $C_e$ [9].

$$C_e/q_e = 1/(K_L q_m) + C_e/q_m \quad (6)$$

The linear form of the Freundlich isotherm, represented by Equation 7, is employed to determine the $n$ and $K_F$, the Freundlich isotherm constants indicating the adsorption intensity and adsorption capacity, respectively [9].

$$log(q_e) = log(K_F) + (1/n) log(C_e) \quad (7)$$

The average absolute percentage deviation (% D) (Equation 8) was tested to prove and the same result were founded

$$D\ \% = (1/N \sum_{i=1}^{N} \Sigma \left|(q_{e,exp} - q_{e,cal})/(q_{e,exp})\right|) x\ 100 \quad (8)$$

Where $N$ is the number of experimental points; and $q_{e,exp}$ and $q_{e,cal}$ are the experimental data and calculated amounts adsorbed, respectively.

Table S.1. Mass of 3D scaffolds discs

| Samples | Mass (g) |
|---|---|
| CHI | (0.007±0.002) |
| CHIMerc | (0.004±0.001) |

Table S.2. pseudo-first-order and pseudo second-order kinetics parameters for sample CHIMerc

| Sample | Pollutant | pseudo-first-order | | pseudo-second-order | |
|---|---|---|---|---|---|
| | | $K_1$ ($min^{-1}$) | $R^2$ | $K_2$ ($g.mg^{-1}.min^{-1}$) | $R^2$ |
| CHIMerc | Methyl orange | 4.78 | 0.8531 | 0.015 | 0.9999 |

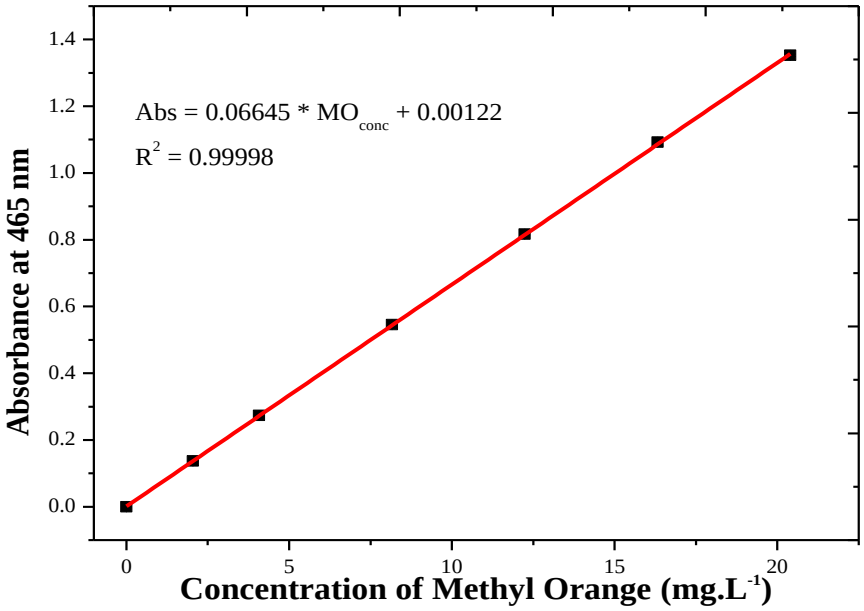


Figure S.1. Calibration curve of Methyl Orange (MO)

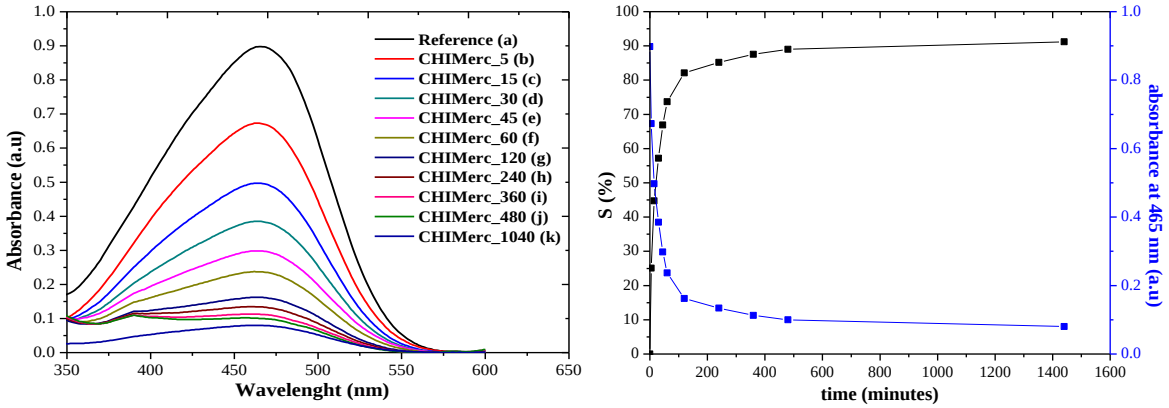


Figure S.2. (A) Absorbance modification of sample CHIMerc function of time contact with MO with the smallest concentration ((a) Reference, (b) CHIMerc_5, (c) CHIMerc_15, (d) CHIMerc_30, (e) CHIMerc_45, (f) CHIMerc_60, (g) CHIMerc_120, (h) CHIMerc_240, (i) CHIMerc_360, (j) CHIMerc_480 and (k) CHIMerc_1040) and (B) Efficiency of absorption (%) of sample CHIMerc as a function of time of contact with MO with the smallest concentration.

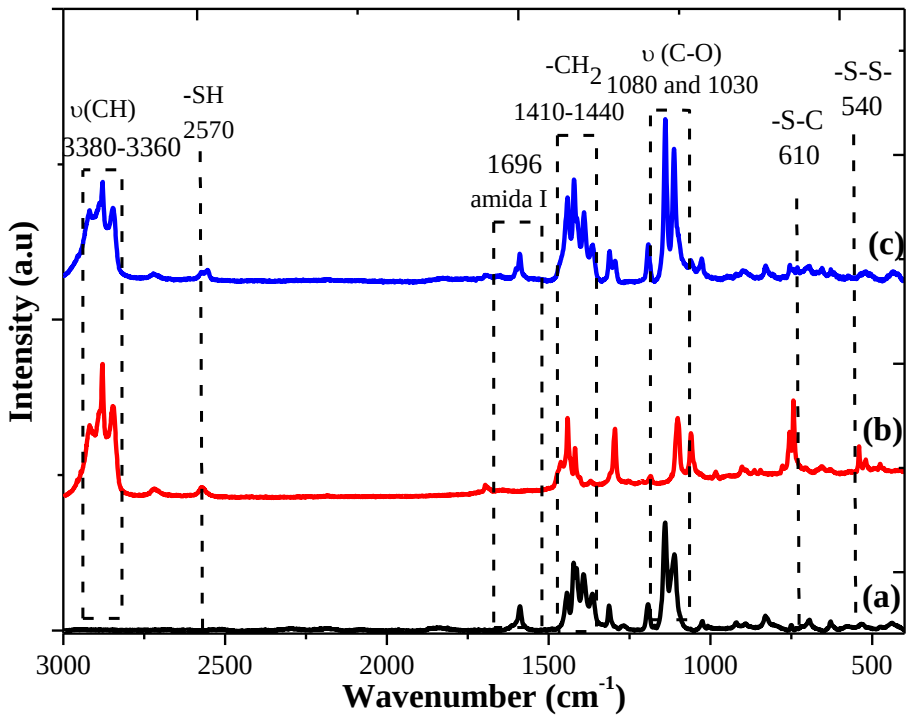


Figure S.3. Raman spectra of (a) MO; (b) CHIMerc and (c) CHIMerc after the adsorption of MO

# Capítulo 5. Conclusões e Considerações Finais

## 5.1 Considerações Finais

O presente trabalho possibilitou a formação de estruturas tridimensionais de quitosana modificada com diferentes precursores contendo o grupo tiol. A viabilidade de funcionalização da quitosana com o ácido mercaptoundodecanóico por uma rota química mais sustentável e eficiente possibilitou uma alta funcionalização comparada com dados da literatura, garantindo um material com uma morfologia tridimensional mais homogênea e uma melhor estabilidade química comparada com a quitosana.

Essas modificações com a inclusão do grupo tiol indicam a potencialidade desse material ser aplicado em diferentes situações, como tratamento de água sendo utilizado como um adsorvente, regeneração do tecido, como por exemplo o tecido cartilaginoso em razão da semelhança com a matriz extracelular pela presença de grupos de acilação, no caso da amostra CHIMerc, ou da incorporação com aminoácido, como na CHICys, porosidade e tamanho de poros adequados para o crescimento celular e não toxicidade. Assim como atividade antibacteriana contra a bactéria *Pseudomona aeroginosa*, uma bactéria bastante resistente e presente em efluentes hospitalares e águas residuais, mostrando então que o presente material possuí um leque de aplicações que podem ser exploradas e a viabilidade de múltiplas ações.

As incorporações mostraram um grau de funcionalização diferente a depender do precursor, também diferenças na lipofilicidade da cadeia e na estabilidade química. Por esse motivo, a funcionalização com o ácido mercaptoundodecanóico mostrou-se mais eficiente e um material bastante promissor em razão da sua multifuncionalidade, apresentando potencial para ser aplicado desde engenharia de tecido, na aplicação de regeneração de tecidos, até tratamento de água contaminada com corantes e bactéria e também tendo potencial para aplicação como biomaterial em feridas queimadas em razão da atividade antibacteriana e semelhança com o tecido epitelial. Concomitantemente, a funcionalização foi bastante eficiente comparada com dados da literatura e mostrando um viés de aplicação amplo desses

materiais, indicando que a incorporação do grupo tiol na cadeia da quitosana é interessante e bem promissora.

## 5.2 Conclusões

Nesse estudo realizou-se o design de estruturas tridimensionais produzidas pelo processo do *frezee-drying* a partir do polissacarídeo quitosana modificado com a incorporação de cadeias contendo o grupo tiol (*L*-cistéina e o ácido mercaptoundodecanóico) por meio de uma rota quimicamente sustentável para aplicações na regeneração do tecido e em tratamento de águas contaminadas com corantes, além de promover atividade antibacteriana contra uma bactéria bastante resistente e presente nos efluentes aquosos, a *Pseudomona aeroginosa*.

Os resultados mostraram que ambas as incorporações possibilitaram a formação de uma estrutura tridimensional com morfologia mais homogênea e estável quimicamente comparada com a quitosana, em razão da presença do grupo tiol (-SH), o qual forma ligações covalentes por meio de dissulfetos. No entanto, o diferente grau de funcionalização (CHICys = 5 % e CHIMerc = 26 %) afetou na estabilidade química dessa estrutura em razão da maior ou menor quantidade de grupos tiol disponíveis e também na lipofilicidade da cadeia.

Ambos os materiais não apresentaram citotoxicidade celular avaliada pelo ensaio colorimétrico de MTT em diferentes tipos celulares (HEK e SAOS), porosidade (> 80 %), interconectividade (> 90 %) e diâmetros de poros (CHICys (223±72) µm e CHIMerc (225±95) µm, por MEV) adequados para o crescimento celular indicando a possibilidade do uso desses *scaffolds* na regeneração de tecido.

Concomitantemente, os ensaios bacterianos contra a bactéria *Pseudomona aeroginosa* mostraram que a diferença na funcionalização e a maior lipofilicidade da amostra CHIMerc viabilizou a atividade antibacteriana dessa amostra. Assim como, o potencial para aplicações em adsorção de corantes, como o laranja de metila, em razão da maior estabilidade química e a afinidade do grupo tiol por esse pigmento.

Os mecanismos de adsorção mostraram uma alta adsorção (400 – 450 $mg.g^{-1}$), predomínio da cinética de pseudo segunda ordem e sendo o modelo matemático de isoterma mais apropriado para explicar o mecanismo, a isoterma de Freundlich, confirmando a quimissorção como mecanismo predominante. Essas propriedades possibilitam a esse *scaffold* a aplicação como adsorvente em tratamentos de águas contaminadas, pois além da alta adsorção, esse material tem atividade antibacteriana contra uma bactéria bastante resistente e que está presente nos meios aquosos, os mais diversos.

A avaliação da adsorção do corante e de água em diferentes pH, mostrou que o grupo tiol apresenta comportamento dependente do pH, sendo que em meios básicos esse grupo sofre oxidação, a qual influencia diretamente no processo de adsorção, evidenciado pela espectroscopia no Raman. Além da viabilidade de reutilização do adsorvente em razão da possível dessorção.

Dessa forma, o presente estudo possibilitou o conhecimento do mecanismo envolvido na funcionalização da quitosana com precursores contendo o grupo tiol, indicando uma grande influência desse grupo nas características físico-químicas dos *scaffolds* produzidos, assim como a influência do grupo em diferentes aplicações. Além disso, ambos os materiais estão passíveis da aplicação em regeneração tecidual em razão da sua morfologia, estrutura química e compatibilidade com meio biológico.

## 5.3 Contribuições originais desse trabalho

- Produção de estruturas tridimensionais com quitosana tiolizada, em especial com o ácido mercaptoundodecanóico (MERC), o qual não havia relatos de sua funcionalização na quitosana, proporcionando um valor de funcionalização entre 300 a 700 % maior do que os da literatura e apresentando multifuncionalidade;
- Síntese desses *scaffolds* por uma rota química mais amigável, utilizando reagentes de funcionalização como o EDC e o sulfo-NHS que não permanecem na estrutura da molécula e são retirados por diálise;

- Compreensão das diferenças físico-químicas e morfológicas proporcionadas pelos diferentes precursores, em especial em relação a estrutura 3D, estabilidade química e ao caráter de lipofilicidade da quitosana, o qual havia poucos relatos na literatura;
- Avaliação de citoxicidade dos *scaffolds* com as células HEK e SAOS mostrando a não toxicidade *in vitro* das estruturas tridimensionais viabilizando a sua aplicação na regeneração de tecido;
- Estudo da quitosana tiolizada pela espectroscopia Raman possibilitando a avaliação dos *scaffolds* em diferentes pH e formação de óxidos em meios básicos que diminuem o processo de adsorção;
- *Scaffold* proporcionando uma alta adsorção do pigmento laranja de metila, com compreensão dos mecanismos envolvidos na adsorção, a cinética da adsorção e avaliação da influência do pH nesse processo, evidenciando uma afinidade química entre a amostra CHIMerc e o pigmento. Assim como a sua reutilização em razão da possível dessorção do mesmo;
- Avaliação da atividade antibacteriana dos *scaffolds* com quitosana tiolizada evidenciando a influência da tiolização na atividade antibacteriana e propondo mecanismos em relação a atividade em razão da maior presença do grupo tiol.

## Capítulo 6. Contribuições para a literatura

### 6.1 Artigos publicados

Medeiros Borsagli, F. G. L.; Carvalho, I. C.; Mansur, H. S. Amino acid-grafted and N-acylated chitosan thiomers: Construction of 3D bio-scaffolds for potential cartilage repair applications. International Journal of Biological Macromolecule, 114 (2018) 270-282. Qualis A2 IF 3,671

### 6.2 Artigos submetidos

Bi-Functional Eco-friendly 3D Scaffolds based on *N*-acyl Thiolated Chitosan for Potential Adsorption of Dye Pollutants and Antibacterial Applications. Artigo submetido ao periódico Biochemical Engineering Journal. Qualis A1 IF 2,892.

### 6.3 Artigos publicados em anais de congresso

**MEDEIROS BORSAGLI, FERNANDA GUERRA LIMA**; MANSUR, H. S. SÍNTESE E CARACTERIZAÇÃO DE QUITOSANA QUIMICAMENTE MODIFICADA POR TIOLIZAÇÃO PARA POTENCIAL APLICAÇÃO BIOMÉDICA In: 14° Congresso Brasileiro de Polímeros, 2017, Águas de Lindóia. **SÍNTESE E CARACTERIZAÇÃO DE QUITOSANA QUIMICAMENTE MODIFICADA POR TIOLIZAÇÃO PARA POTENCIAL APLICAÇÃO BIOMÉDICA**. 2017. v.POST2. p.1 – 5

### 6.5 Outras publicações no decorrer da formação acadêmica

Medeiros Borsagli, F. G., Mansur, A. A. P., Chagas, P., Oliveira, L. C., Mansur, H. S., O-carboxymethyl functionalization of chitosan: Complexation and adsorption of Cd (II) and Cr (VI) as heavy metal pollutant ions, React Func Polym, 97 (2015) 37-47. Qualis A1

Dumont, V. C., Mansur, A. A. P., Carvalho, S. M., Medeiros Borsagli, F. G. L., Pereira, M. M., Mansur, H. S. Chitosan and Carboxymethyl-Chitosan Capping Ligands: Effects on the Nucleation and Growth of Hydroxyapatite Nanoparticles for Producing Biocomposite Membranes. Mater. Sci Eng. C., 59 (2016) 265-277. Qualis A1

Mansur, Alexandra A. P.; Ramanery, Fábio P.; Borsagli, Fernanda G. L. M.; Mansur, Hernan S. Bio-functionalized water-soluble ZnS quantum dots using carboxymethylchitosan. Journal IOP Conference Series: Materials Science and Engineering, 2014. Qualis B1

Borsagli, Fernanda G. L. M.; Mansur, Alexandra A. P.; Mansur, Hernan S. Synthesis and characterization of CMC for potential application as adsorbent in water treatment. Journal Materials Science Forum, 2014. Qualis B1

Ramanery, Fábio P.; Mansur, Alexandra A. P.; Borsagli, Fernanda G. L. M.; Mansur, Hernan S. Green and Facile Synthesis of Water-Soluble ZnS Quantum Dots Nanohybrids using Chitosan Derivative Ligands. Journal Nanoparticle Research, 2014. Qualis A1

## Capítulo 7. Sugestões para trabalhos futuros

- Avaliar a aplicação da CHIMerc como tensoativo para aplicações minerais, como flotação;
- Avaliar a adsorção pela CHIMerc de agrotóxicos, compreender o mecanismo, avaliar a influência do pH e a cinética dessas adsorções;
- Avaliar a adsorção pela CHIMerc dos metais arsênio, prata e cádmio, compreendendo seu mecanismo, avaliando a adsorção em conjunto e afinidade por cada um dos íons analisados, avaliar o pH nessa adsorção e a cinética;
- Avaliar a aplicação da CHIMerc como biomaterial na cicatrização de feridas de queimaduras.

## Apêndice I

The CHICys showed a cumulative adsorption of MO dye up to approximately 480 minutes. At longer times, it was not possible to measure the MO uptake due to the solubilization of the sorbent in the aqueous medium. The investigation with CHICys sample did not proceed due to the low stability of the material in aqueous solution.

Figure A.I. Methyl orange (MO) adsorption and absorbance profile as a function of time for CHICys

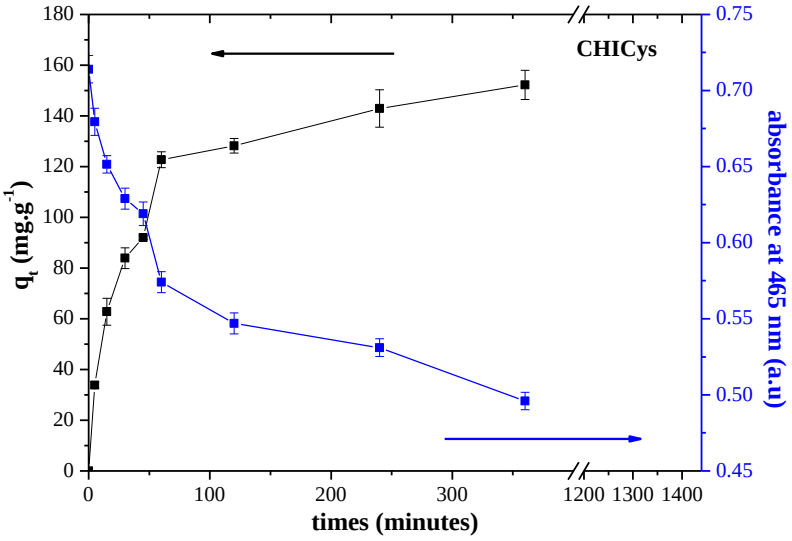


Figure A.II. (A) Change in absorbance of sample CHICys as a function of time of contact with MO with the smallest concentration ((a) Reference, (b) CHICys_5, (c) CHICys_15, (d) CHICys_30, (e) CHICys_45, (f) CHICys_60, (g) CHICys_120, (h) CHICys_240, (i) CHICys_360 and (j) CHICys_480); (B) Efficiency of absorption (%) of sample CHICys as a function of time of contact with MO with the smallest concentration.

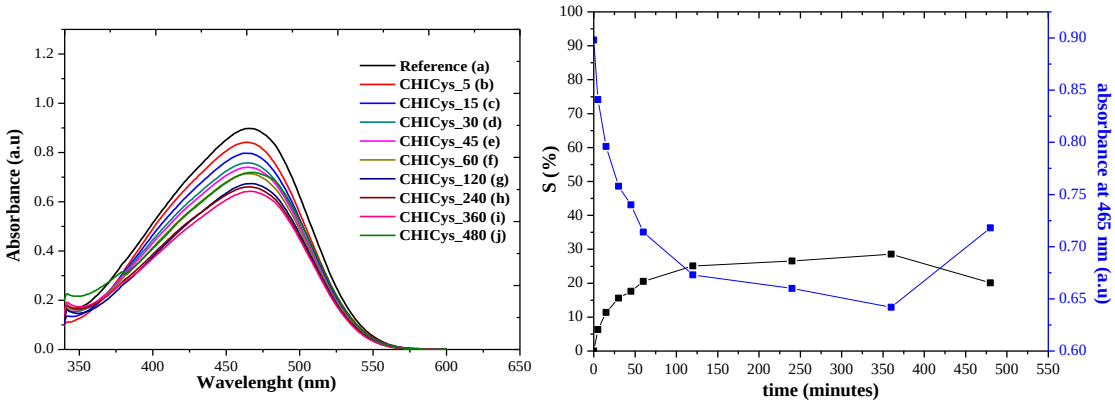


**(A)** **(B)**

Similar to antibacterial activity of CHICys did not proceed due to the absence of antibacterial activity. The detrimental effect on antibacterial activity by the reaction of the thiol-moiety with cysteine, because this group can serve as nutrients for the bacteria [19,22].

International Journal of Biological Macromolecules 114 (2018) 270–282

Contents lists available at ScienceDirect

International Journal of Biological Macromolecules

journal homepage: http://www.elsevier.com/locate/ijbiomac

# Amino acid-grafted and *N*-acylated chitosan thiomers: Construction of 3D bio-scaffolds for potential cartilage repair applications

Fernanda G.L. Medeiros Borsagli, Isadora C. Carvalho, Herman S. Mansur *

*Center of Nanoscience, Nanotechnology and Innovation - CeNano²I, Department of Metallurgical and Materials Engineering, Federal University of Minas Gerais/UFMG, Brazil*

ARTICLE INFO

*Article history:*
Received 31 October 2017
Received in revised form 8 February 2018
Accepted 21 March 2018
Available online 22 March 2018

*Keywords:*
Chitosan
Thiolated chitosan
Thiomers
3D scaffold
Cytocompatibility
Soft tissue biomaterial

ABSTRACT

In this work novel three-dimensional (3D) scaffolds were developed with chitosan thiomer derivatives for potential soft tissue repair applications. Amino acid-grafted chitosan (cysteine, CHICys) and *N*-acylated chitosan (11-mercaptoundecanoic acid, CHIMerc) derivatives were synthesized by covalent coupling reaction and hydrogel scaffolds were produced by freeze-drying process. They were comprehensively characterized by swelling and degradation behaviors, NMR, FTIR and Raman spectroscopy, SEM and X-ray microcomputed tomography. The results demonstrated the synthesis of chitosan thiomers with distinct degree of thiol substitution (CHICys = 5% and CHIMerc = 26%), producing highly porous scaffolds (porosity >80%) with hierarchical interconnected 3D pore structures. Additionally, their physicochemical properties and architectural features were significantly tuned by the thiol-modifier, evidenced by the swelling degrees ranging from approximately 2300% (CHICys) to 1800% (CHIMerc) and chemical stability against degradation. Moreover, they exhibited cytocompatibility based on *in vitro* bioassays, which hold promise as suitable platform in soft tissue engineering applications.



## 1. Introduction

Orthopedic surgeons and researchers worldwide are continuously faced with the challenge of regenerating articular cartilage defects. The human body has a restricted ability to properly auto-regenerate most of its major tissues if the original tissue integrity has been seriously injured because of medical disorders involving an ever-increasing burden of trauma, congenital abnormalities and degenerative diseases [1]. Although the field of tissue engineering has progressed since the landmark article published in *Science* in 1993 by Langer and Vacanti (1993) [2], which listed key strategies for the development of biological substitutes, including building matrices for cells to be seeded on, it is not yet possible to entirely mimic the physicochemical, biochemical and biological properties of articular cartilage using available technology and development strategies [3]. Therefore, the development of mimetic biomaterials with specific properties relevant to articular cartilage native tissue will support the promotion of improved, functional, and novel engineered smart materials for potential clinical application. Essentially, articular cartilage is a connective tissue composed of an extracellular matrix (ECM) containing collagen, glycosaminoglycan (GAG), and water. Due to its complexity, engineering an articular cartilage substitute requires a combination of several fields of research with a multidisciplinary approach such as materials science, materials chemistry, biochemistry, molecular biology, and biomedical engineering [4–9]. Therefore, the biomaterial selection is crucial to the success of the candidate for potential cartilage repair applications, as a large variety of natural and synthetic materials with distinct biological and physicochemical properties have been developed in recent years. Ideally, the biomaterial scaffold should closely mimic the environment occurring in the original articular cartilage tissue structure [10].

To this end, hydrogel scaffolds made from natural and synthetic polymers have become increasingly important within the field of soft tissue repair and restoration, where natural polymers possess more favorable biocompatibility and relative abundance. Among several alternatives of natural polymers, polysaccharides (*e.g.*, chitosan, hyaluronic acid, starch) have attracted the special attention of researchers for producing three-dimensional (3D) scaffolds suitable as extracellular matrix mimics for cell culture in tissue repair applications [11].

Chitosan, which is a partially de-acetylated derivative of chitin, usually extracted from exoskeletons of crustaceans, is an interesting alternative to polysaccharides for producing scaffolds. Chitosan is a linear polysaccharide consisting of $\beta$-(1–4) linked D-glucosamine residues with randomly located *N*-acetyl-glucosamine groups, where its applications depend mostly on the degree of acetylation. In addition, chitosan presents some characteristics similar to several GAGs and hyaluronic acid, which are commonly found in articular cartilage [10]. The *N*-acetylglucosamine moiety in chitosan is a structural feature present in GAGs, which suggests that the analogous structure may also present similar bioactivity. Moreover, one of the most promising features

* Corresponding author at: Department of Metallurgical and Materials Engineering, Federal University of Minas Gerais, Av. Antônio Carlos, 6627– Escola de Engenharia, Bloco 2 – Sala 2233, 31.270-901 Belo Horizonte, MG, Brazil.
*E-mail address:* hmansur@demet.ufmg.br (H.S. Mansur).

https://doi.org/10.1016/j.ijbiomac.2018.03.133
0141-8130/

found in chitosan is related to the exceptional ability to be processed into porous structures to be applied in tissue regeneration. Porous chitosan structures can be shaped by distinct methods such as freezing and lyophilizing slightly acid solutions of chitosan in appropriate molds [10,12].

Despite the numerous advantages of chitosan (*e.g.*, abundant natural polysaccharide, biodegradable and non-toxic), it is soluble only under an acidic aqueous medium, which can restrict some of its potential applications in the biomedical field at a physiological pH and with mildly alkaline environmental conditions. Therefore, chemical derivatization of chitosan provides a powerful means to promote new biological activities and specific properties. The versatility of chitosan functionalization is essentially due to the presence of primary amino groups in the macromolecule (*i.e.*, degree of deacetylation). These groups are reactive and provide a mechanism for side group attachment using a variety of mild reaction conditions. Moreover, by the proper selection of the nature of the side group to be attached to the polymer chains, the physicochemical and biological properties can be tuned to provide specific functionalities. Based on this approach, a myriad of groups (*e.g.*, carboxylates, acyls, alkyls, thiols, quaternized amino, *etc.*) have been inserted into chitosan providing additional characteristics such as improved water solubility, anionic or cationic features, antifouling and antimicrobial activities, amphiphilic behavior and other characteristics [12–14].

Some studies have developed *N*-alkyl derivatives of chitosan exhibiting reasonable water solubility, swelling behavior, and micellar aggregation in solution for applications as drug carriers, nucleic acid transfection in gene therapy and blood compatibility [13,15]. The *N*-acylation of chitosan with fatty acids with different alkyl chain lengths and degree of substitution can add adjustable hydrophobic interactions for use as hydrogel matrices in tissue engineering [15,16].

Another innovative strategy for the derivatization of chitosan is associated with the introduction of amino acid moieties (*i.e.*, monomeric units of proteins) with acidic, basic or hydrophobic characteristics, to the backbone of the polymer chain. This strategy has been used to modify and improve the physicochemical properties of chitosan such as solubility and mucoadhesiveness and gives rise to some interesting synergistic features for using in tissue engineering, as well as other potentially useful biomedical properties, including anticoagulant, antimicrobial, and anti-cholesterol activities as well as the increasing interest in the field of tissue engineering [17,18]. The conjugation reactions of amino acids with chitosan have been conducted principally on the free amino groups of chitosan, usually by direct coupling forming covalent amide bonds [18]. An interesting phenomenon resulting from the functionalization of chitosan with amino acids is the introduction of carboxylic groups and additional amino groups, which in combination, increase the water-solubility of chitosan at neutral and up to alkaline pH values. This characteristic is highly desirable considering the limited solubility of chitosan (*i.e.*, pH >6.0), which can compromise its application in several biomedical areas [18].

Thiomers (or thiolated polymers) are produced by the immobilization of thiol-bearing ligands onto the polymer backbone, which results in a significant improvement in mucoadhesion. Thiolated chitosan has a high level of cohesive-, mucoadhesive-, enzyme inhibitory-, and permeation-enhancing properties. Thus, there is a vast field to be exploited based on the combination of chemical functionalities with the chitosan polysaccharide backbone producing a new class of thiolated chitosan polymers such as *N*-acetyl cysteine-chitosan and *N*-acetyl-chitosan for numerous biomedical applications [19]. The immobilization of thiol groups to form chitosan derivatives (*i.e.*, thiolated chitosan) can promote and enhance numerous biological and biochemical properties due to the formation of disulfide bonds with cysteine-rich subdomains of glycoproteins commonly encountered in biological systems (*e.g.*, cells and tissues) [20–23]. Interestingly, although there is an increasing interest in recent years in the development of thiolated polymers and chitosan derivatives for biomedical applications such as drug delivery carriers, nucleotide transfection for gene therapy, mucoadhesive and antimicrobial activities, no report was found in the published literature investigating the production of 3D porous scaffold hydrogels made of cysteine-chitosan and *N*-acetyl-chitosan for potential applications in soft tissue repair [20,21,23].

Thus, in this study novel multifunctional thiolated polysaccharides were designed and produced based on the chemical functionalization of chitosan backbone with cysteine amino acid and *N*-acyl-thiol moiety for producing 3D scaffolds aiming at potential soft tissue engineering applications. The highly porous 3D scaffold hydrogels with complex interconnected and hierarchical architecture demonstrated physicochemical properties and *in vitro* biocompatibility suitable to be prospectively applied as biomaterial support for cartilage repair in soft tissue engineering.

## 2. Materials and methods

### 2.1. Materials

All the reagents and precursors, sodium hydroxide (Sigma, USA, ≥99%, NaOH), hydrochloric acid (Sigma-Aldrich, USA, 36.5–38.0%, HCl), 11-Mercaptoundecanoic acid (Sigma-Aldrich, USA, ≥95%, MM = 218.36 $g \cdot mol^{-1}$, $HSCH_2(CH_2)_8CH_2COOH$), ethanol (Synth, Brazil, 99.8%, $CH_3CH_2OH$), 2-Propanol (Sigma-Aldrich, USA, anhydrous 99.5%, $(CH_3)_2CHOH$), Acetic acid (Synth, Brazil, 99.8%, MM = 60.05 $g \cdot mol^{-1}$, $CH_3CO_2H$), L-cysteine (Aldrich, USA, $HSCH_2CH(NH_2)CO_2H$, MM = 121.16 $g \cdot mol^{-1}$), *Ellman's* reagent (Sigma-Aldrich, USA, DTNB, 5,5′-Dithiobis (2-nitrobenzoic acid), MM = 396.35 $g \cdot mol^{-1}$, $[—SC_6H_3(NO_2)CO_2H]_2$), EDC (Sigma-Aldrich, USA, $C_8H_{17}N_3 \cdot HCl$ *N*-(3-Dimethylaminopropyl)-*N*′-ethylcarbodiimide hydrochloride, MM = 191.7 $g \cdot mol^{-1}$), Sulfo-NHS (*N*-hydroxysulfosuccinimide sodium salt, Aldrich, USA, ≥98%, $C_4H_4NNaO_6S$, MM = 217.13 $g \cdot mol^{-1}$), sodium phosphate dibasic (Sigma-Aldrich, USA, ≥99.0%, MM = 141.96 $g \cdot mol^{-1}$, $Na_2HPO_4$), potassium phosphate monobasic (Sigma-Aldrich, USA, ≥99.0%, MM = 136.09 $g \cdot mol^{-1}$, $KH_2PO_4$), potassium chloride (Sigma-Aldrich, USA, ≥99.0%, MM = 74.55 $g \cdot mol^{-1}$, KCl), sodium chloride (Sigma-Aldrich, USA, ≥99.0%, MM = 58.44 $g \cdot mol^{-1}$, NaCl) were used as-received. High-molecular-mass chitosan powder (CHI, molar mass, MM = 310.000 to >375.000 $g \cdot mol^{-1}$, deacetylation degree (DD) ≥ 75.0%, and viscosity 800–2000 cPoise, at 1% in 1% acetic acid, Aldrich, USA) was used for polymer modification. Deionized water (DI-water) (Millipore Simplicity™) with a resistivity of 18 MΩ·cm was used to prepare all solutions. All preparations and syntheses were performed at room temperature (RT, 25 ± 2) °C unless otherwise specified.

### 2.2. Synthesis of thiolated chitosan derivatives - Thiomers

#### 2.2.1. Amino acid functionalization of chitosan with cysteine (CHICys)

The synthesis of chitosan (CHI) with cysteine (CYS) was performed according to the molar ratio of reagents 1:2:2 (CHI:EDC:CYS) adapted from the process reported in the literature [17]. Briefly, 0.5 mg of chitosan powder was dissolved in 30 mL of 2% (v/v) acetic acid aqueous solution overnight for complete solubilization. The pH was adjusted to 4.5 ± 0.5 (NaOH, 1.0 $mol \cdot L^{-1}$). In the sequence, 0.7 g of cysteine powder was dissolved in 20 mL of phosphate-buffered saline (PBS) solution, 1.2 g of EDC and 0.32 g of sulfo-NHS were added and maintained under moderate stirring for 1 h at room temperature (referred to as CYS/EDC/NHS solution). Then, the CYS/EDC/NHS solution was added to the chitosan/acetic acid solution (*i.e.*, total volume = 57 mL, molar ratio of 1:2:2/CHI:EDC:CYS) and the pH was adjusted to 5.0 ± 0.5 (NaOH, 1.0 $mol \cdot L^{-1}$). The coupling reaction *via* the formation of amides was performed at room temperature under moderate stirring for 5 h in the darkness. Next, the mixture was dialyzed in the darkness against distilled water using a membrane (12–14 kDa, Sigma, USA) for 7 days at RT to remove unreacted species and water-soluble contaminants for further preparing the hydrogels.

*2.2.2. N-Acylation of chitosan with 11-mercaptoundecanoic acid (CHIMerc)*

Although not previously reported in the literature, the *N*-acylation of chitosan with 11-mercaptoundecanoic acid (MERC), a similar procedure using the modification of chitosan with cysteine was adapted for the synthesis of chitosan functionalized with the hydrophobic acyl chain using MERC. Thus, based on the molar ratio of reagents 1:2:2 (CHI:EDC:MERC), 0.5 mg of chitosan powder was dissolved in 30 mL of 2% (v/v) aqueous acetic acid solution overnight for complete solubilization, and the pH was adjusted to 4.5 ± 0.5 (NaOH, 1.0 mol·$L^{-1}$). In the sequence, 1.36 g of MERC was dissolved in 60 mL of PBS buffer solution/isopropanol (30/30) (v/v). Next, 1.2 g of EDC and 0.32 g of sulfo-NHS were added to the solution and maintained under moderate stirring for 1 h at room temperature (referred to as MERC/EDC/NHS solution). The MERC/EDC/NHS solution was added to chitosan/acetic acid solution (*i.e.*, total volume = 91 mL, molar ratio of 1:2:2/CHI:EDC:MERC), and the pH was adjusted to 5.0 ± 0.5 (NaOH, 1.0 mol·$L^{-1}$). The acylation reaction was performed at room temperature under moderate stirring for 5 h in the darkness. In the sequence, the mixture was dialyzed in the darkness against distilled water using a membrane (12–14 kDa, Sigma, USA) for 7 days at RT to remove unreacted species and water-soluble contaminants for further preparing the hydrogels.

*2.3. Preparation of 3D porous scaffolds of chitosan thiomers*

To obtain polymer matrices with porous three-dimensional structures, samples of the previously prepared solutions (CHICys and CHIMerc) were poured into plastic tubes (1.5 mL in *Eppendorfs*) and frozen at −4 ± 2 °C for 72 h and freeze-dried (ModulyoD, Thermo Electron Corporation, Wathan, Massachusetts, USA) at −50 °C and 400 ± 100 μbar until the samples reached a constant mass (approximately 72 h). The freeze-drying process was the same, and the parameters (temperature, pressure, time) were maintained unchanged for all the samples produced. The thiolated-chitosan scaffolds were produced with a foam-like aspect and stored at 4 ± 2 °C until further use.

*2.4. Characterization of chitosan thiomers and 3D porous scaffolds*

*2.4.1. Determination of thiol functionalization of chitosan by Ellman's reagent protocol*

The determination of the total of the thiol groups in the CHICys chain was performed using the *Ellman's* reagent protocol as reported previously in the literature [24]. Briefly, 5 mg of CHICys polymer was dissolved in 2 mL of deionized water. Next, the test solution was prepared by mixing 100 μL of the CHICys solution with 900 μL of 0.5 M phosphate buffer (PBS, pH 8.0) and 1 mL of *Ellman's* reagent (DTNB, 3 mg in 10 mL of 0.5 M PBS, pH 8.0). After incubation for 2 h at room temperature with light protection, the polymer/PBS/DTNB solution was centrifuged at 4000 rpm for 10 min. The absorbance of the supernatant was measured at a wavelength of λ = 450 nm with a Lambda EZ-2100 spectrophotometer (Perkin Elmer, USA) using a quartz cell with an optical path length of 10 mm. The amount of thiol groups was calculated from a calibration curve of cysteine in a concentration range of 1600–20 μM prepared exactly like the samples (Fig. S1a). Analogously, a similar procedure was performed to determine the total number of thiol groups in the CHIMerc samples, but with the minor alteration of dissolving the chitosan thiomers in ethanol instead of in DI water because of the relative hydrophobicity (*i.e.*, 5 mg of CHIMerc polymer was dissolved in 2 mL of ethanol). Thus, the total amount of thiol functionalization was calculated using the calibration curve of 11-mercaptoundecanoic acid in a concentration range of 2400–90 μM and made in the exactly same way as the samples (Fig. S1b). All experiments were conducted in triplicate (n = 3) unless specifically noted. Statistical analysis of the results was performed using the mean and standard deviation, where necessary.

The degree of functionalization (DF) of chitosan with CYS and MERC was estimated based on the total number of available reaction sites in the chitosan chains before the functionalization reactions and on the results obtained by the *Ellman's* method (Eq. (1)):

$$DF\% = [(N_{Ellman} \times 161)/(W_{CHI} \times DD)] \times 100 \quad (1)$$

where $N_{Ellman}$ is the number of thiol groups obtained by the *Ellman's* method (mol); $W_{CHI}$ is the mass of chitosan used in the synthesis (g); 161 is the average molar mass of 2-amino-2-desoxi-D-glucose units of chitosan (g·$mol^{-1}$); *DD* is the degree of deacetylation of chitosan (DD = 0.85, obtained by NMR in our previous study) [25].

*2.4.2. Spectroscopic characterization of chitosan thiomers and 3D porous scaffolds*

Fourier transform infrared (FTIR) spectra were obtained using an attenuated total reflectance method for all samples (ATR, ZnSe crystal prism, 4000–650 $cm^{-1}$ using 32 scans and a 4 $cm^{-1}$ resolution - Nicolet 6700, Thermo-Fischer). All of the experiments were conducted in triplicate (n = 3) unless specifically noted.

Raman spectroscopy was performed with a LabRam-HR 800 (Horiba/Jobin Yvon) equipped with an Olympus BX-41 microscope provided with lenses of 10×, 50× and 100× and an additional macro lens of 40 mm for all samples. A 632.8 nm excitation from a helium neon laser was focused on a spot of 1–2 $\mu m^2$ in the samples. The back-scattered light collected was dispersed by a monochromator and detected by the $LN_2$ (liquid nitrogen)-cooled CCD (charge-coupled device) system. The spectra ranged from 200 $cm^{-1}$ to 3300 $cm^{-1}$ with a step size of 1.1 $cm^{-1}$. Depending on the background fluorescence, the acquisition time was set from approximately 60 s to 300 s, with a minimum ten replicates to increase the signal-to-noise ratio.

$^1$H NMR (proton nuclear magnetic resonance) spectra of CHI, CHICys and CHIMerc samples were recorded at 50 °C in $D_2O$/DCl using a Bruker-400 MHz Varian spectrometer (90° pulse and 16 scans).

*2.4.3. Characterization of swelling degree and gel-fraction behavior of thiolated-chitosan 3D porous scaffolds*

The swelling degree (SD) of all samples was evaluated in deionized water (pH = 5.5 ± 0.5) as described in the literature [12,26]. Briefly, the samples were weighed before ($W_i$, "dry state") and after immersion in DI water ($W_s$, "swollen state") for the specific time period. After the immersion, any excess of solution was gently removed from the sample surface with a cellulose filter paper and then weighed. In the sequence, the sample was dried at 40 ± 2 °C in an oven for 24 h (*i.e.*, faster drying process compared to room temperature, until mass stabilization) and the final weight was recorded. This process was repeated for different time intervals 1, 2, 3, 4 and 24 h to assess the swelling degree until reaching the equilibrium for the chitosan-based hydrogels, which was evaluated using Eq. (2):

$$SD\ (\%) = [(W_s - W_i)/W_i] \times 100 \quad (2)$$

where $W_s$ is the weight of the swollen polymer, and $W_i$ is the initial weight of the polymer.

The chemical stability *in vitro* in aqueous solution (referred to as the gel fraction, GF) of thiolated chitosan samples was assessed by measuring the GF, according to Eq. (3) [27].

$$GF\ (\%) = \{1 - [(W_i - W_f)/W_i]\} \times 100 \quad (3)$$

where $W_i$ is the initial mass of the polymer, and $W_f$ is the mass of the dried polymer after the swelling procedure.

These experiments were performed with 21 samples for each system (n = 21, 7 samples of 3 different synthesis of each polymer, CHI, CHICys, CHIMerc). The results were averaged and statistical analysis was performed using ANOVA (one way included Tukey's test, $p < 0.05$, software Origin v.8.1, OriginLab Corporation, USA).

*2.4.4. Morphological analysis of thiolated-chitosan 3D porous scaffolds*

The morphologies of the freeze-dried CHICys and CHIMerc scaffolds were evaluated using a scanning electron microscope (SEM, FEI-FEG-FIB-QUANTA 3D) coupled with energy dispersion X-ray spectroscopy (EDX, EDAX Bruker, 0.8 nm). Before examination, the samples were coated with a thin carbon film *via* sputtering using a low deposition rate, cooling the substrate, and ensuring the maximum distance between the target and the sample to avoid sample damage; the film formed was 30 nm. Images of secondary electrons (SEs) were obtained using an accelerating voltage of 15 kV for all samples on two different planes (transversal and superficial). SEM images were collected and the pore size was estimated based on at least 50 random measurements using the open source image processing program (ImageJ v.1.50+, National Institutes of Health, NIH). The results were averaged, and statistical analysis was performed using ANOVA (one way included Tukey's test, $p < 0.05$, software Origin v.8.1, OriginLab Corporation, USA).

The three-dimensional structures of the scaffolds were investigated using 3D microtomography (SkyScan 1174, Bruker micro-CT) at a resolution of 12.18 μm, at 40 kV voltage, 100 μA current, 0.7° rotation step, and no filter. Images were reconstructed using NRecon Reconstruction software (v.1.6.1.18, Bruker micro-CT). CTAn software (v.1.15.4.0, Bruker micro-CT) was used to analyze the micro-CT datasets in 2D and 3D for morphometry and densitometry, and CTVol software (v. 2.3.1.0, Bruker micro-CT) was used for 3D visualization of the scaffolds.

Additionally, the mass of the dry, wet and submerged scaffolds was measured using the accessory SMK-301/400 (Shimadzu) coupled to a balance (±0,0001 g) and the densities ($\rho_a$, Eq. (4)) were calculated according to the equipment manual. The porosities ($\varepsilon$) were calculated according to the *Archimedes's* Method [28] (Eq. (5)). The surface areas ($S_a$) were estimated by a method used to determine the surface area of powder materials (Eq. (6)) [29].

$$\rho_a = (W_{(d)}/(W_{(d)} + W_{(l)})) \times \rho_{(l)} \quad (4)$$

$$\varepsilon\,(\%) = [(W_{(w)} - W_{(d)})/(W_{(w)} - W_{(l)})] \times 100 \quad (5)$$

$$S_a = 3/(\rho_a \cdot (d_m/2)) \quad (6)$$

where $W_{(d)}$ is the mass of sample dry (g), $W_{(w)}$ is the mass of sample in water or alcohol (g), $W_{(l)}$ is the mass of the sample submerged, $\rho_{(l)}$ is the density of water or alcohol at the temperature of experimental analysis (19 °C; 0.9984 and 0.79 $g \cdot cm^{-3}$ to water and alcohol, respectively), $S_a$ is the surface area ($m^2 \cdot g^{-1}$), $\rho_a$ is the bulk density, and $d_m$ is the average diameter ($m$) obtained by micro-CT or by SEM analysis.

*2.4.4.1. Surface Contact Angle (SCA).* The effect of thiolation of chitosan with CYS and MERC moieties on the hydrophilic/hydrophobic behavior was evaluated *via* contact angle measurements. The tests were performed by pouring DI water droplets using a microsyringe (50 μL) onto CHI, CHICys and CHIMerc films and capturing the images for contact angle calculations (Lumix FZ-47 digital camera, Panasonic, Tokyo, Japan and open source image processing program, ImageJ Fijji, NIH).

*2.5. Biological assays of thiolated-chitosan 3D porous scaffolds*

*2.5.1. Cell viability assay by MTT (3-(4,5-dimethylthiazol-2yl) 2,5-diphenyl tetrazolium bromide)*

Human osteosarcoma cells (SAOS) and the kidney cell line of human embryos (HEK 293 T) were kindly provided by Prof. A. Goes of the Department of Immunology and Biochemistry, UFMG. The cells were cultured in Dulbecco's modified eagle medium (DMEM) with 10% fetal bovine serum (FBS), penicillin G sodium (10 units·$mL^{-1}$), streptomycin sulfate (10 mg·$mL^{-1}$), and 25 μg·$mL^{-1}$ amphotericin-b (all from Gibco BRL, NY, USA) in a humidified atmosphere of 5% $CO_2$ at 37 °C. The cells were used for the experiments at passage twelve. All of the biological tests were conducted according to ISO standards (ISO 10993-5:2009/(R)2014 (Biological evaluation of medical devices: Tests for *in vitro* cytotoxicity)). SAOS and HEK 293 T cells were plated ($3 \times 10^4$ cells) on each sample material. The plates were subjected to UV radiation for 60 min in a sterile flow and washed quickly in ice-cold PBS. The samples were sterilized by UV radiation for 60 min in a sterile flow. Controls were created using cells and the DMEM medium (10%); Triton x-100 (1%; Sigma-Aldrich, St. Louis, MO, USA) was used as a positive control, and chips of sterile polypropylene (1 mg·$mL^{-1}$; Eppendorf, Hamburg, Germany) were used as a negative control. After 24 h, all media were aspirated and replaced with 210 μL of culture medium with serum. MTT (170 μL, 5 mg·$mL^{-1}$; Sigma-Aldrich, St. Louis, MO, USA) was added to each well and incubated for 4 h followed by incubation 16 h with SDS/4% HCl. Subsequently, 100 μL was removed from each well and transferred to a 96-well plane, and the absorbance was quantified using a Varioskan Reader (Thermo Scientific) with a 595-nm filter. The values obtained were expressed as the percentage of viable cells according to Eq. (7).

$$\text{Cell viability}\,(\%) = \frac{\text{Absorbance of samples and SAOS cells} \times 100}{\text{Absorbance (control)}} \quad (7)$$

All of the experiments were performed in triplicate ($n = 3$). The results were averaged, and statistical analysis was performed using ANOVA (one way included Tukey's test, $p < 0.05$, software Origin v.8.1, OriginLab Corporation, USA).

*2.5.2. Cell viability assay by LIVE/DEAD®*

SAOS and HEK 293 T cells on passage 13 and 8, respectively, were synchronized in a serum-free medium for 24 h. After this period, cells were trypsinized and seeded ($3 \times 10^5$ cells/well) on hydrogel foams (1 mg hydrogel and 200 μL medium, w/v) and placed in a 96-well plate. The reference controls were cells cultured in the DMEM medium with 10% FBS. After 24 h, all of the media were aspirated, and the cells were washed two times with 10 mL of phosphate buffered saline (PBS, Gibco BRL, NY, USA). Cells were treated with the LIVE/DEAD® Viability/Cytotoxicity kit (Life Technologies of Brazil Ltd., São Paulo, Brazil) for 30 min, according to the manufacturer's specifications. Images of fluorescent emissions were separately acquired, calcein at 530 ± 12 nm, and EthD-1 (ethidium homodimer-1) at 645 ± 20 nm, with an inverted optical microscope (Leica DMIL LED, Germany).

## 3. Results and discussion

*3.1. Characterization of chitosan thiomers and 3D porous scaffolds*

*3.1.1. Characterization of degree of substitution via Ellman's reagent method*

The primary amino group at the 2-position of the glucosamine subunits of chitosan is the main target for the immobilization of thiol groups. The sulfhydryl-bearing reagents can be attached to this primary amino group *via* the formation of covalent amide bonds, using the carboxylic acid groups of the CYS and MERC molecules reacting with the primary amino group of chitosan mediated by a water soluble carbodiimide as schematically depicted in Fig. 1A. The number of thiol groups on the chitosan-based thiomers was determined *via Ellman's* reagent [20]. Fig. 1B shows the chemical structure of the chitosan thiomers of CHICys (a) and CHIMerc (b), respectively. Fig. 1C presents the results of the concentration of thiol groups of CHICys (409 ± 27) μmol·$g^{-1}$ and CHIMerc (2218 ± 100) μmol·$g^{-1}$ obtained by *Ellman's* method. The degree of substitution of thiol groups in this study was relatively higher than others found in the literature [20,24,30,31], although the *N*-acylation of chitosan using 11-mercaptoundecanoic acid has not been reported before. This more effective thiolation process can be assigned to distinct optimized experimental conditions such as the buffer solution and solvent (*i.e.*, PBS in water), the use of sulfo-NHS combined with EDC as a zero-length coupling agent (stabilization of

intermediates formed), temperature, pH, concentration of reagents, time of reaction, degree of deacetylation and molar mass of chitosan and others. In addition, a much higher concentration (over 400%) of thiol groups was verified in the CHIMerc compared to CHICys, which

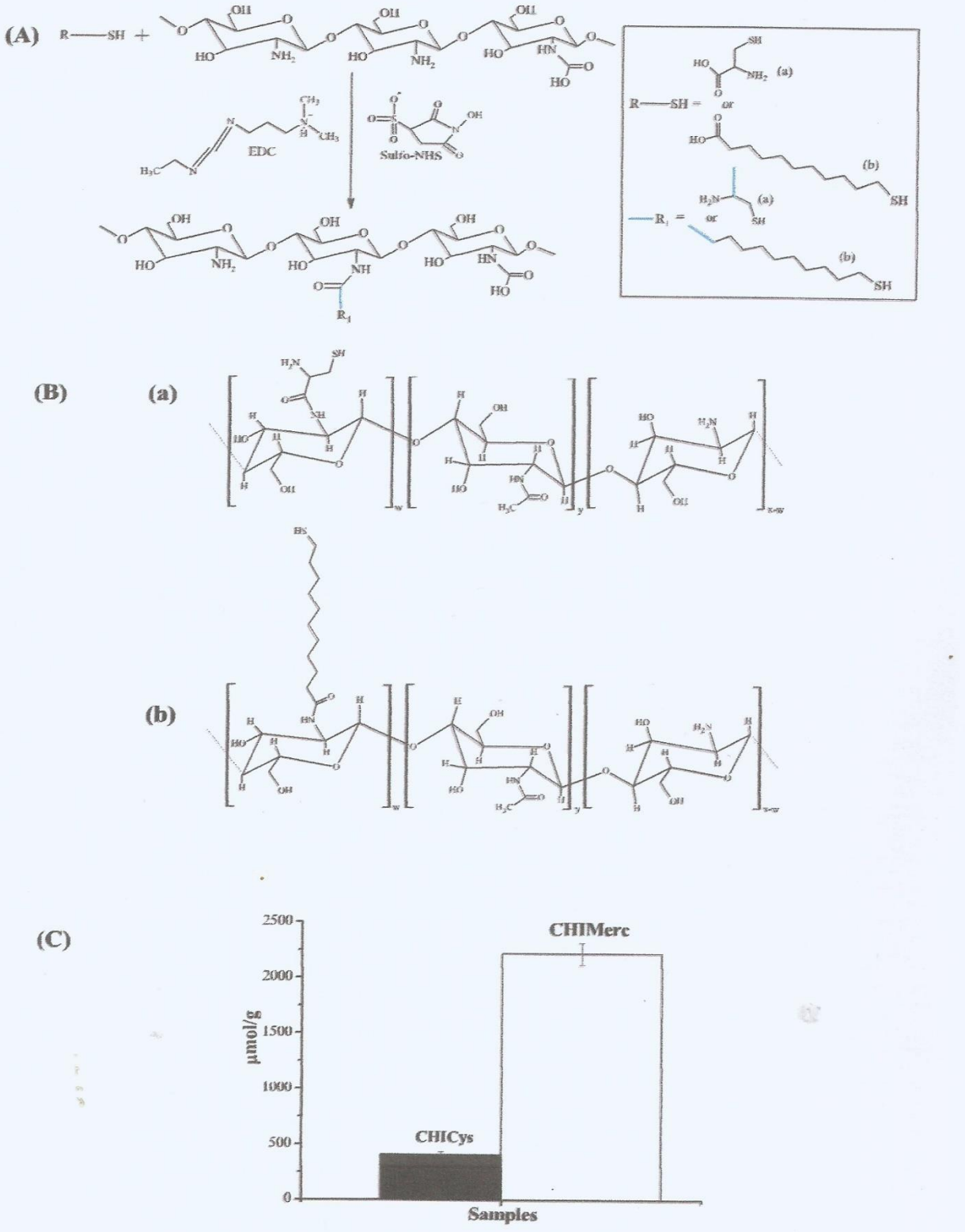


**Fig. 1.** (A) Schematic representation of chemical functionalization of chitosan with thiol precursors (a) CYS and (b) MERC. (B) Chitosan thiomers produced (a) CHICys and (b) CHIMerc (x = 0.85, y = 0.15, and w = 0.85 × DF; DF is 0.05 and 0.26 for CYS and MERC, respectively). (C) Histogram of thiol content inserted in chitosan chain estimated by Ellman's reagent (µmol·$g^{-1}$).

intermediates formed), temperature, pH, concentration of reagents, time of reaction, degree of deacetylation and molar mass of chitosan and others. In addition, a much higher concentration (over 400%) of thiol groups was verified in the CHIMerc compared to CHICys, which

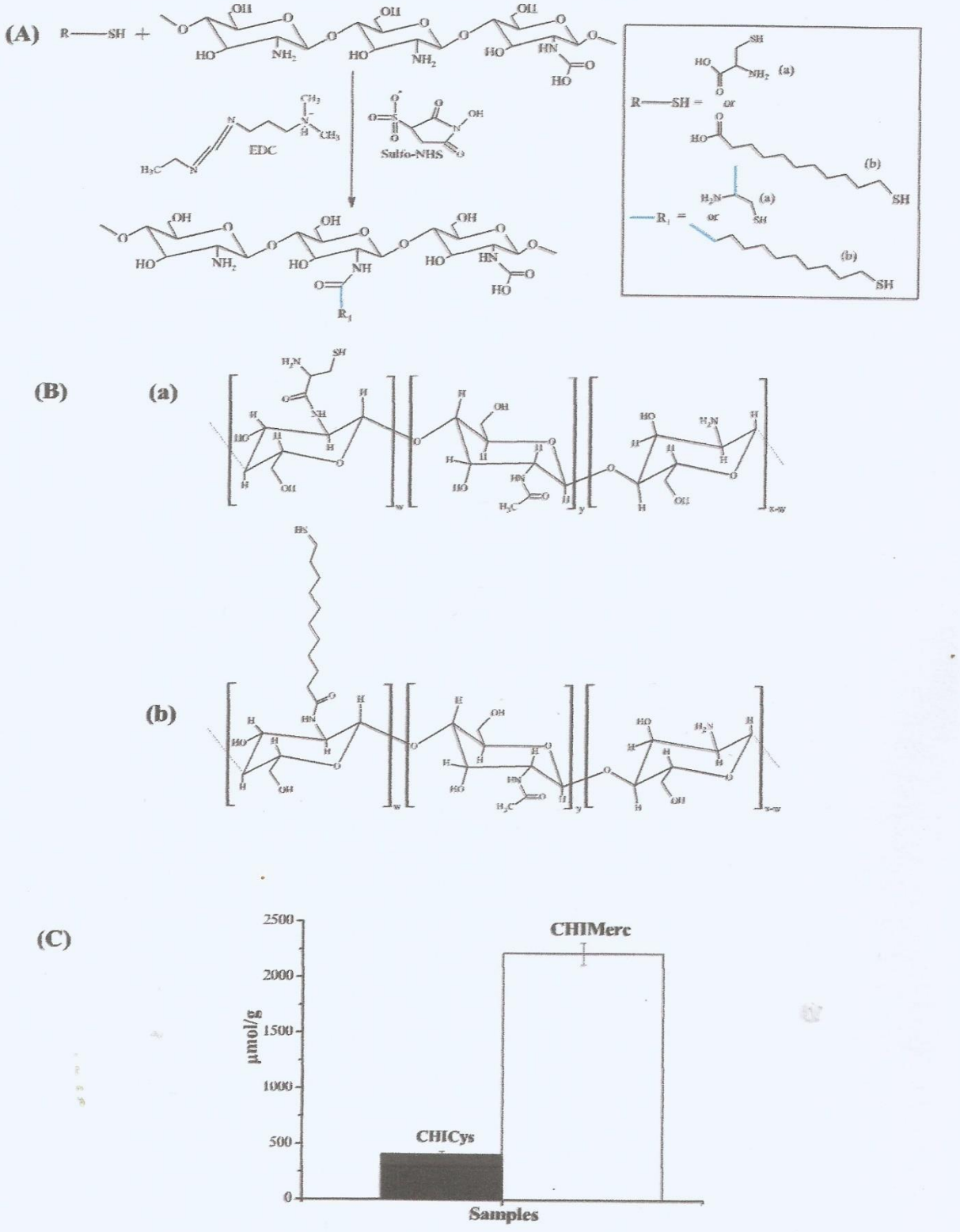


**Fig. 1.** (A) Schematic representation of chemical functionalization of chitosan with thiol precursors (a) CYS and (b) MERC. (B) Chitosan thiomers produced (a) CHICys and (b) CHIMerc (x = 0.85, y = 0.15, and w = 0.85 × DF; DF is 0.05 and 0.26 for CYS and MERC, respectively). (C) Histogram of thiol content inserted in chitosan chain estimated by Ellman's reagent (µmol·g$^{-1}$).

was suggested to be mostly caused by the orientation of the reacting molecule MERC as an amphiphilic molecule (*i.e.*, "polar carboxylic head" and "hydrophobic thiol-acyl tail") favoring the formation of amide bonds with amino groups of chitosan. However, as cysteine is a polarizable amino acid, it can be repelled by electrostatic forces with charged groups of chitosan (amino) leading to a reduction of the degree of substitution [32,33].

Nonetheless, the high concentration of thiol groups found in this study (degree of substitution of 5 ± 1% and 26 ± 2%, CHICys and CHIMerc, respectively) possesses advantages for improving the properties of pristine chitosan in potential biomedical applications such as water solubility, cytocompatibility and mucoadhesion [24,31].

### 3.1.2. Spectroscopic characterization of chitosan thiomers

Chitosan is a copolymer composed of *N*-acetyl-D-glucosamine and D-glucosamine repeating units with several chemical groups, which can be extensively characterized by FTIR spectroscopy. As a general analysis of the FTIR spectra (Fig. 2A), the typical chitosan bands can be identified in all samples: The amide I bands at ~1655 $cm^{-1}$; the amide II band at 1560 $cm^{-1}$; the amide III band at 1315–1320 $cm^{-1}$; the broad OH and NH stretching bands at 3450 $cm^{-1}$; C—H stretching bands between 2800 and 2900 $cm^{-1}$; the —$CH_2$ bending at 1420 $cm^{-1}$; the bands assigned to C—O stretching at 1030 $cm^{-1}$ and 1075 $cm^{-1}$; and the band at 897 $cm^{-1}$, related to C—O—C glycosidic linkage [12,13]. The differences observed by comparing the IR spectra can be associated with the functionalization by the thiol precursors (*i.e.*, CYS and MERC) with the primary amine in chitosan glucosamine units (Fig. 2B In CHIMerc (b), and CHICys (c) spectra, the C—N (1250–1320 $cm^{-1}$) and NH (~1550 $cm^{-1}$) bands shifted towards lower frequencies, which can be attributed to the addition of a heavier group after the amide bond formation [13,16]. In addition, the formation of amide groups also increases the amide I band due to the augmentation of C=O stretching vibrations. Moreover, for both functionalization moieties, *i.e.*, CYS and MERC, there is an insertion of $CH_2$ groups in the chitosan polymer structure, especially for CHIMerc, which possess an alkyl chain with 10 carbons. Therefore, the thiolation of chitosan in this study was qualitatively confirmed by the increase in bands related to $CH_2$ vibrations at approximately 2900 $cm^{-1}$ and 1420 $cm^{-1}$. Moreover, the FTIR spectra indicated the presence of weak signals of sulfur-based groups at approximately 770–730 $cm^{-1}$ (—S—C) and 2560–2500 $cm^{-1}$ (—SH) in thiol-containing chitosan samples (CHICys and CHIMerc).

Considering the glycoside linkage band (897 $cm^{-1}$) of chitosan as the reference, which is not expected to be significantly affected by the chemical reaction at the primary amino group [12], and comparing the relative changes in amide III band (C—N bond) associated with the

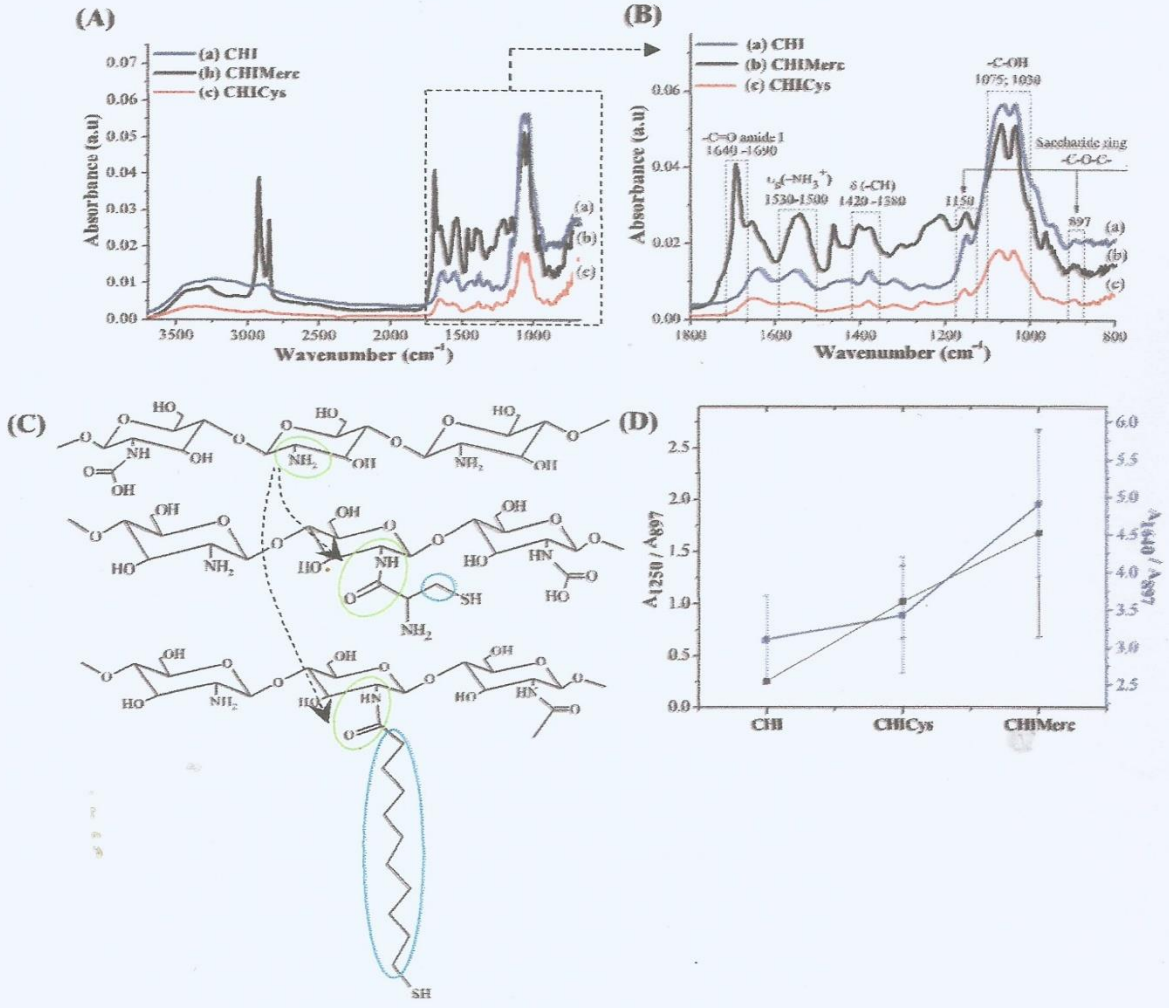


**Fig. 2.** (A) FTIR spectra of samples (a) CHI, (b) CHIMerc, (c) CHICys; (B) FTIR spectra with changes of bands of amine and amide groups (a) CHI, (b) CHIMerc, (c) CHICys; (C) Chemical representation highlighting the changes in the chitosan chains with the thiol functionalization (a) CHI, (b) CHIMerc, (c) CHICys; (D) The relationship between bands at 1640/897 $cm^{-1}$ and 1250/897 $cm^{-1}$ for each sample.

amide bond formation, it was possible to estimate the extension of the functionalization process. Changes in amide I region (~1640 $cm^{-1}$) can also be used to estimate the degree of functionalization. Compared with the CHI spectrum (Fig. 2B (a)), the changes in CHIMerc spectrum (Fig. 2B (b)) are more remarkable than those in the CHICys spectrum (Fig. 2B (c)), attributed to the length of the alkyl chain and the higher degree of functionalization, as verified by *Ellman's* reagent in the previous section. The chemical representations of the changes in chitosan chains with the thiol functionalization, according to the FTIR analysis, are shown in Fig. 2C. The ratio between reference (897 $cm^{-1}$) and amide (1640 $cm^{-1}$ and 1250 $cm^{-1}$) bands (related to both areas and intensities of these selected bands) are shown in Fig. 2D [30,34–36].

As thiol bands are weakly detectable in FTIR, Raman spectroscopy was used as a complementary technique for further characterization of the chitosan thiomers. The results are shown in the Raman spectra in Fig. 3A highlighting the bands related to sulfur groups of thiol chitosan samples (CHICys and CHIMerc) at 2800–2700 $cm^{-1}$ (—S—$CH_2$—$CH_2$), 610 $cm^{-1}$, 530 $cm^{-1}$ (S—S), 770–730 $cm^{-1}$ (—S—C), and 2560–2500 $cm^{-1}$ (—SH) [37,38]. However, the major band related to thiol groups (—SH) at 2560–2500 $cm^{-1}$ appeared only in the CHIMerc (Fig. 3B), most likely due to the much higher degree of substitution compared to CHICys evaluated by *Ellman's* method in the previous section [37,38]. Moreover, the bands associated with stretching and bending vibrations of the $CH_2$ species at 2800–3000 and 1400–1200 $cm^{-1}$ were stronger in the CHIMerc sample than in the CHICys and CHI samples, which were assigned to the contributions of *N*-acylation of the chitosan polymer with the MERC alkyl chain (*i.e.*, inserting 10 $CH_2$ groups) [37,38]. Minor signals were detected at 530 $cm^{-1}$ in the CHICys and the CHIMerc samples, which indicated the formation of disulfide bonds (S—S) by adjacent thiol groups [37,38].

Nuclear magnetic resonance spectroscopy (NMR) has been widely used as a characterization tool for evaluating polysaccharides such as chitosan and its functionalized derivatives. Thus, in this study, $^1$H NMR spectroscopy was used as a supporting technique for further investigating the functionalization of the chitosan backbone by thiol modifiers (*i.e.*, cysteine and MERC). Principally, both samples (CHICys, Fig. S2 and CHIMerc, Fig. 3C) showed the peak at approximately 2.0 ppm indicating the three *N*-acetyl protons of the *N*-acetyl glucosamine residue ($NHCOCH_3$) due to the incomplete deacetylation of chitosan. In addition, the saccharide ring protons of chitosan usually resonating at

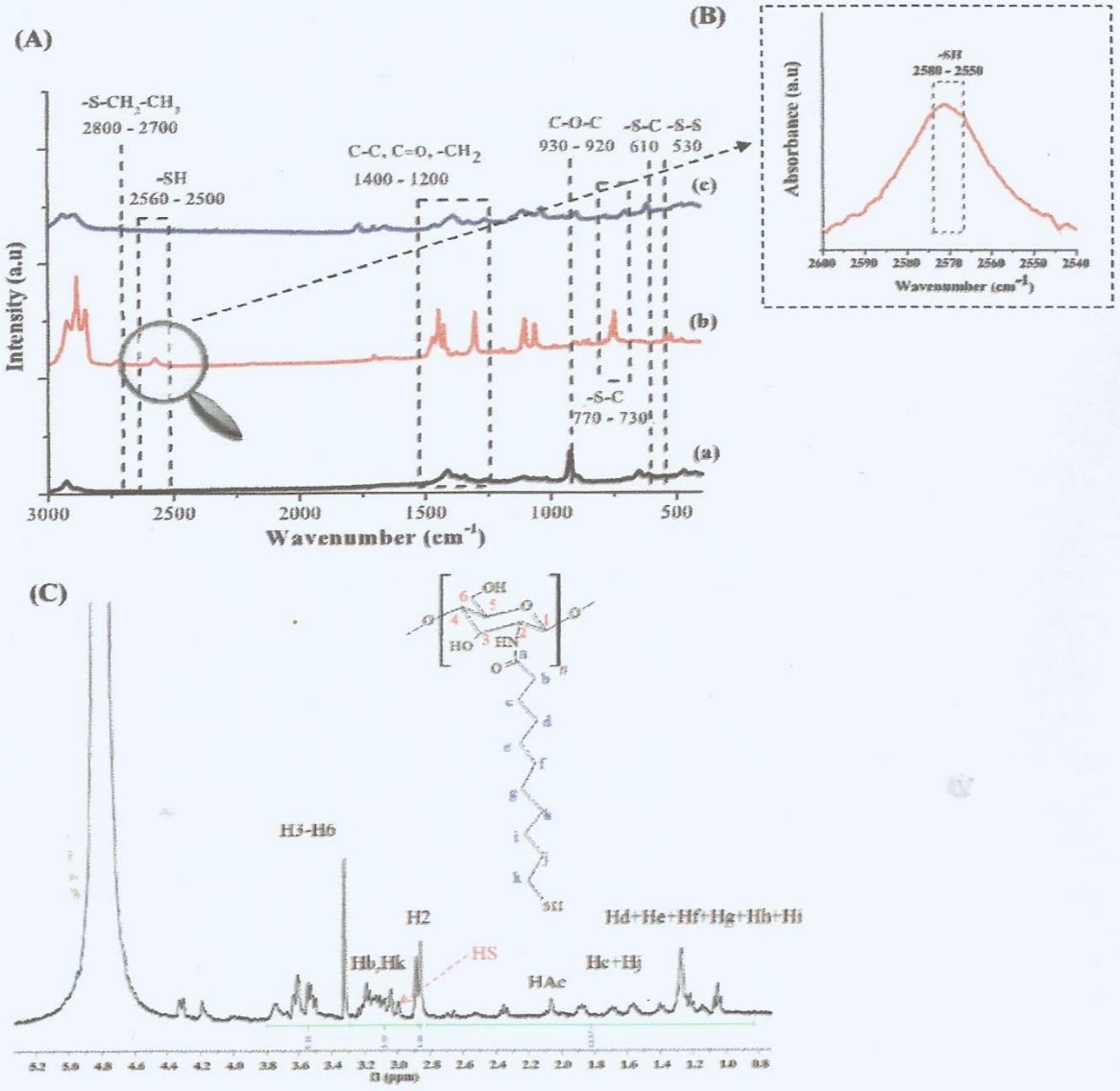


Fig. 3. (A) Raman spectra of samples (a) CHI; (b) CHIMerc and (c) CHICys; (B) Raman spectra of all thiol chitosan samples highlighted the thiol group and (C) $^1$H NMR spectrum of CHIMerc.

approximately 3.4–5.0 ppm were detected [13,24,25,36,39]. Regarding the functionalization of chitosan, the protons in thiol groups can easily be replaced by D in $D_2O$ used for NMR sample preparation, making it undetectable in the NMR spectrum. Nonetheless, the signal at δ 2.7–2.9 ppm is commonly assigned to methylene protons adjacent to thiol groups (—S—$CH_2$), which can be perceived as evidence for the existence of thiol groups immobilized on chitosan backbones [24,36,39,40]. Moreover, the $^1$H NMR spectrum of CHIMerc indicated the incorporation of aliphatic chain residues due to the appearance of signals corresponding to acyl chain protons at 3.1–3.3 ppm, 1.9–1.4 ppm and 1.3–1.0 ppm (greater δ related to α —$CH_2$— and β —$CH_2$— and smaller δ for —$(CH_2)_{d-i}$—) as indicated in Fig. 3C [13]. These results confirmed that CYS and MERC were successfully grafted onto the chitosan backbone forming thiomer-functionalized structures.

### 3.1.3. Swelling and degradation properties of thiolated-chitosan scaffolds

The results of swelling degree of chitosan and chitosan-thiolated scaffolds are presented in Fig. 4A. A significant decrease of the swelling degree (SD) at equilibrium of chitosan from 2600% to 2280% and 1810% for the thiomers, CHICys and CHIMerc, respectively, was observed after 24 h of immersion in deionized water (pH = 5.5 ± 0.5, at room temperature, 26 ± 2 °C). Although several methods are reported in the literature for evaluating the swelling degree of hydrogels, most of them present well-correlated results with no relevant difference for the overall tendency analyzed. These results are consistent with the FTIR findings and the degree of functionalization discussed in the previous sections, where the thiolation of chitosan occurred *via* the formation of amide bonds (*i.e.*, replacing —$NH_2$ groups by —SH groups), which led to a less chemically hydrophilic (or more hydrophobic) polymer matrix for water swelling. In addition, the introduction of thiol groups to the chitosan backbone favored further crosslinking of the polymer network by the formation of disulfide bonds between adjacent groups (*i.e.*, —SH/—SH) [17,24,30]. Therefore, this effect contributed to the reduction of the swelling capacity of the chitosan-thiolated scaffolds produced. To this end, the reduction of swelling degree was more prominent in CHIMerc scaffolds due to the grafting of the hydrophobic acyl chain with terminal sulfhydryl group to the chitosan backbone, associated with a higher degree of functionalization compared to CHICys.

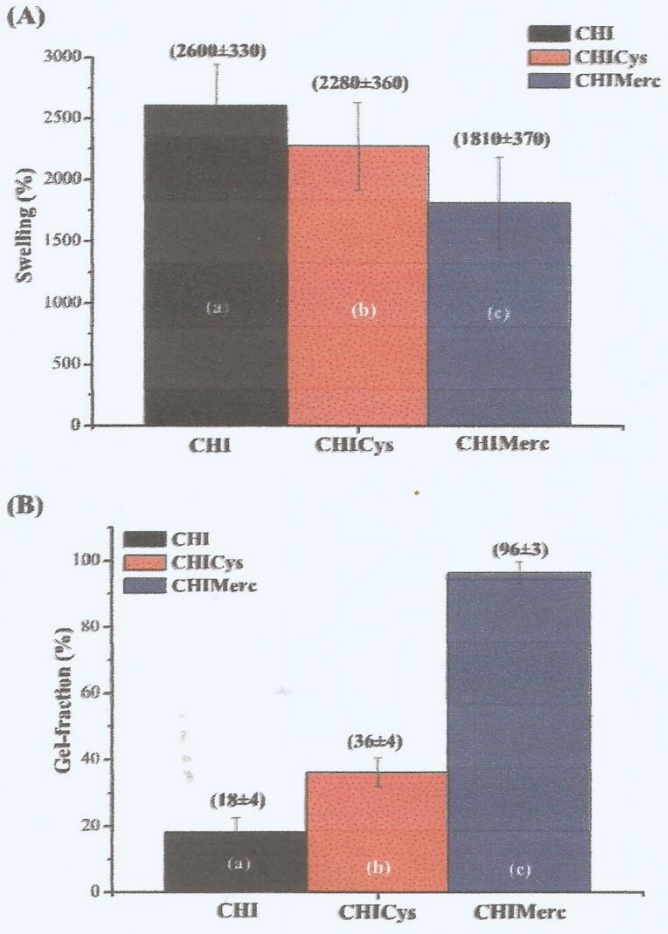


**Fig. 4.** (A) Swelling degree in deionized water (pH = 5.5 ± 0.5) for all samples at 24 h (n = 21) and (B) Gel fraction in deionized water (pH = 5.5 ± 0.5) at 24 h for all samples (n = 21).

Analogously, the *in vitro* chemical stability of these scaffolds was assessed by a gravimetric method after 24 h of immersion in deionized water (pH = 5.5 ± 0.5), at room temperature (26 ± 2 °C), which was applied to estimate the gel fraction (or degradation by solvation), and the results are presented in Fig. 4B. As expected, the opposite trend for the GF compared to the swelling degree was verified. The swelling degree was increased by grafting thiol moieties to the chitosan backbone. The results of GF indicated a higher chemical stability of the scaffolds produced with chitosan derivatives, *i.e.*, GF = 100% and 36% for CHIMerc and CHICys, respectively, and 18% for chitosan. These results endorsed the previous findings, demonstrating the more hydrophobic behavior of thiolated chitosan derivatives due to the substitution of primary amino groups by thiol groups in the polymer chain and the incorporation of the acyl groups by coupling with MERC. Similar trends were reported in the literature for thiolated chitosan derivatives [17,36,41].

Thus, the results of swelling degree and gel fraction measurements demonstrated that these thiomer-based scaffolds made of chitosan derivatives showed physicochemical properties suitable for biomedical applications in soft tissue engineering where hydrophilic networks are highly needed associated with chemical stability in aqueous media. Moreover, the grafting of thiol groups onto the chitosan backbone tuned these properties, which may promote chemical interactions with more hydrophobic molecules (peptides, antibodies, proteins, enzymes, drugs, *etc.*) present in the biological microenvironment (*e.g.*, cells and tissues) [42–45].

### 3.1.4. Morphological analysis by SEM, micro-CT and Archimedes' Method

The presence of thiol groups is a very interesting characteristic because the thiol groups can give the system bio-adhesive characteristics, permeation enhancement and anti-protease properties, and these characteristics are important because they influence the capacity of cells to adhere and proliferate [42]. In addition, if the tissue engineering applications are envisioned, cell adhesion to biomaterials is a crucial prerequisite for tissue repair and regeneration, and in this case, the morphology and structure of the surface of biomaterials are considered key features affecting the capacity of cells to adhere and proliferate [12,46]. Therefore, it is very important to understand the morphology of the scaffold, in particular porosity, because this parameter strongly affects the mechanical and biological performance of the developed structures [12,46]. Among many alternatives, appropriate techniques for this purpose must be selected, because each technique has limitations, and a combination of different techniques is often required to achieve an in-depth study of the morphological properties of the scaffold. Then, for that proposal, scanning electron microscopy (SEM) analysis associated with micro-computed tomography (micro-CT) as nondestructive techniques can provide a comprehensive set of data and fulfill this role. In addition, the surface areas of the scaffolds were estimated based on the results obtained by the *Archimedes'* Method.

SEM is considered a traditional technique to characterize the material surface. This technique presents excellent resolution at the submicrometer range and is available in research centers and universities worldwide. However, the micro-CT, which was used initially to characterize the 3D trabecular microarchitecture of bone, has been exploited

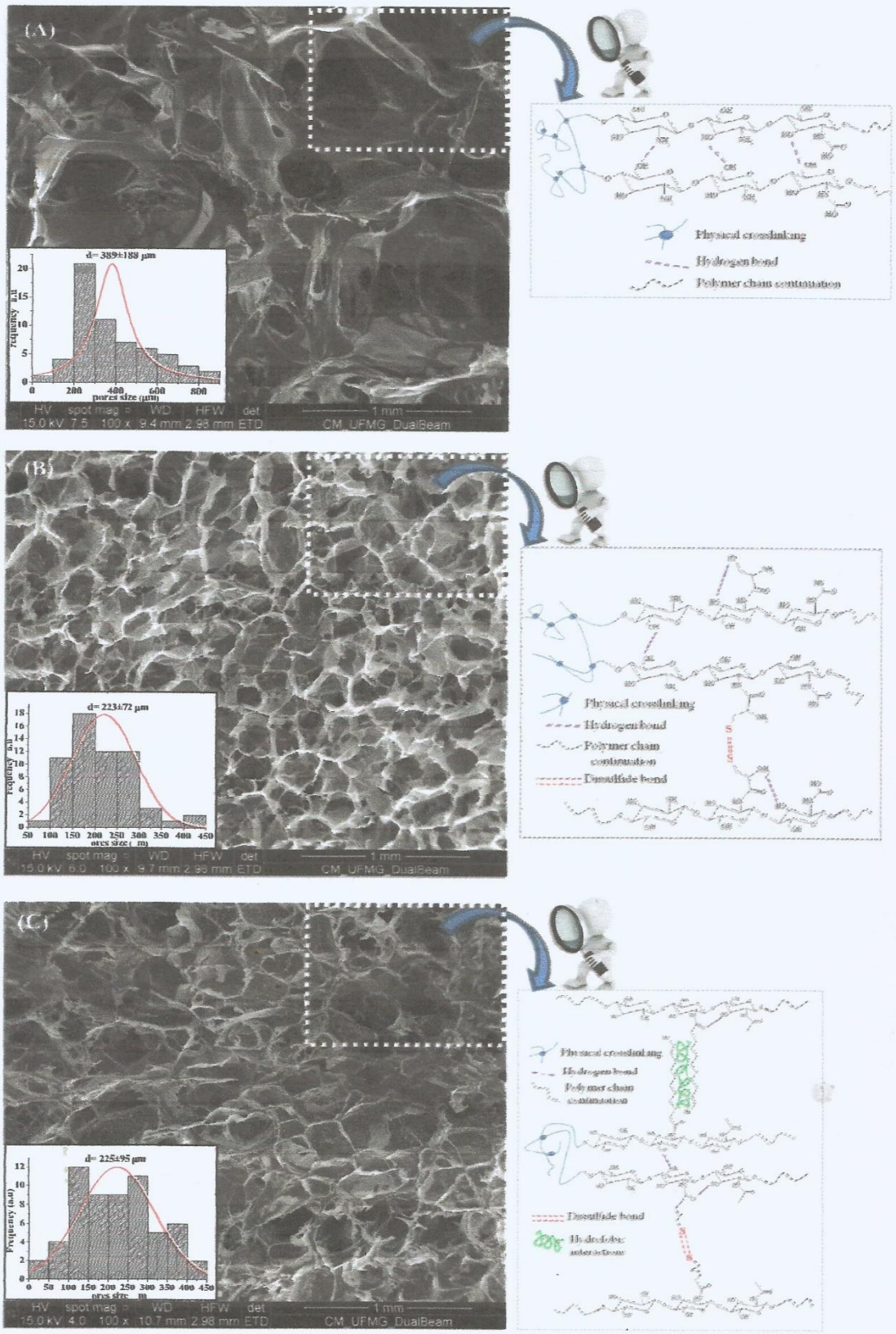


**Fig. 5.** SEM images with 100× at left and distribution of porous size obtained manually with 30 measures and Chemical/Physical crosslinking between the chains at right of (A) CHI, (B) CHICys and (C) CHIMerc.

for several research studies for the morphological porous biomaterial characterization, and this technique enables a full assessment of porous structures, both in terms of pore size and interconnected porosity for the development of scaffold-based tissue engineering applications [12]. In that sense, the SEM analysis was performed, and all samples have presented highly tridimensional porous structure at the micrometer range (Fig. 5). However, although all scaffolds presented sponge-like structures with pore size typically ranging from 100 and 350 μm, they clearly showed distinct morphological aspects. Chitosan scaffolds presented relatively larger average pore size of 389 ± 188 μm than CHICys and CHIMerc thiomer derivatives of 223 ± 72 and 225 ± 95 μm, respectively. Moreover, CHICys scaffolds (Fig. 5B) presented a more uniform pore size distribution than the CHIMerc sample despite similar average pore size values (Fig. 5C), assigned to the possible interactions of the hydrophobic acyl chain of MERC with the water solvent during the freeze-drying process. Nonetheless, as far as biomedical application is concerned, these features of highly porous structures are very important to facilitate the diffusion of nutrients, biomolecules and cell metabolic by-products. In addition, pore sizes ranging from 100 to 350 μm are ideal for cell proliferation and the formation of new tissue [12,47–52].

The X-ray microtomography analysis (micro-CT) showed that the average porosity was higher than 80% in all samples, and the average pore size was 204 ± 6 and 214 ± 3 μm for CHICys and CHIMerc, similar to the values estimated by SEM. The interconnectivity of CHICys and CHIMerc was >90% (Table 1), which is suitable for better cell proliferation aiming at potential biomedical applications in tissue repair [49,52,53] as it allows the flow transport of nutrients and metabolic waste and cell functions pertinent to the new tissue formation and tissue ingrowth.

The *Archimedes'* Method was also used to assess the surface area and the porosity of the scaffolds [54,55]. The results indicated that all chitosan-based thiomer scaffolds presented porosity higher than 90% (like the micro-CT method) but CHIMerc showed the largest surface area and lowest density (Table S1). These results were interpreted as the contribution of the hydrophobic chain inserted in the 3D scaffold of CHIMerc, which caused repulsion to water molecules during the synthesis of the 3D porous structure. In addition to the pores with size ranging from 100 to 350 μm, this has led also to the formation of ultra-small pores in the scaffolds causing a much higher surface area and lower density, which was detected at the higher magnification of the SEM analysis (Fig. S3). Therefore, the contact angles of these systems were evaluated using water droplets spread onto polymer films as a qualitative method for assessing the relative variation of hydrophobic/hydrophilic behavior of the chitosan and thiolated chitosan samples. The results of the contact angle (Fig. 6) were 60 ± 1° for chitosan and 64 ± 1° and 84 ± 2° for CHICys and CHIMerc, respectively. The thiolation of chitosan has significantly increased the average value of the contact angle of almost 40% for CHIMerc, which demonstrated the hydrophobic interactions of the acyl groups inserted into the polymer backbone. To this end, such a large specific surface area, high porosity and tunable hydrophilic/hydrophobic characteristics may promote cell adhesion and proliferation regarding to the potential biomedical applications of these systems [41,51,56].

**Table 1**
Morphological aspects obtained by micro-CT analysis for 3D porous scaffolds of thiolated-chitosan derivatives.

| Morphological aspects | CHICys | CHIMerc |
|---|---|---|
| Average pore size (μm) | (204 ± 6) | (214 ± 3) |
| Porosity (%) | (86 ± 4) | (82 ± 3) |
| S/V ($\mu m^{-1}$) | (0.026 ± 0.003) | (0.085 ± 0.001) |
| Interconnectivity (%) | >90 | >90 |

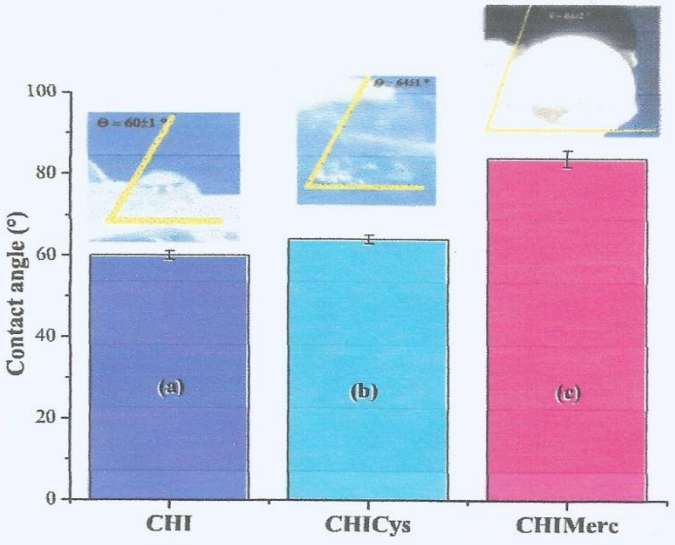


**Fig. 6.** Contact angle measurements of (a) CHI (b) CHICys and (c) CHIMerc films.

### 3.2. Biological characterization of thiolated-chitosan 3D porous scaffolds

#### 3.2.1. Cell viability assay by MTT

The cytocompatibility of the 3D hydrogel scaffolds was characterized through MTT *in vitro* assays to further validate the potential of these hydrogels to be applied in the biomedical field for cartilage repair [12,26]. HEK 293 T and SAOS were used as models, since they share similarities with cells that are involved in the production of ECM components essential for the repair of soft and hard tissues [4–9]. Therefore, in this study, the toxicity of the CHI, CHICys and CHIMerc biopolymeric scaffolds was preliminary evaluated based on analysis of the cell viability using the direct contact method of the MTT assay. This test was specifically used to evaluate mitochondrial function and cell viability and is widely accepted to access the cytotoxicity of novel biomaterials according to the international standard (ISO 10993-5:2009/(R)2014, Biological evaluation of medical devices: Tests for *in vitro* cytotoxicity). Fig. 7A shows the results towards HEK 293 T where no cytotoxic effects were observed for all systems, as there were cell viability responses of over 90%, like the reference control condition (100%, within statistical variation). Despite differences in the morphological and architectural features of CHI, CHICys and CHIMerc scaffolds and their physicochemical properties characterized in the previous sections, they demonstrated equivalent cytocompatibility to HEK 293 T cells, which was attributed to the high biocompatibility of the chitosan biopolymer favoring cell metabolic mitochondrial activity. For the confluence of these cells (Fig. 7B), no significant difference was observed for the polymeric samples compared with the control group with nearly 100% surface coverage after 24 h of incubation in the direct contact method. Analogously, equivalent results were observed for SAOS cells where no cytotoxicity was verified towards all scaffolds tested (Fig. S4).

#### 3.2.2. LIVE/DEAD® assay

Essentially, the LIVE/DEAD® viability/cytotoxicity assay provides a two-color fluorescence cell viability test, based on the simultaneous determination of live (stained in green, $\lambda_{ex}$ 495 nm, $\lambda_{em}$ 515 nm) and dead cells (stained in red, $\lambda_{ex}$ 495 nm, $\lambda_{em}$ 635 nm) with two probes, Calcein AM (acetoxymethyl ester of calcein) and EthD-1 (ethidium homodimer), that measure known parameters of cell viability, the intracellular esterase activity and plasma membrane integrity [57,58]. Therefore, the LIVE/DEAD® cytotoxicity assay was performed to confirm the results of

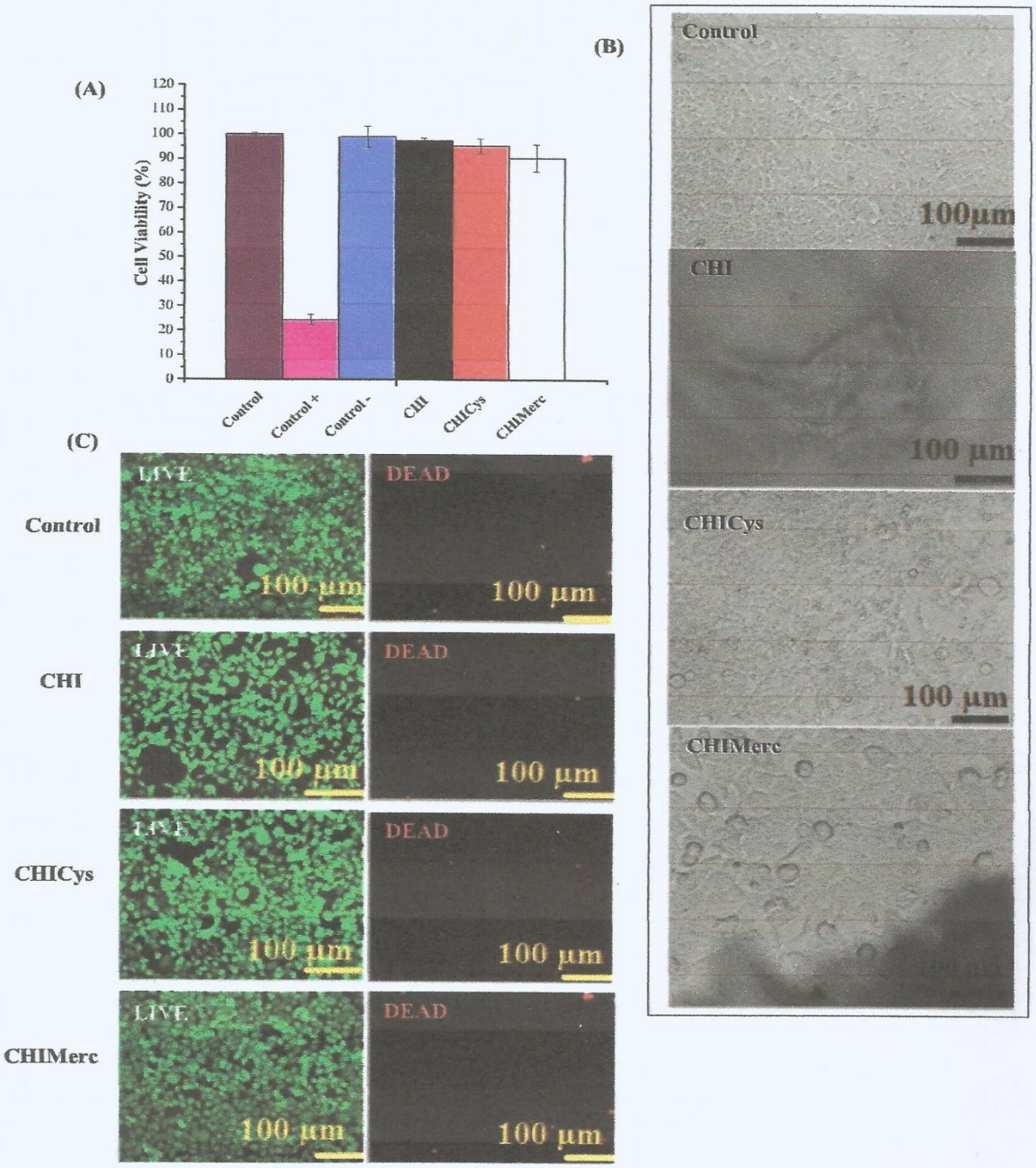


**Fig. 7.** (A) Histogram of cell viability of embryonic cell lines (HEK 293 T) towards all samples; (B) Optical images of HEK 293 T responses after 24 h using MTT assay and (C) The LIVE/DEAD® test with HEK 293 T cells after 24 h incubation. Live cells (green) and Dead cells (red) in control of with 200×. (For interpretation of the references to color in this figure legend, the reader is referred to the web version of this article.)

the MTT tests using the kidney cell line of a human embryo (HEK 293 T) with chitosan and thiolated derivatives (CHICys and CHIMerc). Fig. 7C shows that the cells tested with the samples CHI, CHICys and CHIMerc had a fluorescence pattern similar to the control group, *i.e.*, high green fluorescence (viable cells) and little or no red fluorescence (dead cells). Thus, as expected, the LIVE/DEAD test validated the previous results shown in the cell viability assays by MTT. In that sense, it may be suggested that the CHICys and CHIMerc scaffolds have shown promising potential to find applications as biomaterials for tissue engineering.

## 4. Conclusions

In this study, we focused on the synthesis and comprehensive characterization of new 3D hydrogel scaffolds based on thiol-functionalized high molecular mass chitosan. The hydrogels were produced by the freeze-drying method for obtaining porous scaffolds. The FTIR, Raman and NMR spectroscopy results evidenced the mechanisms involved in the conjugation process *via* the formation of amide bonds between carboxyl groups from thiol precursors (*i.e.*, cysteine and MERC) with amino

groups of the chitosan backbone. Moreover, the results demonstrated that the chitosan and chitosan-thiolated hydrogels were produced with different degree of functionalization and swelling degree depending on the thiol-modifier precursors used in the synthesis. Analogously, degradation behavior was reduced by increasing the hydrophobicity of the thiol precursor and the crosslinking of the network by the formation of disulfide bonds. SEM analysis associated with micro-CT X-ray imaging of the hydrogel scaffolds presented highly porous and interconnected 3D structures, with distinct morphological features such as porosity, surface area and density significantly affected by the thiol moieties inserted in the chitosan polymeric network. These three-dimensional hydrogel scaffolds were cytocompatible, based on the *in vitro* MTT assay with over 90% of the cell viability responses of HEK 293 T and SAOS cells and LIVE/DEAD cell viability results. Therefore, novel biocompatible chitosan-derived thiomer scaffolds were designed and produced with properties that are modified by the selection of sulfhydryl precursors, with the ability to absorb large amounts of water while maintaining their architectural features and three-dimensional stability. The scaffolds are promising for potential use in cartilage tissue repair applications.

## Acknowledgments

The authors acknowledge the financial support from the following Brazilian research agencies: CNPq (140810/2015-3; PQ1B-306306/2014-0; UNIVERSAL-457537/2014-0; PIBIC-2016/2017), CAPES (PROEX-2010-2017; PNPD; PROINFRA2010-2014), FAPEMIG (PPM-00760-16), and FINEP (CTINFRA-PROINFRA 2008/2010/2011). The authors express their gratitude to the staff at the Microscopy Center at UFMG for SEM analysis. Finally, the authors thank the staff at the Center of Nanoscience, Nanotechnology and Innovation-CeNano²I/CEMUCASI/UFMG for the spectroscopy analyses.

## Author contributions

The manuscript was written through equally contributions from all authors. All authors have read and given approval to the final version of the manuscript.

## Conflicts of interest

The authors declare that they have no competing interests.

## Appendix A. Supplementary data

Supplementary data to this article can be found online at https://doi.org/10.1016/j.ijbiomac.2018.03.133.

## References

[1] F.-M. Chen, X. Liu, Advancing biomaterials of human origin for tissue engineering, Prog. Polym. Sci. 53 (2016) 86–168.
[2] R. Langer, J.P. Vacanti, Tissue Engineering, Science, New Series 260 (1993) 920–926.
[3] L.G. Griffith, G. Naughton, Tissue engineering-current challenges and expanding opportunities, Science 295 (2002) 1009–1014.
[4] X. Vial, E.M. Andreopoulos, Novel biomaterials for cartilage tissue engineering, Curr. Rheumatol. Rev. 500 (2009) 51–57.
[5] M.S. Shoichet, Polymer scaffolds for biomaterials applications, Macromolecules 43 (2010) 581–591.
[6] D.F.D. Campos, Supporting biomaterials for articular cartilage repair, Cartilage 3 (2012) 205–221.
[7] M.L. Alves da Silva, A. Martins, A.R. Costa-Pinto, V.M. Correio, P. Sol, M. Bhattacharya, S. Faria, R.L. Reis, N.M. Neves, Chondrogenic differentiation of human bone marrow mesenchymal stem cells in chitosan-based scaffolds using a flow-perfusion bioreactor, J. Tissue Eng. Regen. Med. 5 (2011) 722–732.
[8] A. Abarrategi, Y. Lopiz-Morales, V. Ramos, A. Civantos, L. Lopez-Duran, F. Marco, J.L. López-Lacomba, Chitosan scaffolds for osteochondral tissue regeneration, J. Biomed. Mater. Res. A 95 (2010) 1132–1141.
[9] A. Chevrier, C.D. Hoemann, J. Sun, M.D. Buschmann, Temporal and spatial modulation of chondrogenic foci in subchondral microdrill holes by chitosan-glycerol phosphate/blood implants, Osteoarthr. Cartil. 19 (2011) 136–144.
[10] J.-K.F. Suh, H.W.T. Mathew, Application of chitosan-based polysaccharide biomaterials in cartilage tissue engineering: a review, Biomaterials 21 (2000) 2589–2598.
[11] D. Dickjürgen, D.W. Grainger, Polysaccharide matrices used in 3D in vitro cell culture systems, Biomaterials 141 (2017) 96–115.
[12] I.C. Carvalho, H.S. Mansur, Engineering 3D scaffolds of photocrosslinked chitosan-gelatin hydrogel hybrids for chronic wound dressings and regeneration, Mater. Sci. Eng. C 78 (2017) 690–705.
[13] J.C. Santos, P.M.D. Moreno, A.A.P. Mansur, V. Leiro, H.S. Mansur, A.P. Pêgo, Functionalized chitosan derivatives as nonviral vectors: physicochemical properties of acylated N,N,N-trimethyl chitosan/oligonucleotide nanopolyplexes, Soft Matter (41) (2015) 8113–8125.
[14] H.S. Mansur, A.A.P. Mansur, F. Curti, M.V. Almeida, Bioconjugation of quantum-dots with chitosan and N,N,N-trimethyl chitosan, Carbohydr. Polym. 90 (2012) 189–196.
[15] K.Y. Lee, W.S. Ha, W.H. Park, Blood compatibility and biodegradability of partially N-acylated chitosan derivatives, Biomaterials 16 (1995) 1211–1216.
[16] C. Le Tien, M. Lacroix, P. Ispas-Szabo, M.A. Mateescu, N-acylated chitosan: hydrophobic matrices for controlled drug release, J. Control. Release 93 (2003) 1–13.
[17] T. Schmitz, V. Grabovac, T.F. Palmberger, M.H. Hoffer, A. Bernkop-Schnurch, Synthesis and characterization of a chitosan-N-acetyl cysteine conjugate, Int. J. Pharm. 347 (2008) 79–85.
[18] L. Casettari, Biomedical applications of amino acid-modified chitosans: a review, Biomaterials 33 (2012) 7565–7583.
[19] F. Talaei, E. Azizi, R. Dinarvand, F. Atyabi, Thiolated chitosan nanoparticles as a delivery system for antisense therapy, Int. J. Nanomedicine 6 (2011) 1963–1975.
[20] A. Bernkop-Schnurch, D. Guggi, Y. Pinter, Thiolated chitosans: development and in vitro evaluation of a mucoadhesive, permeation enhancing oral drug delivery system, J. Control. Release 94 (2004) 177–186.
[21] A. Bernkop-Schnurch, Thiomers: a new generation of mucoadhesive polymers, Adv. Drug Deliv. Rev. 57 (2005) 1569–1582.
[22] D. Dheer, D. Arora, S. Jaglan, R.K. Rawal, R. Shankar, Polysaccharides based nanomaterials for targeted anti-cancer drug delivery, J. Drug Target. 25 (2017) 1–16.
[23] K.U. Shah, U.S. Shah, N. Dilawar, G.M. Khan, S. Gibaud, Thiomers and their potential applications in drug delivery, Expert Opin. Drug Deliv. 14 (2017) 601–610.
[24] D. Liu, J. Li, H. Pan, F. He, Z. Liu, Q. Wu, C. Bai, S. Yu, X. Yang, Potential advantages of a novel chitosan-N-acetylcysteine surface modified nanostructured lipid carrier on the performance of ophthalmic delivery of curcumin, Sci. Rep. 6 (28796) (2016) 1–14.
[25] F.G. Medeiros Borsagli, A.A.P. Mansur, P. Chagas, L.C. Oliveira, H.S. Mansur, O-carboxymethyl functionalization of chitosan: complexation and adsorption of Cd (II) and Cr (VI) as heavy metal pollutant ions, React. Funct. Polym. 97 (2015) 37–47.
[26] E.S. Costa Junior, A.A.P. Mansur, E.F. Stancioli, W.L. Vasconcelos, H.S. Mansur, Preparation and characterization of chitosan/poly(vinyl alcohol) chemically crosslinked blends for biomedical applications, Carbohydr. Polym. 76 (2009) 472–481.
[27] W. Mozalewska, R. Czechowska-Biskupa, A.K. Olejnika, R.A. Wacha, P. Ulańskia, J.M. Rosiak, Chitosan-containing hydrogel wound dressings prepared by radiation technique, Radiat. Phys. Chem. 134 (2017) 1–7.
[28] S.T. Ho, D.W. Hutmacher, A comparison of micro CT with other techniques used in the characterization of scaffolds, Biomaterials 27 (2006) 1362–1376.
[29] S. Lowell, J.E. Shields, M.A. Thomas, M. Thommes, Characterization of porous solids and powders: surface area, pore size and density, Springer, New York, 2004.
[30] D.-Y. Teng, Z.-M. Wu, X.-G. Zhang, Y.-X. Wang, C. Zheng, Z. Wang, C.-X. Li, Synthesis and characterization of in situ cross-linked hydrogel based on self-assembly of thiol-modified chitosan with PEG diacrylate using Michael type addition, Polymer 51 (2010) 939–946.
[31] K. Kafedjiiski, K.H. Krauland, M.H. Hoffer, A. Bernkop-Schnurch, Synthesis and in vitro evaluation of a novel thiolated chitosan, Biomaterials 26 (2005) 819–826.
[32] N. Tawill, A. Hatef, E. Sacher, M. Maisonneuve, T. Gervais, R. Mandeville, M. Meunier, Surface Plasmon resonance determination of the binding mechanisms of L-cysteine and mercaptoundecanoic acid on gold, J. Phys. Chem. 117 (2013) 6712–6718.
[33] O. Cavalleri, L. Oliveri, A. Dacca, R. Parodi, R. Rolandi, XPS measurements on L-cysteine and 1-octadecanethiol self-assembled films: a comparative study, Appl. Surf. Sci. 175 (2001) 357–362.
[34] R. Yang, Y. Su, K.B. Aubrecht, X. Wang, H. Ma, R.B. Grubbs, B.S. Hsiao, B. Chu, Thiol-functionalized chitin nanofibers for As (III) adsorption, Polymer 60 (2015) 9–17.
[35] A.S. Robbinson, J. King, Disulphide-bonded intermediate on the folding and assembly pathway of a non-disulphide bonded protein, Nat. Struct. Mol. 4 (1997) 450–455.
[36] G.S. Rajawat, U.A. Shinde, H.A. Nair, Chitosan-N-acetyl cysteine microspheres for ocular delivery of acyclovir: synthesis and in vitro/in vivo evaluation, J. Drug. Deliv. Sci. Technol. 35 (2016) 333–342.
[37] J.T. Edsall, J.W. Otvos, A. Rich, Raman spectra of amino acids and related compounds. VII. Glycylglycine, cysteine, cystine and other amino acids, J. Am. Chem. Soc. 72 (1950) 474–477.
[38] L. Pawlukojc, J. Leciejewicz, A.J. Ramirez-Cuesta, J. Nowicka-Scheibe, L-Cysteine: neutron spectroscopy, Raman, IR and ab initio study, Spectrochim. Acta A Mol. Biomol. Spectrosc. 61 (2005) 2474–2481.

[39] X. Liu, B. Yu, Q. Huang, R. Liu, Q. Feng, Q. Cai, S. Mi, In vitro BMP-2 peptide release from thiolated chitosan based hydrogel, Int. J. Biol. Macromol. 93 (2016) 314–321.
[40] J. Li, D. Liu, Z. Tan, Z. Zhao, X. Yang, W. Pan, A comparative study on the efficiency of chitosan-N-acetylcysteine, chitosan oligosaccharides or carboxymethyl chitosan surface modified nanostructured lipid carrier for ophthalmic delivery of curcumin, Carbohydr. Polym. 146 (2016) 435–444.
[41] J.C. Santos, A.A. Mansur, H.S. Mansur, One-step biofunctionalization of quantum dots with chitosan and N-palmitoyl chitosan for potential biomedical applications, Molecules 18 (2013) 6550–6572.
[42] A. Bernkop-Schnurch, A.H. Krauland, V.M. Leitner, T. Palmberger, Thiomers: potential excipients for non-invasive peptide delivery systems, Eur. J. Pharm. Biopharm. 58 (2004) 253–263.
[43] L. Nobs, F. Buchegger, R. Gurny, E. Alle'mann, Current methods for attaching targeting ligands to liposomes and nanoparticles, J. Pharm. Sci. 93 (2004) 1980–1992.
[44] C.L. Domínguez-Delgado, I.M. Rodríguez-Cruz, E. Fuentes-Prado, J.J. Escobar-Chávez, G. Vidal-Romero, L. García-Gonzáles, R.I. Fuente-Lee, Drug carrier systems using chitosan for non parenteral routes, in: S.J. Thatha Gowder (Ed.), Pharmacology and Toxicological and Pharmaceutics Science, Intech 2014, pp. 273–325.
[45] M. Werle, A. Bernkop-Schnurch, Thiolated chitosans: useful excipients for oral drug delivery, J. Pharm. Pharmacol. 60 (2008) 273–281.
[46] S. Bertoldi, S. Farè, M.C. Tanzi, Assessment of scaffold porosity: the new route of micro-CT, J. Appl. Biomater. Biomech. 9 (2011) 165–175.
[47] I.-H. Bae, B.-C. Jeong, M.-S. Kook, S.-H. Kim, J.-T. Koh, Evaluation of a thiolated chitosan scaffold for local delivery of BMP-2 for osteogenic differentiation and ectopic bone formation, Biomed. Res. Int. 2013 (2013) 1–11.
[48] H.S. Mansur, H.S. Costa, A.A. Mansur, M. Pereira, 3D-macroporous hybrid scaffolds for tissue engineering: network design and mathematical modeling of degradation kinetics, Mater. Sci. Eng. C 32 (2012) 404–415.
[49] B. Mandal, S. Kundu, Cell proliferation and migration in silk fibroin 3D scaffolds, Biomaterials 30 (2009) 2956–2965.
[50] H. Kim, U. Kim, G. Vunjak-Novakovic, B. Min, D. Kaplan, Influence of macroporous protein scaffolds on bone tissue engineering from bone marrow stem cells, Biomaterials 26 (2005) 4442–4452.
[51] G. Akay, M.A. Birch, M.A. Bokhari, Microcellular polyHIPE polymer supports osteoblast growth and bone formation in vitro, Biomaterials 25 (2004) 3991–4000.
[52] C.M. Murphy, F.J. O'Brien, Understanding the effect of mean pore size on cell activity in collagen-glycosaminoglycan scaffolds, Cell Adhes. Migr. 4 (2010) 377–381.
[53] S.M. Lien, L.Y. Ko, T.J. Huang, Effect of pore size on ECM secretion and cell growth in gelatin scaffold for articular cartilage tissue engineering, Acta Biomater. 5 (2009) 670–679.
[54] T. Allen, Particle Size Measurement, Chapman & Hall, Londres, 1990.
[55] L. Svarovski, Solid-Gas Separation, Elsevier Scientific P. Co., New York, 1981.
[56] T. Yasuda, T. Okuno, Contact angle of water on polymer surfaces, Langmuir 10 (1994) 2435–2439.
[57] C.D.F. Moreira, S.M. Carvalho, H.S. Mansur, M.M. Pereira, Thermogelling chitosan-collagen-bioactive glass nanoparticle hybrids as potential injectable system for tissue engineering, Mater. Sci. Eng. C 58 (2016) 1207–1216.
[58] V.C. Dumont, H.S. Mansur, A.A.P. Mansur, S.M. Carvalho, N.S.V. Capanema, B.R. Barrioni, Glycol/chitosan nanohydroxyapatite biocomposites for potential bone tissue engineering and regenerative medicine, Inter. J. Biol. Macromol. 93 (2016) 1465–1478.

Elsevier Editorial System(tm) for
Biochemical Engineering Journal
Manuscript Draft

Manuscript Number:

Title: Bi-Functional Eco-friendly 3D Scaffolds based on N-acyl Thiolated Chitosan for Potential Adsorption of Dye Pollutants and Antibacterial Applications

Article Type: Full Length Article

Section/Category: Bioseparations

Keywords: Biosorbent; Adsorption of Dyes; Antibacterial Hydrogel; Wastewater Treatment; Thiolated-chitosan; Porous Scaffolds.

Corresponding Author: Professor Herman S. Mansur, Ph.D.

Corresponding Author's Institution: UFMG

First Author: Fernanda M Borsagli, MSc

Order of Authors: Fernanda M Borsagli, MSc; Virginia Ciminelli S Ciminelli, PhD; Dionei Joaquim Haas , MSc; Andrey P Lage, PhD; Herman S. Mansur, Ph.D.

Abstract: Unfortunately, the presence of organic dyes in industrial effluents has been continuously polluting waters leading to the formation of toxic sludge and/or carcinogenic compounds. To worsen this scenario, the proliferation of multidrug-resistant microorganisms in waters caused by anthropogenic activities and natural disasters has become major global concern because of serious health and environmental harms. Herein we designed and developed novel three-dimensional (3D) porous scaffolds made of N-acyl thiolated chitosan using 11-mercaptoundecanoic acid. These hydrogels exhibited 3D hierarchical pore structure (porosity > 82%) and high surface area (~ 420 m2.g-1), which demonstrated high adsorption capacity for methyl orange anionic dye pollutant (~ 450 mg.g-1) in water. The adsorption data were well-fitted to a pseudo-second-order kinetics and Freundlich's isotherm. Moreover, the thiolated-chitosan proved antibacterial activity against Pseudomonas aeruginosa regularly found in hospital discharges. Thus, for the first time, bi-functional thiolated-chitosan 3D-scaffolds were produced combining green biosorbent behavior for organic dyes and antimicrobial activity against pathogenic bacteria, which offer innovative strategy for the treatment of multi-polluted and contaminated water bodies.

*Cover Letter

UFMG Universidade Federal de Minas Gerais
Escola de Engenharia

Departamento de Engenharia Metalúrgica e de Materiais e-mail: hmansur@demet.ufmg.br

***To: Editor-in-Chief***
***Ref: Manuscript to Biochemical Engineering Journal, Elsevier.***

*Sunday, June 17, 2018*

Dear Editor,

I, along with my coauthors, would like to ask you to consider our manuscript entitled ***"Bi-Functional Eco-friendly 3D Scaffolds based on N-acyl Thiolated Chitosan for Potential Adsorption of Dye Pollutants and Antibacterial Applications"*** from H. S. Mansur *et al.* to be evaluated by the peer-reviewing process of the ***Biochemical Engineering Journal, Elsevier.***

**Novelty&Contributions:** Despite indisputable advances in the recent decades in the field of water treatment and purification processes the development of innovative adsorbents based on *"smart"* functionalized materials combining high adsorption capacity, low cost, biocompatibility and environmentally-friendly features represents a decisive challenge to be overcome by researchers and professionals. Thus, this research focused on the design, synthesis and comprehensive characterization of novel 3D scaffold hydrogels made of chitosan-based thiomers using 11-mercaptoundecanoic acid as sulfhydryl-bearing reagent for applications as efficient adsorbents of toxic dyes of polluted water bodies associated with antibacterial activity. The results demonstrated the synthesis of chitosan thiomers with degree of thiol substitution of 26 %, producing highly porous scaffolds (porosity > 80 %) with hierarchical interconnected 3D pore structures. Importantly, their physicochemical properties (*e.g.*, swelling behavior and chemical stability) and architectural features were significantly tuned by the thiol-modifier, which proved consistent adsorption properties for the removal of methyl orange (MO) dye from water solution through the formation of polyelectrolyte/dye complexes. The MO adsorption mechanism was well fitted to Langmuir and Freundlich's isotherm models. Moreover, these hydrogels exhibited no ecotoxicity combined with antibacterial activity against *Pseudomonas aeruginosa,* which can be found in contaminated hospital effluents. Hence, these novel systems hold promise as innovative suitable platform for water treatment in *Environmental Biochemical Engineering applications.*
We believe that the findings of this study are relevant to the scope of your journal and it will be of interest to its readership.

We would like to confirm that:
- The authors state that the manuscript is **ORIGINAL**. It has not been published, submitted or under consideration in another journal;
- This article has been written by the stated authors who are all aware of its content and approved its submission;
- The authors declare that there is no conflict of interest;
- If accepted, this article will be under Copyright Terms & Conditions from ***Biochemical Engineering Journal, Elsevier***

Thank you for your consideration. I look forward to hearing from you.
Sincerely yours,
Prof. Herman Mansur

---

**Corresponding author:** Herman Sander Mansur, PhD - Full Professor
***Center of Nanoscience, Nanotechnology, and Innovation-CeNano²I***
Department of Metallurgical and Materials Engineering, Federal University of Minas Gerais
Av. Antônio Carlos, 6627 – Bloco 2 Engenharia – Sala 3639, 31.270-901, Pampulha, Belo Horizonte, MG, Brazil - Tel: +55-31-3409-1843. Fax: +55-31-3409-1815.
email: hmansur@demet.ufmg.br herman.mansur2016@gmail.com

## Highlights

.Thiol-modified chitosan derivatives (thiomer) were prepared *via* amide bond reaction.

.3D porous thiomer scaffolds were obtained by freeze-drying process.

.A facile green route to fabricate novel 3D biosorbent reusable sponges was provided.

.Eco-friendly thiomer sponges exhibited efficient adsorption for toxic anionic dyes.

.Adsorption kinetics mechanisms were tested for the 3D scaffold thiomer adsorbents.

# Bi-Functional Eco-friendly 3D Scaffolds based on *N*-acyl Thiolated Chitosan for Potential Adsorption of Dye Pollutants and Antibacterial Applications

Fernanda G. L. Medeiros Borsagli[1], Virginia S. T. Ciminelli[2], Dionei J. Haas[3], Andrey P. Lage[3], Herman S. Mansur[1*]

[1]*Center of Nanoscience, Nanotechnology, and Innovation - CeNano²I, Department of Metallurgical and Materials Engineering, Federal University of Minas Gerais/UFMG, Belo Horizonte, Brazil.*

[2]*National Institutes of Science and Technology: INCT-Acqua, Department of Metallurgical and Materials Engineering, Federal University of Minas Gerais, Brazil.*

[3]*Department of Preventive Veterinary Medicine, Veterinary School, Federal University of Minas Gerais, Brazil.*

Corresponding author: *hmansur@demet.ufmg.br

**Abstract**

Unfortunately, the presence of organic dyes in industrial effluents has been continuously polluting waters leading to the formation of toxic sludge and/or carcinogenic compounds. To worsen this scenario, the proliferation of multidrug-resistant microorganisms in waters caused by anthropogenic activities and natural disasters has become major global concern because of serious health and environmental harms. Herein we designed and developed novel three-dimensional (3D) porous scaffolds made of *N*-acyl thiolated chitosan using 11-mercaptoundecanoic acid. These hydrogels exhibited 3D hierarchical pore structure (porosity > 82%) and high surface area (~ 420 $m^2.g^{-1}$), which demonstrated high adsorption capacity for methyl orange anionic dye pollutant (~ 450 $mg.g^{-1}$) in water. The adsorption data were well-fitted to a pseudo-second-order kinetics and Freundlich's isotherm. Moreover, the thiolated-chitosan proved antibacterial activity against *Pseudomonas aeruginosa* regularly found in hospital discharges. Thus, for the first time, bi-functional thiolated-chitosan 3D-scaffolds were produced combining *green* biosorbent behavior for organic dyes and antimicrobial activity against pathogenic bacteria, which offer innovative strategy for the treatment of multi-polluted and contaminated water bodies.

**Keywords: Biosorbent; Adsorption of Dyes; Antibacterial Hydrogel; Wastewater Treatment; Thiolated-chitosan; Porous Scaffolds.**

*Corresponding author: Universidade Federal de Minas Gerais, Av. Antônio Carlos, 6627 – Escola de Engenharia, Bloco 2 – Sala 2233, 31.270-901, Belo Horizonte/MG, Brazil; Tel: +55-31-34091843; Fax: +55-31-34091843; E-mail: hmansur@demet.ufmg.br (H. Mansur).

# Graphical abstract

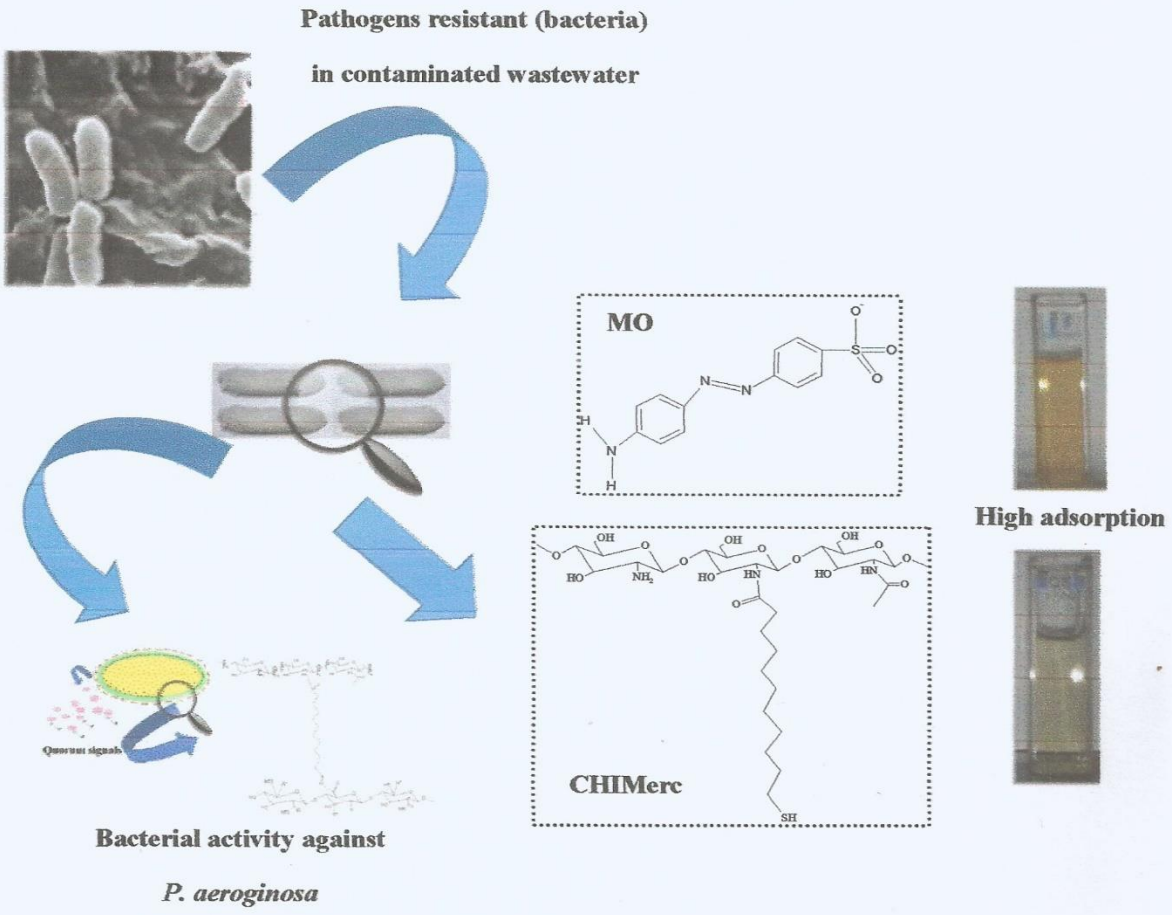


**Green Chemistry meets Environmental Science and Technology: Novel 3D Porous Scaffolds based on Chitosan Thiomers as Biosorbents with Antibacterial Activity for Wastewater Treatment**

## 1. Introduction

Water availability for economic development and conservation of life is a theme of great concern given the increasing occurrence of extreme events related to climate changes combined with the deterioration of water quality due to anthropogenic contamination [1]. Among these pollutants, dyes, phenolics, pharmaceutics, and pesticides have recently become of great concern because of their extreme toxicity and persistence in the environment. Although chemical and biological treatments are available for the removal of organic compounds, the by-products of their degradation can also be harmful and non-degradable [2-4]. Industrial effluents and hospital wastewater are some sources of water pollution. Industrial effluents runoffs may comprise colored substances that are released from textile, paint, paper, varnishes, ink, plastics, pulp, cosmetics, tannery and plastic [5,6]. The presence of dyes in industrial effluents are a significant cause of pollution due to their recalcitrance nature, giving undesirable color to the water and reducing sunlight penetration, associated with the fact that their degradation products may be toxic or even mutagenic and carcinogenic [5]. Approximately 10,000 different types of pigments and over 700,000 tons are produced worldwide annually, being 10 to 15 % lost in the effluent during the dyeing process [4,6,7]. To aggravate this scenario, many types of drugs, including antibiotics usually from inappropriate discard of medical, veterinary, and agricultural applications, heavy metals, and disinfectants are found in wastewater, thus contributing for increasing bacterial resistance [5,6,8,9]. Studies have shown that hospital effluents, in special, contain levels of bacteria with antibiotic resistance higher than effluent derived from other sources [8-10].

Effluents are usually treated by chemical precipitation, membrane separation, evaporation, electrolysis, among other processes. However, some of these methods may be ineffective for the removal of trace amounts from large volumes of wastewater and present shortcomings, such as high maintenance costs, generation of toxic sludge and complicated procedure involved in the treatment [11-14]. For this reason, selective wastewater treatment processes for the capture/immobilization of specific dyes, in addition to the reuse of waste is highly needed. In addition to the adopted adsorbents (*e.g.*, activated carbon) investigations on selective biosorbents based on natural polymers and derivatives have significantly increased under the concept of economic and environmentally friendly materials [15]. The natural polymers such as starch, cellulose, chitosan, and lignin are scientifically and industrially attractive because they present hydrophilic networks with functional groups for developing chemical interactions with metallic ions and organic compounds [16, 17]. Moreover, the presence of pH-sensitive functional groups in the polymer backbone offers an attractive possibility for developing novel soft materials forming polyelectrolyte hydrogel platforms. These hydrogel networks can swell in aqueous medium instead of dissolving in it and

interaction of sulfur-containing groups with MO during adsorption. Based on the results, it is possible to conclude that only a special type of S–S bonds is involved in MO adsorption. In fact, the atoms involved in the disulfide bonds (C–C–S–S–C–C) of adsorbent structure may assume different spatial orientations, causing three different conformations for the chemical bonds: *trans–gauche–trans*, *gauche–gauche–trans*, and *gauche–gauche–gauche* [34]. For the *trans-gauche–trans* and *gauche–gauche–trans* conformations, the expected wavenumbers for the S–S stretching vibration is 540 and 525 $cm^{-1}$, respectively, while for the *gauche–gauche–gauche* it is 510 $cm^{-1}$ [34]. The results indicated that the *trans-gauche–trans* disulfide bridges prevail in the CHIMerc and were preferably consumed during MO adsorption. Moreover, the sharp band at 2550 $cm^{-1}$ ($\nu$(S–H) vibrational mode) shown in the CHIMerc spectrum disappears after reaction with MO, which confirms that the higher concentration of thiol group (2218±100) $\mu mol.g^{-1}$ resulted in the formation of a MO-thiolated chitosan complex on the scaffold surface.

## 4. Conclusions

The application of 3D scaffolds with antibacterial activity, was evaluated for wastewater treatment. These thiolated chitosan derivatives showed a significant high thiolation degree (up to 700% compare to other studies). The antibacterial activity was demonstrated against *P. aeruginosa*, a bacterium highly drug-resistant and an opportunistic pathogen. This feature was related to the presence of sulfhydryl groups, the high DF (26±2) %, the long alkyl-chain, with probable thiol interaction with the alginate biofilm, and the interaction with *quorum signals* (QS). The maximum adsorption capacity, in a range of 400 – 450 $mg.g^{-1}$, is higher than similar studies with other chitosan derivatives. The removal of dyes by thiolated chitosans were not previously reported, to the best of the authors' knowledge. Raman spectroscopy showed that the sulfhydryl groups at the 3D scaffolds are the active groups involved in MO biosorption. The adsorption data were well-fitted to a pseudo-second-order kinetics and Freundlich's isotherm. The desorption showed recoveries over 80 %. Finally, the scaffolds showed MO dye recovery over 80 %. the 3D scaffolds are envisioned as promising bio-sorbents for potential wastewater treatment.

## Acknowledgments

The authors acknowledge the financial support from the following Brazilian research agencies: CNPq (140810/2015-3; PQ1B–306306/2014-0; UNIVERSAL-457537/2014-0; PIBIC-2014/2015), CAPES (PROEX-433/2010; PNPD; PROINFRA2010-2014), FAPEMIG (PPM-00760-16; BCN-TEC 30030/12), and FINEP (CTINFRA-PROINFRA 2008/2010/2011), and they express their gratitude to the Center for Microscopy of the Federal University of Minas Gerais (UFMG) for the